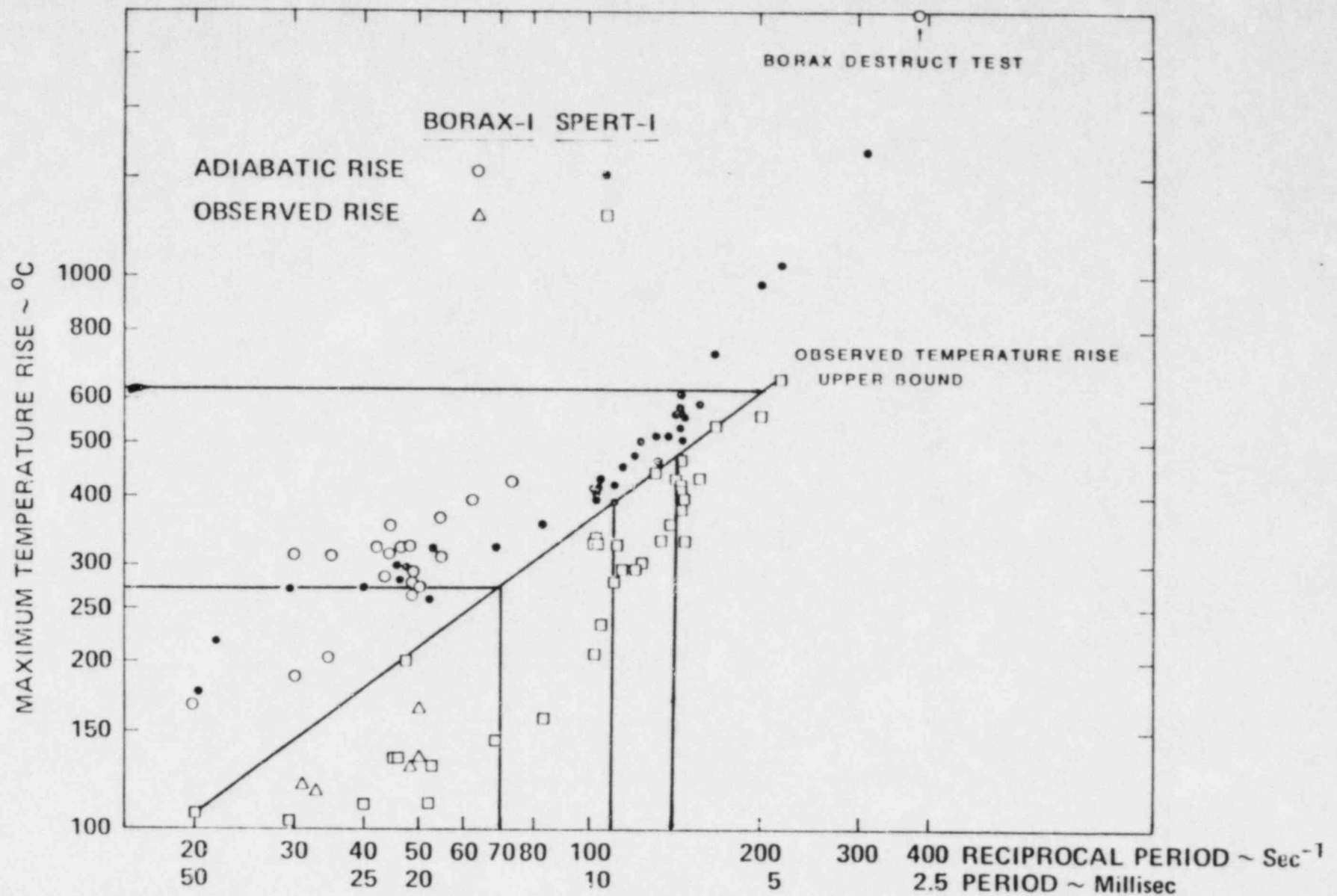


REBUTTAL CONCERNING THE SHUTDOWN MECHANISM IN THE UCLA ARGONAUT

Q.1. Please describe the shutdown mechanism in the UCLA Argonaut reactor.

A.1. The UCLA reactor shuts down in response to rapid and large reactivity insertions by the same fundamental shutdown mechanism that operates in the class of plate-type water-moderated reactors represented by SPERT and Borax: temperature rise in the fuel causing density changes in the fuel and water and followed by the voiding of water as the result of sub-cooled nucleate boiling. In the models that have been developed to describe the mechanism the temperature rise in the fuel plates is a function of the reactor period, which is jointly determined by the reduced prompt neutron lifetime and the reactivity change expressed in dollars, and the shutdown (or reactivity) coefficient. The total energy release is a function of the temperature rise or energy density of the fuel plates and the active mass of the core. In the region of a 14 msec period, which in the UCLA reactor would result from the instantaneous insertion of the proposed licensed limit of \$3.00 excess reactivity, SPERT I-D and Borax-I data indicate that the peak temperature calculated adiabatically would be about 400⁰ C, which would be considerably above the peak temperatures that would be expected on the basis of the temperature rises actually observed during SPERT and Borax tests (see "Figure 3" reproduced here from my earlier testimony). It should be noted that the Battelle generic study analyzed the case of an instantaneous insertion of \$4.00 excess reactivity which put the reactor on a 7.2 msec period. This represents considerable conservatism with respect to the maximum credible reactivity accident at the UCLA reactor.



**ADIABATIC AND OBSERVED TEMPERATURE RISE
VERSUS REACTOR INVERSE PERIOD (seconds⁻¹)**

Q.2. What about the fact that SPERT and Borax were "swimming-pool" type reactors and the UCLA reactor is not.

A.2. The fact that the UCLA Argonaut reactor is not a swimming-pool type reactor does not change the basic conclusion, although it is necessary to examine the shutdown process in more detail to explain how much voiding is required and where it is accommodated. The SPERT-I-A-17/28 swimming-pool core was a closed system in which recriticality was restored after the first power burst for transients of initial periods down to 7 milliseconds. The UCLA Argonaut reactor will behave similarly for an initial period of 14 milliseconds. The system pressure following the first burst will rise to about 35 psig and expel sufficient water in about 100 milliseconds to terminate the event. That expulsion time is short compared to observed oscillatory and chugging periods and none are to be expected for the UCLA Argonaut reactor.

Q.3. How does the analysis of this event proceed?

A.3. There are four steps. The first step is to find the common denominator for a spectrum of reactors characterized by various values of the "shutdown parameter" which is the ratio of the void coefficient to the reduced prompt neutron life time. It is found that the peak power density is inversely proportional to the square root of the shut down parameter. Based on empirical data the constant of proportionality is $73 \pm 16\%$ for reactor periods of 14 milliseconds in the A, B, and D cores of the SPERT-I series. The numerical value yields peak power density in units of kw per cm³.

The second step is to insert the value of the shutdown parameter in the generalized relation to calculate the expected peak power in the UCLA reactor for a transient of the same period. The total energy density generated in the first burst is estimated as if the peak power persisted for two periods, a rectangular power pulse of 28 milliseconds duration. The temperature rise is then calculated.

The third step is to estimate the voiding rate and the disposition of the displaced water. It is found that the air space above the normal core water level is sufficient to accommodate a volume equivalent to about -6.40 dollars of void. The reactor is well on the way to shutdown at this moment.

In the fourth step, the subsequent expulsion of water is treated by an energy imperative, the system pressure will rise to whatever pressure is necessary to expel the water at the same rate that steam is being generated.

Q.4. Please describe the shutdown coefficient discussed by Forbes et al, (IDO-16528, 1959).

Q.4. That shutdown coefficient is a "constant" which relates the instantaneous reactivity, measured in inverse seconds, to some function of the cumulative energy generated. The mathematical form chosen by Forbes et. al is:

$$\frac{1}{\phi} \frac{d\phi}{dt} = \alpha_0 - b[E(t - \tau)]^{1/2}$$

The initial reactivity is α_0 inverse seconds, τ represents a delay time, b is the shut down coefficient, and $E(t - \tau)$ is the cumulative energy generated τ seconds prior to time t . The time t is an independent variable which has no characteristic value. ϕ = power.

Q.5. What do you mean by the phrase reactivity measured in inverse seconds?

A.5. In my previous testimony of June 1983, p. 22, I described a simplified version of the in hour equation as

$$\$ = w \left(\frac{\lambda}{\beta} \right) + 1 .$$

The symbol w represents the inverse period which by algebraic rearrangement is

$$w = \frac{\$ - 1}{\lambda / \beta} .$$

During the time interval between an abrupt positive reactivity insertion and the onset of shutdown, $w = \alpha_0$, the initial inverse period.

Q.6. What factors influence the numerical value of the shutdown coefficient b ?

A.6. The shutdown coefficient is not dimensionless, and certainly the numerical value will depend upon the units that are chosen. In particular, if power density is used instead of total power, and if the void coefficient C_v is expressed in dollars per percent void then for

a 14 millisecond period the four aluminum plate reactors of Forbes and the SPERT-I-D reactor described by Miller, Sola, and McCardell (IDO-16883, 1962), can be represented by

$$\text{Power density (kw/cm}^3\text{)} = k \left(\frac{C_v \beta}{\ell} \right)^{-1/2}$$

with $k = (73 \pm 16\%)$

In other words, for this class of reactor with the proportionality constant $k = 73$, one can predict the peak power density from the known values of the shutdown parameter, $C_v \cdot \beta / \ell$.

Q.7. Please explain why you use power density instead of total power.

A.7. The power density represented by that equation is the maximum power density of the excursion, maximum in time, but average in space. If Forbes had provided total energy, I would have reduced that to energy density. They did not do so, and it is necessary to estimate the maximum energy density.

Q.8. Why do you want to calculate energy density?

A.8. The need for power and energy densities was remarked by Dietrich in discussing the Borax I and Borax II tests. For a fixed energy density, a large reactor will generate more total energy than a small reactor, but the temperatures will be similar. The temperature is important in two ways. First, it is the driving potential for heat transport, steam generation,

and shutdown. This is implicit in the use of temperature coefficients. Second, there is the practical matter of the maximum temperature that a fuel plate reaches in an excursion. Energy density is another name for temperature and it is the temperature that is important, not the total energy.

Q.9. What examples can you cite to illustrate this point?

A.9. Figure 11, p. 21 of Forbes shows the maximum temperature versus reciprocal period for four aluminum plate type reactors. At a reciprocal period of 70 per second the sequence of temperature rises versus core type is the same as that for power density in my Table I which follows.

Q.10. What does the uncertainty of k represent?

A.10. Values of power density for a reactor period of 14 milliseconds were calculated for the five reactors from the graphical total power data of Forbes, et. al, and from the data of Miller, Sola and McCardell for the SPERT-I-D core. The total power was divided by the active fuel plate volume. These power densities were then multiplied by the square root of $C_v \cdot B/\ell$. The value 73 is the arithmetic mean of the extreme values, and the 16% uncertainty encompasses all of the k values.

Table I. 14 Millisecond Transients in Various Reactors

CORE	B-12/64	B-16/40	A-17/28	B-24/32	D-12/25	Argonaut
Number of plates	768	640	476	768	270	264
Number of channels	704	600	448	736	245	240
Water channel cross section, cm ²	2071	1185	812	741		
Active height, cm	60	60	60	60		
1% of water volume	1243	711	487	445		
C_v cents/ml	-0.0093	-0.029	-0.046	-0.073		
C_v %/void	-0.116	-0.206	-0.224	-0.325	-0.35	-0.277
ℓ/R , millisec	11	10	7	7	8.16	29.2
$C_v \cdot R/\ell$, %/sec	10.55	20.6	32	46.4	44.1	9.5
Max. Power, Mw	950	550	400	550	194	} for $\frac{1}{\tau} 70 \text{ sec}^{-1}$
Active volume, cm ³	43500	36240	26960	43500	15300	
Max. Power Density (P), kw/cm ³	21.8	15.2	10.8	12.6	12.7	
$k = P \cdot (C_v \frac{R}{\ell})^{1/2}$	70.8	69.0	61.1	85.8	84.3	

Q.11. What is the source of the uncertainty?

A.11. The reduced prompt neutron life is not recorded to more than about one part in 10 and could introduce an error of approximately 5%. The graphical data for the SPERT A and B cores is difficult to read to within $\pm 5\%$. There appears to be a residual dependence upon $C_v \cdot \beta/\lambda$ with the smaller values of k associated with the smaller values of $C_v \cdot \beta/\lambda$. The various values are shown in Table I.

Q.12. How would you use this data to predict the temperature of a fuel plate in an Argonaut reactor under a 14 millisecond excursion.

A.12 I would take the mean k value, $k = 73$, $C_v = -0.277$ dollars/% void and $\lambda/\beta = 0.0292$ sec. This yields a power density of 23.7 kw/cm^3 . Forbes, et. al, do not provide total energy data, but Dietrich (Borax-I) and Miller, Sola, and McCardell (SPERT-I-D) both indicate that the relation $E(\text{total}) = 2\tau \cdot \phi(\text{max})$ is applicable in the region of $\tau = 0.014$ seconds. With this I calculate 664 joules per cm^3 . For a specific heat of $2.83 \text{ joules/cm}^3 - ^\circ\text{C}$, the average temperature rise would be 235°C . For a peak-to-average power ratio of 1.63, the maximum temperature rise would be 382°C to a final temperature of 402°C .

Q.13. Why did you use $k = 73$?

A.13. It is the mean value for the data that I reviewed. It is conservative. In terms of $C_v \cdot B/\ell$, the Argonaut reactor resembles the B-12/64 core with $C_v \cdot B/\ell = 71$. The calculated adiabatic temperature rise will always exceed the true temperature rise. Forbes in Figure 11 (which follows) indicates a total temperature of about 300°C for the B-12/64 core at a reciprocal period of 70 per second.

Q.14. You take $E(\text{tot}) = 2\tau \cdot \phi(\text{max})$ as some kind of fundamental relation. Please explain that.

A.14. It is really an experimental observation derived from the Borax-I and SPERT-I-D reports. Those two reactors differed markedly in size and in other respects. The rule is independent of whether the Borax-I reactor starts from a subcooled state or near saturation temperature.

It means that the total energy, $E(\text{tot})$ can be represented by the maximum power, $\phi(\text{max})$, acting over a time interval 2τ .

This indicates to me that there is an energy density imperative, the reactor will shut itself down even if it must generate large maximum power and total energy. The energy, power, temperature, and pressure histories may, and did differ appreciably between Borax-I and SPERT-I-D but the 2τ rule was valid for both in the region of $\tau = 14$ milliseconds.

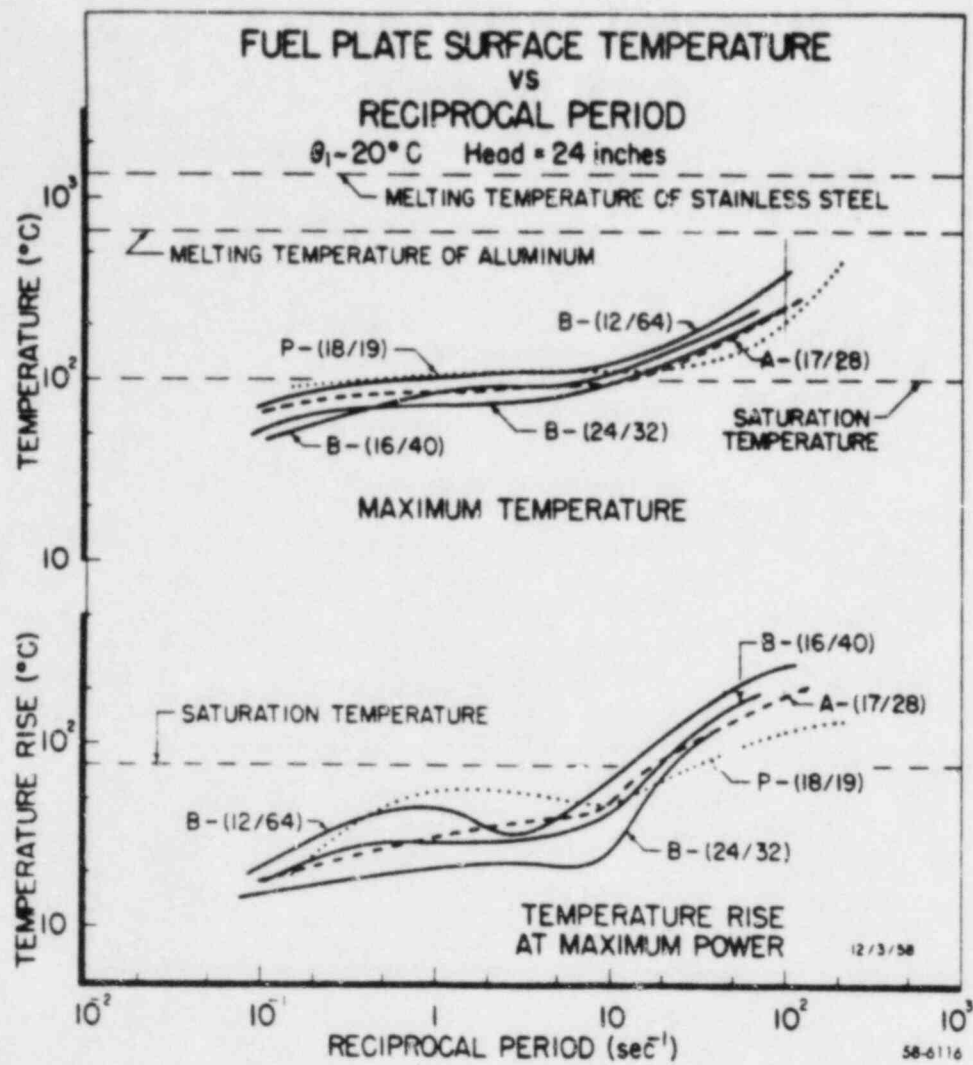


Fig. 11

Reproduced from Forbes et al., 1959 [2]. p.21

Q.15. How did you obtain the void coefficients in units of dollars per percent void?

A.15. The values used are for the uniform void coefficient. A value of \$0.36/% void is given by Miller, Sola, and McCardell for the "D" core. The values for the A and B cores were taken from Forbes in units of dollars per cm^3 , multiplied by the estimated water volume for the core in question and divided by 100 to obtain dollars per percent.

Q.16. What uncertainties are there in choosing void coefficients?

A.16. The principal uncertainty is in knowing what an investigator means when reporting a void coefficient. There are central void coefficients, peripheral void coefficients, and uniform void coefficients. Although these regions are easily identified qualitatively, the precise domain is seldom identified in terms of a description of the volume over which that coefficient is applicable.

Q.17. How was the void coefficient determined for the UCLA reactor?

A.17. The value is derived from measurements described and documented in the startup report for the UCLA reactor. It is the only documented value for the UCLA reactor. The startup was supervised and reported by General Nuclear Engineering. The reactivity effect of local simulant

voids of 110 ml ($1 \text{ ml} = 1 \text{ cm}^3$) was sampled in a number of locations within the core. An average or uniform coefficient for the core was reported to be 23 inhours per void (110 ml), $5.3 \times 10^{-4} \text{ k/ml}$, and 0.2 k/\% void .

Q.18. How do you convert those numbers to dollars per percent void?

A.18. One inhour is approximately 0.00360 dollars, a conversion that is independent of the delayed neutron fraction. I define 100 percent void as all of the water between the fuel plates, $2.845'' \times 24'' \times 0.137'' \times 240$ spaces. For the UCLA reactor, this is approximately 36800 ml and 1% of that volume is 368 ml per % void. The result is

$$C_v = -(23/110) \times 0.00360 \times 368$$

$$C_v = -0.277 \text{ dollars/\% void}$$

Q.19. You have cited other numerical values for the void coefficient in previous testimony. Please explain the apparent discrepancy.

A.19. A lower value was predicted prior to the startup measurement. A still smaller value was reportedly measured by students around 1963. However, there is no existing documentation of such a measurement; nor is it known what units were used to report the coefficient. A member of UCLA's nuclear engineering faculty who participated as a student in the measurement was unable to confirm the measurement. Not much can be done with that kind of information.

I went back to the documented measurements and made a conversion to dollars which does not require speculation concerning the delayed neutron fraction. I related it to a well defined volume of water. I don't know how to find a better value than the value $C_v = -0.277$ dollars/% void. For comparison, if the smallest reported (undocumented) value is used, the predicted temperature rise is increased about 20° C, which is a relatively small effect indicating that the calculation is not particularly sensitive to any uncertainty in the void coefficient measurement.

Q.20. Why do you choose to use a void coefficient in units of dollars per % void rather than in dollars per milliliter?

A.20. If one is analyzing a single reactor, it makes no difference which units are chosen. However, if one is studying a spectrum of cases which range from small, undermoderated reactors to large overmoderated reactors, it is evident that a milliliter of void will have a much larger effect upon a small reactor than a larger reactor. The spectrum of void coefficients is appreciably narrower when expressed in the % unit than when expressed in the milliliter unit.

Q.21. Why did you not use the Borax-I data?

A.21. The Borax-I reactor was superficially very similar to the SPERT-I A core in number of plates, plate dimensions, water channel width and

fuel plate loading. Its performance was quite different. The fuel plates were curved, their configuration in the fuel channels is not clear in the single drawing I have seen (Dietrich, Figure 7) and the static head above the core was 3 to 4.5 feet versus 2 feet above the fuel plates in the SPERT A and B cores. I do not know whether there are other differences which might explain the energy density pulses and the pressure pulses which were significantly higher in Borax-I than in the apparently similar SPERT-I A core.

Q.22. Why did you not consider the Borax-II reactor?

A.22. I did consider that reactor. It was a unique reactor in that it contained perimeter fuel loadings that contained plates of much higher uranium -235 content than the central plates and the plates of Borax-I. The effect was to markedly flatten the flux profile relative to Borax-I.

Borax-II was a remarkably responsive reactor. With an absolutely flat peak-to-average power or flux ratio, all parts of the reactor reach the point of incipient boiling at the same instant and the time scale for shutdown is compressed relative to that for a reactor with a high peak-to-average power. In the latter, steam generation spreads more smoothly throughout the core as successive portions of the core are driven to the point of incipient boiling. This induces a delay, but the pressure pulses will be smaller.

It was this consideration that led to my introduction of the peak-to-average power ratio in my previous testimony.

Q.23. Why did you not use the SPERT-II heavy water test data?

A.23. With the reported value of $\ell/\beta = 0.1$ seconds for the SPERT-II reactor, it would take a reactivity insertion of over 7 dollars to excite a 14 millisecond period. Further, with a void coefficient of 0.07 dollars per % void (about 1/4 the UCLA void coefficient value), $C_v \cdot \beta/\ell = 0.7$ and even with k as small as 60, the resultant energy density of 2000 joules per cm^3 would be well into the melting region.

The UCLA Argonaut core has a shutdown parameter value of above 9.5 which is similar to the SPERT B-12/64 core value of 10.6 and of the same magnitude as the other SPERT I cores. However, the UCLA Argonaut shutdown parameter value is about 14 times that of the SPERT-II reactor. Obviously, the parameters affecting shutdown in the two reactors are sufficiently dissimilar to make useful comparisons unlikely.

Q.24. Why do you think your correlation with $k=73$ should apply to the SPERT-II heavy water?

A.24. I did not mean to imply that the correlation should be applicable to an arbitrarily large class of reactors. I only indicated that the correlation was in qualitative agreement with the observations that had been made

about SPERT II and would remain so even if a k value substantially less than 6J might correlate the non-existent data.

Q.25. Please explain the significance of the Robles data regarding the graphite temperature coefficient.

A.25. The value for the graphite temperature coefficient measured by Robles and reported in his thesis (Robles, Primitivo, "A Theoretical and Experimental Dynamic Analysis of the UCLA 100 kW(t) Nuclear Reactor", UCLA Masters Degree Thesis, 1972) is in excellent agreement with the other reported measurements of the coefficient. Perhaps confusion has resulted from the different choices of temperature that may be used to define the reactivity coefficient. Robles presented a graph which plotted $\% k$ versus temperature. The graph had two essentially straight lines, one for the reactivity change versus a temperature observed near the core center, the other related the reactivity change to an average and lower graphite temperature.

Both lines are correct, but one must be consistent in using the temperature for which the coefficient was defined. In particular, it is improper to "average" coefficients which were differently defined.

Except for the Robles coefficients based upon the average graphite temperature, the other measured values for Argonaut reactors are:

	<u>% k/⁰F</u>
U. of W.	0.0014
UCLA (Robles)	0.0014
UCLA (Ostrander)	0.0013

These values consistently relate to the temperature at the center of the graphite center island. The agreement is excellent.

Q.26. What is the significance of this positive coefficient in influencing a transient?

A.26. None. Most (85%) of the fission neutrons deposit their energy in the water. The graphite is heated primarily by gamma rays. The amount of energy per fission that is promptly released and potentially available to heat the graphite is about 3% of the total event energy. If half of this energy is deposited in the graphite center island (roughly 3 cubic feet of graphite or 145 kilograms of specific heat 0.745 joules per gram-deg C at 25⁰ C) then a 30 mega-joule transient (SPERT-I-D destruct) would yield an energy deposition in the graphite of

$$30 \times 10^6 \times (0.03/2) / 145 \times 10^3 = 3.1 \text{ joules/gm}$$

The resultant adiabatic temperature rise of $3.1/0.745 = 4.2$ deg C to contribute about 1.5¢ of incremental reactivity to the event.

Q.27. Why do you use only one-half of 3%?

A.27. I assume the other half went into the outside reflector.

Q.28. In your earlier testimony you deduced a reactivity change of 1.3 cents for the same event. Why are you changing your testimony?

A.28. This is not a change. The earlier testimony on this point was based upon experimental data regarding the temperature rise in the graphite within 5 minutes of 100 kw operation from a cold start (30 megawatts). At that time I did not know that only 15% of the prompt neutron energy was deposited in the graphite. I am now showing that you can come to nearly the same answer, 1.3 versus 1.5 cents, in a different and independent way.

A.29. Why are you so sure that 85 percent of the neutrons are moderated by the water?

A.29. The question of the relative importance of the graphite as a moderator versus its reflector function has been around for a long time. An answer to that question would clarify the related questions of graphite heating and void coefficient.

The question became fundamental to the discussion of energy deposition in graphite for the Wigner stored energy calculation. It is also relevant to any discussion of graphite radiation damage effects in the

UCLA reactor. I made two calculations, one somewhat intuitive and a second of a confirmatory nature. They agreed very well that approximately 85% of the neutrons are moderated by water. As this was done in the context of the Wigner energy question, I provided my description of the methodology and results to Dr. H. Pearlman. The details are described in my attachment to the testimony on Wigner energy.

Q.30. Why do you use $\lambda/\beta = 29.2$ milliseconds to characterize the UCLA Argonaut transients?

A.30. A number of pile oscillator experiments were performed in the UCLA reactor in the 1960's to obtain measurements for the quantity β/λ . The value of β/λ chosen from measurements in the range 20 to 50, was 34.2 which is consistent with the lowest conceivable β of 0.0065 and a reported prompt neutron lifetime of 1.9×10^{-4} seconds. A recent KENO code calculation of the UCLA prompt neutron lifetime done for the NRC produced a value of 1.88×10^{-4} seconds, which is very close agreement. The reciprocal of 34.2 is about 0.0292 seconds. The basis of that number is experimental observations which were related to plausible values of λ and β .

Q.31. Is the Argonaut reactor an open or closed system?

A.31. For low flow rates, the Argonaut reactor will not sustain a pressure significantly above atmospheric pressure. Also, it can remove any amount of water if the pressure is high enough.

Q.32. Were the Borax and SPERT reactors open systems?

A.32. The Borax-I and SPERT A and B systems were closed in a certain sense. The vessel walls were sufficiently high that for 14 and 16 millisecond pulses, they could not eject enough water to prevent recriticality. After the first pulse they settled to a more or less stable boiling mode (Dietrich, Figure 11 and Schroeder et. al, Figure 8).

Q.33. How would you portray the UCLA Argonaut reactor in this regard?

A.33. In regard to inertial forces, the UCLA Argonaut reactor with a 10 inch water overburden, is less "closed" than either the SPERT-I or Borax-I reactors with overburdens of 2 to 4.5 feet. On the other hand, the larger void requirement demands a greater voiding rate if water eviction is to be achieved in a timely fashion.

Q.34. What is your estimate of the shutdown void and void rate for the UCLA Argonaut reactor?

A.34. It has been commonly recognized that to effect shutdown it is necessary to cancel or compensate only the superprompt critical reactivity. In the UCLA Argonaut reactor experiencing an instantaneous reactivity change of \$3.00 this would mean -2.00 dollars reactivity compensation would be required. However, I chose to consider the introduction of -4.00 dollars of reactivity in order not only to turn the power rise around but also to completely shut down the reactor.

EXPERIMENTS ON WATER-MODERATED REACTORS

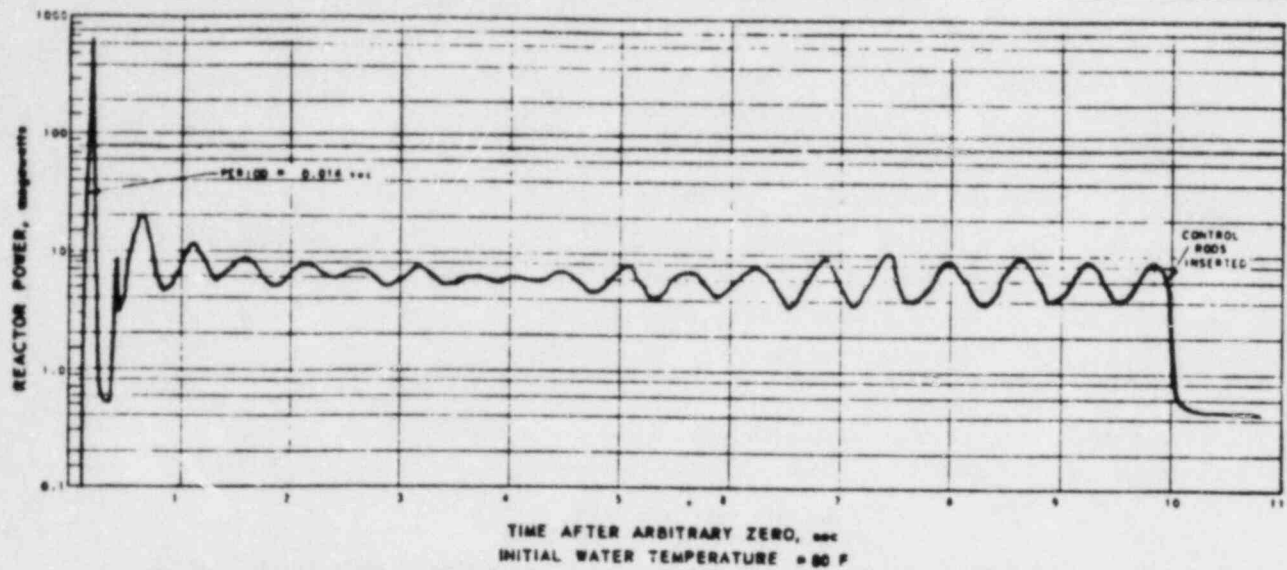


Figure 11. Reactor power variation during 10-second run following initial excursion of 14-millisecond period

BORAX - I

Reproduced from Dietrich, 1955 [3]. p.95

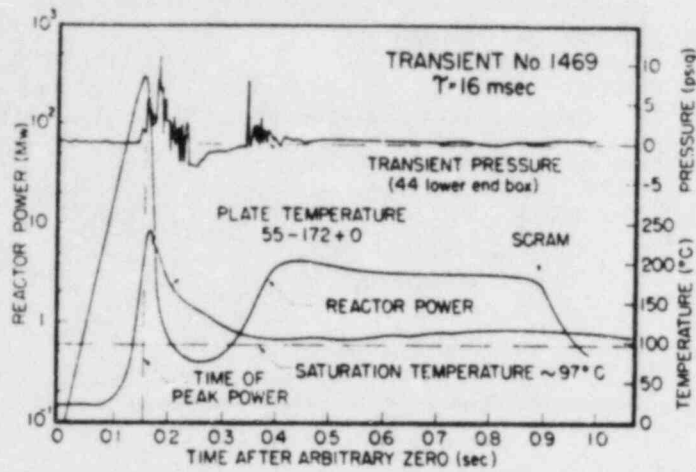


FIG. 8. Representative behavior following 1.0% reactivity addition ($\alpha = 62 \text{ sec}^{-1}$).

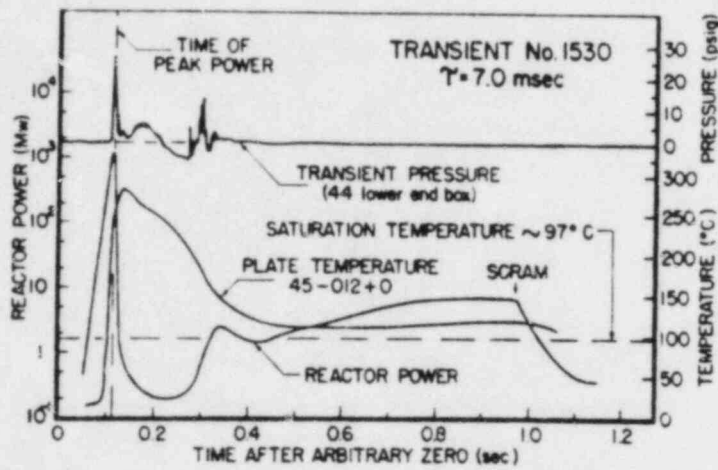


FIG. 9. Representative behavior following 1.4% reactivity addition ($\alpha = 143 \text{ sec}^{-1}$).

Reproduced from Schroeder, 1959 [3]. p.102, 103

The introduction of -4.00 dollars of reactivity with a void coefficient of -0.277 dollar per percent requires a void of 14.4%. The voidable water per fuel box is about 6140 ml of which 886 ml must be displaced by void to create 4.00 dollars of negative reactivity.

The time scale for voiding is approximately 2τ where τ is the initial reactor period. This is based upon the observation that $E(\text{tot}) = 2\tau \cdot P(\text{max})$, and is also the approximate duration of the pressure pulse in a 9 millisecond transient of SPERT-I-D, run number 24 (Miller, Sola, McCardell IDO-16883, p.92). The average flow is about $886/2 \times 0.014 = 31700 \text{ ml/sec}$. for each fuel box.

Q.35. Explain whether the rupture disk will provide a release avenue.

A.35. The rupture disk is not a reasonable avenue for a time scale of 28 milliseconds. The main impediment is the inertia of the water resident in the 30 foot length of 3 inch line that runs from the bottom of the fuel boxes to the rupture disk.

Q.36. What about the overflow lines from the fuel boxes to the dump tank?

A.36. Those lines are one inch in diameter and provide a cross section of 5.07 cm^2 . The velocity in those lines would have to be about 62 meters per second. The principal pressure drops would be entrance and exit losses which if taken as one velocity head ($1/2\rho V^2$) each, will sum to about 570 psi.

Q.37. What about the deflector plate aperture?

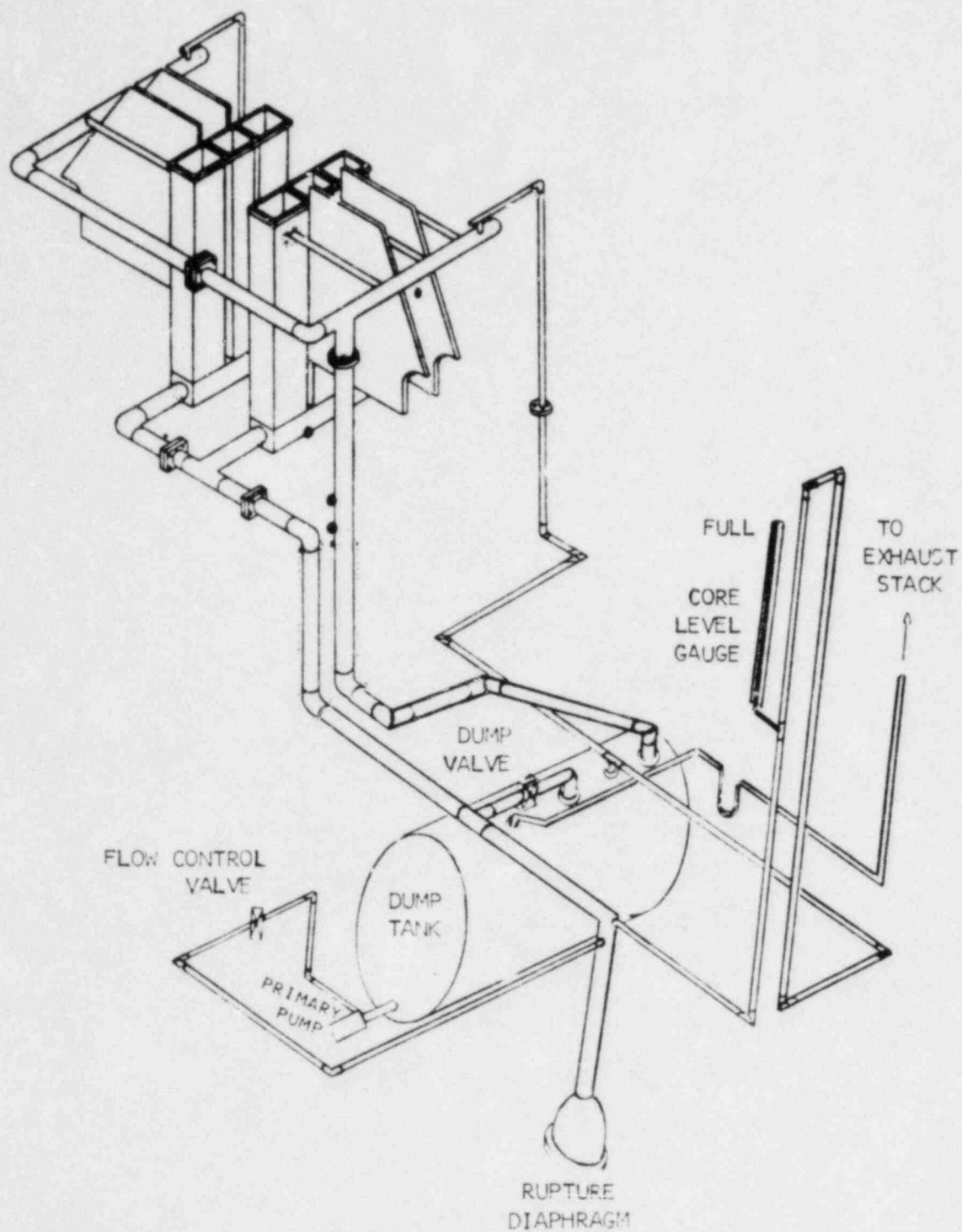
A.37. I misspoke earlier when I said that they faced a graphite wall. They actually face a wall of lead bricks, but the situation is the same. The shield plugs weigh about 100 pounds each and are manually removed and reinserted. To accomplish this, a clearance is required which I and others estimate to be about 1/8 inch. The aperture is 2 inches by 6.5 inches, and the 17 inch perimeter by 1/8 inch clearance provides a flow area of about 13.7 cm^2 . If the water had to escape by that avenue, the velocity would be about 23 meters per second. (Diagrams of the cooling water system and the fuel box and plug assembly follow.)

Q.38. What pressure do you associate with that velocity?

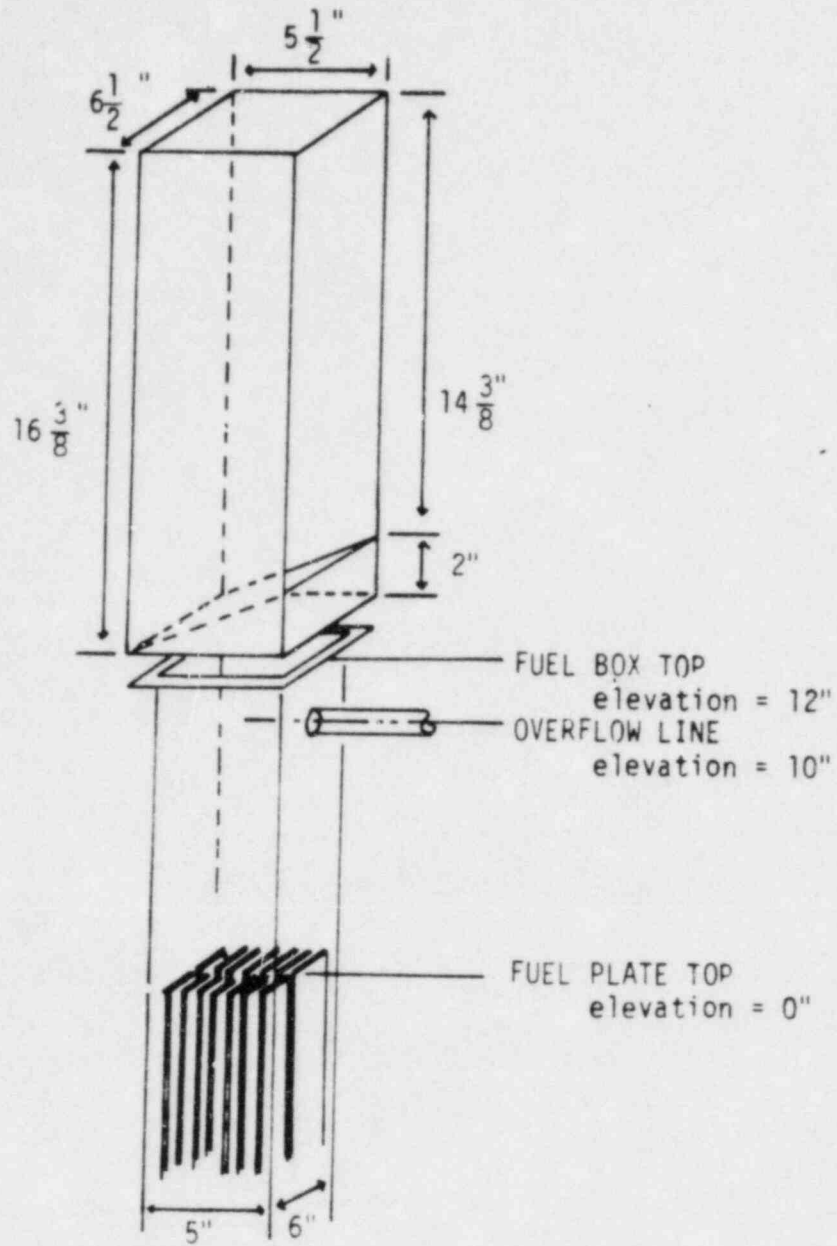
A.38. There are several pressure drops associated with that avenue, but the entrance and exit losses at one velocity head each will sum to about 80 psi.

Q.39. What if you consider these avenues jointly?

A.39. The cross sectional flow area becomes 18.8 cm^2 . Both exits will have the same pressure and hence the same velocity of about 17 meters per second. The required pressure is about 42 psi.



Cooling Water System



Fuel Box and Shield Plug Geometry

Q.40. What other avenues are there for expulsion?

A.40. The shield plugs weigh about 100 pounds each and have a cross sectional area of about 29 square inches. The shield plugs rest on top of the fuel boxes and are not secured in any way. A gap exists between the top of the plugs and the shield blocks on top. The plugs will lift at a pressure of 3.45 pounds per square inch (3.45 psi).

Q.41. Will the air above the normal water level be compressed?

A.41. The peak air displacement rate of 31700 ml/sec could exhaust through the deflector exit aperture gap of 13.7 cm^2 at a speed of 23 meters per second. For air of density 0.0012 grams per ml, the adiabatic expansion requires a pressure of about 0.05 psig to achieve that velocity. The pressure requirement, if doubled is approximately two velocity heads (0.09 psi). The air flow is essentially unrestricted.

Q.42. You are assuming that the air pressure will break the membrane at the bottom of the shield plug. Why do you assume that?

A.42. The membrane is an aluminum rectangle 5 inches by 6 inches and a thickness of 0.020 inches.

Using "Marks" Standard Handbook for Mechanical Engineers, seventh edition (Baumuster, ed, McGraw-Hill), section 5, pages 68, 69, and 70, case 16 leads to a uniform loading of about 1.5 psi to rupture aluminum of 24000 psi ultimate tensile strength. That tensile strength is the upper limit cited in the same reference, same section, page 5.

Q.43. How does this back pressure influence the excursion?

A.43. The effect is negligible. The air pressure will simply rise to about 1.5 psi and rupture the membrane. The water will continue upward to fill the deflector region of approximately 5 inches by 6 inches in horizontal cross section with an average height of one inch. The available air volume above the original water level is about 1430 ml per fuel box.

This volume will be occupied at about 45 milliseconds from the time of peak power.

The steam void that has displaced the water is about 23% of the water volume and has a worth of about -6.40 dollars.

Q.44. What happens to the water.

A.44. It is helpful to look at Figures 8 and 9 Schroeder et. al. At approximately 50 ms after peak power the reactor is approaching a minimum in power after which criticality is restored and the power again rises. This is true for both the 16 ms and 7 ms transients. They did not expel enough water to prevent recriticality, and the same can be expected of the UCLA Argonaut.

To answer the question more directly, the power will rise and generate steam at a pressure that will balance the steam generation rate with the water expulsion rate. That pressure will be about 35 psig and the event will be over in 0.1 to 0.2 seconds after the first minimum.

Q.45. How do you define the event termination?

A.45. The event will be over when enough water is expelled to prevent recriticality. I define that quantity of water as all of the water overburden, 4.8 liters, and 15 percent of the core water, an additional liter. The total quantity to be expelled for termination is 5.8 liters.

Q.46. How do you know the event will be over in 0.1 to 0.2 seconds after the first minimum?

A.46. The prolonged first minimum is because the water cannot get back into the core, there is too much steam from the hot fuel plates. When they cool, water will reenter and restore criticality. The power will rise and generate more steam. Assuming that the Argonaut will rise to an average surface heat flux of 12 watts per cm^2 , the steam generation rate will be about 100 grams/sec - cm^2 . At 35 psig the steam volume rate will be about 54 liters per second per fuel box. Also, the expulsion rate of 54 liters per second can be satisfied at a pressure of 35 psig. The cross section area for expulsion consists of the overflow line (5.1 cm^2), the deflector gaps (13.7 cm^2) and the shield plug gap (16.5 cm^2). The water velocity through those areas will be about 15 meters per second, and the loss of two velocity heads is about 35 psig.

The calculated expulsion time is 5.8 liters divided by 54 liters per second or 0.11 seconds.

Q.47. What will the fuel plate temperatures be during this phase?

A.47. According to Figure 8 of Schroeder et. al, the temperatures are still declining. However, a heat flux of 12 watts/ cm^2 requires a temperature excess of 10 deg C above the saturation temperature. The saturation temperature at 35 psig is about 138 deg C, and the temperature cannot fall below about 150 deg C until the event is over and the system drops to atmospheric pressure.

Q.48. Will there be oscillations or chugging?

A.48. No, the event is over too soon. A second small pulse can be expected, but it can't get very far because the system reactivity is disappearing rapidly.

Q.49. Where did you obtain the heat flux of 12 watts/cm²?

A.49. Figure 8 of Schroeder indicates a peak power at the second pulse of about 4 megawatts. The heat transfer area of that reactor was about $4 \times 10^5 \text{ cm}^2$. The fuel plate temperatures were not far above the saturation temperature, a condition indicative of normal boiling with a heat flux of about 10 watts/cm². The choice of 12 watts/cm² for the Argonaut reactor is in recognition of the smaller surface to volume ratio of the Argonaut reactor relative to the SPERT I A reactor.

Q.50. How long does it take to raise the shield block plug and open that 0.3 inch gap?

A.50. The momentum of the moving water can open the gap. Whether it stays open depends upon the subsequent pressure. With a pressure of 35 psi acting on the 30 square inch projected area of the 100 pound plug will accelerate it at 10.5 g's. Deducting the gravitational acceleration the net upward acceleration will be about 9300 cm/sec². The gap will then open in about 13 milliseconds. The rise time is small compared to the water expulsion time.

Q.51. Please summarize your conclusions regarding the self-limiting shutdown of the UCLA Argonaut Reactor?

A.51. There is more than an adequate margin of safety to preclude fuel melting in the first burst initiated by a 14 millisecond transient. Following the first burst, the rate of water return is limited by evolving steam, and can represent only a ramp insertion of reactivity. The subsequent rise of power will be similar to that of a boiling water reactor with water leaks which remove moderator and in which the energy generation is dissipated by producing steam. Although I have ignored the rupture disk line and the analysis, it could become a useful release route if the boiling stage is at lower pressure and hence more prolonged than I have estimated. I find no phenomena here that can induce melting and fission product release, and hence there is no potential for endangering the public health and safety in such an event.

REFERENCES

1. Dietrich, J. R., "Experimental Determinations of the Self-Regulation and Safety of Operating Water-Moderated Reactors," Peaceful Uses of Atomic Energy, Geneva Convention, V.13, p.88-101, 1955.
2. Forbes et al, "Analysis of Self-Shutdown Behavior in the SPERT-I Reactor," IDO-16528, July 1959.
3. Miller, R. W., Alain Sola, and R. K. McCardell, "Report of the Spert I Destructive Test Program on an Aluminum, Plate-Type, Water-Moderated Reactor," AEC Research and Development Report, IDO-16883, 1964.
4. Schroeder et al, "Experimental Study of Transient Behavior in a Sub cooled, Water Moderated Reactor," Nuclear Science and Engineering, V.2, p.96-115, 1957.

REBUTTAL TO CBG'S PANEL I REBUTTAL

Q.1. Please respond to the claims made in CBG's Table I" concerning the "maximum reactivity potentially available" at the UCLA Argonaut.

A.1. The proposed Technical Specification limit for the fully-loaded UCLA core is \$3.00 excess reactivity. Currently (November 1983), less than \$2.75 is actually available. As the ambient coolant water temperature declines to its mid-winter 1984 seasonal low reactivity will increase. Based on seasonal water temperature data it is projected that the maximum available excess reactivity during mid-winter 1984 will be less than \$2.80. Due to burnup and samarium poisoning, which are related to intensity of operations, the maximum available excess reactivity will decline each year by about \$0.04 until the reactor is refueled, if that becomes necessary.

Loading fresh fuel into the reactor core is a meticulous and time-consuming operation, involving successive additions of fresh fuel plates in a specific pattern to replace spent fuel. At each step reactivity measurements are made as the planned level of the fuel loading is approached. Fuel is loaded to a level of excess reactivity less than the Tech Spec limit to provide for any seasonal variations in reactivity (if, for example, the re-fueling is done during the summer months) and an additional margin to insure that the core does not have to be re-entered to make loading adjustments. After the fuel loading operation is completed, reactivity measurements are made prior to going critical. Reactivity measurements are also

made prior to every reactor run. The measurements are very reliable and there is no possibility that a core loading above the Tech Spec limit would go unobserved. The combined effects of samarium poisoning and burnup will insure that available excess reactivity continues to decline relative to the Tech Spec limit. CBG's claims that greater than \$3.00 (as much as \$10.60 according to Table I) could be available to initiate a fast transient due to several undesirable reactivity effects. However, such claims are based on a misunderstanding of the effects in question.

CBG claims that variations in fuel-bundle spacing within the fuel bundles could result in an \$0.80 reactivity gain. CBG cites a letter report made to the NRC by the University of Washington which identified an \$0.18 drop in reactivity after an unloading and reloading operation. The report by the University of Washington attributes the reactivity drop to the use of a spacer at the top of the bundles that apparently was not effective in repositioning the bundles in the same spot at the bottom of the fuel box. At UCLA, fuel bundles are secured four to a box by an aluminum pins 1 and 2 feet long that are inserted at the junction of the four bundles wedging them tightly in place in all directions top to bottom. The occurrence noted at the University of Washington could not happen with the spacers used at UCLA. More to the point, with either Argonaut reactor once core loading is completed fuel bundle positions are set and the bundles do not shift. Any reactivity changes that result from refueling or other unloading/reloading operations are

always observed in the post-loading reactivity measurements, as was the case in the occurrence reported by the University of Washington. A positive reactivity change from this effect could not appear suddenly to affect the course of a fast transient.

CBG also claims that a reactivity gain of \$2.00 could occur as the result of bowing effects citing "observations of SPERT on the Savannah core" and the "Vitti data." The \$2.00 value is unexplained. The operating experience of the Savannah core has little relevance to the operating experience of the UCLA reactor. The UCLA thesis by Joseph A. Vitti establishes only that if the UCLA fuel elements were redesigned to increase the spacing between plates reactivity increases could be realized. Vitti points out that if fuel plate spacing were increased from the present spacing of 0.137 inches to an "optimum" plate spacing of 0.290 inches the fuel would be maximally moderated. However, CBG overlooks the fact that increasing plate spacing as examined by Vitti would involve redesigning the fuel elements. Moreover, any expansion of the fuel elements would necessitate larger fuel boxes, larger plugs, and redesign of the layout of the graphite reflector and lead shielding. The extreme undermoderation quantified by Vitti is, of course, a designed safety feature of the Argonaut reactor.

Relying on a statement by Hawley, CBG asserts that "cold water" could result in a reactivity increase of \$1.00. CBG uses UCLA's

measured value for the water temperature coefficient of reactivity (-1.8 cents per degree C) and the difference between Hawley's "normal" operating water temperature of approximately 60 degrees C and the temperature of maximum water density 4 degrees C. However, the UCLA reactor could not experience circulating water at 4 degrees C. More to point, UCLA measures its reactivity "cold." That is, except for seasonal changes, the measured reactivity results from water temperatures as cold as they actually get from year to year and season to season. There is no mechanism at UCLA available for cooling the primary coolant water below ambient temperature conditions. Hawley was attempting to make an extremely conservative adjustment to excess reactivity measurements made at the various Argonaut facilities on the assumption that these facilities measured reactivity "at normal operating temperatures." Such a "correction" is not needed for the UCLA facility since reactivity is not measured at normal operating temperatures but ambient temperature conditions.

CBG claims that a "warm graphite" effect could result in a reactivity increase of 0.80 cents but does not explain its value except to state that it is derived from "Robles measurements" of the positive graphite coefficient. CBG claims that the value cited in Robles thesis for the positive graphite coefficient is "slightly lower" than the coefficient reported in the AEC inspection report in June, 1968 (the "0.006%Δk" per degree F). As has been pointed out, the value in the AEC inspection report is clearly a typographical error. The error becomes obvious when the correspondence preceding that

June, 1968 report is examined. In a letter dated January 4, 1968 the University of Washington reported that they had measured a graphite temperature coefficient of reactivity of "+0.0014%Δk/°F." An NRC inspector reviewed the University of Washington measurement and in an inspection report dated April 5, 1968 confirmed the reported value of "+0.0014%Δk/°F -- net effect at power, approximately 0.04%Δk." During an inspection at UCLA the inspector does a rough on-the-spot calculation of the graphite effect based on temperature data reported in the operating log for a long run at full power. In the subsequent inspection report of June 7, 1968 he observes that his measurement was "about one-half of the coefficient measured during the University of Washington experiment" (emphasis added). However, instead of reporting the measurement as +0.0006%Δk/°F, which is about one-half of the University of Washington value, the inspection report reads +0.006%Δk/°F.

CBG believes it has found support for the value erroneously reported in the Robles thesis. However, CBG has misinterpreted the measurements reported in the Robles thesis. Robles actually reports a measured value of +0.0014%Δk/°F which is the same as the University of Washington value and nearly identical to the value measured by Ostrander of +0.0013%Δk/°F. Several recent measurements of the graphite component of the overall temperature coefficient of reactivity have been made at UCLA and invariably they demonstrate that the graphite component is worth 1/6 to 1/5 of a cent/°F (+0.0011 to +0.0013%Δk/°F). These measured values are very reliable and are an order of magnitude lower than the value assumed by CBG.

Furthermore, the specific situation that CBG assumes will result in a pronounced positive reactivity effect (due to its "warm graphite" effect) has been examined experimentally by UCLA. After a lengthy run heating the graphite the reactor is shut down, the heat is removed from the coolant and fuel by circulation. Then the reactor is immediately brought back up to power. The largest positive reactivity effect observed under these unusual conditions was 10 cents, which occurred about 45 minutes after shutdown. This result is consistent with the values reported by UCLA and University of Washington for the graphite coefficient. Thermal conductivity of the graphite and fuel temperature effects preclude any pronounced reactivity effects even under the extremely unusual experimental conditions proposed by CBG. CBG overlooks the fact that the primary coolant water circulates in a loop and it takes time for the water to cool down. During this time the graphite also cools due to its high thermal conductivity. The graphite temperature coefficient is approximately 1/5 that of the water temperature coefficient and is very slow in its effect. The positive graphite component of reactivity is of no importance in the analysis of fast transient accidents.

CBG claims that replacement of the Ra-Be neutron start-up source with the Pu-Be neutron source will result in a \$0.50 reactivity gain. The suggested replacement is nonsense; and, the calculated reactivity gain is incorrect. The reactor graphite must be completely unstacked to replace the start-up source. There is no reason to substitute the Pu-Be source for the Ra-Be source and there are several good reasons not to. Such a replacement could not occur accidentally. But even

assuming the replacement is made CBG has miscalculated the reactivity worth of the change by using a mass coefficient that applies only to actual fuel in the core and not to a Pu-Be neutron source that exhibits absorption as well as fission effects. Reactivity measurements were made of both sources during reactor start-up. As installed both the Ra-Be and the Pu-Be represent negative reactivity. Replacement of the Ra-Be source with the Pu-Be will result in a reactivity gain of less than 1 cent, based on reactivity measurement during start-up which show that the Pu-Be source is a little less negative than the Ra-Be source. The mistake in CBG's calculation was to treat the plutonium in the Pu-Be source as pure fissionable material ignoring the actual neutron interactions and the absorption qualities of the container.

Besides the reactivity effects CBG purported to quantify, CBG speculates about the existence of other effects which "were not readily quantifiable." The only one of the effects that could conceivably have any relation to a fast transient accident is the "positive void effect." Positive voids do not exist in the UCLA reactor. The design of the fuel plate spacing results in a significantly undermoderated core which insures that negative temperature and void coefficients are maintained at all places in the fuel box under all credible circumstances.

Q.2. Explain why UCLA needs \$3.00 excess reactivity.

A.2. UCLA is seeking a license limit of \$3.00 on the level of excess reactivity that can be loaded in the reactor. The excess reactivity currently available in the UCLA reactor is about \$2.75. Available excess reactivity will continue to decline at the rate of about \$0.04 per year. At some future time available excess reactivity will have declined so that reactor operations are adversely affected. At that time the reactor will be refueled. By permitting the reactor to be refueled to a level of excess reactivity approaching \$3.00 means that the reactor will have to be refueled less often. In fact, if the current operating intensity continues it will be well into the 1990's before any refueling would be required and certainly no further refueling would be needed during the proposed license renewal period. Since refueling operations are the most hazardous and disruptive of reactor operations it is the objective of the UCLA Staff to minimize the number of such refuelings. Clearly, something less than \$3.00 excess reactivity is satisfactory for day-to-day reactor operations. But \$3.00 is a safe excess reactivity level and a level that will insure that the UCLA reactor will not have to be refueled more than once during the license renewal period.

Q.3. What "use" is made of available excess reactivity.

A.3. The available excess reactivity of the UCLA reactor will be about \$2.80 in mid-winter 1984. During the license renewal period samarium poisoning and burnup will consume about 40 cents based on the current intensity of operations (about 50% licensed level of operations). Seasonal variations in the ambient cooling water temperature, which ranges from a mid-winter low of about 50⁰ F and a summer high of about 75⁰ F, accounts for about 25 cents. The increase in water temperature as the reactor goes from zero to full power (100 kW), which is about 40⁰ F, requires 40 cents. The regulating blade is designed to operate best at between 20-40% withdrawn. Assuming about 30% withdrawn the rod worth curves indicate that the reg-rod is worth 90 cents in this position. When these negative reactivity effects are subtracted from the available excess, 85 cents remains. This 85 cents is left to be allocated between the remaining three safety rods and all samples. For example, if the total worth of samples in the core was about 60 cents the remaining safety rods would have to be nearly 100% withdrawn for the reactor to go critical. The preferred position for the safety rods is about 50% withdrawn. In order for the safety rods to be in their preferred position much less sample worth can be accepted by the reactor. However, to conserve operating time and thereby reduce Argon emissions it is desirable to run several sample irradiations at the same time. Therefore, even though the worth of individual

samples irradiated in the reactor is generally low (5-35 cents), the actual available excess reactivity requirements are consistent with the requested Tech Spec limit.

Q.4. Respond to CBG's claim that a SPERT/SL-1 type excursion could occur at UCLA because of similar "reactivity insertion rate possibilities"

A.4. The SPERT 1-D (and Borax) destruct tests and the SL-1 accident resulted from reactivity changes that occurred rapidly enough to induce particularly short reactor periods. Within this plate-type, water-moderated class of reactors the reactor period is the controlling parameter for examining the consequences of the excursion. It is, of course, the uncontrolled or uncompensated rate of power growth, represented by the reactor period, that threatens a destructive excursion. Reactivity insertion rates in different reactors must be related to the reactor period each excites in the particular reactor.

The Borax, SPERT 1-D and SL-1 reactors were all destroyed when the available excess reactivity of each of the reactors was inserted in an exceedingly short period of time. For Borax I, insertion of all the available excess reactivity put the reactor on a destructive reactor period of 2.6 msec; in SPERT 1-D the destructive period was 3.2 msec; in SL-1 the destructive period was estimated at approximately 4 msec. Even if the UCLA reactor maximum limit of excess reactivity

(\$3.00) is inserted instantaneously (and there is no credible scenario in which this could occur accidentally) the resulting reactor period is approximately 14 msec, or about 4 times longer than the longest period that produced core destruction in the three other plate-type reactors. Stated another way, for the UCLA reactor to experience a 2.6 msec period, as occurred in the Borax I destruct test, would require the instantaneous insertion of over \$12.00 excess reactivity as measured in UCLA units; for the 3.2 msec period as occurred in the SPERT 1-D destruct test over \$10.00 would be required; over \$8.00 would be required for the 4 msec period estimated to have resulted in the SL-1 accident. In all the SPERT and Borax testing of various plate-type fuel, light-water-moderated reactor cores no significant core destruction nor any melting occurred in reactor periods of 14 msec or longer.

In addition to the fact that the UCLA reactor cannot achieve a reactor period in the range where core destruction occurred, there is no credible mechanism at the UCLA reactor comparable to the mechanisms at Borax, SPERT and SL-1 that produced the instantaneous reactivity change. Borax, SPERT and SL-1 each employed a transient rod that was capable of taking the reactor supercritical in an exceedingly short period of time. In Borax I the transient rod was designed to fall with gravity assisted by springs at an acceleration that would result in the rod traversing the core in 200 msec. For

the SPERT 1-D destruct test considerable time and effort was devoted to designing a pneumatically-launched transient rod that could traverse the core in 85 msec, which required an acceleration of approximately 33 g's.

The SL-1 reactor accident resulted when a single, central cruciform transient rod was withdrawn manually less than 4 inches beyond the critical position which put the reactor on a 4 msec period. The central rod was worth about \$7.00. At the time of the accident the shutdown margin for the reactor (all rods fully in) was about \$3.50 meaning that even partial withdrawal of the central rod would put the reactor on a destructive power excursion. Obviously, with a rod of such great worth compared to the shutdown margin of the reactor, manual withdrawal of the rod through a distance of a few inches could produce a reactivity change which could place the reactor on a very short period even though all the other rods remained fully inserted and the central rod was still partially in the core.

Neither the SL-1, Borax, nor SPERT reactors satisfied the "stuck rod" criterion. That criterion states that it should be impossible for a reactor to be made critical on the withdrawal of a single control rod or, conversely, it should always be possible to shut down the reactor with one rod (the rod of greatest worth) stuck in the outermost position. The UCLA reactor well satisfies that criterion. The UCLA

reactor loaded with \$3.00 excess reactivity remains subcritical even with the two of the four control blades with greatest worth in the fully withdrawn position.

Q.5. Please explain the relevance of the November 16, 1981 letter from UCLA to the NRC reporting a possible violation which is cited in paragraph 128 of Panel I as a potential precursor of a reactivity accident.

A.5. The incident reported in UCLA's letter of November 16, 1981 has little relevance to reactivity accidents. The controlled experiment was an attempt to identify a positive worth reactivity sample in response to CBG's assertion that such samples do exist. UCLA had never seen a positive sample and the reactor supervisor decided to investigate a polyethylene plug to see if it could induce a positive reactivity charge. In fact, as with all other samples investigated at UCLA, the plug turned out to be negative. The reason UCLA noticed a possible violation was because of an ambiguity in a Tech Spec limit pertaining to whether procedures applicable to a "critical" reactor must be observed during a sub-critical operation involving a sample of known reactivity. The procedure employed by the senior reactor operator involved no hazard. There was no accident of any kind. Although UCLA informed the NRC that the operation may have constituted a technical violation of a Tech Spec limit, the NRC did not find that any violation occurred.

Q.6. What is the relevance of CBG's Exhibits C-III-5, 6, 7 which relate to the time the reactor core was entered after a shutdown of operations.

A.6. None. Exhibits C-III-5, 6, 7 are UCLA reactor operating log entries from the 1963-65 period, when most core entries were made with less than a three week holding period. CBG claims on the basis of these log entries that UCLA could not be expected to observe the three-week holding period proposed as a Tech Spec limitation. CBG overlooks the fact that these early core entries were made when the fission product inventory of the fuel was relatively low. CBG also overlooks the fact that for each of the four core entries that were made since 1970, the observed shutdown time varied from three to seven weeks, despite the fact that there was no Tech Spec requirement that such a shutdown period be observed. Of course, it is in the interest of the UCLA staff to observe long shutdown periods for health physics reasons and to be consistent with the ALARA principle.

Q.7. What is the significance of core water level changes to the maximum credible reactivity accident.

A.7. None. At standard operating conditions, the flow rate through the core is 16 gallons per minute. The water rises through the fuel boxes and exists the outlet pipe which is about 10 inches above the

top of the plates. Measurements of the reactivity effect of the core water level height have shown that if the water level drops to an "optimum" level of 2.8 inches above the core, a reactivity gain of 15 cents (maximum) could result. However, during normal operations the only time the water level drops below the outlet pipe is during regular shutdown (control blades fully inserted, water drained sometime afterward) or during a full scram. In either case reactivity is effectively canceled by the action of the control blades and a positive reactivity effect is never experienced. The dump valve has leaked in the past but this problem was remedied in 1979 with the addition of a back-up air supply system which supports the system that keeps the valve closed. In any case, a leaking dump valve could not result in a reactivity change that could exacerbate any credible fast transient accident.

Q.8. Please respond to CBG's assertion that the presence of the graphite island tends to reduce the effectiveness of voiding, because obviously part of the moderator is solid and cannot be voided.

A.8. The voiding characteristics of the Argonaut reactor are fully represented by the void coefficient. No additional account need be taken of the fact that part of the moderator is the solid graphite. It is to be noted that about 85% of the energetic neutron flux is absorbed in the water moderator of the UCLA Argonaut. It is interesting to note that the value of the UCLA void coefficient is

about 75-85% of the values of the void coefficients reported for the SPERT I-D and Borax-I reactors.

Q.9. Respond to CBG claim that Mr. Ostrander's analysis is an attempt to explain all reactor behavior differences on the basis of different masses of the core.

A.9. Mr. Ostrander makes no such attempt; CBG apparently misunderstands the analysis.

REBUTTAL TO CBG'S WIGNER ENERGY TESTIMONY

Q.1. Please provide a general response to the new arguments made in the "Wigner Energy Rebuttal" of CBG.

A.1. CBG's rebuttal testimony does not materially affect the calculation of stored energy which has been done by Dr. Pearlman and which is explained in this testimony nor the general conclusion that stored energy in the graphite of the UCLA reactor can make only a negligible contribution to a postulated fast transient accident or any other kind of thermal accident such as fire.

Q.2. Please respond to the specific claims made by CBG in its "Wigner Energy Rebuttal" questions and answers.

A.2. The following comments are provided with respect to the issues raised by CBG in its answers (noted parenthetically).

Volume of graphite potentially affected (A-1)

CBG's discussion of where the fast flux peaks is irrelevant to the point being made by Pearlman about the volume of potentially-affected graphite; moreover, it is irrelevant to Pearlman's calculations. First, the potentially most heavily irradiated graphite is clearly in the center island, plus the volume immediately adjacent to the fuel boxes on the sides opposite the center island. The mass of the center island in the fueled region is about 180 kg, which is to be compared to the

total mass of the graphite in the reactor which is about 8500 kg. Making use for the moment of "Figure D-4" (which appears in CBG's rebuttal) from the UCLA 1960 Hazards Analysis Report, it is evident that the fast flux shown decreases substantially faster outside the center island than inside. Even doubling or tripling the center island graphite mass to estimate the total affected graphite, the volume of affected graphite is a very small percent of the total graphite volume. The point to be made is that the far greater amount of unaffected graphite is available to absorb any heat that could be released by the potentially affected graphite. Where the fast flux peaks is unrelated to this conclusion.

Second it is simply not correct to state as CBG does in the first answer of its rebuttal that Pearlman "errs" when he "assumes" that the maximum damage occurs in the region of maximum temperature. His calculations do not in any way depend on where the fast flux peaks. His calculations do take into account the distribution of graphite temperature, which he correctly took to be lowest near the fuel boxes. He even calculates a value for the graphite temperature in the hypothetical case where all the graphite is assumed to be damaged at 30 degrees C, and an adiabatic release occurred from that temperature base. The temperature rise at 30 degrees C is higher than the temperature rise for the case in which all the graphite is assumed to be damaged at 65 degrees C.

Incidentally, it is to be noted that the "fast flux" plotted in "Figure D-4" is not additionally characterized as to actual neutron energy spectrum. As a consequence, it is not possible to ascertain the effect of this particular flux -- and its spatial distribution -- in producing stored energy. As for the flux plots from UCLA Exhibit 2, Pearlman made it clear that his only use of the data was to obtain a value of the peak thermal flux, which was taken as 1.5×10^{12} n/cm²-sec. Although Pearlman was asked questions about other of the flux plots contained in UCLA Exhibit 2, specifically certain plots purporting to be of the fast flux, he made it clear that his only use of the document was to obtain a value for the thermal flux. It is the thermal flux and only the thermal flux that enters into the calculation of the stored energy in the method which has been used by the parties. Finally, the conceptual flux plots from Nightingale's "Figure 7.15" for the Hanford reactor, referred to in CBG's Rebuttal, have very little relevance to the UCLA core.

Graphite temperature in the high-rate volume (A-2)

CBG claims Dr. Pearlman failed to properly account for graphite temperatures in the high-rate volume. But again CBG has made the mistake of assuming that Pearlman's calculations depend on where the fast flux peaks, that is, where the high-rate volume is. In fact, the calculations do take into account the effects of temperature (a range of temperatures from 30 degrees C to 82 degrees C is considered) in the high-rate volume wherever that is assumed to be located.

Estimated total exposure in the year 2000 (A-3)

CBG claims that the integrated thermal flux estimated by Dr. Pearlman is low by a factor of two because his flux value is low by a factor of two. Pearlman uses a flux value of 1.5×10^{12} n/cm²-sec which yields a fluence of 6.9×10^{19} nvt. The flux value was provided by the UCLA staff and has been verified as a reasonable value for the peak thermal flux by several recent detailed measurements. It is to be noted that CBG's DuPont, who claims responsibility for CBG's Wigner energy calculation, used a flux value of 3.3×10^{12} n/cm²-sec the source of which was identified as page 53 of the 1965 thesis by G. B. Bradshaw (CBG's Exhibit C-II-3). In fact, the values reported on page 53 of the Bradshaw thesis were values for the total neutron flux at 1 kW (which are multiplied by 100 to get the flux at 100 kW). On page 33 of the Bradshaw thesis is cited a thermal flux value of 1.5×10^{10} n/cm²-sec, which converts to 1.5×10^{12} n/cm²-sec at 10 kW. (A later thesis by Wilson cites a thermal neutron flux value in the same range. Measurements made by students as part of one of the classes taught at the laboratory are routinely in the same range.) For its calculation CBG used the total neutron flux value from the Bradshaw thesis although the calculational method clearly requires the use of the thermal neutron flux. Subsequent to Dr. Pearlman's testimony on this point CBG has substituted a new value for the thermal flux of 3.0×10^{12} n/cm²-sec which it obtained in a 1962 thesis by Taylor. That value derived for a different core configuration has no relation to current thermal flux values.

Graphite temperature assumed in the Battelle study (A-4)

CBG takes issue with Dr. Pearlman's claim that an assumed operating temperature of 50 degrees C is too low. In fact, the difference in effect between 50 degrees C and 65 degrees C (assumed by Pearlman) are taken into account in Pearlman's calculation which covers the range of temperatures between 30 degrees C and 82 degrees C. This allows for any corrections that may be needed for different operating temperatures. CBG also overlooks two important points. One is the annealing effected by operation at a higher temperature subsequent to operation at a lower temperature. The other is that reactor operations are generally at full power (100 kW) or very low power (less than 1 kW). At very low power, the temperatures are lower and the flux is very much lower. It is inappropriate to assume the "average condition" is represented by the arithmetic average power level.

Storage rate assumed in CBG's direct testimony (A-5)

CBG is incorrect in its assertions about what Dr. Nightingale intended to convey in the discussion of storage rates for low exposure, on page 345 of "Nuclear Graphite." The 0.6 to 1.0 $\frac{\text{cal/gm}}{\text{Mwd/AT}}$ values were intended for determining displacement rates of carbon atoms at essentially zero exposure. They were not intended for practical estimation of stored energy at the exposure level of the UCLA reactor. A value of 0.5 cal/gm, or higher, may quite possibly be better than the one Pearlman used -- but not for the reasons set forth by CBG.

Specific heat values used by CBG (A-7)

CBG takes issue with Pearlman's testimony that the values of specific heat used by CBG were too low. CBG's calculation is contained in DuPont's affidavit. DuPont derives stored energy values of 125 and 208 cal/gm for which he estimates adiabatic temperature increases of 600 degrees C and 1000 degrees C, respectively, following hypothetical stored energy releases. The specific heat, C_p , corresponding to these energies and temperatures can only be 0.21 cal/gm-°C. The correct average values of C_p over the ranges 50 degrees C to 600 degrees C and 50 degrees C to 1000 degrees C are, respectively 0.32 and 0.37 cal/gm-°C. The original CBG specific heat values are too low. It is to be noted that subsequent to Dr. Pearlman's testimony CBG has dropped, without explanation, the 1000 degrees C adiabatic temperature rise estimate.

Comparison of 1 Mwd_{UCLA} with 1 (Mwd/AT)_{Hanford} (A-8)

In its answer CBG attempts, essentially, a re-definition of exposure units. First it should be noted that Pearlman explicitly stated that he assumed that these units were equivalent, although he stated that this assumption appeared to be conservative -- that is, it would overestimate the UCLA graphite exposure. This same assumption was made implicitly in the Battelle study and by CBG.

Second, the Mwd/AT unit was developed for use in reactors like Hanford, BEPO, Windscale and Calder Hall -- where there is a repeating natural uranium -- graphite lattice extending over distances of many tens of feet. It is not an appropriate unit for the UCLA reactor, and therefore cannot be used to directly compare exposures in the two reactors.

CBG's value of 1120 Mwd/AT is without basis and grossly exaggerates exposure for the UCLA reactor.

The assertion that "the only way to truly know the stored energy content is to measure it," is not relevant. It is possible to analyze available data and utilize the considerable amount of knowledge and experience that has been acquired on this subject to conservatively estimate the stored energy content of the UCLA reactor graphite.

Influence of water moderation on neutron damage in graphite (A-9)

In its very confused answer CBG attempts to disprove, by essentially qualitative arguments and assertions, the general validity of Pearlman's calculational method; the specific value of the conversion rates he used between Hanford units and BEPO units; the comparisons he cited between Hanford (water-cooled, graphite moderated) and gas-cooled, graphite moderated natural-uranium fuel reactor (BEPO, Windscale, Calder Hall); and the claim he makes in his testimony that the presence of the water moderator in UCLA greatly reduces the

neutron energy available to damage the graphite, compared to reactors where all the moderation is in graphite.

CBG also repeats its inaccurate assertion that Pearlman assumes the fast flux peaks in the core center. As previously stated, neither Pearlman's calculations nor his conclusions depend upon where the fast flux peaks. As for CBG's other assertions:

1) Pearlman's calculational procedure is essentially identical to that used by Battelle and CBG. He chose it because it offered the most direct method of comparing estimates of stored energy and maximum temperature. He clearly identified its assumptions (and limitations) and indicated that they tended to drive up the peak graphite temperature. Thus, the final values were conservative.

2) The BEPO conversion factor, 6.4×10^{17} thermal neutrons per 1 (Mwd/AT)_{Hanford}, is the correct value to use to relate Hanford exposures to equivalent thermal neutron fluence in an all graphite-moderated reactor. CBG's claim that a different factor should be used to relate to Hanford thermal flux is simply not valid. That factor comes from a 1959 paper by Nightingale and is not even given in his 1961 book. It was superseded by the BEPO factor, which is specific for comparison of stored energy, rather than any other radiation effect in graphite (such as electrical or mechanical property changes).

By an inappropriate use of the Mwd/AT unit to compare Hanford graphite damage to UCLA, A-9 asserts that the stored energy in UCLA graphite would be 300 cal/gm by the year 2000 -- a grossly overestimated value. The conversion between stored energy produced at Hanford per Mwd/AT exposure and gas-cooled reactors of otherwise generally similar design, is that the same energy is produced by about 0.6 Mwd/AT in the case of the gas-cooled reactors. These data are cited in Nightingale's book. CBG's claim that the thermal-to-fast fluence ratio equivalent to 1 (Mwd/AT)_{Hanford} shows that Hanford exposure would result in more stored energy than gas-cooled reactors is based on data in a 1959 paper by Nightingale that was superseded by the information presented in his 1961 book.

3) CBG's confusing discussion of water-moderation affects appears to be based on a value of 3/4 inches for the water in the Hanford reactor which CBG wishes to compare with the 1 1/2 inches of water at UCLA. The correct value for the water layer around the fuel at Hanford is 0.083 inches for all reactors except one where it is 0.102 inches. It is true that the test-hole water-cooling at Hanford provides more moderation; but that is at a different location. Also, for a neutron born in fission in the UCLA reactor the length of the path in water to reach graphite can be as great as 2.1 inches, rather than 1.5 inches.

4) CBG's assertion that the fast flux plot in "Figure D-4" rules out any significant effect of water is not substantiated by data on the fast neutron energy range depicted in that figure.

5) Moreover, UCLA has calculated the effect of the water coolant/moderator on the relative energy deposition by fission neutrons in water and graphite. The conclusion is that down to 100 kev, the neutrons deposit only about 15% of their energy in the graphite. The balance is dissipated in water.

Q.3. What is the current value of the thermal neutron flux in the center of the reactor?

A.3. UCLA has reported a value of 1.5×10^{12} n/cm²-sec at 100 kW in its Safety Analysis Report. In response to claims made by CBG that the thermal flux could be as high as 3.0×10^{11} n/cm²-sec, or even higher, UCLA performed a detailed measurement of the thermal neutron flux in the center vertical hole (CVH). The measurement was made by researchers from the principal academic user group of the neutron activation analysis laboratory at the Institute of Geophysics and Planetary Physics (UCLA). A measured value of 1.66×10^{12} n/cm²-sec \pm 0.06 (one standard deviation) at 100 kW was obtained by a standard method based on the General Activation Equation and counts from small dilute solutions of gold, cobalt and scandium. The

measurement procedure used is known to overstate the actual flux by a small amount and actually supports a value of 1.5×10^{12} n/cm²-sec (100 kW). A second, independent calculation was made utilizing the delayed-neutron counting technique and measurements obtained in the west vertical hole (WVH) by means of the rabbit system. This calculated value, 1.2×10^{12} n/cm²-sec (100 kW), when properly adjusted to the CVH using flux profiles supports the 1.5×10^{12} n/cm²-sec as the "best" average value for thermal neutron flux in the UCLA reactor. Details of these measurements and calculations are attached.

Q.4. Please describe the Wigner Energy calculation of Dr. Pearlman.

A.4. Dr. Pearlman's Wigner Energy calculation follows. It includes a calculation of the amount of neutron energy that is deposited in the graphite of the UCLA reactor by Mr. Ostrander.

Calculation of Wigner Energy Release for the UCLA Reactor by Dr. H. Pearlman with Supporting Calculation by N. Ostrander.

Q.1. What procedure did you use to calculate the effects of a Wigner release?

A.1. The procedure used is the same as in NUREG/CR-2079 (PNL-3691) (also known as "Hawley") and in Intervenor Panel II (June 14, 1983). The procedure calculates the value of the temperature rise in the graphite, due to the instantaneous release of the Wigner energy. This temperature rise, ΔT_{ad} , is measured in degrees centigrade.

This quantity is computed by dividing the value of the stored energy ("Wigner energy"), S_T , by the specific heat of graphite, \bar{C}_p . This is the average specific heat, for the temperature range of interest. Values were obtained from Table 6.3, p. 122, Nightingale; S_T is measured in calories per gram of graphite. \bar{C}_p is measured in units of calories per gram per degree centigrade (cal/gm-°C). Thus,

$$\Delta T_{ad} = S_T / \bar{C}_p$$

Q.2. How did you calculate the stored energy?

A.2. To obtain the value of S_T , I started with equation 12.1

(Nightingale, p. 329). The designation S_T signifies that S depends on the temperature of the graphite, during its exposure in the reactor.

The equation is $S_{30} = 685 (1 - e^{-0.526E})$ cal/gm, where S_{30} is the stored energy, in calories per gram, accumulated by graphite

during exposure at 30°C. Units of E are in 1000 megawatt-days per adjacent ton (Mwd/AT). The unit is a measure of the neutron fluence received by a graphite sample during the time required for the release of one thousand megawatt-days of fission energy in 2000 lbs. of uranium surrounding the location where the graphite is being exposed. The equation adequately represents the 30°C data plotted in the graphs, Figure 12.2 page 329, Nightingale.

Differentiating Eq. (12.1) gives the rate at which stored energy is accumulated as a function of exposure, (dS_{30}/dE) in units of calories per gram per 1000 megawatt-days per adjacent ton exposure:

$$(dS_{30}/dE) = 360 e^{-0.526 E} \frac{\text{cal/gm}}{1000 \text{ Mwd/AT}} .$$

Because the rate is a function of the exposure, I initially obtained an average rate by integrating the rate equation over the entire exposure range, and dividing by the exposure interval. Thus, the average exposure rate $(\overline{dS_{30}/dE})$ is

$$360 \int_0^{0.0531} e^{-0.526 E} dE \int_0^{0.0531} dE = 354 \frac{\text{cal/gm}}{1000 \text{ Mwd/AT}} = 0.35 \frac{\text{cal/gm}}{\text{Mwd/AT}} .$$

Here, 0.0531 is the total exposure in the UCLA reactor, estimated by the year 2000, in units of 1000 Mwd. (The exposures, 53.08 Mwd by 2000, and 20.23 Mwd as of 1983, were obtained from the UCLA staff.)

It is worth noting here that higher values of the accumulation rate, cited on page 345 Nightingale, are not appropriate for this calculation. Those are asymptotic values, at essentially zero exposure, and at very low temperature. They are intended for solid state physics calculations of displacement rates in graphite without any interfering vacancies or interstitials created by neutrons. The UCLA reactor graphite exposure is relatively low, but not zero. What is needed is an average rate over the actual exposure range, which this procedure based on Eq. (12.1) was intended to supply.

The choice of an appropriate rate is complex and in my earlier testimony I explained the difficulty I had in understanding Dr. Nightingale's comment on this subject. Subsequently, I have communicated with Dr. Nightingale and have established that his intended meaning on page 345 of "Nuclear Graphite" is equivalent to using an average rate of $0.5 \frac{\text{cal/gm}}{\text{Mwd/AT}}$ for exposures in the UCLA graphite, but not the 0.6 to 1.0 values which were meant for exposures near zero. Additional research turned up some experimentally determined data on stored energies in graphite irradiated to low exposures, at a temperature within the range of interest for UCLA. This data could be interpreted as suggesting a rate as high as two times my calculated value of dS_{30}/dE , or about $0.7 \frac{\text{cal/gm}}{\text{Mwd/AT}}$. I have adopted this value for further calculations, rather than 0.35, or Nightingale's suggested 0.5. The use of the higher value adds conservatism to the calculation.

At 30°C, the average stored energy is converted to thermal fluence (thermal nvt, or N_{th}/cm^2) by the relation on p. 328, Nightingale, called the BEPG equivalent:

$$\frac{\text{Thermal nvt}}{\text{Mwd/AT}} = 6.4 \times 10^{17}$$

Here, nvt, or N_{th}/cm^2 , refers to the number of neutrons of thermal energy (about 1/40 of an electron volt) that pass through a one square centimeter area in the graphite. Utilizing this conversion factor, I obtained a stored energy (Wigner energy) average accumulation rate, per unit thermal neutron fluence. Thus

$$\overline{(dS_{30}/dE)} = 1.1 \times 10^{-18} \frac{\text{cal/gm}}{n_{th}/cm^2}.$$

The total thermal fluences are obtained by multiplying the thermal neutron flux at 100 kW power level (=0.1 Mw), by the times equivalent to the Mwd's of exposure for the years 1983 and 2000. The flux value, $1.5 \times 10^{12} n_{th}/cm^2\text{-sec}$, is the value reported by the UCLA staff for the thermal flux. Maximum fluences are estimated to be 2.6×10^{19} and 6.9×10^{19} , respectively, in the years 1983 and 2000. The product of the average storage rate, $\overline{(dS_{30}/dE)}$, and the fluence yields the stored energy, S_{30} .

Q.3. How did you calculate the stored energy for other operating temperatures?

A.3. The UCLA reactor graphite though does not operate isothermally at 30°C. The three dimensional temperature distribution peaks at the center of the graphite island, from minimum values near the fuel boxes. To determine the S_T values at other temperatures, I used Eq. 12.3, p. 331 (Nightingale) which relates the stored energy at 30°C to that stored at different temperatures of accumulation. Thus

$$S(T) = e^{-T/71.2} \text{ cal/gm}$$

where $S(T)$ = stored energy accumulated at $T(^{\circ}\text{C})$
 = constant for a given reactor

Taking the 30°C value as unity, the fractions of this value at higher temperatures are summarized in the following table:

<u>T(°C)</u>	<u>S(T)/S(30)</u>
30°	1
40°	0.87
50°	0.76
60°	0.66
65°	0.61
70°	0.57
82°	0.481

From my review of reactor operations, I chose 65° as the graphite damage temperature for this calculation. This value is derived from considering a typical three-hour run at 100 kw. For one such run, the graphite temperature in the thermocouple well at the center island between the fuel boxes reached 82°C in 110 minutes of operation (Figure 4, N.C. Ostrander testimony, 1983). Based on water inlet and outlet temperatures obtained from NEL staff, I calculated that the graphite temperatures next to the fuel boxes are 50°C and 72°C respectively at the water inlet and outlet locations. The 65°C value was selected as representative of the graphite temperature during this kind of exposure. The maximum temperature reached by the graphite after a Wigner release is the sum of the starting temperature, plus ΔT_{ad} . I assumed a starting temperature of 82°C. (If a starting temperature lower than 82°C is assumed the calculations show that the maximum temperature is lower). Therefore,

$$(dS/dE)_{65} = (0.61) (0.7) \frac{\text{cal/gm}}{\text{Mwd/at}} = 0.43 \frac{\text{cal/gm}}{\text{Mwd/at}} \text{ at } 65^{\circ}\text{C} .$$

Q.4. What value of \bar{C}_p did you use?

A.4. For an estimated 100°C temperature rise, the \bar{C}_p value is 0.24 cal/gm-°C. This is approximately the average specific heat over the temperature range 82°-182°C. For an estimated 200°C temperature rise (for the range 82° - 282°C), the \bar{C}_p value is 0.27 cal/gm-°C.

Q.5. What were your numerical results?

A.5. Based on the above, I calculate ΔT_{ad} values of 74°C in 1983, and 175°C in 2000. However, these calculated values do not take into account the significant moderating effect of the water in reducing the high energetic flux incident on the graphite.

To obtain the peak temperatures in these years, I use a starting temperature of 82°C . The 82°C value, as stated above, is the measured temperature at the thermocouple well in the graphite center island. (Regarding this, an inadvertent mistake appears in my testimony, Tr. 1801, Line 19. It is not correct to use 65°C as the starting temperature. That is the exposure temperature.)

Q.6. Could you give us a simple comparative breakdown of the factors that go into computing T_{ad} and the respective values chosen by Hawley, Intervenor and yourself?

$$A.6. \Delta T_{Ad} = B \times C \times D \times E \times F$$

where ΔT_{Ad} = Temperature rise in $^{\circ}\text{C}$.

B = thermal neutron flux in $\text{n/cm}^2\text{-sec}$

C = time at full power equivalent in seconds

D = 1/BEPO equivalent in $1/ \frac{\text{nth/cm}^2}{\text{Mwd/AT}}$

E = energy storage rate in $\frac{\text{cal/gm}}{\text{Mwd/AT}}$

F = (1/specific heat) in $\frac{1}{\text{cal/gm-}^{\circ}\text{C}}$.

Stored energy per gram of graphite, S , in cal/gm is equal to the partial product ($B \times C \times D \times E$). If the moderating effect of the coolant water is properly characterized by the percentage of fission neutron energy deposited in the graphite, we can make use of a Neutron Moderation Factor, G . If $(\Delta T_{Ad})_{mod}$ is the corrected temperature increase, then $(\Delta T_{Ad})_{mod} = \Delta T_{Ad} \times G$.

Table 1. Comparison of Parameters & Results

<u>Item</u>	<u>Hawley</u>	<u>Intervenor Panel II</u>	<u>Pearlman</u>
B	1×10^{12}	3.3×10^{12} (a)	1.5×10^{12}
C	1×10^7	4.8×10^7	4.58×10^7
D	1.56×10^{-18}	1.56×10^{-18}	1.56×10^{-18}
E	0.30	0.5 to 0.83	0.43 (e)
S	5	125 to 210 (b)	17.8 (1983) to 47.3 (2000)
F	---	1/0.21 (c)	1/0.24 to 1/0.27
ΔT_{ad}	---	600° to 1000° (d)	74°C (1983) to 175°C (2000)
G	---	---	0.15 (f)
$(\Delta T_{ad})_{mod}$	---	---	11°C (1983) to 26°C (2000) (g)

NOTES

- (a) Correction by CBG, September 26, 1983, changed this to 3×10^{12} .
- (b) Correction (see above) changed this to 115 and 190, without explanation, on their p. 11. (On their p. 13, the corrected values are 113 and 189).
- (c) The value of 0.21 cal/gm $^{\circ}\text{C}$ is the specific heat at about 77°C . For comparison, the correct average value to 600°C is 0.32 cal/gm $^{\circ}\text{C}$.
- (d) Correction (see above) eliminates the 1000° value, without explanation.
- (e) For an exposure temperature of 65°C .
- (f) Neutron Moderation Factor. As explained below, this correction should properly be applied to factor "D"; however, to facilitate the comparison and to make explicit the effect of water moderation on resultant ΔT_{ad} , factor "G" has been applied after calculating a temperature rise assuming no water moderation effect.
- (g) Ignores minor \bar{C}_p correction.

Q.7. What are the conservatisms in your calculations of the temperature rise?

A.7. There are at least three, each of which results in too high a calculated temperature rise.

The first is the difference in neutron spectra between the UCLA reactor and BEPO. The conversion factor from the exposure units (Mwd/AT) to the thermal neutron fluence (N_{th}/cm^2), that is utilized above (see Table), is strictly valid for a single test position in BEPO, which is a graphite-moderated, natural uranium-fueled air-cooled reactor. In BEPO, all of the neutron moderation takes place in graphite. Although the Hanford reactors are also graphite-moderated (essentially) and natural uranium-fueled, their neutron spectra are different from BEPO because they are water-cooled, which means water performs some (small) moderation. This difference is manifested by the experimental fact that the Wigner energy per unit exposure (that is, per Mwd/AT) is smaller in Hanford than in BEPO. Qualitatively, it is to be expected that the Wigner energy would be still smaller in UCLA reactor graphite, because the water there substantially moderates as well as cools.

A quantitative calculation has been completed that provides definite values for the relative neutron energy absorption in graphite and in water. (The computer calculation by N.C. Ostrander is described in the Appendix.) Utilizing a Monte Carlo method to track 45 neutrons from 2 Mev (Mega electron-volts) to

100 kev (kilo electron-volts), as well as other calculations of the uncollided flux, Ostrander computes that only 14.7% of the neutron energy is absorbed in and therefore moderated by the graphite. If the stored energy effect scales directly with the energy absorption, the thermal flux equivalent of one Mwd/AT exposure would be $4.4 \times 10^{18} \text{ n}_{\text{th}}/\text{cm}^2$, so that the factor "D" in the Table becomes 2.3×10^{-19} (rather than 1.56×10^{-18}). The important consequence of this result is to reduce the calculated value of ΔT_{ad} in the year 2000 to less than 30°C .

A second conservatism is in the assumption that the Wigner energy release occurs adiabatically--with no heat transfer to the surroundings. This means that every gram of graphite must absorb its released stored energy, which it can only do by increasing its temperature. In fact, the portion of the UCLA graphite that is susceptible to Wigner energy storage and release is relatively small, about 6% of the nearly 20,000 pounds of graphite present. Any heat conducted by the cooler contiguous graphite would reduce the maximum temperature below the calculated values.

The effect of heat transfer in a real reactor situation is shown in "BEPO Wigner Energy Release," by J. L. Dickson and others, in Proceedings of the Second U.N. Conference on Peaceful Uses of Atomic Energy, Geneva 1958, 7, 250 (1959). Figure 9, on page 254 shows that the peak temperature in the real situation is 80°C lower than in the carefully contrived laboratory adiabatic rise experiment. Further, the peak temperature occurs approximately

six hours after initiation in the real reactor case, compared with about 1 hour for the laboratory adiabatic experiment.

Finally, the assumption (made in the calculations) that the Wigner energy is released instantaneously, results in an unrealistically high temperature rise. There is ample evidence from carefully conducted Wigner energy release experiments--for example, at the Brookhaven graphite reactor as well as the BEPO experience cited above--that the release occurs gradually. The literature reports releases starting at temperatures as low as 80°C, with the rate of release increasing to a maximum rate at higher temperatures and then decreasing. The energy release pattern is not instantaneous. Among other results, this behavior allows time for heat transfer away from the graphite in which the release occurs.

Q.8. What is your conclusion with respect to Wigner Energy storage in graphite for the UCLA reactor?

A.8. The Wigner Energy phenomenon can make only a negligible contribution to the course of a postulated transient accident in the UCLA reactor, or any other kind of thermal accident such as fire.

APPENDIX A

The Distribution of Fission Neutron Energy Deposition between
Fuel Regions and Graphite in an Argonaut Research Reactor

by

N. C. Ostrander

The Argonaut Reactor Geometry (Idealized)

The UCLA Argonaut reactor consists of two fueled sections or slabs separated by twelve inches of graphite. The graphite central island has been variously called an internal thermal column or a flux trap. A plan view is shown in Figure 1. Each "slab" is composed of three fuel boxes, however only the center box of each slab is shown completely in Figure 1. Control blades in shrouds (not illustrated) occupy the space of approximately one inch between the fuel boxes. Each fuel box contains four fuel bundles of eleven plates each. The plates are 0.070 inches thick and include 0.015 inches of aluminum alloy containing 13.7 weight percent (2.2 volume percent) uranium-235. The water channel width is 0.137 inches and the volume ratio of metal to water is about 0.51.

The region containing the fuel boxes and graphite center island is about 20 inches in the east-west direction by 22 inches in the north-south direction. That region is further surrounded by graphite to provide 19 to 20 inches of graphite reflector on each side.

For simplicity, the geometry will be idealized by assuming that the two slabs are continuous and extend indefinitely in the east-west and vertical directions. The geometry thus becomes one-dimensional with distance, z , measured toward the south from the center-line of

the north slab. The fueled region is treated as a homogenous mixture containing 33.8 volume percent aluminum and 66.2 volume percent water.

The Uncollided Flux

The uncollided flux is defined here as the fission neutrons which escape from the fuel slab into the graphite without having a collision with a hydrogen atom. In this definition, collisions with oxygen or aluminum don't count because the post-collision neutron will have nearly the same energy as the pre-collision neutron.

The calculation assumes a uniform spatial distribution of neutron births in the fuel region. The fraction of the newly born neutrons which escapes the fuel region without any collision can be represented by an integral which leads to

$$f_1 = \frac{1}{8\ell\Sigma} \cdot$$

The fuel region half thickness is $\ell = 6.35$ cm, and at 2 mev, the total cross section of the H - O - Al mixture in the fuel region is about 0.215 cm^{-1} . Thus the fraction directly escaping is about 0.0916.

Of the remaining neutron fraction (0.9084) which experiences some kind of collision in the fuel region, approximately 58% will occur with a hydrogen atom and 42% will occur with a heavier atom (oxygen or aluminum). These latter collisions will be referred to as M collisions.

$$\begin{aligned} f_1 &= 0.916 && \text{(no collision)} \\ f_2 &0.9084 \times 0.58 = 0.5269 && \text{(H collision)} \\ f_3 &0.9084 \times 0.42 = 0.3815 && \text{(M collision)} \end{aligned}$$

The probability that a fission neutron will experience a sequence of n collisions of kind M and then escape the fuel region on the next trial is $f_3^n f_1$. Thus the cumulative probability that the neutron will escape directly, or after one M event, or after two M events, or after n events of kind M is

$$F_1 = f_1(1 + f_3 + f_3^2 + \dots + f_3^n) = \frac{f_1(1 - f_3^{n+1})}{1 - f_3} .$$

If n is large, then f_3^{n+1} becomes negligible with respect to unity and

$$F_1 \xrightarrow{n \text{ large}} \frac{f_1}{(1 - f_3)} = 0.148 .$$

Accordingly, the uncollided fraction reaching the graphite is approximately 0.148, the uncollided fraction in the fuel region approaches zero, and the fraction of the fission neutrons which have at least one collision with hydrogen is

$$1 - 0.148 = 0.852.$$

It is worth noting that the number n used in the preceding calculation need not be extremely large. The probability of ten successive collisions with a heavy atom is 0.3815 to the tenth power or about 7×10^{-5} . On the other hand, the average logarithmic energy decrement in such a collision is about 0.089 per collision and after 10 collisions the average neutron energy will have fallen from 2 mev to about 0.82 mev. In a single collision with a hydrogen atom, the 2 mev neutron will depart that collision with an average energy of 0.74 mev. In going from 2 mev to 0.8 mev, the neutron mean free path in

the fuel region decreases by more than 40%, and below 0.8 mev, neutron escape from the fuel region becomes increasingly improbable. For these reasons, the distribution of energetic neutrons between the fuel region and the graphite tends to be "frozen" at fairly high energies.

The simple conclusion of the foregoing is that whereas all of the fission neutron energy is transferred to the graphite in a graphite moderated, gas cooled reactor, only about 14.7% of the fission neutron energy is transferred to the graphite reflector of an Argonaut reactor.

A Monte Carlo Calculation

A variation of the preceeding calculation involves tracking sample neutrons from birth until their energy falls below some cut-off value of interest. Although it is time consuming, this approach does incorporate the variation in cross-sections with energy and does permit migration of neutrons across the fuel-graphite interface in either direction.

This calculation has been done for a sample of 45 neutrons, born at 2 mev and tracked down to 100 kev (5% of their birth energy). The choice of the 100 kev cut-off was made for two reasons:

- a) it accounts for 95% of the fission neutron energy; and
- b) the computation process becomes slow, particularly for the small fraction of the neutrons which are well into the graphite, have mean free paths of only about 1.20 cm and do not move very far from their 100 kev locations in subsequent collisions down to 30 kev (tested with a sample of 15 neutrons).

Given a limited amount of time there is a choice between tracking a few neutrons to very low energy versus tracking a larger number to improve the statistics and to account for a substantial fraction (95%) of the fission neutron energy distribution between the fuel region and the graphite reflector. Ten to twenty minutes are required to acquire a single neutron history with a Hewlett-Packard HP-41 CV, depending upon how much detail one wishes to record at each collision.

The computation starts with a 2 mev neutron created at a random (uniform) location in the core and moving in a random (isotropic) direction. The path length, r , to the point of first collision is chosen by

$$r = - \frac{1}{\Sigma} \ln N$$

where N is a random number uniformly distributed between zero and unity. The path length must be adjusted if the neutron moves from one region to the other because of the generally different values of macroscopic scattering cross sections, Σ in the different regions.

At the point of first collision, the scattering atom is identified. If the neutron is in the graphite, the collision is necessarily with a graphite atom. However, if the collision occurs in the core, the neutron will collide with hydrogen, oxygen, or aluminum with probabilities proportional to the cross-section of those atoms relative to the total cross-section of the medium. The decision is based upon a new random number ($0 < N < 1$).

Collisions are treated isotropically and three dimensionally in the center-of-mass coordinate system and hence preferentially scatter the neutron forward relative to its incident direction. However, the

neutron progress is tracked only in one dimension, the projection of r upon the axis normal to the core-graphite interface. Neutron energy losses are calculated from the scattering angle and the mass of the scattering atom. Energy losses are accumulated separately in core and reflector regions for successive scatterings.

The geometry is that of Figure 1, specifically the region $0 < z < 21.6$ cm. The fuel slab center plane and the graphite island center plane are both treated as reflecting boundaries. Thus neutrons never leak from the system.

The calculations to date have tracked 45 neutrons from 2 mev until their energy fell below 100 kev. At this cut-off, the neutron was assumed to deposit its residual energy in the medium in which the neutron then resided. From the tabulated results, the effect of other cut-off energies (above 100 kev) can be examined. The summary data are:

Cut-Off Energy mev	Fraction of Initial Energy	
	In Graphite	In Fuel Box
1.0	0.136	0.864
0.2	0.145	0.855
0.1	0.147	0.853

These results support the assumption that the neutron distribution is strongly determined at high energy and is then nearly frozen for the lower energies. The statistical calculation agrees very well with the uncollided flux calculation in indicating that less than 15% of the fission neutron energy is transferred to the graphite of an Argonaut reactor.

Thermal Neutron Flux Determination by

Dr. G. W. Kallemeyn
Instrumental Neutron Activation Analysis Laboratory
Institute of Geophysics and Planetary Physics

The equation which relates the activity of a nuclide due to thermal neutron bombardment in a nuclear reactor is called the general activation equation and can be written as follows:

$$\phi_{\text{thermal}} = \frac{A_{\text{th}}}{fN\sigma \sqrt{\frac{\pi}{2}} \left(\frac{T_0}{T}\right)^{1/2} G_f(1 - e^{-\lambda t_1})e^{-\lambda t_2}}$$

$$A = \frac{\text{measured cps}}{E P m F}$$

$$A_{\text{th}} = A_{\text{bare}} - A_{\text{covered}}$$

Counting equipment: Nuclear Data ND66 multichannel analyzer

Harshaw 3" x 3" NaI(Tl) detector @ 10 cm

-Gamma ray peaks plotted on DEC VT640 graphics terminal, background stripped, and integrated using VAX 11/780 computer.

- $T_{1/2}$, f and F (absolute gamma intensities) taken from "Chart of Nuclides" General Electric Co. (1972) and from Table of Isotopes, by C. M. Lederer and V. S. Shirley (1978), 7th ed.

- E (abs. det. eff.) and P (peak-to-total) from Scintillation Spectrometry Gamma-Ray Spectrum Catalogue by R. L. Heath (1957)

Measurements and Calculations:

1. Sc-46 (1120 keV peak)

$$A_{\text{bare}} = \frac{8.04 \pm 0.08 \text{ cps}}{(.0173)(.392)(2.486 \times 10^{-6} \text{ g})(1.0)} = 4.77 \times 10^8 \text{ dps/g} \pm .05$$

$$A_{\text{covered}} = \frac{0.017 \pm .002 \text{ cps}}{(.0173)(.392)(2.457 \times 10^{-6} \text{ g})(1.0)} = 0.010 \times 10^8 \text{ dps/g} \pm .001$$

$$A_{\text{thermal}} = 4.76 \times 10^8 \text{ dps/g} \pm .05$$

$$\phi_{\text{thermal}} = \frac{4.76 \times 10^8 \text{ dps/g}}{fN\sigma(0.8862)(0.9495)(1.0)(1 - e^{-\lambda t_1})e^{-\lambda t_2}}$$

$$t_1 = 3\text{h}; \quad t_2 = 50.4 \text{ h}$$

$$\phi_{\text{thermal}} = \frac{4.76 \times 10^8}{(1.0)(1.340 \times 10^{22})(26 \times 10^{-24})(0.8862)(0.9495)(1.0)(.0010)(.9828)}$$

$$\phi_{\text{thermal}} = 1.65 \times 10^{12} \text{ n cm}^{-2} \text{ s}^{-1} \pm .02$$

2. Co-60 (1333 keV peak)

$$A_{\text{bare}} = \frac{5.13 \pm .05 \text{ cps}}{(.0165)(.345)(31.97 \times 10^{-6} \text{ g})(1.0)} = 2.82 \times 10^7 \text{ dps/g} \pm .03$$

$$A_{\text{covered}} = \frac{0.500 \pm .011}{(.0165)(.345)(31.97 \times 10^{-6})(1.0)} = 0.275 \times 10^7 \text{ dps/g} \pm .006$$

$$A_{\text{thermal}} = 2.54 \times 10^7 \text{ dps/g} \pm .03$$

$$\phi_{\text{thermal}} = \frac{2.54 \times 10^7 \text{ dps/g}}{fN\sigma(0.8862)(0.9495)(1.0)(1 - e^{-\lambda t_1})e^{-\lambda t_2}}$$

$$t_1 = 3h; t_2 = 50.8 h$$

$$\phi_{\text{thermal}} = \frac{2.54 \times 10^7}{1.0(1.022 \times 10^{22})(37 \times 10^{-24})(0.8862)(.9495)(1.0)(4.503 \times 10^{-5})(9.992 \times 10^{-1})}$$

$$\phi_{\text{thermal}} = 1.77 \times 10^{12} \text{ n cm}^{-2} \text{ s}^{-1} \pm .02$$

3. Au-198 (412 keV peak)

$$A_{\text{bare}} = \frac{507 \pm 2 \text{ cps}}{(0.0230)(0.730)(6.989 \times 10^{-6} \text{ g})(.986)} = 4.38 \times 10^9 \text{ dps/g} \pm .02$$

$$A_{\text{covered}} = \frac{212 \pm 1 \text{ cps}}{(0.0230)(0.730)(6.989 \times 10^{-6} \text{ g})(.986)} = 1.83 \times 10^9 \text{ dps/g} \pm .01$$

$$A_{\text{thermal}} = 2.55 \times 10^9 \text{ dps/g} \pm .02$$

$$\phi_{\text{thermal}} = \frac{2.55 \times 10^9 \text{ dps/g}}{fN_{\sigma}(0.8862)(0.9495)(1.0)(1 - e^{-\lambda t_1})e^{-\lambda t_2}}$$

$$t_1 = 3h; t_2 = 148.8 h$$

$$\phi_{\text{thermal}} = \frac{2.55 \times 10^9}{(1.0)(3.057 \times 10^{21})(98.8 \times 10^{-24})(.8862)(.9495)(1.0)(3.169 \times 10^{-2})(.2024)}$$

$$\phi_{\text{thermal}} = 1.56 \times 10^{12} \text{ n cm}^{-2} \text{ s}^{-1} \pm .03$$

$$\text{Average } \phi_{\text{thermal}} = 1.66 \times 10^{12} \text{ n/cm}^2 \text{-sec (100kw)} \pm 0.06$$

CALIBRATION OF THE UCLA NUCLEAR REACTOR

EMIL K. KALIL, PH.D.

This paper presents the thermal neutron flux calculation of the UCLA Nuclear Reactor. The delayed neutron counter is used to count the delayed fission neutrons from irradiated uranium standards. The neutrons counted are directly proportional to the number of fissions which is related directly to the flux.

There are many steps leading to the actual flux calculation. The first is the absolute calibration of the neutron detector. The neutron detector (counter) is described fully in Dr. Kalil's dissertation, with excerpts included in Appendix 1. Briefly, it is a 55 gallon drum, filled with over 300 pounds of paraffin. There are 8 BF-3 neutron counting tubes situated in a circle in the middle of the drum. The tubes are 2 inches in diameter and 24 inches long. There is an annular cylinder of lead in the center of the drum that surrounds the sample during counting and also acts as a gamma absorber. The actual count is recorded from the electronic digital scaler.

The counter first needed to be calibrated against a known source. An AmBe source, serial number MRC-N-SSW-AmBe-631 was used. It has an activity of 1.3×10^5 neutrons/second. The detector efficiency for these neutrons was $0.1373 \pm 0.15\%$. (The error is based solely on counting statistics.) This means the neutron counter system is 13.73 percent efficient. According to published sources (N.H. Gale, 1967, SM-87/38) the efficiency for Gale's detector system was approximately 17% as calculated from a known reactor flux. The 13.73% is a respectable number but may be a bit off due to two factors: (1) the neutrons from the source are at a higher energy than the delayed fission neutrons and (2) the high count rate could have changed the dead time.

Once the detector is calibrated, a known uranium sample was irradiated and counted. I have been doing this type of measurement for 9 years and have uranium standards that are extremely accurate. They are NBL (New Brunswick Lab) standards and they concur with my cross calibration with other major labs in the United States.

A computer program is included to illustrate the flux calculation. I will describe the variables of interest and the general program flow.

CALCULATION

The recorded count must first be corrected for counter dead time. This is the time the BF-3 tube uses to process a pulse. Dead time was determined by the dual sample method to be 16.56 micro seconds. 10 to 20 micro seconds are very typical dead times for BF-3 tubes, depending on their length and operating voltage. The dead time I use works extremely well for correcting

counting losses on high count rate samples.

The delayed neutrons are counted for 29 seconds exactly. All timing is done with custom digital times so the timing does not introduce any error. The count is started exactly 17 seconds after the end of irradiation. The recorded count is first corrected for dead time. Then it is converted to a count rate at the beginning of the count. This initial count rate is then decay corrected to the count rate at the end of irradiation. The count rate is then converted to neutrons by division of the detecto

efficiency. It is then divided by neutron yield to give the number of fissions per neutron.

We now have a fission production rate at the end of irradiation. This is equal to the flux times the cross section times the number of U-235 atoms times the saturation factor. The flux is calculated from all these.

There is a decay constant, λ , for the delayed neutrons. I have used a half life of 25 seconds. This is based on actual plots of counts per second during the count period. There are many different delayed neutron emitters, I-137, Br-87, Br-88 and Br-89 being the most dominant during the counting period. These are listed in Table 3-1 of Appendix 1. Most texts usually divide the delayed neutron emitters into decay groups (LaMarsh, J.R., Nuclear Reactor Theory, 1966, Addison-Wesley Publishing Company). The groups are similar to those listed in Table 3-1. Group 1 has a 55.72 second half life with a yield of .00063 neutrons per fission. Group 2 has a 22.72 second half life and a yield of .00351 neutrons per fission. Group 3 has a half life of 6.22 seconds with a yield of .00310 neutrons per fission. The remaining groups have half lives too short to be of any concern.

The observed delayed neutron half life, shown in Figures 1, 2 and 3 is approximately 22 to 25 seconds. This is a mixture of groups 1, 2 and 3. Group 3 is not very important because I do not start counting until 17 seconds after irradiation. By this time, Group 3 has undergone almost 3 half lives and is down to 15.4 % of its original activity.

$$\text{Activity} = \lambda_1 * N_1 + \lambda_2 * N_2 + \lambda_3 * N_3$$

$$\text{also, Activity} = \lambda * N$$

$$\text{and } \lambda = \ln(2) / \text{Half Life.}$$

$$\lambda_1 \text{ is group 1, 55.7 seconds, } N_1 = .00063$$

$$\lambda_2 \text{ is group 2, 22.7 seconds, } N_2 = .00351$$

$$\lambda_3 \text{ is group 3, 6.22 seconds, } N_3 = .0031 * .147$$

The .147 factor on group 3 is the amount of group 3 that is available for decay during the count period. This calculates to a neutron yield of .00459 with a half life of 19.24 seconds. However, the observed half life is longer, 22 to 25 seconds during the count period. Substituting the 22 to 25 second half life in the above equations, gives a neutron yield of .0047 to

Table 1 lists a variety of combinations for the flux calculation. In the first part, the observed half life of the delayed neutrons is varied from 20 to 25 seconds by 1 second. The neutron yield changes proportionately and so does the flux. Holding the half life constant and just changing the detector dead time also causes a change in flux. Finally, changing the detector efficiency also causes a change in flux.

Table 2 is almost the same as Table 1, except a much higher count sample is used. It is not an NBL standard, but just a high count sample. This gives a much higher flux because it is much more sensitive to counter dead time.

ERRORS

There are 4 places where error can occur. The first is the counter dead time. By varying counter dead time over the maximum allowable range, from 6 to 20 micro seconds, the flux does not appreciably change. The total error is 5.6% (.08 delta flux/1.42 mean flux).

By changing the detector efficiency by one percentage, from 13.73 to 14.73 or to 12.73 induces a 7% change in the final flux. As mentioned earlier, the detector efficiency could be off due to the different neutron energy spectrum of the standard source (negligible), and from errors in the dead time at this count rate. The standard source recorded an average count of 399458 counts in a 29 second count.

The last two errors are tied together in the neutron half life and the neutron yield. Theoretically, the half life should be about 19.24 seconds with a yield of .0047 neutrons per fission. However, the observed half life is much longer during the count period. The count period does not start until 17 after irradiation and last only 29 seconds. The three multiscaled plots clearly indicate a longer half life. Varying the half life from 20 to 25 seconds changes the flux for the low count sample from 1.6 to 1.2. This represents a net change of +/- 0.2 over a mean of 1.4 for a 14% maximum error.

FLUX

Using the mean of 3 NBL standard counts, the mean flux for the West Vertical Port of the UCLA Reactor is calculated to be 1.23×10^{12} neutrons/cm²/second +/- 16%. The error is a combination of the 4 errors mentioned above. Applying the 1.5 to 1.2 flux ratio of west vertical to center vertical ports, the center vertical port would have a flux of 1.5×10^{12} .

$$\text{ERROR} = \sqrt{5.6\%^2 + 7\%^2 + 14\%^2}$$

FLUX CALCULATION USING LOW COUNT RATES

DETECTOR		DELAYED NEUTRONS		SAMPLE		FLUX
Dead time	Eff.	Half Life	Yield	Counts	Grams U	n/cm^2/sec
1.66E-05	.1373	20.0	.004781	114453	.001681	1.63E+12
1.66E-05	.1373	21.0	.005020	114453	.001681	1.53E+12
1.66E-05	.1373	22.0	.005259	114453	.001681	1.43E+12
1.66E-05	.1373	23.0	.005498	114453	.001681	1.35E+12
1.66E-05	.1373	24.0	.005737	114453	.001681	1.28E+12
1.66E-05	.1373	25.0	.005976	114453	.001681	1.22E+12

VARY DETECTOR DEAD TIME

DETECTOR		DELAYED NEUTRONS		SAMPLE		FLUX
Dead time	Eff.	Half Life	Yield	Counts	Grams U	n/cm^2/sec
4.56E-06	.1131	25.0	.005976	114453	.001681	1.41E+12
8.56E-06	.1201	25.0	.005976	114453	.001681	1.35E+12
1.26E-05	.1281	25.0	.005976	114453	.001681	1.29E+12
1.66E-05	.1373	25.0	.005976	114453	.001681	1.22E+12
2.06E-05	.1478	25.0	.005976	114453	.001681	1.15E+12

VARY DETECTOR EFFICIENCY

DETECTOR				DELAYED NEUTRONS		SAMPLE		FLUX
Dead time	Eff.	Half Life	Yield	Counts	Grams U	n/cm^2/sec		
1.66E-05	.1173	25.0	.005976	114453	.001681	1.43E+12		
1.66E-05	.1273	25.0	.005976	114453	.001681	1.32E+12		
1.66E-05	.1373	25.0	.005976	114453	.001681	1.22E+12		
1.66E-05	.1473	25.0	.005976	114453	.001681	1.14E+12		
1.66E-05	.1573	25.0	.005976	114453	.001681	1.07E+12		

DETECTOR		DELAYED NEUTRONS		SAMPLE		FLUX
Dead time	Eff.	Half Life	Yield	Counts	Grams U	n/cm ² /sec
4.56E-06	.1131	25.0	.005976	484473	.007912	1.35E+12
8.56E-06	.1201	25.0	.005976	484473	.007912	1.37E+12
1.26E-05	.1281	25.0	.005976	484473	.007912	1.39E+12
1.66E-05	.1373	25.0	.005976	484473	.007912	1.42E+12
2.06E-05	.1478	25.0	.005976	484473	.007912	1.45E+12

VARY HALF LIFE FROM 20 TO 25 SECONDS, HOLD DEAD TIME CONSTANT

DETECTOR		DELAYED NEUTRONS		SAMPLE		FLUX
Dead time	Eff.	Half Life	Yield	Counts	Grams U	n/cm ² /sec
1.66E-05	.1373	20.0	.004781	484473	.007912	1.90E+12
1.66E-05	.1373	21.0	.005020	484473	.007912	1.77E+12
1.66E-05	.1373	22.0	.005259	484473	.007912	1.67E+12
1.66E-05	.1373	23.0	.005498	484473	.007912	1.57E+12
1.66E-05	.1373	24.0	.005737	484473	.007912	1.49E+12

VARY DETECTOR EFFICIENCY, DEAD TIME AND HALF LIFE CONSTANT

DETECTOR		DELAYED NEUTRONS		SAMPLE		FLUX
Dead time	Eff.	Half Life	Yield	Counts	Grams U	n/cm ² /sec
1.66E-05	.1173	25.0	.005976	484473	.007912	1.66E+12
1.66E-05	.1273	25.0	.005976	484473	.007912	1.53E+12
1.66E-05	.1373	25.0	.005976	484473	.007912	1.42E+12
1.66E-05	.1473	25.0	.005976	484473	.007912	1.32E+12
1.66E-05	.1573	25.0	.005976	484473	.007912	1.24E+12

TRY DIFFERENT URANIUM SAMPLES, COUNTS & MICROGRAMS OF URANIUM
HOLD EVERYTHING ELSE CONSTANT

DETECTOR		DELAYED NEUTRONS		SAMPLE		FLUX
Dead time	Eff.	Half Life	Yield	Counts	Grams U	n/cm ² /sec
1.66E-05	.1373	25.0	.005976	500957	.008592	1.37E+12
1.66E-05	.1373	25.0	.005976	644458	.011397	1.50E+12
1.66E-05	.1373	25.0	.005976	473113	.007844	1.39E+12
1.66E-05	.1373	25.0	.005976	518497	.009035	1.37E+12
1.66E-05	.1373	25.0	.005976	56412	.000803	1.22E+12
1.66E-05	.1373	25.0	.005976	60376	.000843	1.24E+12
1.66E-05	.1373	25.0	.005976	114453	.001681	1.22E+12

```

10 REM      FLUX.BAS
20 REM      3-NOV-83              EMIL K. KALIL
30 REM
40 REM      USE DELAYED NEUTRON COUNTER TO CALIBRATE UCLA REACTOR FLUX
50 REM
60 REM      CORRECT COUNT FOR DEAD TIME
70 REM
80 REM      ACTUAL COUNT RECORDED FROM COUNTER
90 REM      GRAMS.URANIUM = .000843
100 REM     REC.COUNT = 114000!
110 INPUT "GRAMS URANIUM: ",GRAMS.URANIUM
120 INPUT "COUNT AT 100 KW: ",REC.COUNT
130 GRAMS.URANIUM = .007912
140 REC.COUNT = 484473!
145 LPRINT " DETECTOR      DELAYED NEUTRONS      SAMPLE      FLUX"
146 LPRINT "Dead time Eff. Half Life Yield Counts Grams U n/cm^2/sec"
150 REM
160 REM      DEAD TIME IN SECONDS
165 REM
166 INPUT "GRAMS URANIUM: ",GRAMS.URANIUM
167 INPUT "COUNT AT 100 KW: ",REC.COUNT
170 DEAD.TIME = 1.656E-05
180 REM
190 REM      CALCULATE EFFICIENCY BASED ON DEAD.TIME
200 REM      SOURCE IS  $1.3 \times 10^5$  NEUTRONS/SEC
210 REM
220 EFFICIENCY = (399458!/29)/(1 - (399458!/29)*DEAD.TIME)/130000!
230 REM
260 REM
270 REM      COUNT PERIOD FOR LONG COUNT
280 COUNT.PERIOD = 29
290 RAD.TIME = 30
300 REM
310 REM
320 REM      CALCULATE COUNT CORRECTED FOR DEAD TIME
330 CPS = REC.COUNT/COUNT.PERIOD
340 REAL.COUNT.RATE = CPS/(1 - CPS * DEAD.TIME)
350 REAL.COUNT = REAL.COUNT.RATE * COUNT.PERIOD
360 REM
370 REM      CONVERT TO COUNT RATE AT BEGINNING OF COUNT ALLOWING FOR
380 REM      DECAY DURING THE COUNT PERIOD.
390 REM      USE FORMULA  $N * \text{LANDA} / (1 - \exp(-\text{LANDA} * \text{COUNT.PERIOD}))$ 
400 REM
410 REM      SET LANDA, USE AVERAGE OBSERVED HALF LIFE
420 REM      HALF LIFE IN SECONDS
430 REM      ALSO SET NEUTRON YIELD AS A FUNCTION OF OBSERVED HALF LIFE
440 REM
450 REM      OBSERVED HALF LIFE IS A COMBINATION OF 3 ISOTOPE GROUPS
460 REM
470 REM      GROUP 1 = 54.5 SECONDS      .00063 NEUTRONS/FISSION
480 REM      GROUP 2 = 22.7 SECONDS      .00351 NEUTRONS/FISSION
490 REM      GROUP 3 = 6.22 SECONDS      .00310 NEUTRONS/FISSION
500 REM
510 REM       $\text{LANDA} * N = \text{LANDA1} * N1 + \text{LANDA2} * N2 + \text{LANDA3} * N3$ 
520 REM
530 REM N IS THE NEUTRON YIELD, LANDA IS  $\ln(2)/\text{HALF.LIFE}$  (OBSERVED)
540 HALF.LIFE = 25
550 LANDA =  $\ln(2)/\text{HALF.LIFE}$ 
560 REM
570 REM      CALCULATE NEUTRON YIELD AS FUNCTION OF 3 ISOTOPE GROUPS
580 REM
590 NEUTRON.YIELD = ( $\ln(2)/55.72 * .00063 + \ln(2)/22.7 * .00351 + \ln(2)/6.22 * .00310$ ) / LANDA

```

```

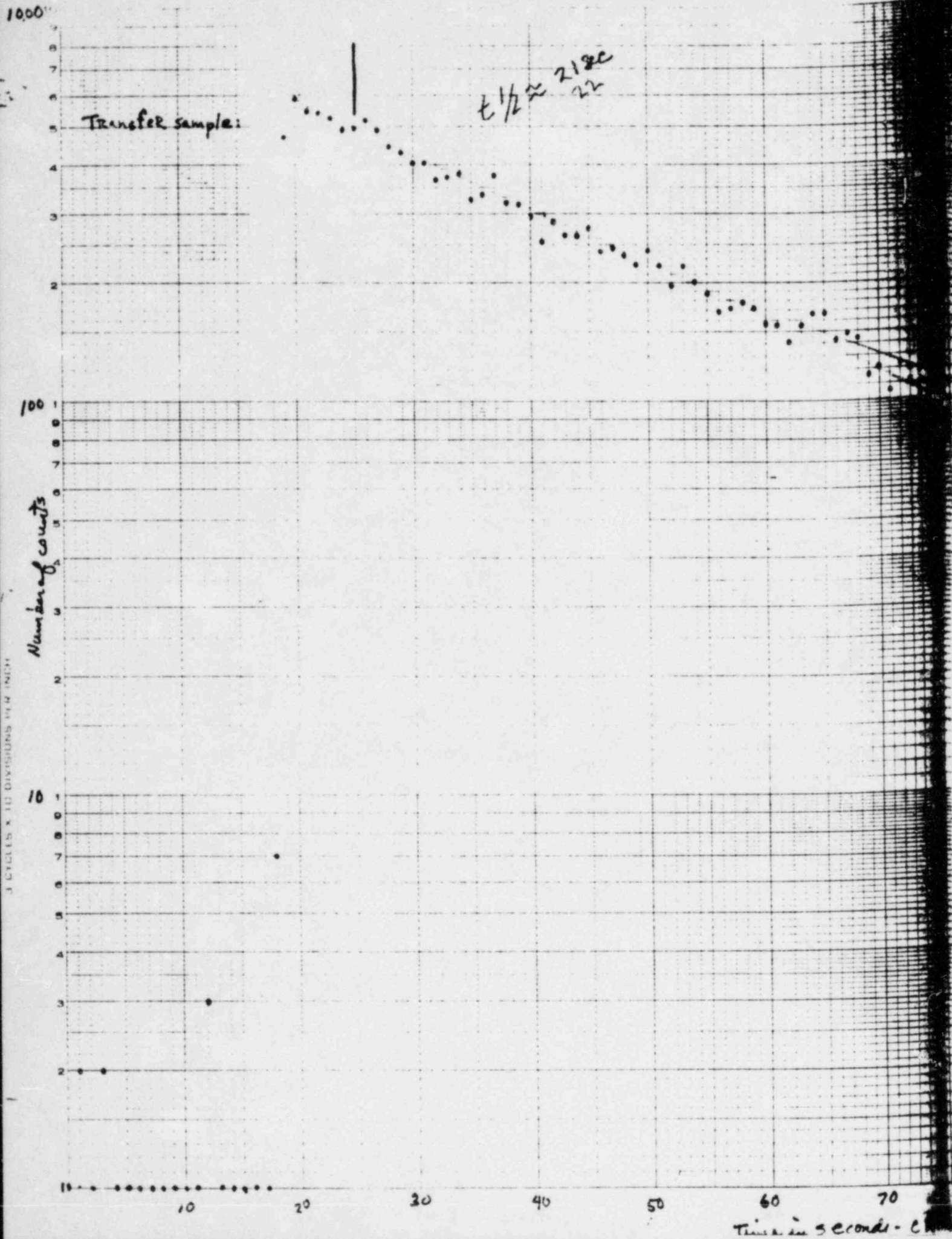
600 REM
610 REM
620 START.COUNT.RATE = REAL.COUNT * LANDA / (1 - EXP(-LANDA * COUNT.PERIOD))
630 REM
640 REM      CORRECT COUNT RATE FOR DETECTOR EFFICIENCY
650 REM
660 REAL.START.COUNT.RATE = START.COUNT.RATE / EFFICIENCY
670 REM
680 REM
690 REM      CORRECT COUNT RATE TO END OF IRRADIATION
700 REM      COUNT DOES NOT START UNTIL 17 SECONDS AFTER IRRADIATION
710 REM
720 INIT.COUNT.RATE = REAL.START.COUNT.RATE * EXP(LANDA * 17)
730 REM
740 REM      THIS COUNT RATE IS PROPORTIONAL TO THE FLUX
750 NEUTRON.RATE = INIT.COUNT.RATE / NEUTRON.YIELD
760 REM
770 REM
780 REM      THE FLUX IS RELATED TO THE NEUTRON RATE DIVIDED BY THE
790 REM      CROSS SECTION, SIGMA, AND THE NUMBER OF U-235 ATOMS PRESENT
800 REM      SET UP VARIABLES FOR ATOMS AND SIGMA
810 REM      ABUNDANCE OF U-235 IS .71% IN NATURAL STANDARDS
820 REM
830 ABUNDANCE = .0071
840 MOLECULAR.WT = 238.3
850 REM
860 REM      AVAGADRO'S NUMBER IS 6.02 * 1023
870 REM
880 U.235.ATOMS = GRAMS.URANIUM/MOLECULAR.WT*ABUNDANCE*6.02E+23
890 REM
900 REM
910 REM      DEFINE CROSS SECTION FOR U-235 FISSION FROM THERMAL NEUTRONS
920 REM
930 SIGMA = 5.77E-22
940 REM
950 REM
960 REM
970 REM      NOW READY TO CALCULATE FLUX DIRECTLY
980 REM
990 FLUX = NEUTRON.RATE/(SIGMA*U.235.ATOMS*(1-EXP(-LANDA*RAD.TIME)))
1000 REM      LPRINT "COUNT: ";REC.COUNT;" ";
1010 REM      LPRINT "FLUX, n/cm2/sec: ";FLUX;" "; "YIELD FACTOR: ";NEUTRON.YIELD
1020 REM      LPRINT
1030 PRINT "FLUX, N/CM2/SEC: ",FLUX
1040 PRINT "NEUTRON YIELD: ", NEUTRON.YIELD
1050 REM PRINT "  DETECTOR      DELAYED NEUTRONS      SAMPLE      FLUX"
1060 REM PRINT "Dead time Eff. Half Life Yield Counts Grams U n/cm^2/sec"
1070 MASK$ = "00.000000  .0000  00.0  .000000  000000  .000000  00.000000"
1080 LPRINT USING MASK$;DEAD.TIME,EFFICIENCY,HALF.LIFE,NEUTRON.YIELD,REC.COUNT,GRAMS.URANIUM,FLUX
1090 GOTO 165

```

3 June 1973

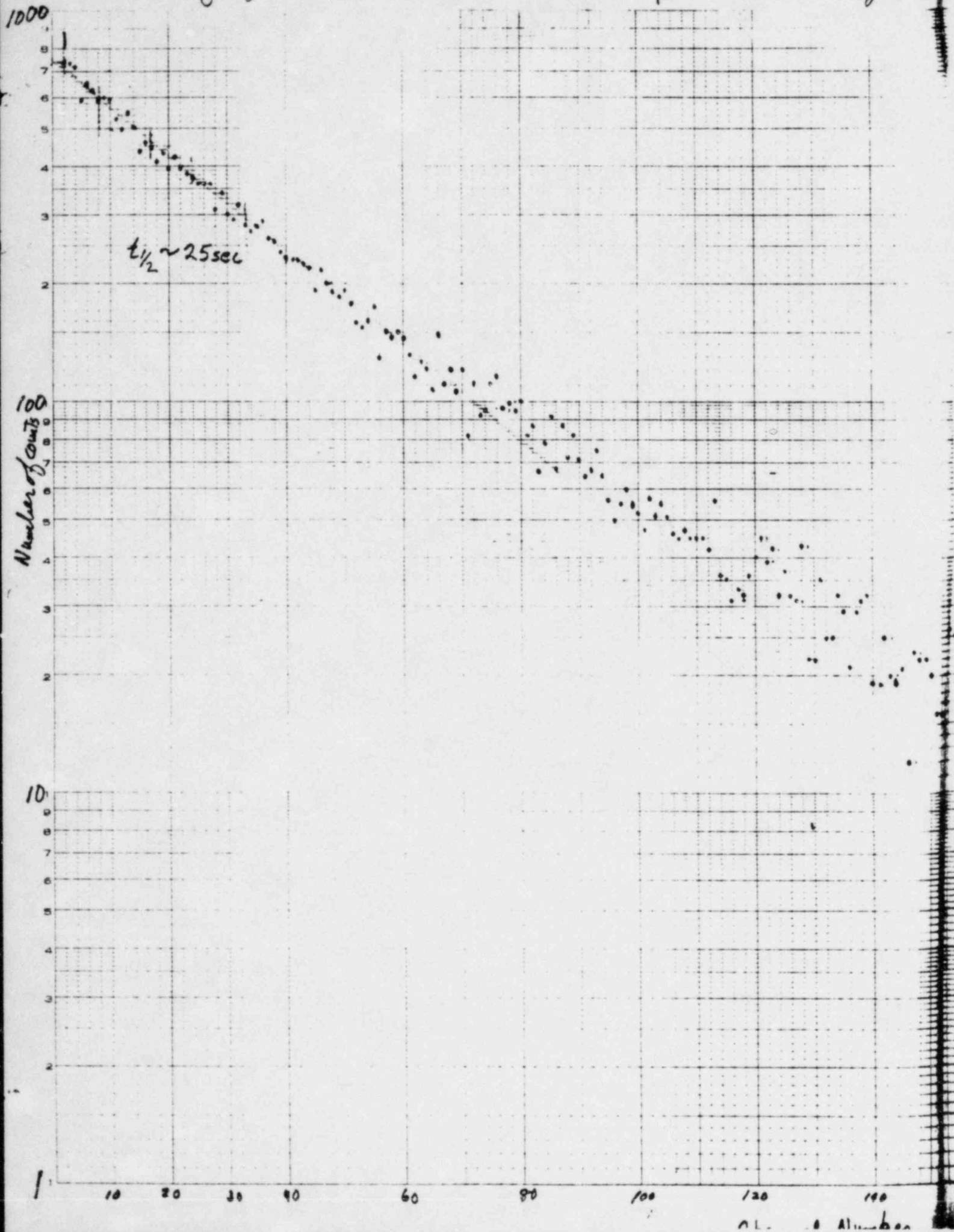
Multi. scaling of Sample K-14, 104.15 mg U

1 channel per sec



Multiscaling of K-9 First Run.

1 second per channel, Begin 25



20 1000
 25 500
 62 250

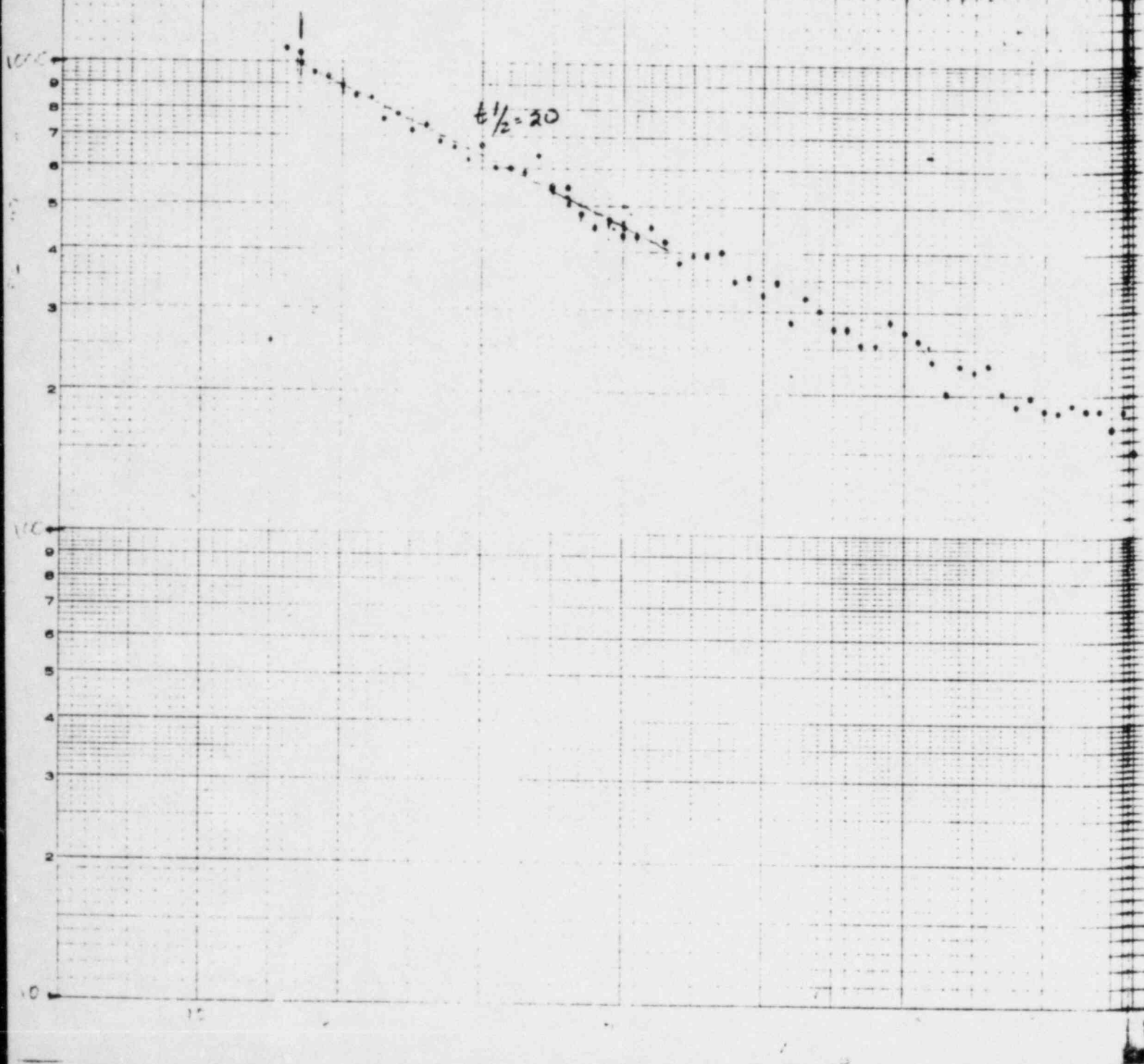


(Table 3-1) for the products of ^{235}U thermal neutron fission. ^{235}U has a large (n, f) cross section (577 barns) for thermalized neutrons. ^{238}U and ^{232}Th can be determined by another technique, fast neutron fission, which was not used in this study.

3.2.2 Equipment

The neutron counter consists of eight BF-3 tubes radially aligned in a paraffin shield. BF-3 tubes (Model 20314, LND, Inc.) are 2 inch diameter by 20 inch sensitive length, stainless-steel tubes, filled to 70 mm Hg pressure with BF_3 . The tubes were arranged in a 10 1/2 inch diameter circle around the sample in a 55-gallon drum, Figure 3-1. A cylinder of low level lead of 7 inch o.d. by 2 1/4 inch i.d. and 12 inch length was situated on centers with the sample and counters to reduce the gamma flux. About 300 lbs of paraffin were used to thermalize the delayed neutrons.

The eight BF_3 tubes were wired in parallel to a junction box leading into an ORTEC 109PC preamplifier. The amplifier was an ORTEC-410 Linear Amplifier which provided the necessary pulse shaping. To discriminate against gammas, a single channel analyzer was used (ORTEC 420) to drive an ORTEC 430 scaler. The scaler was controlled by a CMOS timer. High voltage was supplied by a Power Designs (Model HV-1544) power supply operated at 2000 volts.

Delayed neutrons are also emitted from ^{17}N formed by ^{17}O (^{17}O) (n, p) ^{17}N ; ^{17}N , n, $t_{1/2} = 4.2$ sec) present, and by ^9Li , 0.17 sec. A 25 sec delay at the end of irradiation and before counting allows for minimum interference from ^9Li and ^{17}N , and maximum sensitivity and accuracy. Timing was automatically controlled by the

Table 3-1. Neutron emitting fission
products of ^{235}U

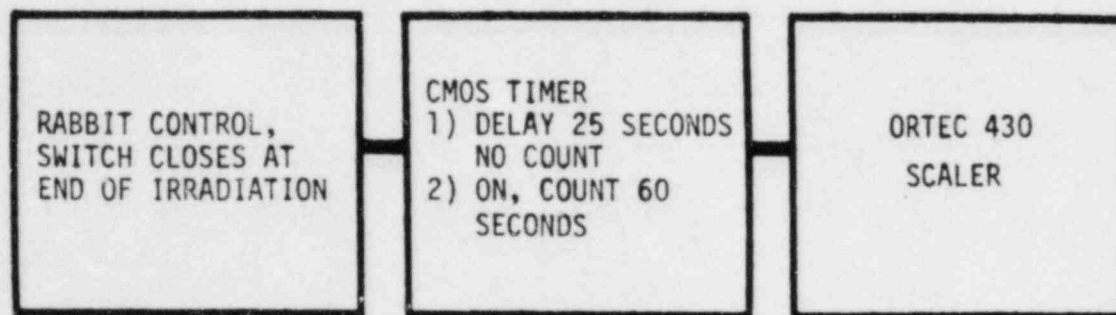
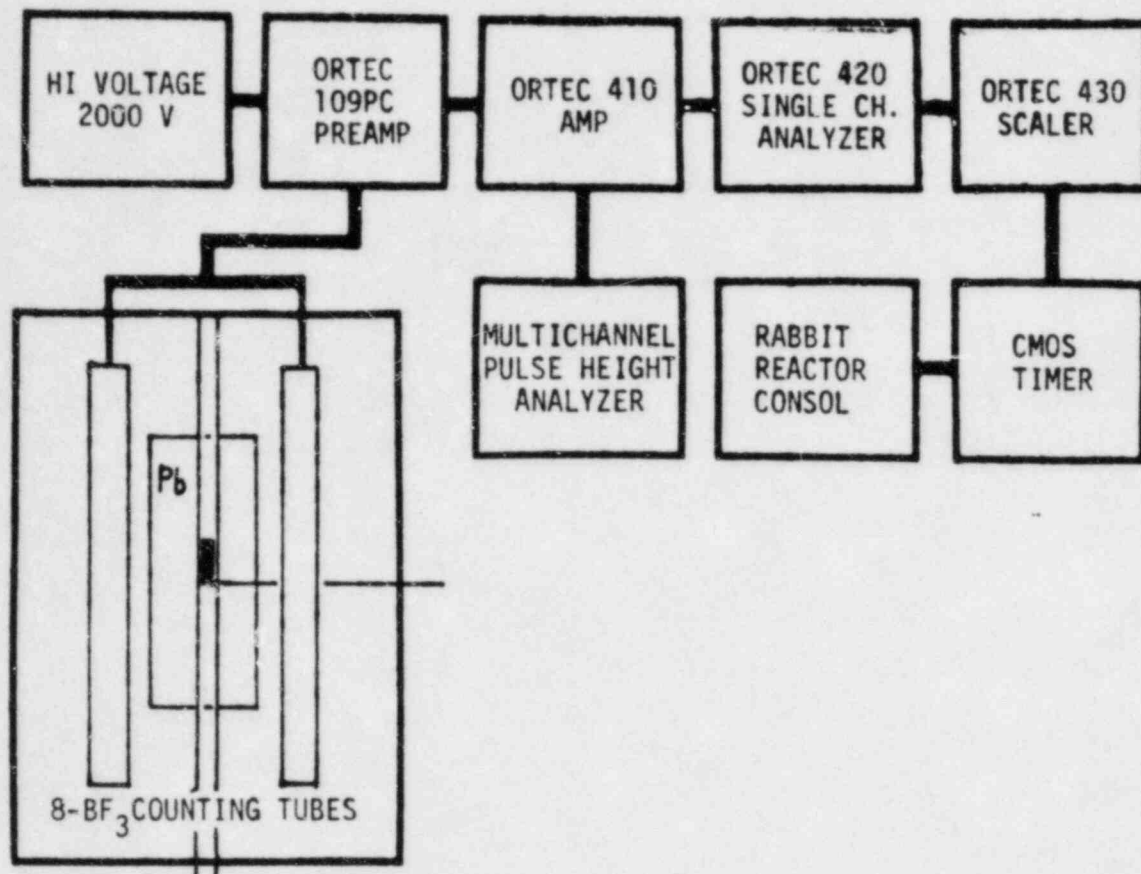
Isotope	$t_{1/2}$	Absolute Yield*
^{87}Br	54.5 sec	0.063
^{137}I	24.4 sec	0.351
^{88}Br	16.3 sec	
^{138}I	6.3 sec	0.310
^{89}Br	4.4 sec	0.672
^{139}I	2.0 sec	
^{90}Br	1.6 sec	
^{85}As	0.43 sec	0.254

Total = 1.65 delayed neutrons/100 fissions

*Neutrons per 100 fissions

Data from Dyer, Emery and Leddicotte (1962).

Figure 3-1. Block diagram of the delayed neutron counting system.



ERROR IN URANIUM DETERMINATION

$\leq 1\%$ for ± 0.25 SEC. (of 60 second count)

0.3 % for ± 0.1 SEC. (of 25 second delay)

REBUTTAL ON CREDIBILITY OF A GRAPHITE FIRE AT THE UCLA REACTOR

Q.1. Respond to CBG's assertions contained in CBG's "Fire Rebuttal" concerning the combustibility of graphite.

A.1. Graphite is commonly regarded as "non-combustible," although, as with other "non-combustibles," under certain conditions it can be made to undergo rapid oxidation. CBG's "Fire Rebuttal," however, obscures the only relevant questions: Under what conditions and at what rate does graphite oxidize? Are such conditions present with the graphite at the UCLA reactor? Considerable experience and research with reactor graphite shows that a self-sustaining and propagating "graphite fire" requires high initiating temperature, sufficient airflow, and little or no heat loss from the oxidizing mass. These conditions cannot be met with the UCLA reactor.

Q.2. Respond to CBG's criticism of the examples used by Dr. Wegst to demonstrate the non-combustibility of graphite.

A.2. Dr. Wegst's statement was that graphite does not burn under "ordinary conditions." The oxidation of the high temperature graphite electrode and the graphite rod under the application of an oxy-acetylene torch is not disputed. CBG misses the relevant point. Despite the extremely high initiating temperatures and the small mass of graphite, when the ignition source is out off the reaction stops. Neither one exhibits self-sustaining and propagating combustion. Quoting from one of CBG's references the following is noted concerning the oxidation of

a carbon arc electrode operating in the open air with a tip temperature of 4000⁰K: "When the arc current is interrupted, the electrode cools. Self-sustained combustion does not occur, even after heating to high temperatures." (Mantell, op. cit., p. 349.)

Q.3. Of what significance is the Windscale reactor accident.

A.3. CBG cites the graphite fire that occurred at Windscale, England in 1957 as an example of what could occur at the UCLA Reactor. That is nonsense. The reactors have nothing in common except the use of graphite. The Windscale reactor was a huge block of graphite and fuel; it has 500 times the volume of the UCLA reactor. The Windscale reactor consisted of natural uranium fuel rods in long channels in an evenly distributed array throughout the graphite moderator. The highly-enriched plate-type fuel in the UCLA reactor is water-moderated and concentrated in two rows of fuel boxes in the center of the graphite mass. The neutron spectrum at Windscale was considerably more energetic than at UCLA where the water moderation greatly reduces the fast-to-thermal neutron ratio. As a result, for the same thermal neutron flux at the two reactors, the graphite damage per unit volume at Windscale would be far greater than at UCLA. Moreover, the graphite damage in the Windscale reactor would affect the entire core. With the UCLA reactor the damage would not only be much less but also it would be confined to the area around the fuel boxes. The table on the following page lists the other fundamental differences between Windscale and UCLA and indicates the significance of the differences relative to the possibility of a graphite fire.

A COMPARISON OF GRAPHITE FIRE POTENTIAL: WINDSCALE AND UCLA

<u>WINDSCALE</u>	<u>UCLA</u>
1) Graphite cube approximately 50 feet by 50 feet by 25 feet. Area/vol. = 0.18 Effect: Internal heat escapes from UCLA 10x faster than from Windscale.	Graphite approximately 5 feet on a side. Area/vol. = 1.2
2) Graphite penetrated by many holes for fuel and cooling air. Effect: Much greater oxygen supply throughout Windscale graphite pile.	No holes in graphite.
3) Cooling air forcefully pushed through reactor. Effect: Air flow is orders of magnitude lower in UCLA reactor.	Air diffusing into reactor collected by small bleed line.
4) Reactor cooling channels directly connected to 400 foot stack (40 ft. diameter). Effect: No way that convection currents (either from a stack induced draft or fire induced draft) can be established at UCLA.	No air cooling channels in graphite or reactor. Bleed air flows through 3/4" pipe.
5) Graphite preheated by operating reactor to at least 400°C. Effect: Exothermic oxygen-graphite reaction requires preheating graphite to at least 650°C.	<u>Impossible</u> to use reactor to raise graphite temperature to greater than 105°C.
6) Initially, "fire" was due to U metal and possibly Li/Mg cartridges, hence further raising graphite temperature. Effect: Insufficient energy to preheat graphite to "ignition" temperature.	No credible way U metal fire could occur. No Li/Mg cartridges in UCLA reactor.
7) During accident, air forced through graphite in attempt to cool it. Effect: Subsequent research showed that large amounts of air are needed to cause graphite to sustain combustion. This leads to peculiar case that graphite temperature falls when coolant air is reduced.	No analogous situation.

SUMMARY: There is no source of energy in or around the UCLA reactor of sufficient magnitude to preheat graphite to the minimum combustion temperature of 650°C. Further, there is no way that sufficient air supply could reach hot graphite, since air must be forced over the hot graphite surface to sustain combustion (smoldering).

Q.4. Describe the graphite oxidation reaction.

A.4. When graphite oxidizes in air, the graphite (carbon) atoms do not vaporize and leave the surface of the solid. In order for graphite to oxidize, oxygen must diffuse across any gaseous boundary layer (CO and CO₂) that may exist and then diffuse into the graphite solid. It is for this reason that the oxidizing gas must be moving across the graphite surface to provide the force necessary to break through the gaseous boundary layer above the surface of oxidizing graphite. Further, it is in this sense that the oxidation of graphite is similar to the rusting of iron. Both are surface reactions, and in both cases the oxygen must diffuse into the solid surface before oxidation can occur. The rates of reaction are irrelevant. However, in some cases the reaction rates are probably not orders of magnitude different. For example, it is reported that the oxidation of graphite at 350°C produces a weight loss of only 0.4% after more than 60 days. To quote from one of the references cited by CBG: "In the range 400 to 650°C, the oxidation is primarily penetrative. The weight loss is greater than the volume loss. At higher temperatures the oxidation is diffusion-controlled with oxidation taking place at the outside surface, and oxidation is sensitive to air velocity." (Mantell, Carbon and Graphite Handbook, p. 351.) Quoting from another of CBG's references: "On the other hand diffusional control of the oxidation reaction begins to have an effect at higher rates of oxidation and materially raises the temperature at which self-sustaining oxidation can arise." (Nairn and Wilkinson, "The Predictions of Conditions for Self-Sustaining Graphite Combustion in Air"; emphasis added.)

Q.5. What is the significance of graphite contamination?

A.5. It is true that contaminants on the graphite can increase oxidation rates. However, the magnitude of this affect as a function of contaminant concentration is not well known. The Nairn article cited by CBG does not specify the concentration of solutions in which the graphite was soaked prior to measuring the effect on the oxidation rate. It is worth noting that the samples were soaked in various aqueous solutions containing the impurity and that the samples were small (hence they had a large surface to volume ratio). It is well known that the oxidation rate of graphite is dependent on the surface-to-volume ratio and whether the effects of contaminants on small samples scale directly to large samples (with much smaller surface-to-volume ratios) is uncertain. However, we are again talking about a surface affect and any increased oxidation rate will quickly disappear as the surface contaminant is removed by oxidation. Note that the Nairn article does state that "the depth of penetration in the case of graphite exposed to burning magnesium in a combustion experiment was so small (much less than 1/8 in.) that the average increase for the block as a whole was only 30 percent." It is very unlikely that the graphite in the UCLA reactor has become contaminated to any significant extent because contamination would show up in a decline of reflector properties and loss of reactivity. In any case, contamination would be a surface effect and would not be a factor in sustaining oxidation.

Q.6. What about the irradiation effects on oxidation rate claimed by CBG.

A.6. CBG claims that "other studies" have found an 18-fold increase in the oxidation rate due to irradiation. However, CBG neglects to mention that the samples were irradiated to a total thermal neutron fluence of 4×10^{20} nvt. The UCLA reactor operating at full power for 40 years under the license limitation of 5% of the year (440 hours) will generate a total thermal neutron fluence of about 1×10^{20} nvt. CBG fails to mention that the samples were very small (1/8" in diameter by 2 in. long), hence the neutron damage to the sample was essentially uniform throughout the volume. In the UCLA reactor, the thick (4") stringers of graphite would suffer maximum neutron damage only near the surface, with much less damage deeper into the graphite volume. Moreover, it is the fast flux that causes the damage and as Ostrander has shown less than 15% of the fast neutron energy reaches the graphite in the UCLA reactor which is to be compared to graphite moderated reactors and to experiments where all of the damaging fast neutron energy is transferred to the graphite. CBG fails to mention that the oxidation experiments they cite were done at 300°C and that raising the oxidation temperature to 450°C reduces the effect by a factor of 2 or 3. It is known that all of the radiation damage effects in graphite anneal out at higher temperatures. Therefore, the radiation effects in graphite subjected to the high temperatures of a fire would be greatly reduced from the magnitude measured at 300°C. Kosiba and Dienes have shown that the ratio of the oxidation rate of irradiated to unirradiated graphite at 450°C is only 2.3. When one

corrects for the ratio of total nvt exposure (4×10^{20} vs 1×10^{20} after 40 years of UCLA operation), the effect becomes negligible.

Q.7. What about the reduction in thermal conductivity due to radiation damage claimed by CBG.

A.7. The reduction in thermal conductivity due to irradiation is also cited by CBG as an effect that would make it easier to ignite graphite in a fire scenario. However, they again omit many important facts and quote a figure ("roughly twenty-fold") that has no relevance to UCLA. For example, the experiments described by Woods indicate that graphite irradiated at 25°C to a total thermal neutron fluence of 1.55×10^{20} nvt (the lowest dose used in these experiments) showed a decrease in thermal conductivity of a factor of 16. (Woods, et al, "Irradiation Damage to Artificial Graphite", Peaceful Uses of Atomic Energy, Proceedings of International Conference in Geneva, Vol. 7 (1955).) It would require 65 years of operation of the UCLA reactor at 440 full power hours per year to reach this dose. The same reference indicates that the radiation damage to graphite is highly dependent on the temperature during irradiation and that, "irradiation at 150°C effects an order-of-magnitude reduction in the changes of most physical properties compared with those incurred by irradiating at 30°C ." Based on this data it could be estimated that at the UCLA reactor temperature of 75°C the overall effect would be reduced by a factor of about 3. (Figure 5 in Woods shows a factor of about 2 reduction from irradiation at 30°C to 80°C .) However, again the important fact is that in the UCLA reactor, contrasted with experimental conditions and

empirical data from graphite reactors, less than 15% of the energetic, damaging flux reaches the graphite due to water moderation effects.

Further, there is an annealing which occurs as the graphite temperature is raised after irradiation. At 400°C the overall change in thermal conductivity drops to about 2 (for UCLA total nvt dose) and at 600°C the ratio drops to about 1.5 (Woods, et al, pg. 470, fig. 44). Thus, combining the lower UCLA dose (approximately 1.0×10^{20} nvt in 40 years), with the higher irradiation temperature (75°C vs 30°C), and with the effect of annealing as external fire temperatures heat the graphite, the overall effect on thermal conductivity would be negligible. Note that the effect of irradiation temperature quoted above would also apply to the magnitude of the oxidation rate increases due to radiation damage. Results obtained from irradiations done at temperatures of 30°C would be significantly reduced at the UCLA reactor operating temperature of 75°C.

Finally, it must be recognized that whatever radiation damage effects there are in the UCLA reactor they are confined to the small volume of graphite adjacent to the fuel boxes (including the graphite island). The irradiated volume of approximately 620 pounds is only 6% of the total graphite in the reactor. The remaining graphite, including the thermal column suffers no radiation damage.

Q.8. Could you summerize the radiation damage and contamination effects relative to the possibility of a graphite fire in the UCLA reactor?

A.8. It must be emphasized that the many studies done to determine changes in thermal conductivity and oxidation rate vs. radiation dose, and those on oxidation rate vs. contamination, were all directed toward elucidating the properties of the long term slow oxidation of graphite that occurs in gas cooled, graphite reactors operating at relatively low temperatures. The test samples were always small (often only 1/8" diam.) and the post-irradiation tests were done at graphite temperatures below 450°C. The magnitude of the radiation damage effects steadily decreases as the temperature of the graphite is raised (due to annealing of the damage done to the crystalline lattice). The radiation damage studies were not directed at determining the bulk properties of graphite at temperatures where self-sustaining oxidation might occur (650°C). However, some of the experiments did show that annealing at temperatures above 600°C reduced the radiation damage affects by factors of up to 5. Further, as far as can be determined, no attempt was made to try to scale the effects from small samples with large surface to volume ratios, to large samples with small surface-to-volume ratios. Because of the surface nature of the oxidation of graphite and the importance of the diffusion rate of oxygen into the graphite, it is recognized that scaling from small to large samples at high rates of oxidation is not linear and that surface affects are relatively more important in small samples than in large samples. Therefore one would expect radiation effects in large volumes of graphite to be proportionately less than

in small samples. More importantly, any empirical data derived from graphite-moderated systems on radiation damage effects will greatly over-predict the effects in the UCLA reactor where, because of the water moderation: 85% of the fast neutron energy (the damaging flux) never reaches the graphite.

Q.9. Please respond to CBG's claims that the graphite blocks in the UCLA reactor are stacked like "logs" with significant air gaps present.

A.9. To liken the graphite stringers (or blocks) in the UCLA reactor to logs or charcoal briquettes, is simply ludicrous. The graphite stringers are carefully machined and stacked tightly together. Their own weight and the additional weight of lead shielding above the core compresses the graphite stack, squeezing the stringers closely together. If there were appreciable gaps between the stringers (particularly near the fuel), the reactor would not work due to loss of neutrons in the reflector. The stringers fit so tightly that one in the middle of the stack cannot be pulled out without unpiling the stack (even though graphite is an excellent lubricant). The tight fit of these blocks can be seen in photographs of the reactor core. The graphite stringers in the UCLA reactor do not have air gaps between them, contrary to CBG's claims.

It is true that the stringers next to the fuel boxes are stacked vertically. However, they are pushed tightly together as evidenced by the fact that they work as an efficient neutron reflector. If there were visible air gaps, the effectiveness of the graphite as a

reflector would be greatly reduced and this reduced effectiveness would be observable. Further, the entire top of the reactor including the graphite stringers close to the fuel boxes is covered with a horizontal layer of lead bricks which block any vertical channels. Thus the chimney effects claimed by the Intervenor could not occur. It is also interesting to note that lead melts at 327°C . Any event in the vicinity of the core that raised the graphite to anywhere near the self-sustaining oxidation temperature of 650°C , would have long since melted the lead, effectively plugging all of the imaginary air channels between the graphite stringers near the core.

Q.10. Respond to CBG's claim that the reactor is a porous structure which permits substantial air flow.

A.10. To characterize the reactor, as CBG has done, as a porous structure of graphite blocks is patently ridiculous. The UCLA reactor is not like a gas-cooled graphite reactor in which the entire graphite mass is penetrated by many holes for fuel cartridges and cooling air passages.

The Battelle study does quote an airflow figure of 250 cfm for the generic Argonaut UTR reactor class. However, at the UCLA reactor the actual flow rate is currently about 50 cubic feet per hour and in the past has been as high as 300 cfh. Since we are discussing the UCLA reactor and not a generic class of reactors, we use the flow rates applicable to the UCLA reactor. It should be pointed out what Professor Robkin actually said in the Battelle study. "Most of the air flows between the graphite and the shield, with little flow

between the individual graphite stringers, and the airflow rates range up to 250 cfm." Incidentally, in a phone conversation with Professor Robkin, he has agreed that the high thermal conductivity and large thermal inertia of the pile of reactor graphite would make it extremely difficult if not impossible to ignite the graphite with a fire external to the graphite stack.

The gap size in the Dahl burning rig experiments was 0.125 inches. The gaps around the graphite stack in the UCLA reactor are of this order of magnitude, but the cracks between the graphite block are at least two orders of magnitude smaller. CBG mentions the adiabatic conditions of the Dahl experiment as simulating the conditions inside a large mass of hot graphite. They are correct, but they fail to mention that the graphite in the Dahl experiment had to be preheated to hundreds of degrees Celsius before a self-sustaining oxidation reaction could be started, even using preheated air for oxidation. No one has identified any method for preheating the UCLA graphite stack to 650°C. The reactor certainly couldn't do it, since water boils at 100°C, at which point the reactor shuts down.

Q.11. Respond to CBG's claims about credible means for initiating a graphite fire.

A.11. In his previous testimony Dr. Wegst stated that any solvent running down between the cracks in the concrete shield would be cooled well below the ignition point. This statement, of course, is not contradicted by CBG's claim that a pool of solvent on top of the

shield (or a stream of gasoline in the street) would continue to burn. There is no dispute that a pool of solvent on top of the reactor shield could burn. The point is that solvent running down small cracks between massive concrete blocks would not burn -- both due to the cooling effect of the concrete and lack of oxygen.

Heating of one surface of the graphite stack by an external fire would tend to draw air toward the fire, hence away from the graphite. In this case, convection currents would not draw hot air toward the graphite. Emphasizing again that graphite does not vaporize until extremely high temperatures and hence the oxidation reaction must occur on the surface, it is not reasonable that a fire external to any one side of the graphite could "ignite" the pile.

CBG claims that the Battelle study finds a graphite fire to be "credible." In fact, the following statement was made in the summary of that study. "A graphite fire can be postulated from many different scenarios, including a major building fire. Given an initiating event, such a fire could result in core melting and fission product release. However, except for a major building conflagration with essentially no suppression, itself a highly unlikely event, there appear to be no credible initiating events," (emphasis added). Therefore, it appears that Professor Robkin and the UCLA staff agree on all aspects of this question, except the potential for a building fire initiating a graphite fire.

Q.12. Could a major building fire lead to a graphite fire.

A.12. No. The thick concrete shielding offers significant protection. The thermal inertia of the graphite is very large and it would take a very long and very hot fire to heat the stack to the point where self-sustaining oxidation would occur. In any case, there is insufficient airflow into, around and through the graphite stringers. The reactor shield tank contains 2700 gallons of water in direct contact with the graphite. This tank would not be removed, even in the case of shield blocks being removed (partially open shielding) and 2700 gallons of water represents an additional very large thermal sink that would help keep the graphite well below the so-called ignition temperature of 650°C . Finally, the temperatures in a building fire seldom reach 1000°C , even after two hours of uninterrupted burning and that temperature is considerably below the melting point of concrete.

REBUTTAL ON CREDIBILITY OF CBG'S FISSION PRODUCT RELEASE MODEL

Q.1. Please respond to Professor Anderson's criticism of Professor Olander's testimony on the fission product release fraction to be assumed in a fuel-handling or core-crushing accident.

A.1. Professor Anderson seeks to dismiss Professor Olander's testimony on the conservatism of the Hawley release fraction calculation (NUREG/CR-2079, the "Battelle Study", pp. 44-51) as irrelevant because "he is analyzing the wrong accident and the wrong release mechanism" (CBG "Fuel Handling/Core-Crushing Rebuttal", p.2). Anderson characterizes Hawley's calculation as an attempt to model the maximum surface area of fuel plates that could be exposed in a severe accident and the "skin depth" from which releases of all the noble gases and iodines would occur. Anderson criticizes Olander for regarding Hawley's model as an attempt to represent "actual physical phenomena rather than modelling parameters" (id.). Anderson concedes that there could be no release by recoil during fuel handling; he views Hawley's calculation as indicating only an "equivalent" release fraction. Anderson's criticism is without merit.

The Battelle Study was intended as an analysis of credible accidents for Argonaut reactors. The study concludes that a fuel-handling accident scenario appeared to be the only realistic postulated accident that might result in significant fission product releases. The calculated release and dose assessments, although

conservative, were intended to be based on a realistic release mechanism. As the Battelle Study states:

"The amount of activity released would depend on circumstances of the accident, primarily on the temperature and exposed surface area of the fuel. Following normal operation even at full power, the fuel temperature would be low and diffusion would be essentially zero. Hence, any release of fission products would be from the surface of the fuel, through kinetic energy imparted by the fission fragment recoil. This places a finite limit on the range of the recoil." (p. 46; emphasis added.)

It seems clear that the Battelle Study was postulating a realistic release mechanism. Regardless, for the analysis of credible accidents it is necessary to relate the postulated "model" to what is known about actual releases from metal fuels.

The substance of Professor Olander's testimony is that there is no credible release mechanism outside of melting that can result in fission product releases from the UCLA plate-type fuel on the order of magnitude suggested by the Hawley calculation. Professor Olander concludes that the fission product release estimates calculated by Hawley are extremely conservative, representing severe upper limits on fission product releases that could actually result from any fuel-handling or core-crushing accident. Hawley's "equivalent" release fraction is very conservative with respect to all real mechanisms of release.

Hawley's calculations were not based on any description of the physics and chemistry of the processes that take place in plate-type fuel. The purpose of Olander's testimony was to examine the actual physical principles that govern the interactions of ions with solids, the structure and properties of the UCLA fuel and realistic mechanisms for fission gas release from such fuels. The conservatism of Hawley's model depends on the degree to which it corresponds with actual physical reality. Olander expressly intended to relate the model to the empirical evidence that has accumulated during the past twenty-five years of experience and research with nuclear metal fuels.

Q.2. Please analyze the model for fission product releases proposed by Professor Anderson and his graduate student Ms. Reid.

A.2. The model proposed by Professor Anderson and Ms. Reid is based on the assumption that gas bubbles exist within the aluminum-uranium crystals of the UCLA fuel. Having postulated the existence of the bubbles, Anderson and Reid postulated the mechanism for the release of the gases that are assumed to accumulate in the bubbles. The bubbles are assumed to interconnect under stress to produce microcracking in the material, depending on the size and density of the bubbles, strength of the material and other things that the model would propose to calculate. Reid conceded that the model does not explain how the bubbles got in the crystal but just how they behave based largely on the anisotropy of the UAl_4 lattice structure. Although this part of the model is not clear, apparently the bubble

dislocations in the lattice are assumed to migrate out of the lattice by microdiffusion after prolonged periods of irradiation of the material. Reid proposed several techniques for measuring these bubbles that are supposed to exist in the UAl_4 particles. No calculations nor empirical data were presented. The only evidence presented that was supposed to suggest the existence of bubbles in the UCLA aluminum plate-type fuel consisted of certain electron micrographs that Ms. Reid claimed demonstrated that fission tracks could be found in the fuel.

There is no empirical basis for the model of fission product releases proposed for the UCLA fuel by Anderson and Reid. The model is based instead on speculations about phenomena that may exist under certain conditions in highly irradiated fuel in reactors operating at temperature extremes and under other conditions not relevant to the case of the UCLA fuel. Even as applied to highly irradiated fuels the model is contradicted by the available empirical evidence. The model proposed by Anderson and Reid to explain fission product releases in the UCLA fuel is flawed for several other reasons.

In the first place the assumption that the products of a fission event in the UAl_4 crystals will exist as gases in bubbles is without empirical support. The fission fragments come off as atoms of material. They do not form gases unless they can combine as gas molecules (in the case of the iodines) and will not form microbubbles until hundreds of thousands of these gas molecules coalesce. The products of a

fission event form single atom dislocations in the lattice structure of the crystal. They do not migrate and they do not coalesce to form bubbles. The only way fission products can escape the UAL_4 crystals is by recoil during fissioning in which case the fragments become implanted in the matrix material. After fissioning stops nothing escapes the intermetallic compound UAL_4 .

In particular, each escaping iodine atom will plunge into a sea of aluminum atoms with which it combines readily as aluminum iodine, which remains buried in the matrix. In this "implantation", where a single iodine atom is swallowed in a sea of aluminum as distinguished from bulk reactions between aluminum and iodine, there is no opportunity for an iodine gas molecule to form. The only way the iodine can be released is by the melting of the fuel. Even in that case competition between the vapor pressures of the aluminum-iodide and the matrix material tends to reduce the emissions of iodine gas. Certainly under non-molten conditions there is no mechanism for release.

Secondly, the proposed model apparently assumes matrix material will be subject to microcracking along the lines of fission track tunnels. Ms. Reid apparently relies on the existence of fission track "tunnels" for molecules to collect as gases for eventual escape. However, tunnel-like effects can only be produced in dielectrics and

not in conductors like aluminum which have free electrons available. The paths traveled by the fission fragments through the aluminum lattice are immediately annealed out. Ms. Reid is mistaken in relying on the electron micrographs she identified as evidence of such tunnels. The tracks formed in the thin metal films that have been vaporized are not gas bubbles at all but an absence of material that results when the surface of the film melts and surface tension pulls in the solidifying material forming tracks along the path of the fragment. The tracks are not the result of gases blowing the material up, but instead are due solely to heating effects: the heat applied to the small volume of material greatly exceeds the boiling point of the material and it evaporates. The track represents the path the particle takes in heating up the material. In bulk material (a fuel plate) the heat capacity is too great to permit vaporization. When the material is irradiated in bulk first, then thinned down by etching and submitted to transmission electron microscopy, no fission tracks are identified. The bulk material that has been irradiated first then thinned down exhibits the same "fat" grain structure that is seen in all wrought materials. In contrast, the grain structure in the vaporized film experiments is very fine, almost amorphous and the lattice structure it tends to pick up is that of the underlying material (generally NaCl, in the identified micrographs). The bulk material never reaches vaporization temperatures and therefore will never exhibit the "fission tracks" that result from "thin film" vaporization experiments.

Even if tunnels, gaps, or other voids are assumed to exist in the matrix material, the empirical evidence is that the fission fragments do not collect in the void space but instead traverse the space and become implanted in the matrix. "Catcher-foil" experiments with various types of ceramic and metal fuels demonstrate that the vast majority of fission products become buried in the foils and are not released. But there is no empirical evidence to support the existence of fission tracks in the aluminum matrix fuel in use at UCLA. "Microcracking" could occur in the brittle UAl_4 particles, but there is no mechanism for extending the microcracking into the aluminum matrix.

Thirdly, the model proposed by Anderson and Reid is concerned with how the fission fragments get out of the intermetallic UAl_4 . It overlooks the characteristics of the matrix material and fails to explain how the fission products escape the matrix material. The UAl_4 crystals (the "raisins") represent about 2% of the volume of the aluminum matrix fuel meat (the "cake"). The fuel meat is 40 mils thick (approximately 1000 microns). Aluminum cladding adds 15 mils to each side of the meat. The range of fission fragment recoil in the aluminum matrix material is about 14 microns. The range of recoil within the intermetallic UAl_4 crystals would be considerably less. The extremely ductile and malleable aluminum matrix material will be little affected by the fissioning that occurs in the UAl_4 crystals. Fission products that escape the crystals will become buried in the matrix material. The volume of material affected by

the fission events will remain very small relative to the total material. Microcracking, even if it existed outside of the UAL₄ could not extend across the volume of the matrix material. But the concern with "equivalent" surface area exposed in an accident misses the point. The xenon, krypton and iodine atoms will be implanted in the matrix, unable to disengage and migrate to coalesce and form bubbles. It makes no difference what the surface area is, there is no mechanism for release in the absence of melting. Once the fission fragments become implanted in the aluminum no amount of cutting, slicing, squeezing, or crushing of the fuel plate will result in any significant releases.

Q.3. What about micro-diffusion or thermal-cycling as release mechanisms.

A.3. It has been asserted that radiation damage creates vacancies in the metal lattice which will enhance diffusion of fission products in the material. Such diffusion can only occur in very highly irradiated material and has no relevance to the UCLA fuel with its very low irradiation levels. Moreover, the formation of gas bubbles requires an accumulation of large numbers of atoms. Micro-diffusion of individual atoms in a sea of aluminum cannot result in any significant coalescing of atoms.

It was suggested that "thermal cycling" could cause bubbles to form. The maximum "thermal cycle" for the UCLA fuel is about 75

degrees C. There is no empirical evidence that cycling over that small range has any effects on the fuel.

Q.4. Please respond to CBG's assertion, contradicting Hawley, that the Parker and Creek study (ORNL-3547) indicates that an immediate release from molten fuel of at least 50% of radioiodines and nearly 100% of noble gases would be expected in the case of the UCLA fuel.

A.4. CBG misuses the Parker and Creek study. In the first place the temperatures in the table from the study used by CBG begin at 750 degrees C. Total burnup of the UCLA fuel in the year 2000 will be approximately 1.4% assuming the maximum operating schedule permitted by the license (53 Mwd). More importantly, the Parker and Creek experiments were done with very small fuel samples, less than an inch in diameter and less than 1/10 inch thick. There is a known surface-to-volume ratio effect on the amount of material that gets released. In melting a large piece of material such as a UCLA fuel plate the lump size of the melt is large and the surface-to-volume ratio is much smaller than the experimental samples. As a result the releases from an actual fuel plate are much smaller (an order of magnitude smaller at 750 degrees C, according to George Parker) than the values in the table. Taking surface-to-volume effects and burnup for the UCLA fuel into account Hawley's estimates are not unreasonable.

Q.5. What is the empirical evidence concerning the releases of iodine gas from MTR plate-type fuel.

A.5. There have been few problems with metal plate-type fuel. Most of the empirical evidence relevant to the fission product releases to be expected from plate-type fuel comes from studies of releases in fuel-clad gaps of intact LWR and LMFBR fuels. The empirical data supports the following general conclusion concerning the chemical form of fission product iodine in irradiated fuel.

Alkali metals, located in group I-A of the Periodic Table of the elements, have strong chemical affinities for group VII-A halogens. Thus, sodium, cesium and potassium readily combine with iodine to form iodides. In fact, cesium iodide is one of the most stable compounds of iodine known. (R. L. Ritzman and D. Cubicciotti, "Release Rates in Chemical States of Volatile Fission Products," Proc ANS/ENS Intl Meet Thermal Reactor Safety, Chicago, IL, Aug. 29-Sept. 2, 1982, NUREG/CP-0027 (1983).) Since the fission process produces approximately six times more cesium than iodine, and since the free energy of formation of cesium iodide is quite negative, it could be expected that cesium iodide would be the chemical form of iodine in the gap and plenum of intact fuel pins. (D. R. Olander, "Fundamental Aspects of Nuclear Reactor Fuel Elements," NTIS: Springfield, Virginia, TID-26711-P1 (1976).) Post-irradiation examination of LMFBR fuels have confirmed that iodine does not exist in the elemental state within the fuel rod gas gap and plenum. (W. H. McCarthy, et al, "Performance of Unencapsulated (U,Pu)O₂ Fuel Pins

(Series F3A) Irradiated in EBR-II to 50,000 MWd/Te," General Electric Co, FBRD Report: GEAP 13735 (November 1971); C. A. Guderjahn, "Release of Volatile Fission Products," Rockwell International, Atomics International Division Report: AI-N707-TI-100-011 (1975); M. G. Adamson, "Distribution of Fission Products," in Gen. Elec. Co. LMFBR Program Reference Fuel Studies 2nd Semi-Annual Report: GEAP-14032-4 (1976).) Rather, the iodine is present as cesium iodide. Similar results have been obtained from the electron beam microprobe examination of the crystals deposited on the interior of the cladding from high burnup LWR fuel. (D. Cubicciotti and J. E. Saneki, "Characterization of the Deposits on the Inside Surfaces of LWR Cladding," J. Nuc. Mater. 78, 96 (1970).) A recent NRC research document has suggested that greater than 95% of the iodine inventory in intact LWR fuel rods was in the form of CsI. (M. Silberberg (Coordinator), "Technical Basis for Estimating Fission Product Behavior During LMFBR Accidents," NUREG-0772 (1981).)

Q.6. Will fission product iodine and cesium react chemically with the aluminum in the fuel.

A.6. Yes. When the fission fragments come to rest in the aluminum lattice, they can react with the lattice atoms or with other nearby fission fragments, forming compounds such as AlI_3 and CsI, which have low mobility in the aluminum lattice and low volatility, compared to molecular iodine, when released to the atmosphere.

Q.7. Do the reactor and building structural materials act to remove iodine and cesium fission products from the atmosphere once they have been released from the fuel.

A.7. Yes. If steel or aluminum surfaces are exposed to elemental iodine, it can be expected that the iodine will be removed by chemisorption. Such an effect has been observed in the removal of elemental iodine from helium by unoxidized stainless steel surfaces to form the metal iodides FeI_2 , CrI_2 , and NiI_2 . (A. W. Barsell, et al, "Safety Research on Iodine Plateout During Postulated HTGR Core Heatup Events," General Atomic Co. Report: GA-A-16169 (1980).) In the case of aluminum surfaces it can be expected that iodine will form AlI_3 , which like the other metal iodides has a much lower vapor pressure than molecular iodine and is water soluble.

Fission product cesium and cesium hydroxide (formed by reacting cesium with water or water vapor) corrode both aluminum and stainless steel surfaces by diffusing along grain boundaries and then forming ferrite or chromite compounds. (C. G. Allan and T. A. H. Taylor, "Activity Deposition in DFR Primary Cold Traps," Proc Int Conf Liquid Metal Tech in Energy Production, Champion, PA, 1976, M. H. Cooper (ed), p35, ANS, Hinsdale, IL, CONF-760503-P2 (1976).) The diffusion of cesium into stainless steel has been studied by Sagawa, et al who found a diffusion coefficient of $7.4 \times 10^{-14} \text{ cm}^2/\text{s}$ for cesium on stainless steel at 569 degrees C. (N. Sagawa, et al, "Transport and Deposition of Metals in Sodium-Stainless Steel Systems V: An Experiment

on the Thermal Diffusion of Zinc, Antimony, and Cesium in Liquid Sodium," J. Nuc Sci Tech 12,626 (1975); (N. Sagawa, et al, "Transport and Deposition of Metals in Sodium-Stainless Steel Systems VI: Diffusion of Diffusion of Deposited Radioisotopes in Stainless Steel," J. Nuc Sci Tech, 13,358 (1976).) Simple decontamination with alcohol or water washing will not remove all of the sodium/cesium from the stainless steel surfaces. (H. Feuerstein, et al, "Mechanisms of Release of Radionuclide Products into Liquid-Metal Coolants, Their Transfer Within Circuits and Removal from LMFBRs," Atomic Energy Review 17, #3, 697 (1979).) (For example, analysis of the radioactivity of a control rod lead screw removed from TMI-2 showed that the major activity was cesium. Washing with water removed very little activity, but etching with nitric acid removed much but not all of the activity.) Thus, reactions between iodine and cesium to form CsI in and on the aluminum and steel surfaces could also be expected.

Q.8. Is there any recent evidence relevant to the existence of microcracks or interlinked fission gas bubbles in the irradiated U-Al fuel of the type used in the UCLA reactor?

A.8. Yes, Gerald L. Hofman of the Materials Science Division of the Argonne National Laboratory has been studying dispersion-type research reactor fuels (of which the U-Al fuel is one type) as part of a program supported by the U.S. Department of Energy. Hofman is a specialist on transmission and scanning electron microscopy of irradiated materials, which is one of the specialties of ANL. He has

recently examined highly-irradiated U-Si dispersion fuel for fission gases. In Fig. 1, he shows isolated fission gas bubbles after irradiation to 5×10^{21} fissions/cm³. These are about 400 Å diameter and appear only in the irradiated specimens and are with high probability fission gas bubbles.

On the other hand, the fracture surfaces of U-Al fuel meat specimens following irradiation to 3.5×10^{21} fissions/cm³ show no cavities which can be identified as fission gas bubbles (see Figs. 2 and 3). The large cavities visible in the SEM photos are fabricated pores; they decrease in size with increasing burnup. Figs. 4 and 5 show these pores at higher magnification.

Hofman states that in all of his work with a variety of dispersion fuels (including U-Al), he has found no evidence for the proposed model of "dot-connecting" or microcracks proposed by Ms. Reid. The photographic evidence presented here corroborates our assertion that the irradiation features imagined by Anderson and Reid are just that.

It should be noted that in preparing the specimens for SEM examination the fuel plates had to be fractured. This mechanical process is very similar to the postulated core-crushing accident on which the gas release debate centers. Even with the severe distortion required to fracture the fuel plates in the ANL tests, the purported microcracks do not appear. Neither do fission gas bubbles larger than 400 Å, even though the fuel burnup was one hundred times larger than that of the UCLA reactor.

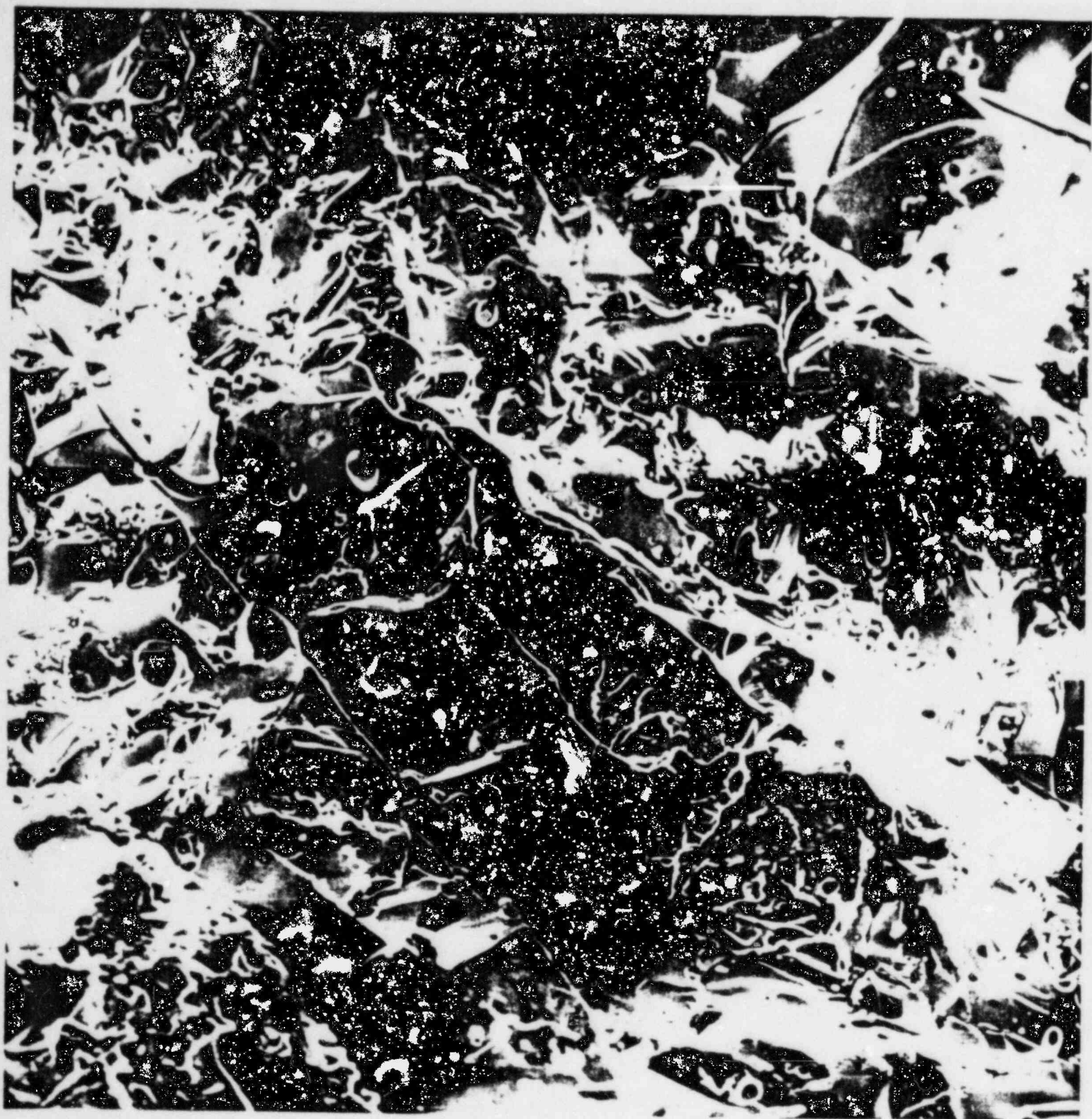
001.0 u |-----|

31.3 20.0 11 214 165

U₃Si

Figure 1 U₃Si

5 x 10⁴ eV Astor 1



18.2

Fracture surface of fuel meat.

U_{Al} (500x)

$\sim 2.5 \times 10^2$ f/s/cc

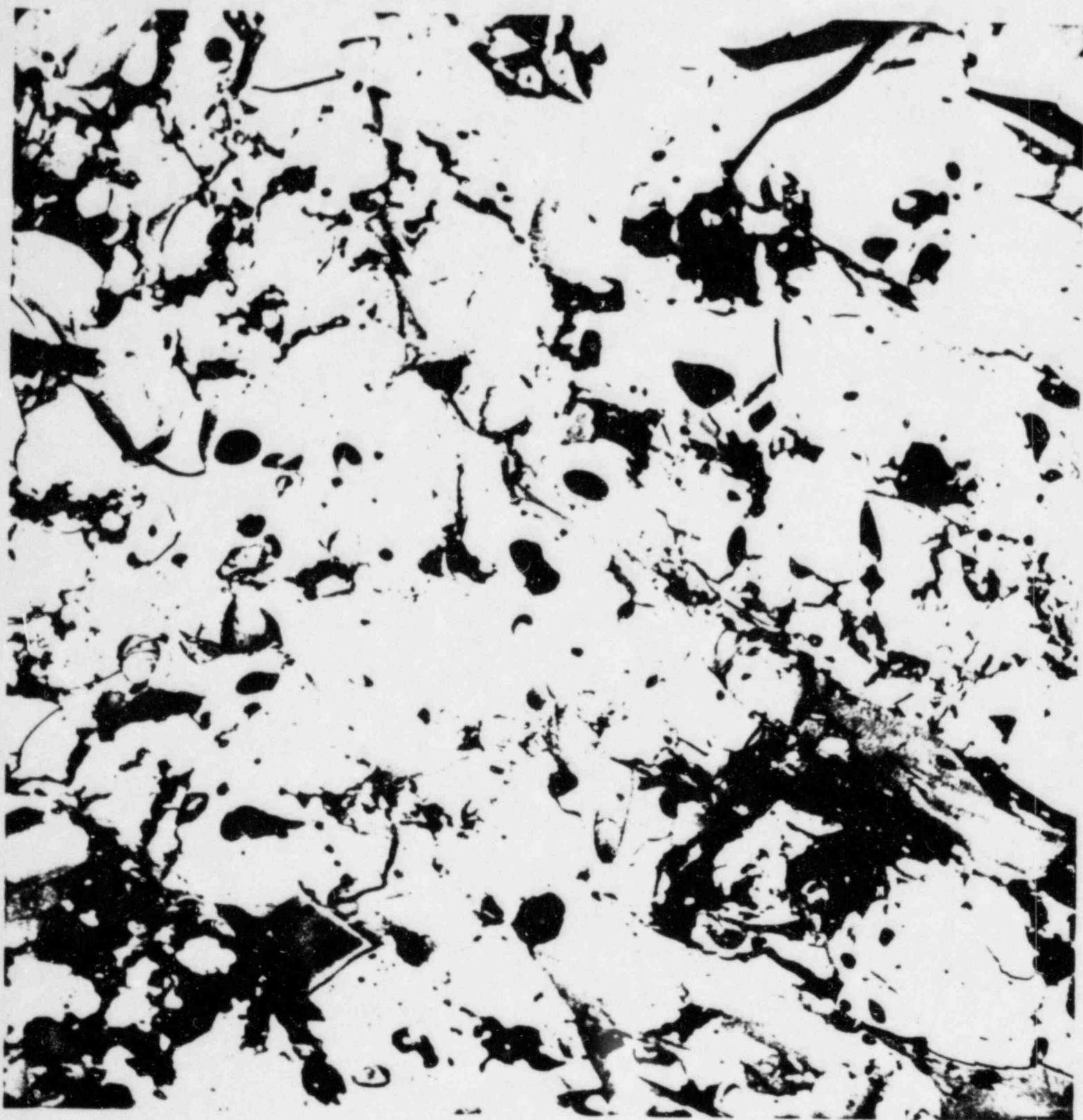


Fig. 3

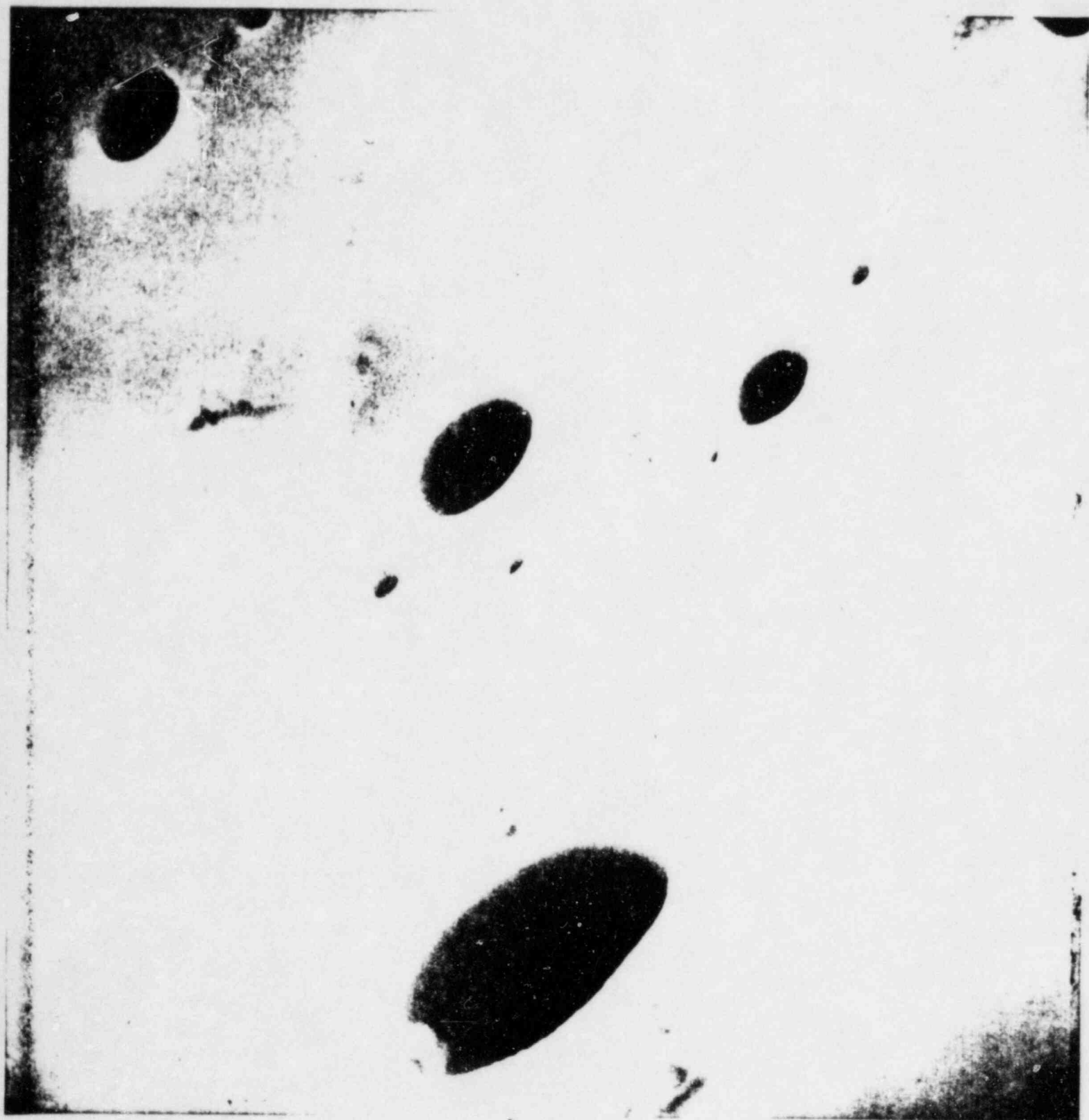
(black = matrix)

Backscatter el. UAl₄ (500x)



Fig. 4

Uth₄ detail (N 2000x)



↑
3 μm diameter

Fig. 5

Uthx detail (10,000x)

REBUTTAL TO CBG's TESTIMONY ON DISPERSION

Q-1 : What are the meteorological conditions at the UCLA reactor site?

A-1: Observations of the meteorological conditions at UCLA show that it is a typical ocean breeze regime. A southwesterly wind ($\bar{V} = 3.36$ m/s) prevails 70% of the daylight hours⁽¹⁾. In the lower atmosphere, both wind speed and direction fluctuate rapidly and randomly in elevation and azimuth. Observed azimuthal fluctuations ($\sigma_A = 29.5^\circ$) classify the UCLA atmosphere as extremely unstable, i.e. stability class "A".⁽²⁾ The UCLA atmosphere is a typical ocean breeze regime in which the air is highly turbulent, gusting with eddys that will distort the plume and produce highly variable local concentrations over periods of 10s to a few minutes.

Q-2: Can the Gaussian plume model be used with confidence under the UCLA site conditions?

A-2: Prof. L. G. Wurtele, UCLA Department of Meteorology has already stated⁽³⁾ that the Turner workbook⁽⁴⁾ formulae are not appropriate to the UCLA situation and cannot be expected to yield reasonable results. Further, a comparison of the Gaussian plume atmospheric dispersion model with validation experiments has shown that the model is extremely unreliable in sea breeze regimes⁽⁵⁾ and under low wind speed, inversion conditions in hilly terrain. UCLA is situated in the foothills of the Santa Monica mountains and faces the Pacific Ocean 12 miles away.

Q-3: Would you comment on Q-8 of the CBG's Panel 4 rebuttal which stated that X/Q is a function of relative dispersion some distance from a source and thus cannot be a measure of dispersion at the source?

A-3: This is another case in which the intervenors exhibit either their technical incompetence or their willingness to obfuscate the issues.

In the wake of large structures such as the UCLA Engineering Building (or a reactor complex such as Rancho Seco) building induced turbulent fluctuations in the atmospheric flow field cause an accelerated rate of dilution of effluent over that predicted by point - source diffusion formulae. Photographs of smoke released from the NEL vent on the roof of the UCLA engineering building show rapid dilution of the plume in a distance of a few meters due to roof top turbulence. Similarly at Rancho Seco, the building induced turbulence diluted the plume much more than predicted by the simple Gaussian plume model.

In addition, the close-in flow field downwind from large structures is "well-mixed" so that X/Q is approximately constant in the range 50 to 200 m down wind.

In the case of the EBR - II₁ complex where the building heights varied from 4 to 29m high, the measured C/Q under inversion conditons at 100 m down wind was identical to that at 200 m down wind⁽⁶⁾ i.e. close-in X/Q was not a function of distance from the source. Similarly, the maximum of 95% cumulative frequency levels of C/Q values were approximately flat from 50 to 120 m for the EOCR and from 80 to 180 m for Rancho Seco. (The upper 5% of the values of C/Q exceeding the 95% cumulative frequency occurred only during F stability conditions.) See Table 1, below.

TABLE 1

Site	Maximum Building Height	Cross Section (m^2)	Stability Class	Region Of Constant X/Q
EBR-II	29 m	665	F	100 - 200 meters
EOCR	22.9m	1090	A to E	50 - 120 meters
Rancho Seco	42.9m	2050	A to E	80 - 180 meters

Sangendorf, et al,⁽⁷⁾ have investigated the near building wind diffusion by means of atmospheric tracer experiments at Rancho Seco⁽⁸⁾ and EOCR⁽⁹⁾. When the plume travel distance from the release location to the samplers was plotted in a scatter diagram against C/Q (the concentration normalized source strength) it was found that for both experiments that the maximum C/Q for A type stability was 2.07×10^{-3} and the maximum C/Q for F type stability was 5.72×10^{-3} . These measurements can be compared with the largest measured X/Q at UCLA⁽¹⁾, $X/Q = 6.98 \times 10^{-3}$ (for a 0.1 minute sampling time) at a distance of 8.2 meters down wind from the stack.

Sangendorf, et al point out "that there is enough turbulence generated close to buildings within a surface boundary or skin layer that values of C/Q much larger than 6×10^{-3} will not be measured for sixty minute averaging times. For shorter averaging times, somewhat larger values may be expected." Thus the relative concentration factor of 7×10^{-3} assumed by the NRC staff is probably conservative by a factor of 3 for the UCLA atmospheric conditions.

REFERENCES

1. M. P. Rubin, "Atmospheric Dispersion of Argon-41 from the UCLA Nuclear Reactor," UCLA Masters Thesis, UCLA School of Engineering (1976).
2. "Answer to Question 8 (8-22-80)", UCLA's September 5, 1980 Response to NRC Questions, UCLA's Exhibit 3.
3. M. G. Wurtele, "The Non-Buoyant-Bent Over Plume," Attached to Answer to Question 8 (8-22-80). Ibid.
4. B. D. Turner, "Workbook of Atmospheric Dispersion Estimates," EPA Publication No. AP-26 (1969).
5. C. A. Little and C. W. Miller, "The Uncertainty Associated with Selected Environmental Transport Models," Oak Ridge National Laboratory Report, ORNL-5528 (1979).
6. C. R. Dickson, et. al., "Aerodynamic Effects of EBR-II Reactor Complex on Effluent Concentration," Nuclear Safety, 10, No. 3, p.228 (1969).
7. J. F. Sagendorf, Jr., et. al., "Near-Building Diffusion From Atmospheric Tracer Experiments," AMS Fourth Symposium on Turbulence, Diffusion and Air Pollution, Reno, Nevada, Jan. 15-18, 1979.
8. G. E. Start, et. al., "Rancho Seco Building Wake Effects on Atmospheric Diffusion," NUREG/CR-0456 (1978).
9. G. E. Start, et. al., "EOCR Building Wake Effects on Atmospheric Diffusion," NOAA Tech. Memo, cited by reference 7 (1978).

Q-4: What is the evidence that molecular iodine attaches to available aerosols and thereafter is transportable only as an aerosol?

A-4: Baurmash, et al⁽¹⁾, have studied the behavior of elemental iodine and NaI(v) in the presence of sodium oxide aerosols produced from a sodium pool fire. In the first experiment, the sodium was contaminated with NaI and heated to 540°C in an inert atmosphere. The molten sodium was exposed to air and allowed to burn as a pool, releasing a mixture of NaI and Na₂O. Both the NaI and the Na₂O evolved at the same rate and, after reaching maximum concentrations, decayed at the same rate. Both compounds took 40 minutes to decay to 50% of their peak concentrations. At six hours, the airborne concentrations for both compounds were 0.5% of their maximum values. The compounds had coagglomerated and behaved as a composite aerosol.

In the second experiment, 148 mg of elemental iodine was first vaporized into the chamber, where it disappeared with a half time of 400 minutes. After 20 minutes, heated liquid sodium in a pan was exposed to the air in the chamber and 0.92 g of sodium were promptly released to the chamber atmosphere as Na₂O aerosols. The iodine vapor fraction fell immediately by a factor of 100, which increased in time to a factor of 1000, demonstrating the rapid scavenging effect of the particulate oxide. After the peak concentration of sodium oxide was reached, both the sodium oxide and iodine concentrations decreased with a sixty minute half time, showing the attachment of the iodine to the particulate.

These two experiments illustrate the fact that in a reactor accident even if the iodine is originally released in elemental form, the iodine transport will be governed by aerosol behavior, not gas behavior.

REFERENCE:

1. L. Baurmash, et al, " Behavior of Iodine in the Presence of Sodium Oxide Aerosols," 11th AEC Air Cleaning Conference, Richland, WA, 31 Aug-3 Sept 1970.
CONF-700816,2, 373 (1970)

Q-5: Do aerosols pass through cracks and crevices as if they were gases?

A-5: No. Aerosols are removed from gas streams as they pass through cracks and crevices. The removal mechanisms include: turbulent impaction, settling, turbulent agglomeration, etc. A recent review⁽¹⁾ suggested that the removal of aerosols in passing through cracks and ducts was so large that, in many cases, the passages would plug gas leak tight. This means that even in the event that the UCLA engineering building collapsed, and crushed the core so that somehow the fission product inventory was released from the fuel, nevertheless only the noble gases would escape from the rubble.

REFERENCE:

1. H. A. Morewitz, " Leakage of Aerosols from Containment Buildings," Health Physics, 42, 195 (1982)

Q-6: What is the evidence that little plutonium would become airborne as a result of a fire involving the Pu-Be source?

A-6a: PLUTONIUM BURNING TEST

A set of glove box experiments on the oxidation in air of 1 to 2 g amounts of vaporized plutonium was carried out at the Argonne National Laboratory⁽¹⁾. The glove box was exhausted at a high rate through a series of HEPA filters. It was found that 5.5×10^{-6} of the plutonium burned was collected as an aerosol on the filters. The average particle size of the plutonium oxide was determined by electron microscopy to be $0.016 \mu\text{m}$.

A-6b: ACCIDENTAL RELEASES OF PLUTONIUM

A number of accidental plutonium releases^(2,3) have occurred over the past thirty years as a result of fires and explosions in plutonium handling facilities. In no case was there more than slight environmental contamination. (See Table 2)

A-6c: WEAPONS SYSTEMS ACCIDENTS

Several accidents involving nuclear weapons also provide information on the dispersal characteristics of plutonium oxide derived from burning plutonium metal in air.

In 1960, a fire occurred at McGuire Air Force Base in New Jersey. A missile containing a nuclear warhead caught fire and both jet fuel and high explosives burned at high temperature for over an hour until the missile bunker was flooded with water. The plutonium metal melted and puddled under the burned out missile. No ground contamination was found beyond 100 ft. from the bunker. Close-in contamination was found associated with the water run-off. No air contamination

was detected⁽³⁾.

In 1966, a B-52 bomber collided with a KC-135 tanker over Palomares, Spain during refueling operations. Four nuclear bombs broke loose and fell to earth. The high explosives on two of the bombs detonated on impact and spread $> 500 \text{ mg/m}^2$ of plutonium over a 160 m diameter, in one case, and a 130 m diameter in the other case. The topsoil from this five acre area of highest contamination was removed and 1200 additional acres of ground was plowed to a depth of ten inches to decontaminate the surface. All determinations for plutonium uptake by the inhabitants of Palomares were negative^(2,3).

In 1968, a B-52 bomber crashed on the sea ice at Bylot Sound near Thule, Greenland. Conventional explosives contained in the four nuclear weapons carried by the bomber and the aircraft fuel produced an explosion and fire that scattered some kilograms of plutonium over a 700 m by 150 m area of sea ice. A cloud of smoke and debris⁽³⁾, estimated by radar to be 850 m high, 800 m long and 800 m in depth rose from the crash site carrying one to five Ci of plutonium and deposited it in uncertain amounts on the sea ice and landscape⁽⁴⁾. A month later, the maximum deposition on the snow measured outside of the impact area was 40 pCi/cm^2 and the geometric mean of all samples was 0.44 pCi/cm^2 (4 mCi/km^2). From this survey it was estimated that the total contamination of the environment outside of the impact area was a few curies of plutonium⁽⁵⁾. Six months later, local sea water contained twice the fall-out background of plutonium. Examination of urine samples of the nearby population showed no traces of plutonium.

In these two aircraft accidents, "The dispersal of appreciable quantities of plutonium did not create a catastrophe in terms of human impairment and death or in terms of property damage, but instead, were incidents that, with modern technology, were brought under rather complete control."⁽²⁾

TABLE 2

Accidental Releases of Plutonium

Date	Site	Amount Pu Metal	Fire/ Explosion/ Overpressure	Contaminated Area	Environmental Release Fract.
12/51	Hanford	1-4g	fire	Inside Bldg	Slight Deposit
1/55	Richland	900g	fire	Inside Bldg	None
9/55	Rocky Flats	80g	fire	Inside Box	None
9/57	Rocky Flats	22kg	fire	Inside Boxes	3×10^{-6}
7/59	LASL	N/A	fire	Inside Room	Vicinity Bldg.
10/65	Rocky Flats	20-30kg	fire	Inside Bldg	Slight
5/69	Rocky Flats	Large	fire	Inside Bldg	3×10^{-8}
5/59	Richland	N/A	explosion	Lab Room	Slight
11/59	ORNL	165g	explosion	2 acres	3.6×10^{-3}
10/64	Miamisberg	17g	explosion	Inside Bldg	Not Detected
11/51	Richland	N/A	overpressure	Inside Bldg	Not Detected
5/61	Miamisberg	N/A	overpressure	Inside Bldg	None
1/65	Livermore	N/A	overpressure	Inside Room	None

REFERENCES:

1. C. L. Cheever, "Recent Air Cleaning Developments at ANL," in Seventh USAEC Air Cleaning Conf. BNL, Oct 10-12, 1961, TID-7627, 308 (1962)
2. H. S. Jordan, "Distribution of Plutonium from Accidents and Field Experiments," Los Alamos Natl Lab Report: LA-4756 (1971)
3. B. W. Wachholz (Comp) "Plutonium and Other Transuranium Elements: Sources, Environmental Distribution, and Biomedical Effects", USAEC Report: WASH-1359 (1974)
4. W. C. Hanson, "Plutonium in Lichen Communities of the Thule, Greenland Region During the Summer of 1968," Health Physics 20, 39 (1971)
5. A. Aarkrog, "Radioecological Investigations of Plutonium in Arctic Marine Environments," Health Physics 20, 31 (1971)



IDO-16883
AEC Research and Development Report
Reactor Technology
TID-4500 (30th Ed.)
Issued: June 1964

REPORT OF THE SPERT I DESTRUCTIVE TEST PROGRAM
ON AN ALUMINUM, PLATE-TYPE, WATER-MODERATED REACTOR

Reported By

R. W. Miller
Alain Sola (Euratom)
R. K. McCardell

PHILLIPS
PETROLEUM
COMPANY



Atomic Energy Division

Contract AT(10-1)-203

Idaho Operations Office

U. S. ATOMIC ENERGY COMMISSION

ABSTRACT

In response to the need for an understanding of destructive mechanisms in aluminum plate-type cores, the Spert project conducted a series of reactor tests in which sudden insertions of excess reactivity were successively increased for each test until, in two such tests, melting temperatures had been experienced over small fractions of the core but with no other unusual behavior noted. In a final test which partially melted approximately 35 percent of the core, large pressures were suddenly produced after the power excursion. These pressures in combination with widespread melting were responsible for completely destroying the core, dispersing melted fuel, damaging other reactor hardware, and causing the release of about 0.7 percent of the fissionable content of the core to the atmosphere. The explosion phenomenon was qualitatively absent in all previous tests and was in that sense not predictable. A chemical reaction between aluminum and water was detected and estimated to have released about 4 MW-sec of energy. However, results of the test indicate the existence of a triggering mechanism which dispersed the melted fractions of the core into fragments which were conducive to the chemical reaction. Conditions in the core were favorable for the initiation of a "steam explosion", and consequently this mechanism has been proposed both as a triggering device and as a contributor to the overall explosion.

SUMMARY

This report describes the results of a program of reactor testing conducted at Spert during the calendar year 1962 to demonstrate the behavior of an aluminum, plate-type, water-moderated, highly-enriched reactor when subjected to large reactivity insertions sufficient to induce very short-period power excursions. Previous test programs performed on reactors of this type had produced extensive data on reactor behavior characteristics but only at periods longer than about 8 msec, in which fuel temperatures remained well below melting. Tests in this period region were nondestructive, resulting in only minor fuel plate distortion, due to thermal stresses, in even the most severe cases. However, data had been obtained at a 2.6-msec period in the 1954 Borax I test in which an explosion was produced which completely destroyed the reactor. Thus, the period region between about 8 msec and 2.6 msec, which contained an abrupt transition from minor thermal distortion of core components (accompanied by small transient pressures) to violent destruction of the reactor, was relatively unexplored.

The Spert I destructive test program was, therefore, directed toward investigating this unexplored period region with the specific objective of studying the results of each test in search of evidence of a destructive threshold and relating, if possible, the onset of explosive pressures to the other measured or programmed test parameters. A sequence of transient tests was called for in which increasing insertions of reactivity were used to obtain successively shorter periods and greater energy releases. Portions of the core which might be destroyed or damaged beyond further use in each test were to be replaced in preparation for subsequent tests. Testing in this manner would continue to shorter periods until complete destruction of the core occurred in a single test.

The core was loaded in the Spert I facility in 1961, and by June of 1962 all calibrations, measurements, and nondestructive transients with periods ranging down to about 6 msec had been completed. Damage resulting from these tests was confined to thermal distortion and was not severe. Preparations were then made for shorter period tests which were predicted to yield more extensive damage to the core in the form of plate distortion and plate melting. Extrapolation of measured transient pressures to the shorter periods did not indicate expected pressures of destructive magnitude; however, it was recognized and anticipated that thresholds (in the sense of a change in pressure-producing phenomena) could occur either with the attainment of various degrees of fuel melting and subsequent dispersion of fuel in the water moderator or as a consequence of an aluminum-water reaction.

Two tests were conducted with periods of 5.0 msec and 4.6 msec, respectively, each of which resulted in both thermal distortion of the plates and in fuel plate melting. The combination of distortion with localized melting caused a few fuel plates to become permanently fused together. The transient pressures measured during both of these tests were in agreement with the extrapolations of pressure data from the longer period tests and there was no indication that the attainment of fuel plate melting, which had spread to about three percent of the core, constituted a threshold for the development of a new pressure source. Nor was there any indication that increasing the degree of melting in the core such as was expected in the next (3 msec) test would or would not provide such a threshold.

On November 5, 1962, the next test (which proved to be the final test) was conducted with a reactivity insertion of about 3.5 dollars producing a period of 3.2 msec. A typical self-limiting power excursion occurred, releasing about 31 MW-sec of nuclear energy. As the power excursion neared completion, approximately 15 msec following the peak of the power burst, a sharp pressure rise was recorded. The pressure pulse which occurred demolished the core, damaged most of the associated hardware and part of the control system, and bulged the earth-backed reactor vessel. Virtually no damage to the facility occurred outside the vessel.

Contamination of the facility and fission release to the atmosphere was generally very slight since the fission content of the core was small. Water was removed from the vessel for criticality control shortly after the test, and, even with this reduction in shielding protection, personnel were able to enter the area for observation of the reactor about four hours after the test.

It is estimated from radiological measurements taken in the area around the reactor building during the test that less than 0.7 percent of the fission content of the core was released to the atmosphere. Radioiodines were not detected, but less than 0.01 percent of the iodines are calculated to have been released to the atmosphere.

Calculations indicate that the fuel plates at the core hot-spot reached a maximum temperature of approximately 1360°C and had probably cooled to about 1000°C at the time of the explosion. About 8 percent of the core was completely melted and about 35 percent of the core was partially melted prior to the explosion.

Since the explosion occurred at a time after the power excursion when the reactor was completely self-shutdown, it was possible to conclude from the power burst shape that thermal expansion and steam formation took place in a predictable mode and were effective as shutdown mechanisms and that, further, the explosion was not a consequence of either a failure or a change in the nature of these mechanisms.

A possible implication of this result is that the explosion which occurred during the Borax I test (but which could not, on the basis of the recorded data, be similarly separated from the power excursion) also was not due to failure of shutdown mechanisms. Both explosions appear to be the result of a process or reaction qualitatively absent in all other transient tests.

Analysis of residual solids collected from the Spert I vessel after the destructive test indicates that a chemical reaction between aluminum and water released about 4 MW-sec of energy. However, consideration of the metal temperatures attained during the test and the initially undivided state of the fuel has resulted in the conclusion that the chemical reaction likely was not responsible for initiation of the Spert I explosion. It is considered more likely that the chemical reaction took place only after being triggered by an initial disturbance in the core which dispersed hot fragments of the melted and semi-melted fuel plates into water, thereby producing an arrangement more favorable for the chemical reaction to proceed, and that the reaction in this way may have contributed to the overall severity of the explosion.

It is known from the temperature data obtained that immediately prior to the destructive pressure pulse a significant fraction of the core was at melting temperature and could, therefore, have been dispersed into the water moderator as a result of any triggering mechanism which would produce a slight pressure surge. However, the available evidence does not permit a definitive description of the mode of initiation and propagation of the explosion and various mechanisms may be postulated as triggering devices. One of these mechanisms which appears likely is a steam explosion since it is consistent with the environment and has sufficient potential both in speed and magnitude to account for the results obtained. From a study of the fuel plate damage observed during longer period nondestructive tests it appears that conditions within the core just prior to the explosion were very favorable for the entrapment of water between the melting fuel plates. Conditions somewhat similar to this have been known to cause violent steam explosions, and this mechanism of super-heating and subsequent expansion of small quantities of water is suggested as a sufficient source for the dispersal of molten fuel in the water moderator of the Spert I core. It is further argued that once such a disturbance of the core has been initiated, further steam formation and pressure generation would be self-propagating as melted and otherwise weakened hot fuel plates become fragmented and come into intimate contact with water.

REPORT OF THE SPERT I DESTRUCTIVE TEST PROGRAM
ON AN ALUMINUM, PLATE-TYPE, WATER-MODERATED REACTOR

CONTENTS

ABSTRACT	11
SUMMARY	111
I. INTRODUCTION	1
II. DESCRIPTION OF THE REACTOR FACILITY AND INSTRUMENTATION	3
1. REACTOR FACILITY	3
1.1 Reactor Site	3
1.2 Reactor	3
2. OPERATIONAL INSTRUMENTATION	6
3. TRANSIENT INSTRUMENTATION	6
III. NONDESTRUCTIVE TEST RESULTS	7
1. INITIAL STATIC MEASUREMENTS	7
2. POWER EXCURSIONS	7
2.1 General Behavior of Nondestructive Tests	8
2.2 Transient Data	10
2.3 Reactivity Compensation Characteristics	13
2.4 Energy Coefficient	13
2.5 Time Dependent Reactivity Compensation	14
2.6 Maximum Reactivity Compensation	17
2.7 Fuel Plate Damage	17
IV. THE DESTRUCTIVE TEST	32
1. PREDICTABILITY OF TEST RESULTS	32
2. TEST CONDITIONS	32
3. TEST EVENTS	33
4. REENTRY	34
V. DESTRUCTIVE TEST RESULTS	36
1. DAMAGE TO THE CORE AND FACILITY	36
2. TEST DATA	43

2.1 General Behavior	43
2.2 Discussion of the Destructive Pressure History	44
2.3 Fissile Release	46
VI. ANALYSIS	48
1. METAL-WATER CHEMICAL REACTION	48
1.1 Chemical Analysis	48
1.2 Interpretation	50
2. CONDITION OF THE CORE AT THE TIME OF THE EXPLOSION	51
VII. CONCLUSIONS	52
VIII. REFERENCES	56
APPENDIX A - START-UP AND STATIC EXPERIMENTS	59
1. INITIAL CORE LOADING	61
2. ROD CALIBRATIONS	61
2.1 Control Rod	61
2.2 Transient Rod	61
3. VOID COEFFICIENT	62
3.1 Uniform Void Coefficient	62
3.2 Central Void Coefficient	63
3.3 Void Interaction of Central and Peripheral Regions	64
4. NEUTRON FLUX DISTRIBUTION	65
5. POWER DISTRIBUTION IN A VOIDED CORE	65
6. ISOTHERMAL TEMPERATURE COEFFICIENT	68
7. REDUCED PROMPT NEUTRON LIFETIME	68
APPENDIX B - DETAILS OF TRANSIENT INSTRUMENTATION FOR RUN 54	71
1. POWER	73
2. ENERGY RELEASE	73
3. TEMPERATURE	74
4. PRESSURE	75
5. STRAIN	76
6. FLOW	78

7. PHOTOGRAPHY	78
8. RADIOLOGICAL MEASUREMENTS	79
9. SPECIAL EQUIPMENT FOR DESTRUCTIVE TEST	80
APPENDIX C - DATA SUMMARY	87
APPENDIX D - MELTDOWN DATA	105
APPENDIX E - SUPPLEMENTARY PHOTOGRAPHS OF DESTRUCTIVE TEST RESULTS	113
APPENDIX F - MEASUREMENT AND CALCULATION OF MAXIMUM TEMPERATURE IN THE DESTRUCTIVE TEST	141
1. EXPERIMENTAL RESULTS	143
1.1 Surface Thermocouple Temperature Measurements	143
1.2 Buried Thermocouple Temperature Measurements	143
1.3 Fuel Capsule Temperature Measurement	145
2. CALCULATIONS OF MAXIMUM TEMPERATURE	146
2.1 Maximum Average Temperature of a Fuel Plate Near the Core Hot Spot: Location E5 (7W) - 3	146
2.2 Maximum Average Temperature in the Capsule	146
2.3 Temperature Distribution in Fuel Plate at E5 (7W) 0	146
APPENDIX G - CALCULATION OF FISSIDE RELEASE FROM THE DESTRUCTIVE TEST	151
APPENDIX H - METALLOGRAPHIC EXAMINATION OF DAMAGED FUEL PLATES FROM THE DESTRUCTIVE TEST	157
APPENDIX I - RECOVERY AND CLEANUP OPERATIONS	167

FIGURES

1. Outside view of Spert I reactor building showing electronic bunker on left	3
2. Inside view of Spert I reactor building showing upper bridge with drive motors and top of vessel	3
3. Cutaway view of the Spert I reactor	4
4. Cross section of Spert I D-12/25 core showing positions of transient rod and control rods	4
5. Cutaway views of Spert I D-core fuel assemblies	4
6. General behavior of D-12/25 core during 6.0-msec power excursion	9

7. Peak power vs reciprocal period	11
8. Total energy release and energy release to time of peak power vs reciprocal period	11
9. Maximum fuel plate temperatures as a function of the reciprocal period. Δh is the heat of fusion of aluminum. The notation TC is an abbreviation for thermocouple	11
10. Fuel plate temperatures at the time of peak power as a function of reciprocal period	12
11. Plot of the maximum measured transient pressures at various positions outside the core	12
12. $k_c(t_m)$ and Δk_0 vs reciprocal period α_0	14
13. Energy coefficient of the reactivity evaluated at the time of peak power as a function of the reciprocal period, α_0	14
14. Various power profiles for several different periods normalized at peak power	15
15. The time dependent compensation of reactivity for several short-period power excursions of decreasing period	16
16. Two fuel plates warped and fused together as a result of a 5-msec test	19
17. Fuel plate from 5-msec test showing melting and warping	20
18. Close view of fuel plate showing melt region, cracking of clad, and a thermocouple -- 5-msec test	21
19. Two fuel plates fused together -- 5-msec test	22
20. Two fuel plates fused together -- 5-msec test	23
21. Typical melt eruptions and clad fracture of fuel plate -- 5-msec test	24
22. Typical square-topped ripples and melt of fuel plate -- 5-msec test	25
23. Top fuel plate of central assembly showing warpage and melting -- 4.6-msec test. Regions of complete clad melting are visible	26
24. Side view of central assembly showing extent of plate fusion -- 4.6-msec test	27
25. Melting and plate constriction in center assembly -- 4.6-msec test	28
26. Edge view of fused plates, position D5 -- 4.6-msec test	29

27. Edge view of fused plates, position E6 -- 4.6-msec test	30
28. Edge view of fused plates, position F5 -- 4.6-msec test	31
29. Plume of water rising about Spert I during 3.2-msec test	34
30. Front view of reactor building showing damage incurred to control rods	37
31. Rear view of control rods and lower bridge	37
32. Side view of reactor building showing bent roof purlin	38
33. Close view of bent roof purlin	38
34. View of reactor before destructive test	39
35. View of reactor after destructive test	39
36. Close view in vessel after destructive test	40
37. Close view in vessel after destructive test	40
38. Typical plates from peripheral assembly-edge view, position G6	41
39. Fuel plate end fragments from assembly D5	42
40. Plot of data from Run 54, the destructive test	43
41. One of four oscillograph records obtained during Run 54, the destructive test	44
42. Pressure recording obtained during Run 54, the destructive test	45
43. Static and pulse calibration of permanent deformation of diaphragms of 0 - 300 psig range pressure transducers	46
44. Map of peak pressures around core during destructive test	46
45. Diagram of analysis and results of a typical sample of metallic debris collected from the Spert I vessel after Run 54	49
46. Particle size distributions obtained from two samples of debris taken after the Spert Destructive Test	49
A-1. Differential and integral control rod calibration curves	62
A-2. Integral transient rod calibration curve	62
A-3. Reactivity loss as a function of void fraction for a uniform distribution of voids	63

A-4. Reactivity worth of centrally-located, 4-inch long void strips as a function of height above the bottom of the core	63
A-5. Flux wire activation positions	65
A-6. Vertical flux profiles in fuel assemblies E-3, E-4, and E-5	66
A-7. Vertical flux profiles in fuel assemblies F-3, F-4, and F-5	66
A-8. Vertical flux profiles in fuel assemblies G-3, G-4, and G-5.	67
A-9. Horizontal flux profiles along direction A-B (Fig. A-5)	67
A-10. Horizontal flux profiles along direction A-C (Fig. A-5)	67
A-11. Location of uranium-aluminum alloy foils for comparison of the flux in voided and unvoided core	68
A-12. Comparison of horizontal flux profile in voided and unvoided core	69
B-1. Mounting technique for thermocouples	74
B-2. Photograph of typical surface-type thermocouple	75
B-3. Photograph of fuel-bearing capsule	76
B-4. Location of pressure transducers for destructive test	76
B-5. Photograph of displacement transducers mounted on fuel assembly	78
B-6. Miniature ionization chamber used for in-core power level monitoring	81
B-7. Typical installation of pressure transducers	82
B-8. Typical installation of strain gauges	83
B-9. Installation of camera No. 6 for long distance photography	84
B-10. High speed (600 fps) camera No. 3 installation at the rear of the reactor building	85
B-11. View of high speed camera inside of protective housing	86
C-1. General behavior plot showing power and temperature for a 880-msec period transient test	90
C-2. General behavior plot showing power and temperature for a 355-msec period transient test	90
C-3. General behavior plot showing power and temperature for a 118-msec period transient test	91

C-4. General behavior plot showing power and temperature for a 19.3-msec period transient test	91
C-5. General behavior plot showing power, pressure, and temperature for a 9-msec period transient test	92
C-6. General behavior plot showing power, pressure, and temperature for a 7-msec period transient test	92
C-7. General behavior plot showing power, pressure, and temperature for a 6-msec period transient test	93
C-8. General behavior plot showing power, pressure, and temperature for a 5-msec period transient test	93
C-9. Vertical pressure profile showing pressure measured about five feet above the center of the core (No. 1), about two feet above the center of the core (No. 3), and 20 inches below the center of the core	94
C-10. Horizontal pressure profile showing pressures measured respectively, 52 inches (No. 11), 35 inches (No. 12), and 17 inches (No. 13) horizontally from the core center	94
C-11. General behavior plot showing power, pressure, and temperature for a 4.6-msec period transient test	95
C-12. Vertical temperature profile measured on the west side of plate No. 7 in assembly E-5	96
C-13. Horizontal temperature profile measured in the $z = 0$ plane	97
C-14. A comparison of fuel capsule and fuel plate temperatures during the destructive test	98
C-15. The strain response of the horizontal and 45° gauges of a rosette attached to the outside of a peripheral fuel assembly	98
C-16. Temperatures measured on the west side of the plate No. 7, assembly E-5, during the destructive test	99
C-17. Vertical temperature profile as measured by surface-mounted thermocouples attached to the west side of plate No. 12, assembly E-5, during the destructive test	100
C-18. Horizontal temperature profile measured in the $z = + 8$ plane by buried thermocouples during the destructive test	100
C-19. Pressure associated with moderator boiling as measured about 2 feet above the core center (No. 3 d), 20 inches below the core center (No. 4 d), and 53 inches below the core center (No. 6 d), during the destructive test	101

C-20. Pressure associated with moderator boiling as measured at the side of the core and 17 inches from the core center during the destructive test	101
C-21. Maximum measured temperatures versus total energy release	102
C-22. Burst parameter versus reciprocal period	102
D-1. Cross section drawing of the core showing distribution of melted regions on fuel plates after 5.0-msec test	108
D-2. Vertical drawing of assemblies showing melted regions on fuel plates after 5.0-msec test	109
D-3. Cross section drawing of the core showing distribution of melted regions on fuel plates after 4.6-msec test	110
D-4. Vertical drawing of assemblies showing melted regions on fuel plates after 4.6-msec test	111
D-5. Vertical drawing of assemblies showing melted and disassembled regions of fuel plates after destructive test	112
E-1. Fuel plates recovered from position C3 -- one of the two corners of the core in which the melted portions of the plates were relatively undisturbed	116
E-2. Assembly from position C4	117
E-3. Control rod bearing assembly from position E7	118
E-4. Control rod bearing assemblies from core positions G5 (left) and E3 (right)	119
E-5. Control rod bearing assembly from position E7 after being opened for inspection	120
E-6. Assembly from position G4 showing damage typical for internal assemblies	121
E-7. Control rod bearing assembly from position C5	122
E-8. Upper (nonpoison) section of transient rod blades as recovered from the reactor vessel	123
E-9. Several fuel plates from position G6 showing a stage in the progression from warping to melting and fusion of the plates	124
E-10. A fracture in the concrete floor which circumscribed the reactor vessel	125
E-11. Section of an air filled tube located in the core during the destructive test	126

E-12. Objective lens of periscope	127
E-13. $t = -143$ msec	128
E-14. $t = 87$ msec	128
E-15. $t = 130$ msec	128
E-16. $t = 220$ msec	128
E-17. $t = 360$ msec	129
E-18. $t = 620$ msec	129
E-19. $t = 900$ msec	129
E-20. $t = 1030$ msec	129
E-21. $t = 1300$ msec	130
E-22. $t = 1620$ msec	130
E-23. $t = 2160$ msec	130
E-24. $t = 2830$ msec	130
E-25. $t = 3280$ msec	131
E-26. $t = 3820$ msec	131
E-27. $t = 4400$ msec	131
E-28. $t = 5300$ msec	131
E-29. $t = -73$ msec	132
E-30. $t = 57$ msec	132
E-31. $t = 65$ msec	132
E-32. $t = 70$ msec	132
E-33. $t = 72$ msec	133
E-34. $t = 74$ msec	133
E-35. $t = 79$ msec	133
E-36. $t = 85$ msec	133
E-37. $t = 94$ msec	134
E-38. $t = 97$ msec	134

E-39. t = 105 msec	134
E-40. t = 114 msec	134
E-41. t = 124 msec	135
E-42. t = 135 msec	135
E-43. t = 155 msec	135
E-44. t = ≈ 4 sec	135
E-45. t = -153 msec	136
E-46. t = 70 msec	136
E-47. t = 85 msec	136
E-48. t = 100 msec	136
E-49. t = 115 msec	137
E-50. t = 130 msec	137
E-51. t = 145 msec	137
E-52. t = 160 msec	137
E-53. t = 175 msec	138
E-54. t = 190 msec	138
E-55. t = 205 msec	138
E-56. t = 295 msec	138
E-57. t = 445 msec	139
E-58. t = 1040 msec	139
E-59. t = 1940 msec	139
E-60. t = 4340 msec	139
F-1. Temperatures at various points in the core in a horizontal plane eight inches above core center at about the time when destructive pressures arose (t = +15 msec)	145
F-2. Calculated results of centerline meat temperature and of heat transfer rates from fuel plate surface to moderator	147
F-3. Calculated temperature distributions of a fuel plate section near the hot spot of the core	148

I. INTRODUCTION

In recognition of the need to obtain an understanding of reactor kinetic behavior and reactor accidents, the Atomic Energy Commission contracted Phillips Petroleum Company in 1954 to undertake a long range reactor safety program which included both nondestructive tests and integral core destructive tests.

The completion of a substantial portion of these investigations which could be performed in Spert I and the construction of the Spert II, III, and IV facilities to continue such studies, made it appropriate in 1962 to initiate a program of destructive tests. This phase of the program had been deferred in favor of extending the nondestructive studies on various core configurations in order to better understand and evaluate the reactivity compensating mechanisms.

The first extensive experimental kinetics studies of reactors prior to the Spert Program were the GODIVA tests [1] for fast systems, and the BORAX tests [2] for thermal systems. In the Borax-I tests, self-limiting power excursions were performed with exponential periods ranging between about 100 msec and 5 msec at boiling temperatures and between 100 msec and 13 msec at ambient temperatures. While only minor damage to the core occurred during these tests, the results indicated that shorter periods with larger energy releases could lead to extensive core damage. The Borax-I program was concluded with a test having a period of 2.6 msec at ambient temperature. This test yielded a maximum power of 19 GW and a burst energy of about 135 MW-sec, and resulted in nearly total destruction of the core and partial destruction of the facility.

Although the Borax destructive test constituted a major step forward in providing an understanding of accidental excursions, the nature of the explosion and factors influencing it could not be learned from the available data, and other damage effects such as plate distortion, channel blockage, and melting were concealed by the over-riding effects of the explosion.

The destructive program in Spert I, therefore, had as its objective a systematic exploration of the destructive region of reactivity insertions in order to describe damage effects encountered, to search for any explosive threshold, and finally to demonstrate a full-scale explosion in an effort to contribute to the understanding of these responses and consequences.

Since the results of the Spert I explosion tests are best understood in context with the entire testing program, this report presents the results of the preceding nondestructive and partially destructive tests but with particular emphasis on the destructive test which concluded the program. Briefly, the report is divided as follows: Section II contains a description of the reactor facility and the experimental methods used in the execution of this program; Section III presents data and analysis of all tests exclusive of the final destructive test; and Section IV and V present, respectively, a description of the destructive test and the results obtained from that test. Results of the entire program are finally discussed and analyzed in Section VI and some of the main conclusions are expressed in Section VII. In many cases where supporting information or peripheral studies are needed but are otherwise not pertinent to the main body of the report, this information has been included in the appendices. These appendices contain, for instance, details of transient instrumentation, representative data for various periods,

calculations of temperature, fission release, etc, and results of metallurgical studies.

II. DESCRIPTION OF THE REACTOR FACILITY AND INSTRUMENTATION

In the following section, brief descriptions of the Spert I reactor facility including the building, the reactor, reactor control system, operational instrumentation, and auxiliary equipment are presented. A more detailed description of the reactor facility has been published [3].

1. REACTOR FACILITY

1.1 Reactor Site

The Spert I reactor is located at the National Reactor Testing Station in Idaho. The reactor is approximately one half mile from the reactor control room at the Spert control center building and approximately one half mile from the nearest other reactor facility. Spert I consists of the reactor building (shown in Figures 1 and 2) and an attached earth-shielded, instrumentation bunker containing electronic equipment for amplifying and sending instrumentation signals to the control center. A small service building located about 400 feet from the reactor building, houses the water-treatment equipment, air-compressor, and other auxiliary equipment. The reactor is operated remotely from a control console located in the control center building.



Fig. 1 Outside view of Spert I reactor building showing electronic bunker on left.

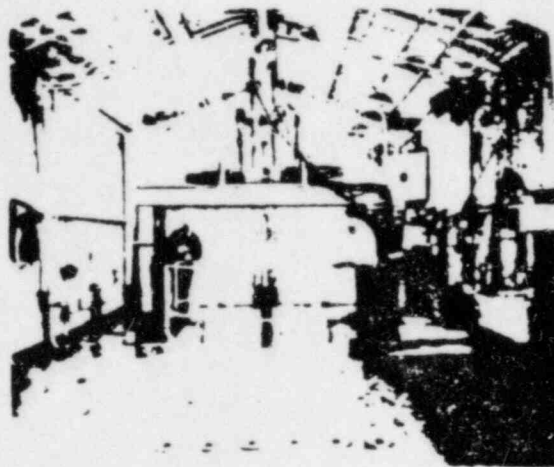


Fig. 2 Inside view of Spert I reactor building showing upper bridge with drive motors and top of vessel

1.2 Reactor

Figure 3 is a cutaway view of the Spert I reactor. The reactor vessel is an open, unpressurized, 10-foot diameter by 16-foot deep, carbon-steel tank. The reactor which was moderated and cooled by light water had no provision for forced coolant circulation through the core. The water level in the reactor vessel was nominally 4.5 feet above the top of the fuel plates for the tests described here.

The test core was comprised of 25 fuel assemblies, mounted in a 5 x 5 rectangular grid structure as shown in Figure 4.

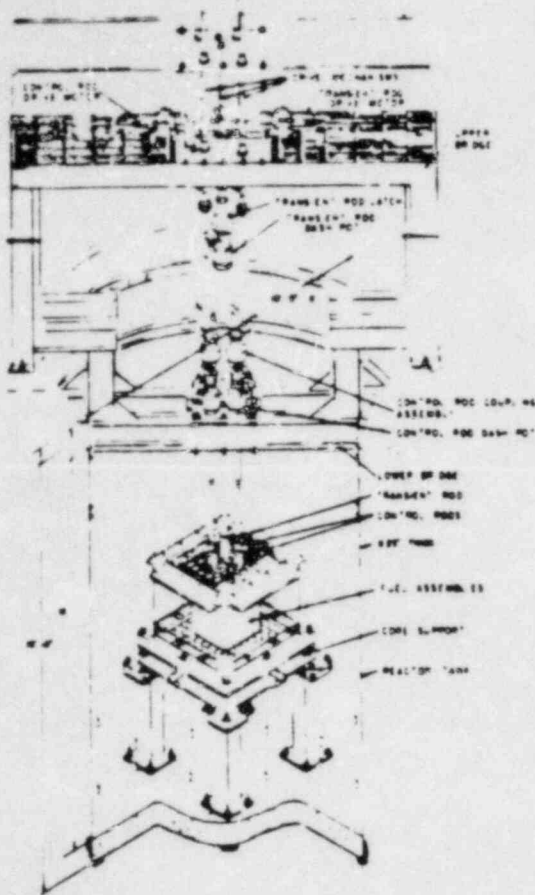


Fig. 3 Cutaway view of the Spert I reactor.

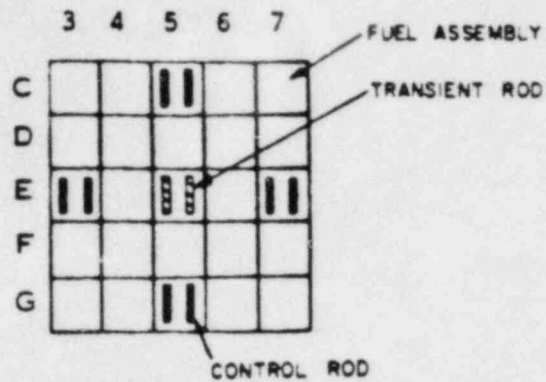


Fig. 4 Cross section of Spert I D-12/25 core showing positions of transient rod and control rods. (Each is identified by a letter and a number, ie, the fuel assembly in the central position with the transient rod is designated E-5.)

Four symmetrically-placed, gang-operated control rod assemblies, each consisting of a pair of seven weight percent boron-aluminum poison blades with aluminum followers provided reactor control. An additional, centrally-located "transient" rod assembly consisting of two aluminum blades with poison follower blades was used to initiate power transients.

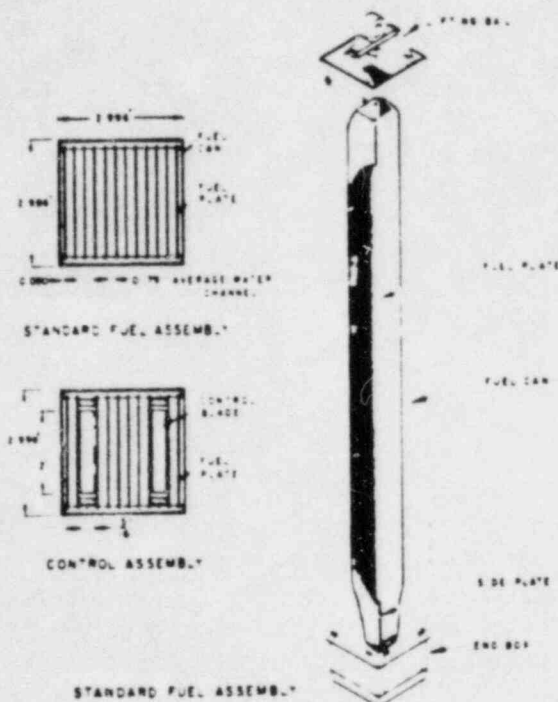


Fig. 5 Cutaway views of Spert I D-core fuel assemblies.

The Spert I D-type fuel assembly is shown in Figure 5. It consisted of a square aluminum box, with two grooved aluminum side plates used for supporting removable fuel plates. The end-box section at the bottom of the fuel assembly fits into the lower core support grid structure, and a lifting bail at the top was used for handling. The standard assembly contained 12, highly enriched, U-Al alloy, aluminum-clad fuel plates, which could be removed from the fuel assembly box to permit fuel plate inspection, and installation and replacement of instrumentation. The four control-rod and one transient-rod fuel assemblies contained six fuel plates; the remaining six fuel plate positions were occupied by two blades and blade-guide channels. Fuel assembly design characteristics are included in Table I together with physical properties of the core.

TABLE I
PHYSICAL PROPERTIES OF SPERT I D-12/25 REACTOR

Reactor Type	Open Pool
Moderator-Reflector	H ₂ O
Vessel	10-ft ID x 16-ft High Right Cylinder
Vessel Material	Carbon Steel
Number of Fuel Assemblies	25
Standard (12-plate) Fuel Assemblies	20
Rod Bearing (6-plate) Fuel Assemblies	5
Approximate Fuel Assembly Size	3 x 3 x 25 in.
Total Number of Fuel Plates in Core	270
Fuel Plate Dimensions	0.060 x 2.704 x 25-1/8 in.
Clad Material	6061 Aluminum
Clad Thickness	0.020 in.
Meat Composition	93 percent enriched, U-Al Alloy (24 weight percent U-235)
Meat Dimensions	0.020 x 2.454 x 23-1/2 in.
U-235 Per Fuel Plate	14 g
Total U-235 in Core	3.8 kg
Coolant Channel Thickness	0.179 in.
Total Core Volume (inclusive of all materials and moderator)	5.3 x 10 ³ in. ³
Moderator Volume	3.2 x 10 ³ in. ³
Metal-to-Water Ratio	0.66
Heat Transfer Area	3.4 x 10 ⁴ in. ²
Control Rods	4 double-bladed, gang-operated
Transient Rod	1 double-bladed
Control and Transient Rod Poison Material	Binal ^[a] (7 weight percent natural boron-Al alloy)

[a] Binal - Trademark for the Sintercast Corporation aluminum-boron powder-metallurgy process material.

2. OPERATIONAL INSTRUMENTATION

The Spert I operational instrumentation included neutron instrumentation, a reactor bulk water thermopile, a reactor water level indicator, and radiation-detection equipment.

Operational neutron instrumentation included several B^{10} -lined pulse chambers with amplifiers and counters, a B^{10} -lined gamma-compensated ion chamber connected through a linear electrometer to a 6-decade linear power recorder, and a B^{10} -lined uncompensated ion chamber connected through a logarithmic electrometer to a 6-decade log-power recorder. The chambers and electronic amplifiers were located in the reactor building and instrument bunker, respectively, and the counters and recorders were located in the Spert I control room at the control center.

Bulk water temperature in the reactor was measured by a thermopile positioned near the tank wall and leads from the thermopile extended to a constant-temperature reference junction from which the signal was transmitted without amplification to a temperature recorder at the control center.

Gamma radiation levels directly over the reactor vessel and at other points in the reactor area were measured by gamma-sensitive ion chambers, the signals from which were transmitted to indicators in the Spert I control room and to a recorder in the health physics office at the control center.

3. TRANSIENT INSTRUMENTATION

This section contains a brief description of methods used to obtain data on the kinetic response of the reactor during transient tests. Structural details, locations, limitations, etc, of the instruments are discussed more extensively in Appendix B along with a description of the data system.

Reactor power was measured by neutron-sensitive ion chambers, which with the exception of one miniature chamber located inside of the core, were all located exterior to the core in the reflector where they detected leakage neutrons and, to a lesser extent, gammas.

Nuclear energy release was determined both by integration of the power data and in the case of the total energy, E_T , by activation of cobalt wires.

Fuel plate temperatures were measured by thermocouples attached either to the surface of the fuel plates or buried within the meat. Many locations in the core, especially in the region of the flux peak, were instrumented for each test in order to obtain measurements of the temperature distribution in the core. The flux peak occurred in the central fuel assembly, E5, (Figure 4) about three inches below the center-plane of the core.

Pressure measurements were obtained in the reflector at several positions surrounding the core by unbonded, strain-gage type, diaphragm transducers. The transducers were located close to the x, y, and z, core-centered axes of the reactor and at several radial distances from the core up to about four feet.

III. NONDESTRUCTIVE TEST RESULTS

1. INITIAL STATIC MEASUREMENTS

After the D-12/25 core (so designated because it contained 25 nominal 12-plate assemblies) had been loaded in Spert I, a series of tests was performed to measure characteristics of the core and to obtain various calibration information necessary for transient operation. These latter included primarily a calibration of the control rods by the reactor period method using both boric acid and the transient rod as poison shims. Integration of the control rod worth indicated that the total available excess reactivity was about 8.2\$, and by inter-calibrating the transient rod against the control rods, it was determined that the transient rod was worth about 7\$. Table II summarizes the nuclear characteristics of the core.

TABLE II

NUCLEAR CHARACTERISTICS OF THE SPERT I D-12/25 CORE

Total U-235	3.8 kg
Excess Reactivity	8.2\$
M/W Ratio	0.66
H/U Ratio	360
Max/Ave Flux Ratio	2.4
Void Coefficient	
Average	-36¢/%
Average	-0.067¢/cm ³
Maximum	-0.16¢/cm ³
Temperature Coefficient, Isothermal	
@ 20°C	-2.1¢/°C
Reduced Prompt Neutron Generation	
Time, ℓ/\bar{E}	8.16 \pm 0.04 msec
nv/Watt (Average)	7.6 $\times 10^6$

Detailed descriptions and results of most of the statics experiments are presented in Appendix A.

2. POWER EXCURSIONS

Measurements of the dynamic characteristics of the Spert I D-12/25 core were obtained from transient power excursions produced in the core by rapidly ejecting a poisonous "transient" rod from the core while the core was at very

low power levels (usually less than 10 watts). By this means, a step-wise increase of reactivity occurs in the reactor, with the amount of reactivity being predetermined by a measured displacement of the control rods above their normal critical position. The ensuing power excursion is initially exponential and finally self-limited and quenched by inherent "shutdown" mechanisms which cause a loss of reactivity.

The magnitudes of the measured variables during these self-limiting power excursions (power, fuel plate temperature, pressure generation, etc) and the relative times at which specific events occur during the course of an excursion are affected considerably by the initial excess reactivity insertion, Δk_0 . In this section, some of these transient behavior characteristics of the test core are discussed briefly with respect to the variations taking place in each as Δk_0 is increased from about 1.0\$ to about 3.5\$. Nearly all aspects of the transient behavior of this core were qualitatively the same as those previously obtained at Spert with several other aluminum plate type cores. The results of these tests are presented here and discussed, especially to indicate the basis for predicting the results of the very short period tests.

2.1 General Behavior of Nondestructive Tests

In the region of relatively long periods, 50 msec and greater, (or $\Delta k_0 < 1.15$) the initial power rise during the transients was found to gradually deviate from the exponential while still at low power levels, and then to slowly pass through a maximum. Maximum power was normally followed by a slow power decline with the rate of the decline again being small but increasing with shorter initial periods (Figures C-1, C-2, and C-3 on pages 90-91). Power levels always remained low during these excursions (ie, in the range of several megawatts) and there was, consequently, no appreciable peaking of the temperature in the meat portions of the fuel plate. Ordinary conductive heat transfer processes were adequate in these cases to nearly suppress temperature peaking in the fuel plate and distribute the heat in both the metal cladding of the fuel plate and in the water moderator. Boiling temperatures, if attained at all during the course of these long-period transients, always occurred after the time of peak power and the compensation of reactivity before peak power was attributed principally to thermal expansion of metal and water[a].

When the initial reactivity insertion, Δk_0 , was further increased to obtain shorter periods, more energy was required to compensate the increased reactivity and it was found that the maximum power attained during the tests increased approximately as the square of the initial asymptotic reciprocal period, λ_0 , (empirically, the exponent was found to be about 1.7). The reason for this (near) "square-law" dependence of peak power on λ_0 arises from the two separate facts that the energy under an exponential power rise varies as the inverse of λ_0 , whereas the prompt reactivity increases directly as λ_0 [b].

It is possible, at least in theory, for the thermal expansion mechanisms alone to compensate the prompt reactivity and to arrest the initial power rise of a power excursion provided enough energy is released. However, at some point,

[a] It should be noted however that attempts to make a quantitative computation of the reactivity compensation purely on the basis of thermal expansion of materials have not been successful (see Reference 4).

[b] See page 9 for footnote.

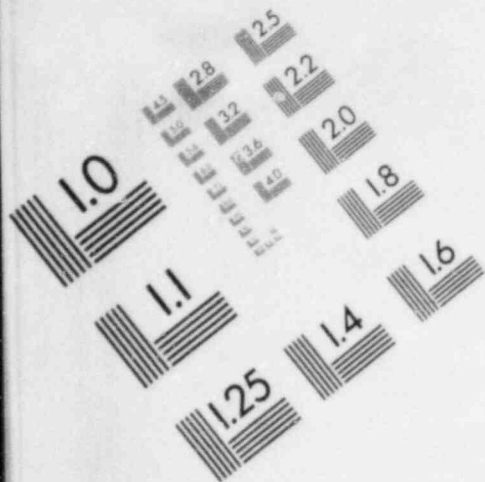
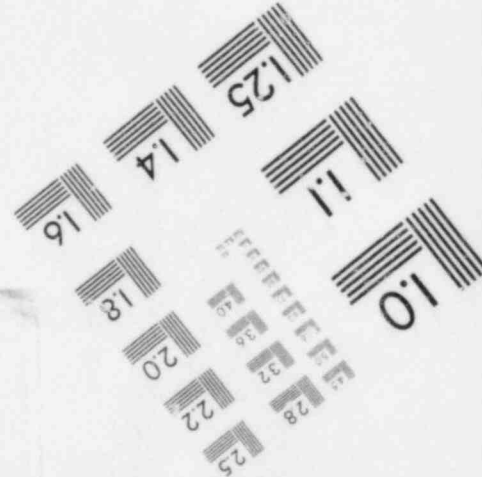
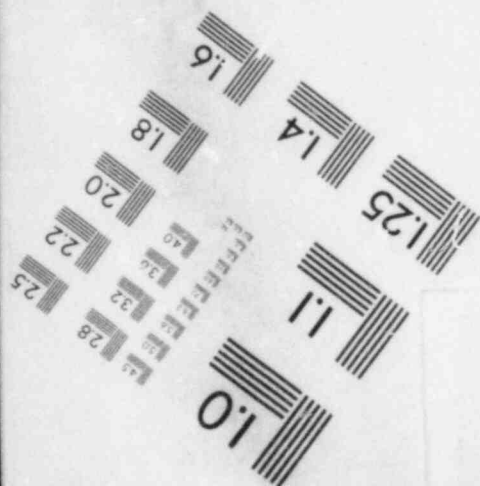
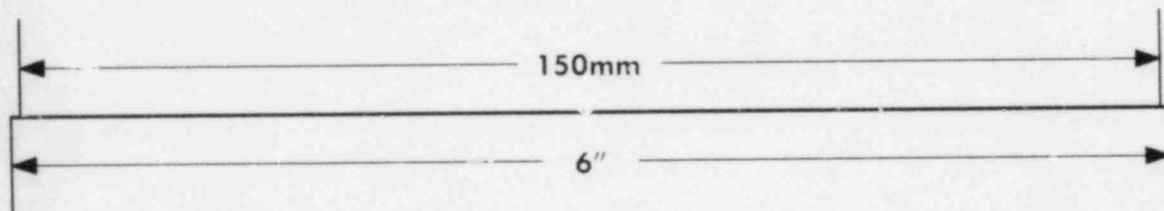
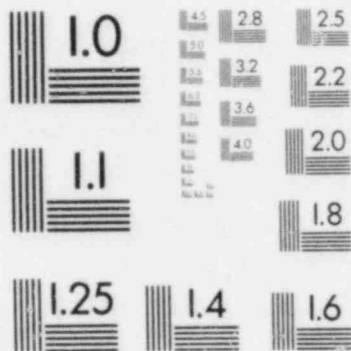
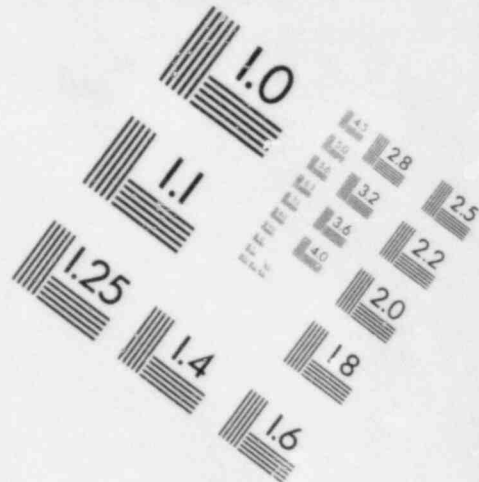


IMAGE EVALUATION
TEST TARGET (MT-3)



which for this core occurred at a period of about 50 msec, fuel plate temperatures were attained which allowed moderator boiling to commence and to contribute to the compensation of prompt reactivity by producing steam voids. Boiling void growth is extremely fast (often requiring less than 1 msec for the growth of a bubble) and the region over which boiling occurs generally spreads rapidly over the entire core, and as a consequence, peak power has never been observed to lag behind the onset of boiling by more than a few milliseconds regardless of the period. Although some reactivity is still compensated by thermal expansion, power behavior after the onset of boiling is primarily controlled by the dynamics of this single reactivity compensating mechanism, i.e., production and condensation of steam.

The typical short-period transient is illustrated in Figure 6. As a result of the higher energy releases obtained in short-period excursions, boiling temperatures are eventually reached at nearly every point in the core, and voiding in all water channels is extensive. Reactivity compensation produced by steam voiding during short-period excursions has been found to greatly exceed the initial excess reactivity insertion and establish, as a consequence, a highly shutdown condition in the reactor. Due to this shutdown condition of the core the power will fall to a level approximately two to three decades below peak power and level off at this point. Further decline of the power is resisted by the release of delayed neutrons.

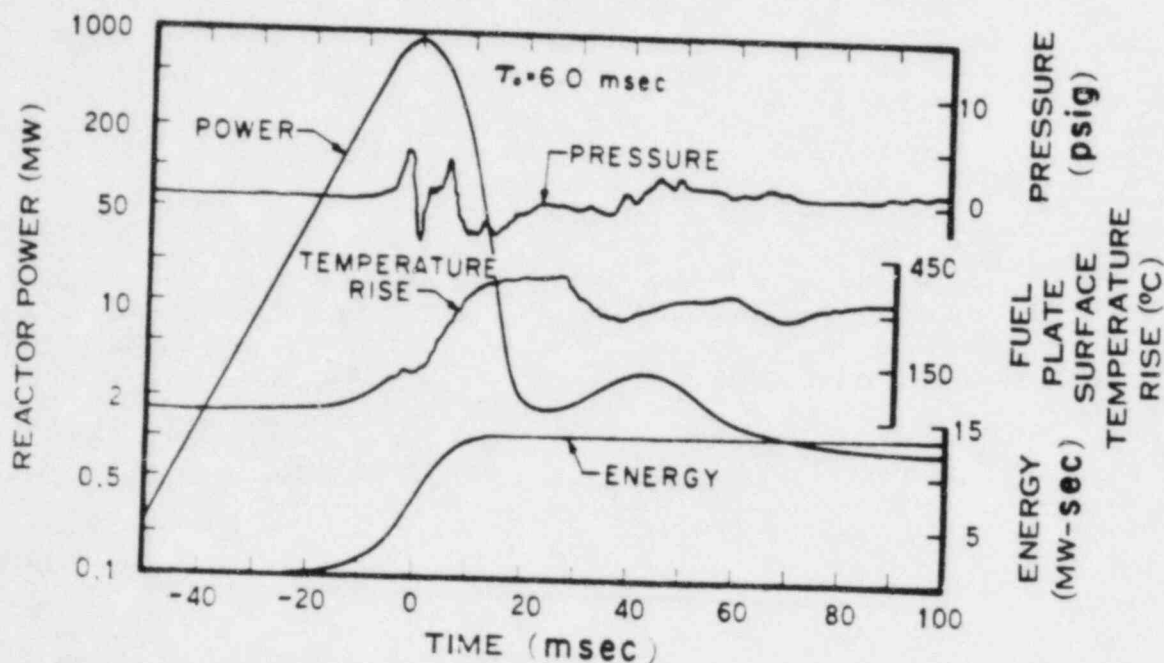


Fig. 6 General behavior of D-12/25 core during 6.0-msec power excursion.

- [b] If the power, $\phi(t)$, varies as $e^{\lambda t}$ up to the time of peak power, t_m , then the energy release at time of peak power, $E(t_m)$, is equal to $\phi(t_m)/\lambda_0$. For short-period tests, the reactivity compensation at the time of peak power $k_c(t_m)$ is proportional to λ_0 [5]. If $k_c(t_m)$ also is assumed to be proportional to $E(t_m)$, then, it appears that $\phi(t_m)$ is proportional to λ_0^2 , a result which is only approximate since ordinary power excursions deviate from an exponential near peak power.

The ability of this reactor to self-limit itself during power excursions has been demonstrated for periods as short as 3.2 msec. Reactivity compensation (discussed in Section III-2.5) took place in a predictable manner for each test and demonstrated an ability to over-compensate the initial excess reactivity insertion by several dollars.

Nevertheless, the energy release resulting from these short-period tests was reaching to potentially damaging magnitudes. At periods around 5 msec and below, maximum temperatures of the fuel plates were expected to exceed the melting point of aluminum, a threshold which had been avoided in previous Spert testing on aluminum cores, and it was not known what new effects might arise as a result. Another consequence of these short-period tests was an increased temperature peaking within the fuel plates which produced thermal gradient stresses and consequent severe warping of the plates along with cracking of the clad. Permanent damage to fuel plates from thermal distortion first became significant in the 7- to 8-msec period region, and, although in these tests there was no apparent change in the effectiveness of reactivity compensation as a consequence of the damage produced, warping was often severe enough to completely block several water channels.

Finally, a pressure pulse arising from the initial super-heating of water prior to the onset of boiling was of concern. Although only small pressures were attributed to this mechanism (ie, about 6 psi at a 5-msec period), these pressures tended to increase with decreasing period. By extrapolation, it was expected that this pressure source could cause damage in tests with periods of less than about 2 msec.

2.2 Transient Data

In this section and in those following, specific results of the 54 transient tests conducted on the D-12/25 core are presented in the form of plotted relationships of several measured variables against the inverse period, ω_0 . Further summary of the data including illustration of the temporal relationship between these quantities, general behavior plots of the power, energy, temperature, and others are presented in Appendix C.

Peak power data as shown in Figure 7, were found to be nearly collinear (on a log-plot) for all tests. A least-squares fit to peak power data, $\phi(t_m)$, yields the form:

$$\phi(t_m) = 0.13 \omega_0^{1.72} \text{ MW}$$

over the range, $10 < \omega_0 < 300 \text{ sec}^{-1}$. The regularity of the data made it possible to obtain accurate extrapolations of peak power during the entire test series.

As seen in Figure 8 the energy released at peak power, $E(t_m)$, and the total energy, E_T , vary linearly with reciprocal period, ω_0 , for ω_0 less than about 125 sec^{-1} . At shorter periods, however, both sets of data were observed to rise steeply. This change in slope (as shown below) appears to be a consequence of the boiling shutdown process and its effect upon the burst shape.

Figure 9 is a plot of peak fuel plate temperature data obtained during the test series as a function of the reciprocal period, ω_0 . The highest temperatures

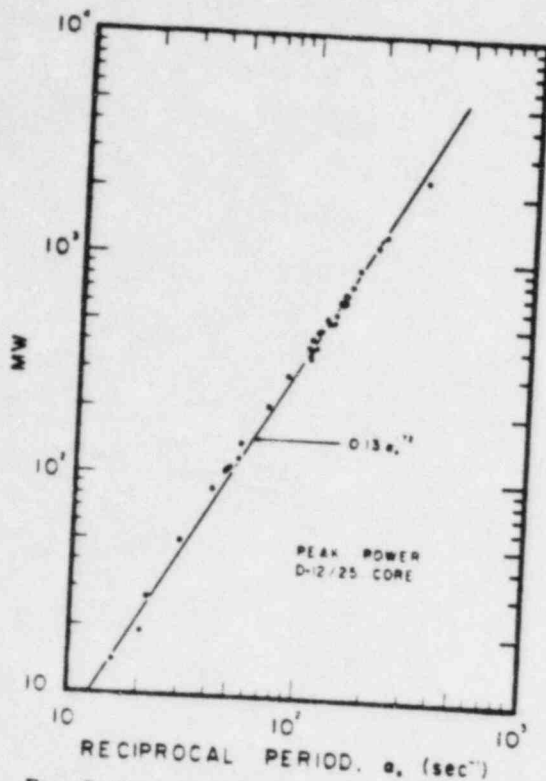


Fig. 7 Peak power vs reciprocal period.

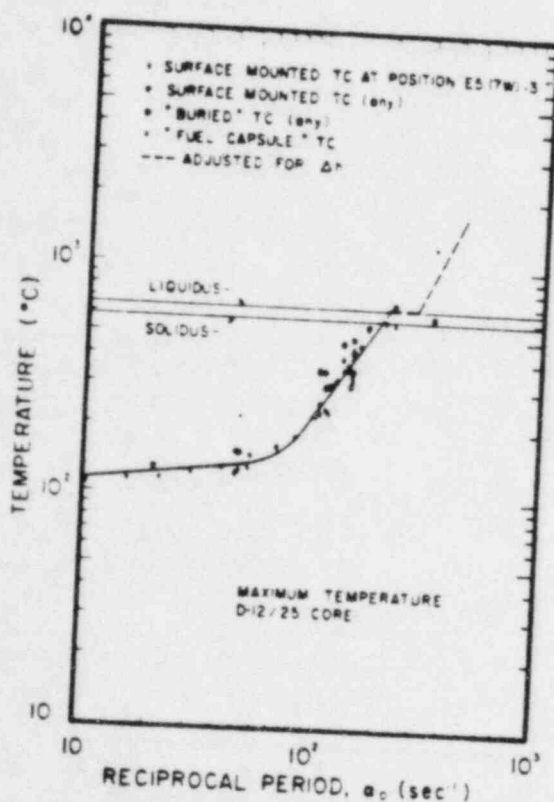


Fig. 9 Maximum fuel plate temperatures as a function of the reciprocal period. Δh is the heat of fusion of aluminum. The notation TC is an abbreviation for thermocouple.

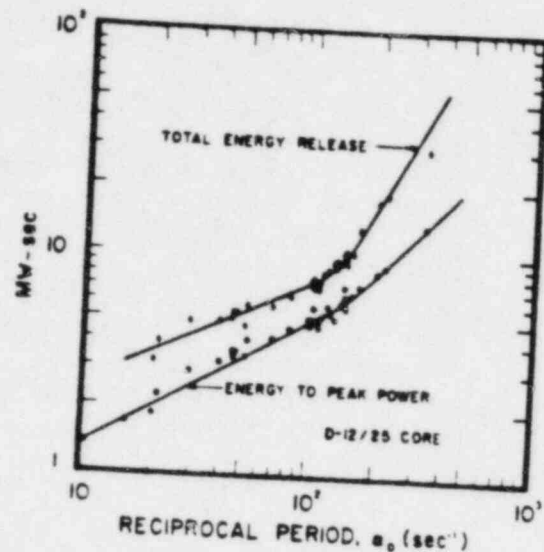


Fig. 8 Total energy release and energy release to time of peak power vs reciprocal period.

were usually observed in the center of the central assembly of the core and about three inches below the midplane of the core. This position (denoted as position E5(7W)-3) was the nearest instrumented point to the flux peak. The solid line in Figure 9 has been faired through the data points and the dashed line is an extrapolation of these data adjusted at the melting point for the heat of fusion of aluminum, Δh .

The fact that temperature data are not exactly proportional to the energy data is interpreted as a consequence of the variation of heat capacity with temperature and of a variation in the fraction of the nuclear heat which is transferred from the fuel plate to the water. From an extrapolation of the temperature data, it was possible to predict closely the onset of melting, which occurred first at a period of 5 msec ($\omega_0 = 200 \text{ sec}^{-1}$).

The functional relationship of $\theta(t_m)$, the measured fuel plate temperature at the time of peak power, with ω_0 in Figure 10 is explained as follows: In the longer period region, ω_0 greater than 50 msec, ($\omega_0 < 20 \text{ sec}^{-1}$), peak power occurs while surface temperatures of the fuel plates are still rising (but below 100°C). At about

$\alpha_0 = 50 \text{ sec}^{-1}$, peak power occurs almost simultaneously with maximum temperature, $\theta(\text{max})$, so that $\theta(t_m) \approx \theta(\text{max})$. Energy which is released after peak power (in this range of periods) is apparently lost rapidly from the fuel plates to the moderator by boiling heat transfer so that higher fuel plate temperatures are never obtained. The rise in $\theta(t_m)$ between $\alpha_0 = 50 \text{ sec}^{-1}$ and $\alpha_0 = 160 \text{ sec}^{-1}$ reflects the fact that boiling heat transfer eventually becomes unable to offset the rapidly increasing power levels of the short-period excursions; and finally, the apparent jump of $\theta(t_m)$ at $\alpha_0 \approx 160 \text{ sec}^{-1}$ indicates that film boiling also has occurred before peak power so that $\theta(t_m)$

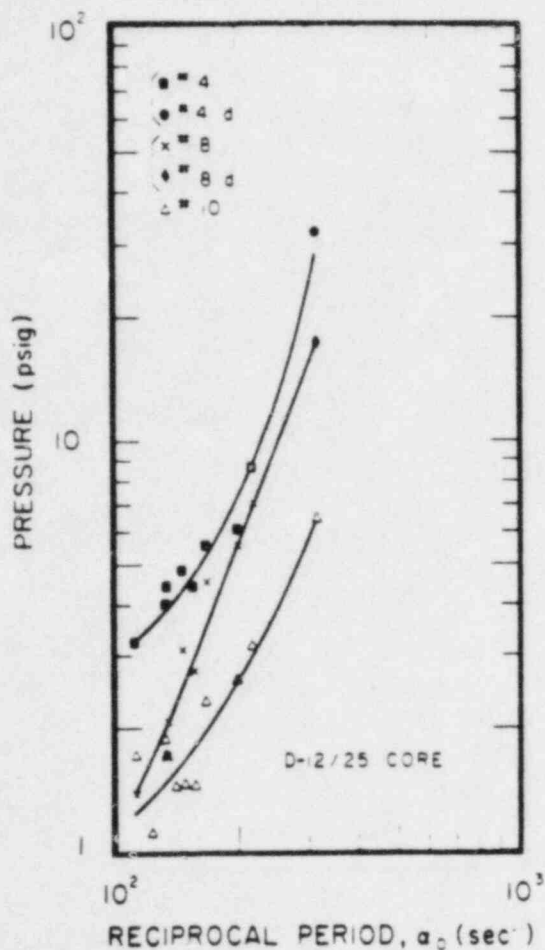


Fig. 11 Plot of the maximum measured transient pressures at various positions outside the core. Location #'s indicated refer to Table B-II, Appendix B. Positions 4 and 4d are several inches below core; positions 8 and 8d are at the side of the core; and position 10 is near the vessel wall.

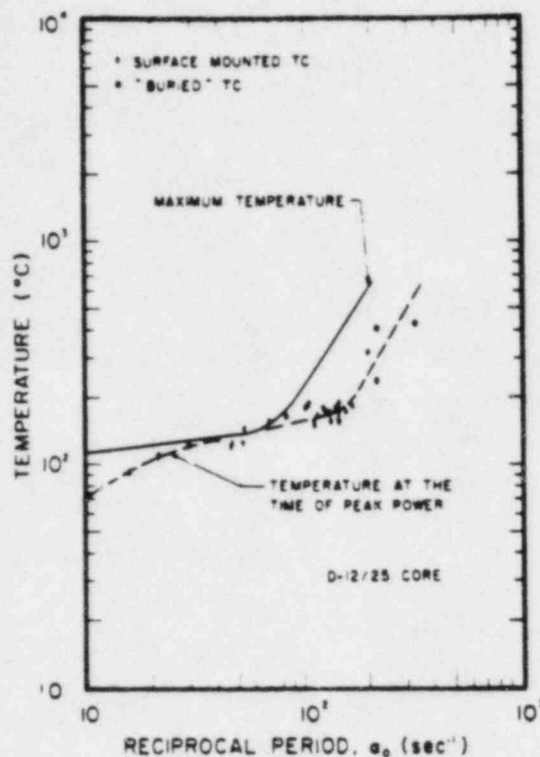


Fig. 10 Fuel plate temperatures at the time of peak power as a function of reciprocal period.

includes part of a nearly adiabatic temperature rise after vapor blanketing on the fuel plates [6].

The maximum transient pressures as measured in the reflector water at several positions around the core are shown in Figure 11. While the maximum pressures measured at any location demonstrate a fairly regular dependence upon the reciprocal period, both the period-dependence and the pressure magnitudes were found to vary considerably with the location of the pressure transducer [a]. The lines shown in Figure 11 are only faired-in to connect related data points. Pressure profiles differed greatly according to position and highest

[a] Reference 9 contains a summary of reactor dynamic pressure measurements made during previous transient testing programs at Spert. It constitutes a comprehensive source of information on the problems and interpretations of pressure measurements.

pressures were measured below the core. Position numbers shown in Figure 11 refer to locations as shown in Appendix B, Figure B-4. Actual coordinates of these positions are shown in Table B-II of Appendix B, page 77.

The pressure data in Figure 11 were recorded at times always immediately after the onset of boiling in the core and are, therefore, associated with the vapor pressure of superheated water on the fuel plate surfaces just prior to the initiation of boiling. The moderate superheats of water indicated by the data (for instance about 35°C for the destructive test) are probably less than actually achieved in the core since the pressures are measured external to the core after undergoing some attenuation.

2.3 Reactivity Compensation Characteristics

It has been shown that a super prompt critical power excursion may be temporarily terminated by compensation of only a part of the original reactivity insertion, Δk_0 ; [7, 8] the reason being that when the reactor power is greatly in excess of the delayed neutron equilibrium value, up to one dollar of reactivity is lost in the buildup of neutron precursors. The actual amount of reactivity compensated at the time of peak power, $k_c(t_m)$, therefore, is usually less than the initial excess reactivity by as much as one dollar, but may increase depending upon the rate of shutdown. Thus, if the initial reactivity compensation in a transient occurs very slowly (as in the case of extremely long period transients, i.e., $\lambda_0 > 1$ sec) then it is possible for delayed neutron precursors to approach equilibrium with the power, and a compensation of nearly all of the inserted excess reactivity is required to halt the power rise. On the other hand, it was found with this core as with many others, that in the case of short period transients, self-shutdown from both thermal expansion and from boiling occurred very rapidly and arrestment of the power rise occurred after a compensation of only the prompt reactivity, $\Delta k_p \approx (\Delta k_0 - 1)\$$. Figure 12 shows the empirical relationships of $k_c(t_m)$ to the prompt reactivity and to the total reactivity for the D-12/25 core. As with all other light-water moderated, highly-enriched cores studied at Spert, $k_c(t_m)$ departs from Δk_0 (for extremely long periods) and approaches the prompt reactivity in the region of $\lambda_0 \approx 10$ sec⁻¹.

2.4 Energy Coefficient

Since compensation of reactivity arises primarily from thermal processes taking place in response to the release of energy during a power excursion, the ratio, $b(t)$, of the compensated reactivity to the energy can be defined as an "energy coefficient" which is an indicator of the efficiency of the shutdown mechanisms in the arrestment of power excursions. In Figure 13, the energy coefficient evaluated at the time of peak power, $b(t_m)$, has been shown for most of the D-core power excursions. For excursions in which boiling did not occur before peak power (i.e., $\lambda_0 \leq 20$ sec⁻¹), characteristically low values of $b(t_m)$ approximately 10¢/MW-sec are obtained. The slight decrease in $b(t_m)$ with increasing λ_0 may be attributed to the change in energy partition between the fuel plate and the water moderator. That is, with shorter periods, a relatively greater amount of energy remains in the fuel plate which has a lower coefficient of thermal expansion than does water. The effect of boiling shutdown begins to appear at about $\lambda_0 = 30$ sec⁻¹, causing the reactivity coefficient to turn upward to larger values (i.e., more efficient shutdown). Although very large volumes of steam can be produced by extracting only a small fraction of the heat from the plates, it takes a few milliseconds for boiling to spread over the core and the modest rate of increase of $b(t_m)$ for λ_0 above 30 sec⁻¹ (rather than a stepwise

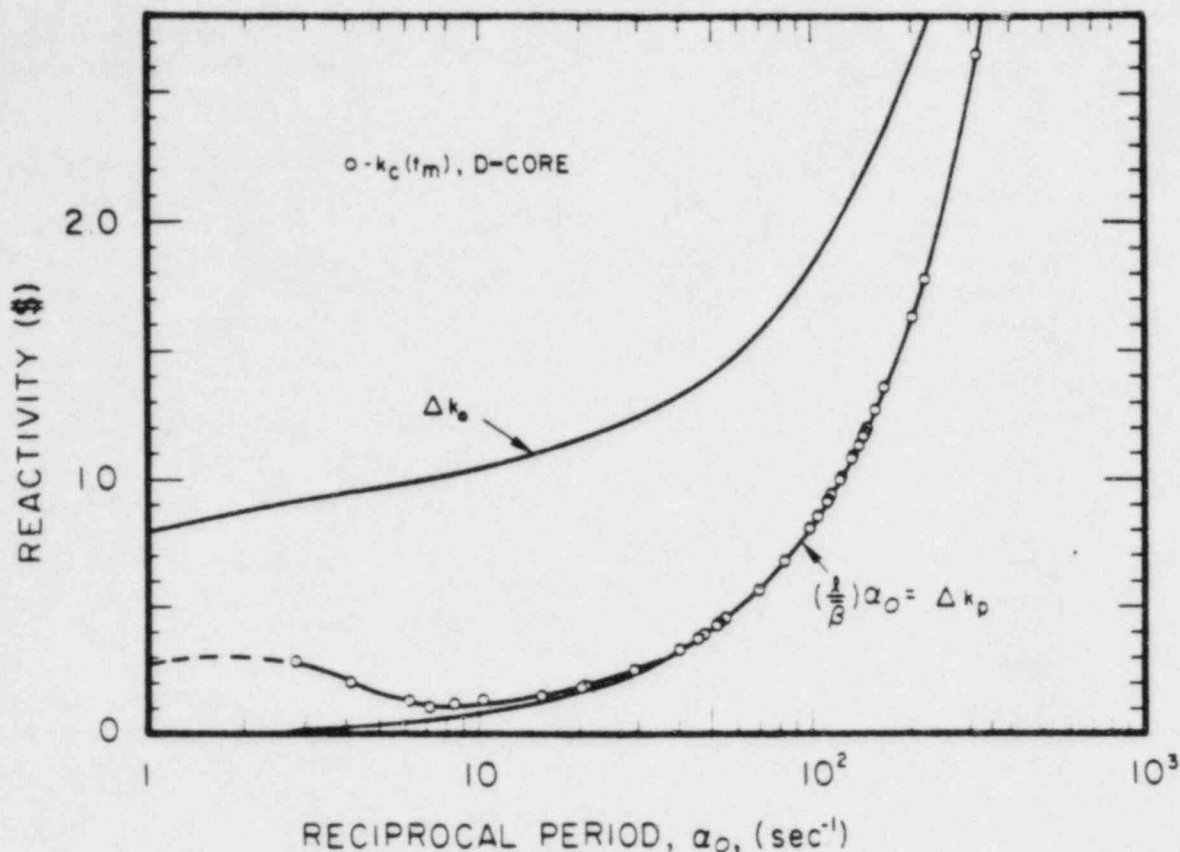


Fig. 12 $k_c(t_m)$, and Δk_0 , vs reciprocal period α_0 .

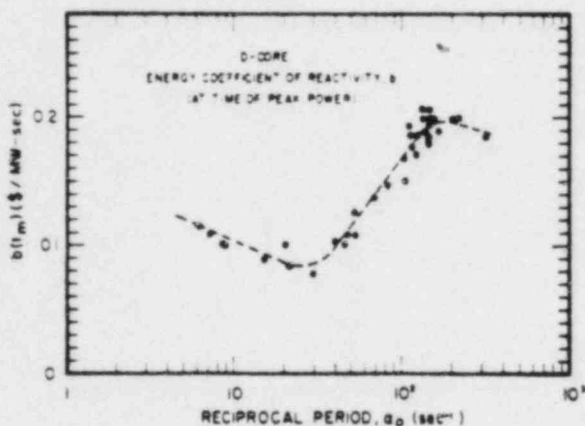


Fig. 13 Energy coefficient of the reactivity evaluated at the time of peak power as a function of the reciprocal period, α_0 .

jump) reflects this fact since at the time of peak power, void growth from boiling is only partially complete. Above $\alpha_0 = 100 \text{ sec}^{-1}$, it appears that the energy coefficient reaches a maximum and begins to decline, probably because of the onset of film boiling and the resultant decrease in heat transfer rate to the water.

2.5 Time Dependent Reactivity Compensation

Information on the dynamic condition of the reactor as indicated by the compensated reactivity has been obtained from analysis of the power data for tests with periods less than 10 msec. Two

aspects of the compensated reactivity behavior were carefully considered, viz, whether there was any evidence of the existence or proximity of, first, an upper limit to the amount of reactivity which could be compensated by boiling and, second, a significant change (specifically a reduction) in the rate at which self-compensation occurs. Possible failure of the existing shutdown mechanisms to terminate a power excursion for either reason might be anticipated by

computing the compensated reactivity for each test and extrapolating to the shorter periods.

The first step in this examination was to compare power burst shapes in order to observe any changes. The curves in Figure 14, drawn for this purpose, have been normalized at peak power both in magnitude and in time. For excursions with periods less than 9 msec ($\alpha_0 > 111 \text{ sec}^{-1}$), the power bursts were observed to become increasingly broad. That is, after passing through peak power, high power levels were sustained momentarily, prior to the fast decline which normally took place. At still shorter periods, this broadening began to occur before peak power. This effect resulted in excursions with greater relative energy releases and consequently increased the slopes of the energy versus reciprocal period curves as shown in Figure 8 for the region $\alpha_0 \geq 125 \text{ sec}^{-1}$. Broadening of the power burst is indicative of less rapid rate of reactivity compensation occurring around the time of peak power. This effect also was noted in the decrease in the energy coefficient as shown in Figure 13.

A possible explanation of the burst shape can be made from what is known about moderator boiling in the core. As the period is shortened film boiling arises over larger portions of the core and is established earlier in the burst with respect to peak power. This film boiling can inhibit the formation of larger amounts of steam and retard the self-shutdown process, leading to the observed broadening of the power peak. The power decrease is equally delayed but, when a sufficient degree of superheat exists, it appears that instabilities in film

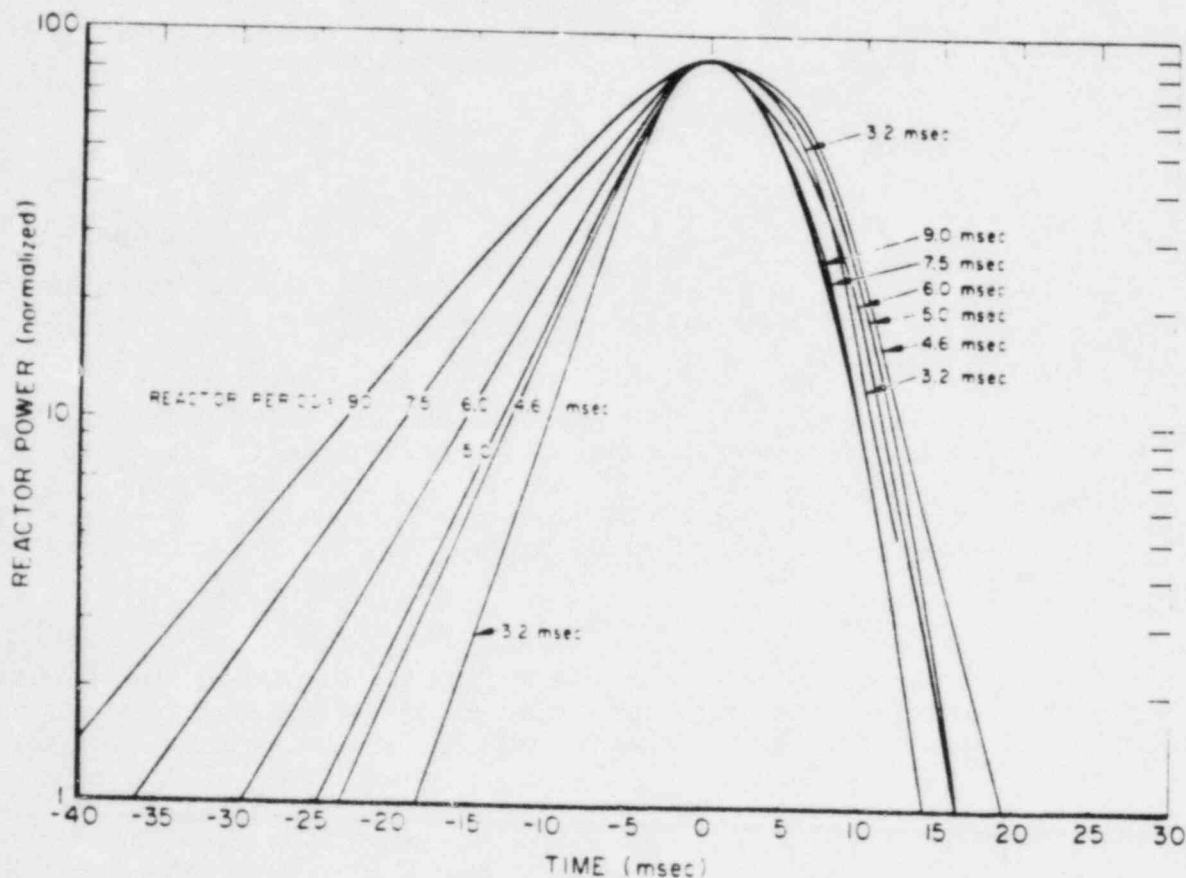


Fig. 14 Various power profiles for several different periods normalized at peak power.

boiling arise, resulting in the production of a larger amount of steam and, therefore, increasing the rate of production of shutdown reactivity. The eventual sharp power decline after peak power, which becomes sharper with shorter periods, might thus be associated with a break in film boiling.

To study the specific compensated reactivity, Δk_C , responsible for the change in burst shape, the time dependent reactivity was computed, for several excursions in the short period region, by solving the space independent kinetics equation (Figure 15). The results of this study showed that the rate of reactivity compensation during tests in the intermediate period range, say between 20 msec and about 8 msec, is characterized by a curve such as that in Figure 15 corresponding to $\tau_0 = 9.5$ msec, which demonstrates a fairly rapid but smooth compensation to several dollars. However, an inflection in the compensation reactivity curve was observed to occur at periods of about 7.5 msec (not shown) and this inflection became more abrupt at shorter periods. For $\tau_0 = 6.4$ msec, peak power is established as the value of Δk_C passes through about 1.30\$. Fully another dollar is compensated before the inflection occurs, so that for this case, at least, considerable power decline occurred before the shutdown rate was significantly reduced by the inflection.

For tests with shorter periods, around 5 msec, peak power was established at about the beginning of the inflection, and shutdown of the power was consequently delayed. Finally, for $\tau_0 = 3.2$ msec, peak power occurred during (rather than before) the inflection resulting in the observed broadening of the burst both before and after peak power.

Two conclusions are drawn concerning this behavior of the reactivity compensation. First, it might be expected that at still shorter periods ($\tau_0 < 3$ msec) the inflection in the compensation curves would occur prior to peak power, giving somewhat the effect of a transient with two periods (ie, the initial asymptotic period will be followed by a transition region as initial compensation takes place and, then, during the inflection another and longer "period" may be established).

Second, since the compensated reactivity is primarily a consequence of the steam content within the core, the inflection indicates an inhibition in the rate of void growth, which might have resulted from a nonuniform process in the rate of steam void production under transient conditions such as exponentially heating of fuel plates.

Behavior somewhat of this nature was anticipated from the results of previous in-pile studies of transient boiling [6] conducted at Spert. These studies revealed that during short-period power excursions, the initial growth of steam bubbles was often suppressed momentarily and that complete vapor blanketing of the fuel plate finally arose from a second generation of bubbles.

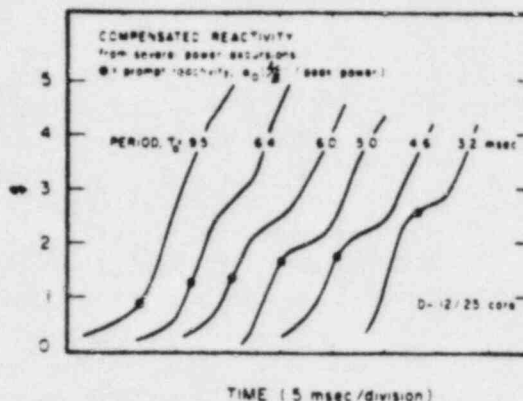


Fig. 15 The time dependent compensation of reactivity for several short-period power excursions of decreasing period. The occurrence of peak power is indicated on each curve and is coincident with the compensation of the prompt reactivity.

The calculations of reactivity compensation are obtained from the space-independent kinetics equations and would not reflect the above described void behavior unless nearly all regions of the core gave rise to the same process of boiling simultaneously. However, during very short-period power excursions, the time-lag between high and low flux regions of the core is correspondingly decreased, and the specific behavior of boiling void production (and condensation) should become increasingly apparent in the reactivity calculations. It is possible that this effect is responsible for the enhancement of the reactivity inflection noted in Figure 15 as shorter periods are achieved.

2.6 Maximum Reactivity Compensation

The maximum reactivity compensation attained during a power excursion, $\Delta k_C(\text{max})$, has also been computed for several of the shortest period tests and values ranging between 6\$ and 7\$ have been found. It is not apparent from these data just what functional relationship exists between $\Delta k_C(\text{max})$ and the reciprocal period in this region, but it does appear that in the region investigated (ie, between $\lambda_0 = 150$ and $\lambda_0 = 312 \text{ sec}^{-1}$), $\Delta k_C(\text{max})$ is not rapidly changing. The excess reactivity, Δk_0 , however, increases rapidly over this region (Figure 12) and it can be expected that at some period complete shutdown will become difficult. As the calculations indicate, such a condition may arise for initial reactivity insertions above 6\$ which would yield periods less than about 1.6-msec.

2.7 Fuel Plate Damage

After each test in which measured temperatures exceeded a few hundred degrees, fuel plates were inspected in order to ascertain the amount of damage sustained from thermal distortion. The first indications of permanent warping were obtained in a test with a period of 7 msec, for which the maximum recorded temperatures were about 400°C.

During shorter period tests, damage to the plates gradually increased from slight, lengthwise bowing to more localized bowing around the hot spot of the plate, succeeded by a type of sinusoidal rippling along the length of the fuel plates. The amplitude of these ripples was greatest a few inches below the center of the plate at a position corresponding to the peak flux, and attenuated toward either end of the plate in low flux regions.

Rippling of the plates was apparently caused by the constraint against expansion existing within the fuel plates both by the cladding and the edge of the fuel plates since these nonfuel-bearing materials remained comparatively cold during the power excursions while the central meat was heated.

It was observed that following excursions in which high plate temperatures were reached (ie, 550 to 650°C) the ripples became flat-topped or "square-wave" in profile, creating, as a consequence, regions on the plate of very high curvature. Failure of the clad by cracking was common in these regions.

Warping of the fuel plates was sufficient in several cases to cause complete channel blockage. The amplitudes of the ripples were often greater than the plate spacing (0.179 inch), and occasionally adjacent plates having rippled in opposite directions would come together and close off the water channel.

In the test with a period of 5 msec, eruptions of molten fuel occurred over about a 6-inch-high region on each of the six fuel plates in the central fuel

assembly, and over a small region of one additional fuel plate in an adjacent fuel assembly. About 0.5 percent of the total fuel plate area of the core showed signs of melting. Figures 16 through 22 show several damaged fuel plates of the central assembly from this test. Rippling and particularly the "square-wave" character of thermal deformation is apparent in most of the photographs.

Failure of the cladding by hot short cracking was widespread but most severe at the corners of the ripples. The actual surface of the cladding does not appear to have melted during the 5.0-msec period test. The molten material seen in the photographs from this test was mostly the uranium-aluminum alloy which had escaped through clad fractures. Eruptions of molten fuel (Figures 17 and 22) were preferentially located in high curvature regions.

Hot short cracking of the cladding is characteristic of the aluminum alloy used for these plates (6061 alloy) and probably promoted early failure of the clad. As seen in several of the photographs, the melted metal occurring in the 5.0-msec period test appears to have originated in the meat portion of the fuel plate and escaped through fractures in the yet unmelted clad. It is possible that another alloy of aluminum (such as 2S) less susceptible to hot, short cracking might have contained the molten fuel in this test. The results of a metallographic examination of the fuel plates are discussed in Appendix H, and a more complete discussion of fuel plate damage may be found in Reference 10.

For the test with a period of 4.6 msec, fuel plate thermal distortion and melting were more severe as seen in Figures 23 through 28. In this test, nearly 80 percent of the plates were warped and rippled to the extent that they could not be reused for subsequent tests. The region of melting was again centered about the hot spot of the core with a diameter (on a horizontal plane) of about six inches and a height of about nine inches. About two percent of the total plate area of the core was affected by melting and most of the melted plates were fused to adjacent plates as shown in Figures 26 through 28. Figure 23 illustrates the extent of melting as it occurred during the 4.6-msec test on a single plate located in the center (transient rod) assembly. It may be seen that, in contrast to the damage observed in the 5.0-msec test, melting of the clad surface did occur during the 4.6-msec test. Several plates from the same assembly, Figure 25, show severe constriction as a consequence of fuel melting and subsequent runout.

Maps of the melting regions for both the 5.0-msec and 4.6-msec tests are shown in Appendix D.



59

Fig. 16 Two fuel plates warped and fused together as a result of a 5-msec test.



59

Fig. 17 Fuel plate from 5-msec test showing melting and warping.



Fig. 15 Close view of fuel plate showing melt region, cracking of clad, and a thermocouple -- 5-msec test.

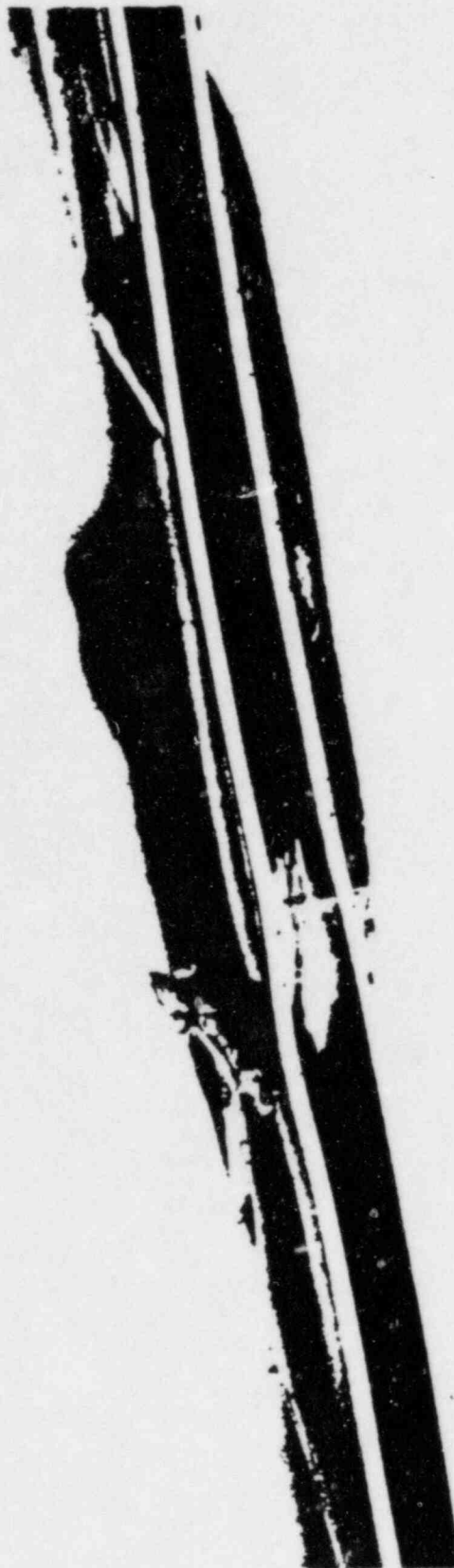


Fig. 19 Two fuel plates fused together -- 5-msec test.

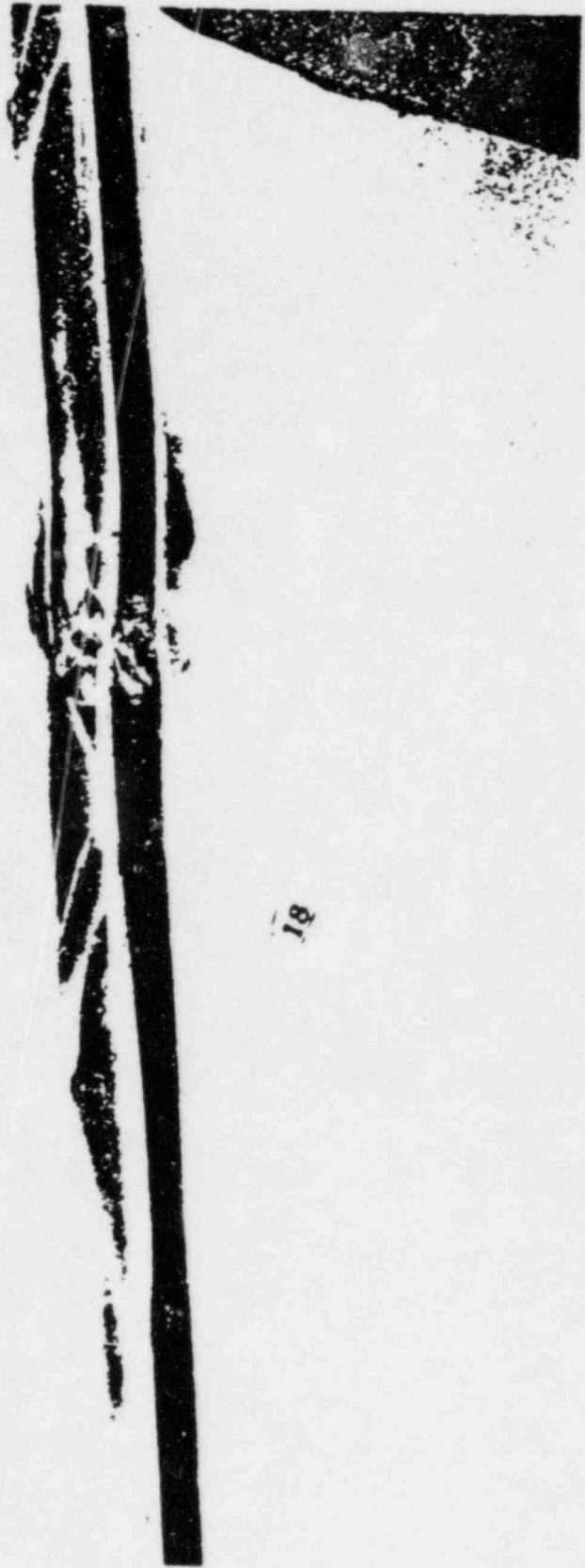


Fig. 20 Two fuel plates fused together -- 5-msec test.



Fig. 21 Typical melt eruptions and clad fracture of fuel plate -- 5-msec test.

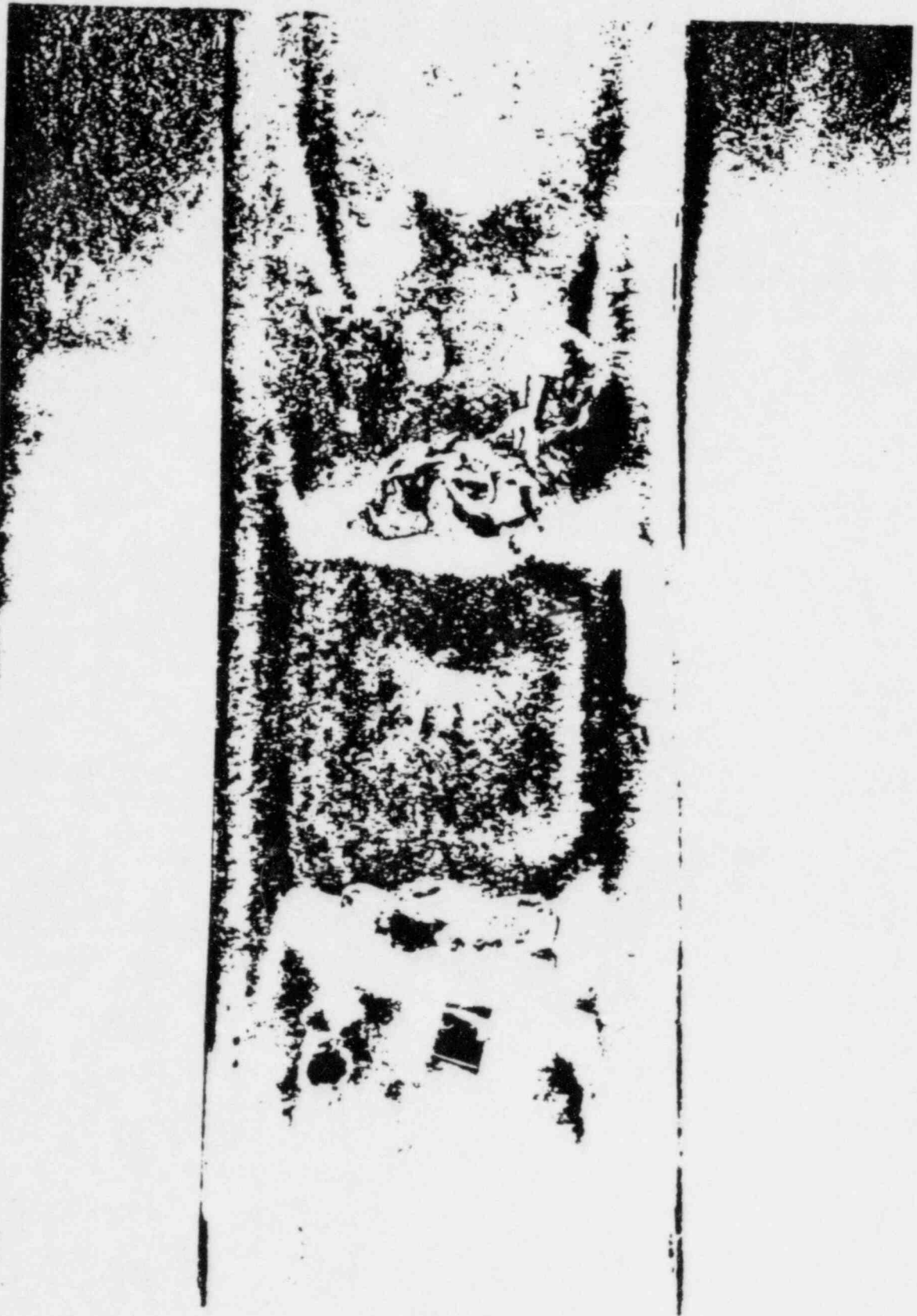


Fig. 22. Typical square-topped ripples and melt of fuel plate -- 5-msec test.

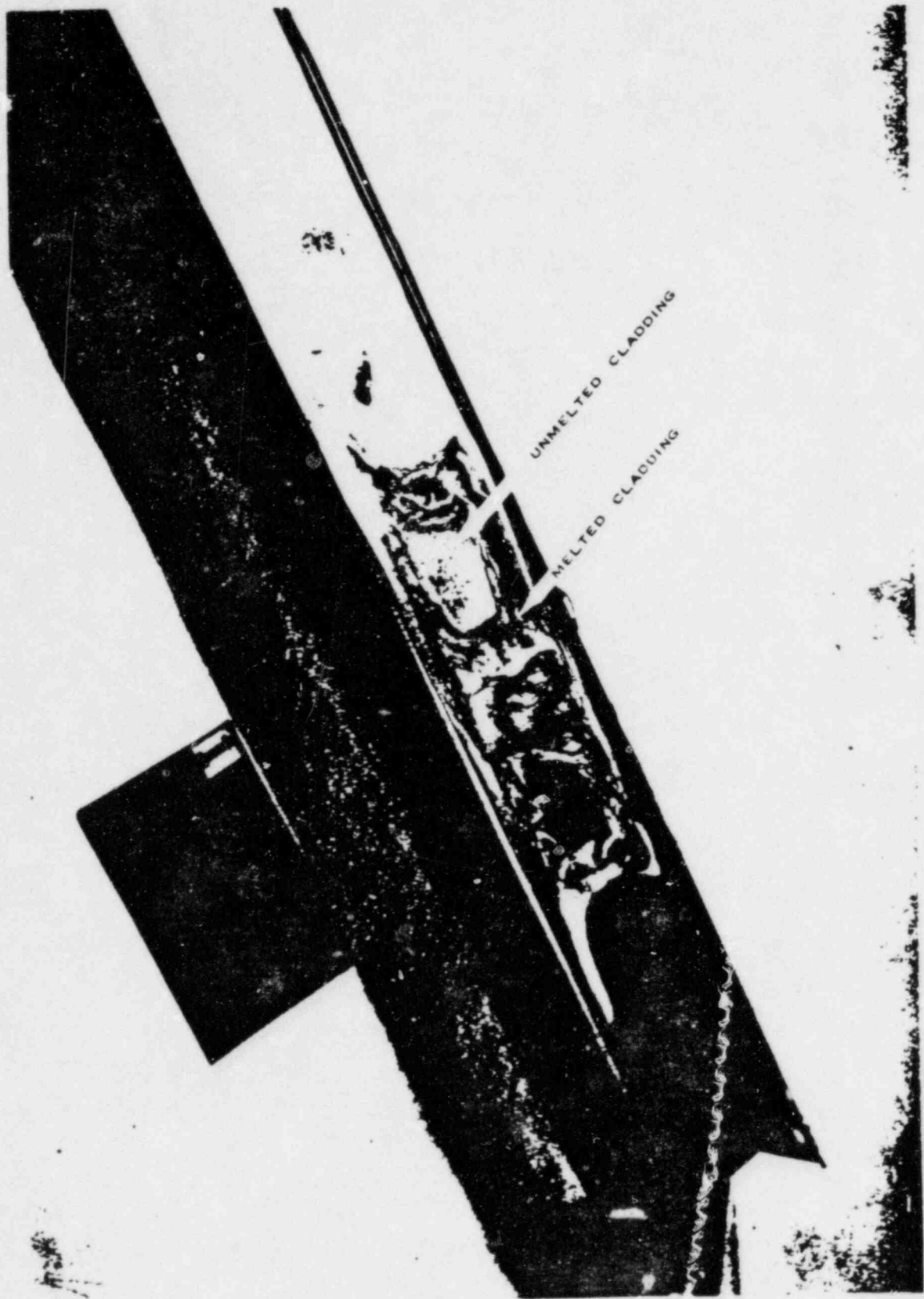


Fig. 23 Top fuel plate of central assembly showing warpage and melting -- 4.6-msec test. Regions of complete clad melting are visible.

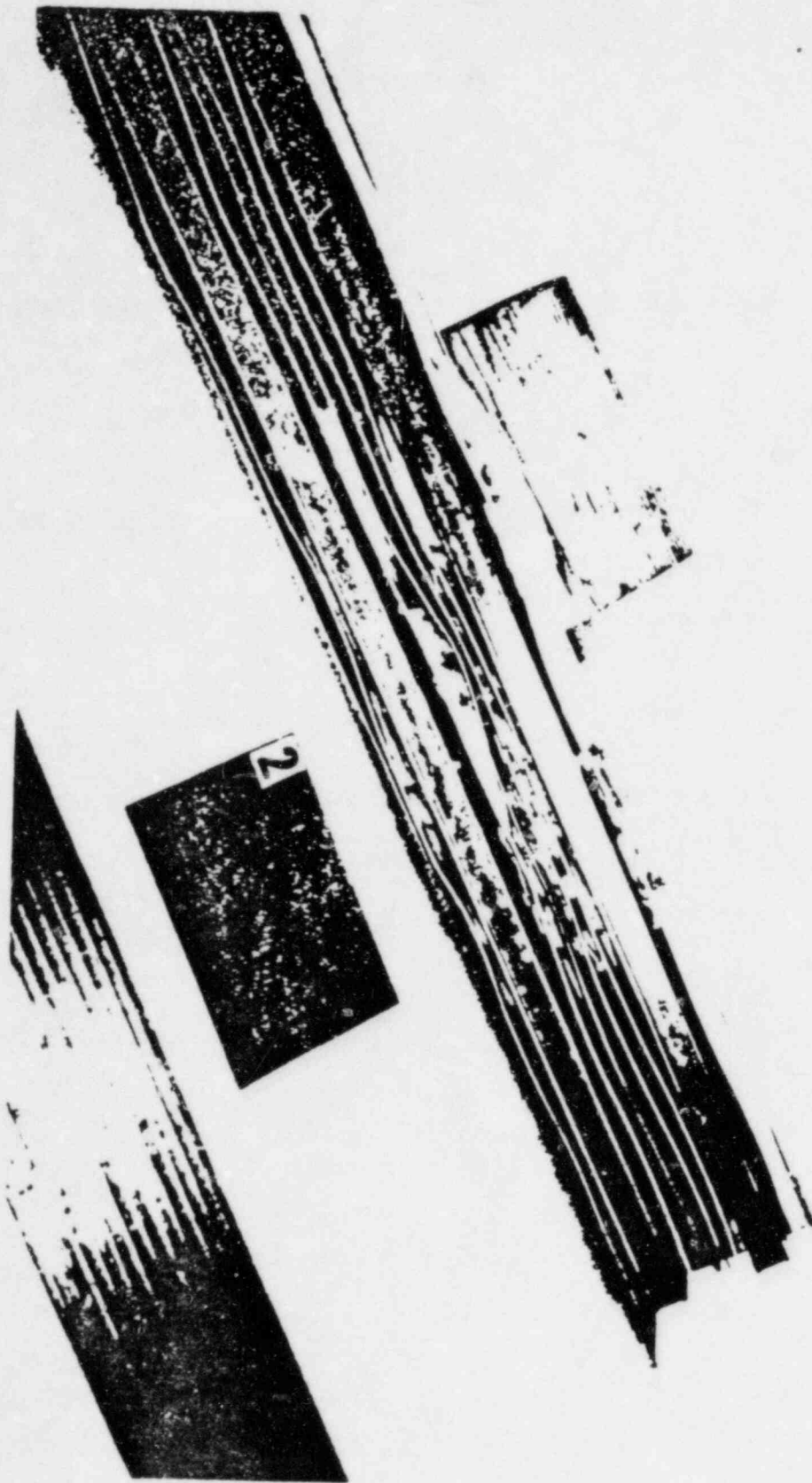


Fig. 24 Side view of central assembly showing extent of plate fusion -- 4.6-msec test.

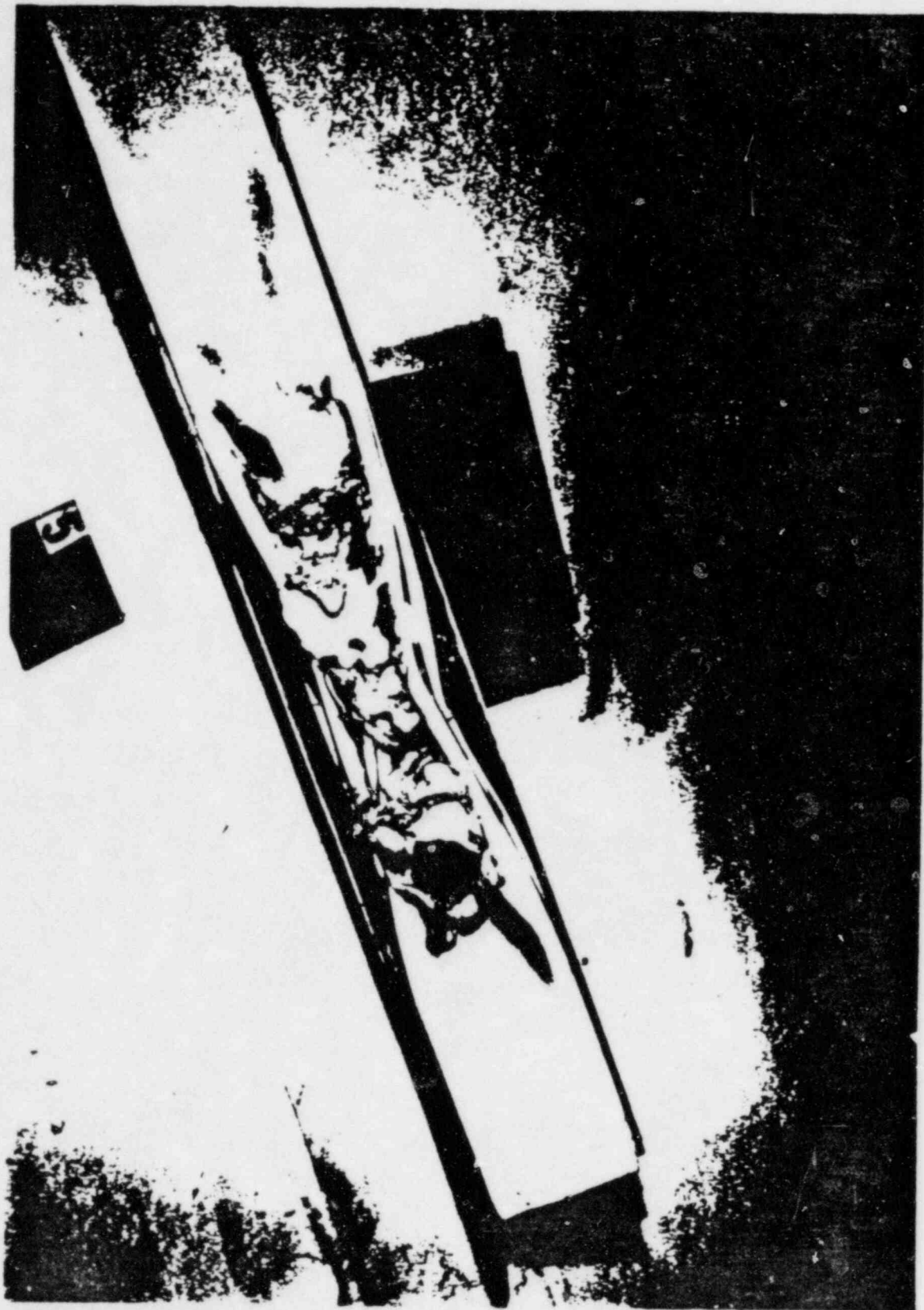


Fig. 25 Melting and plate constriction in center assembly -- 4.6-msec test.

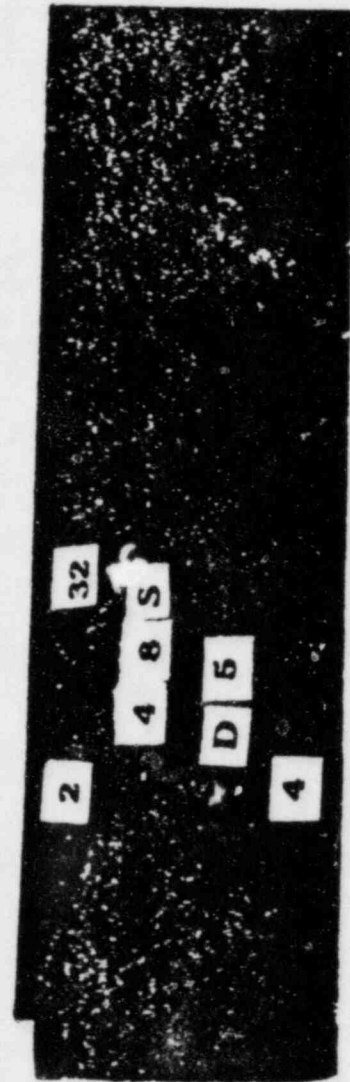
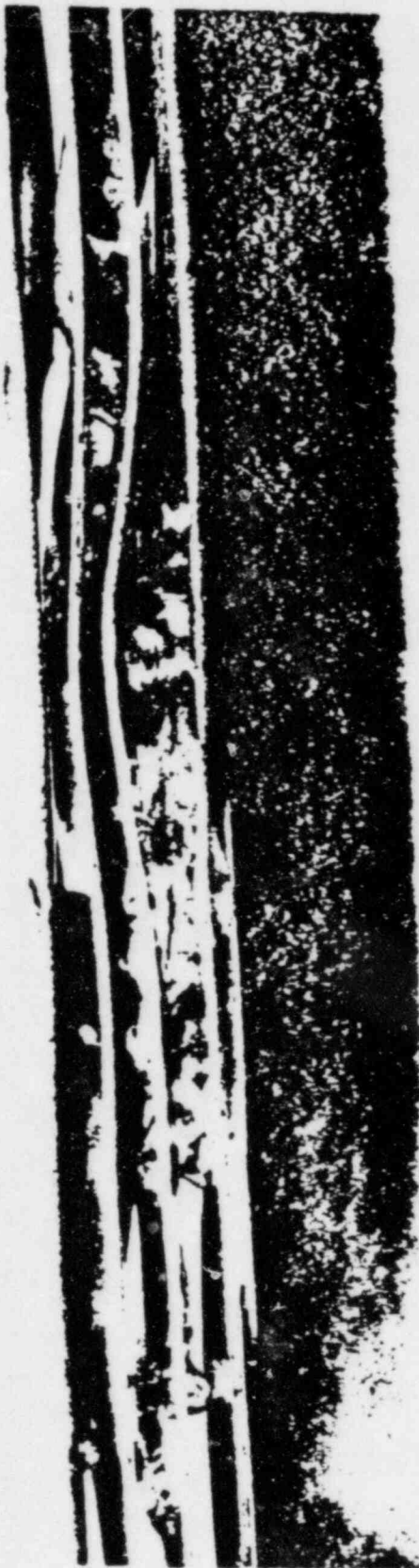


Fig. 26 Edge view of fused plates, position D5 -- 4.6-msec test



Fig. 27 Edge view of fused plates, position E6 -- 4 6-msec test.

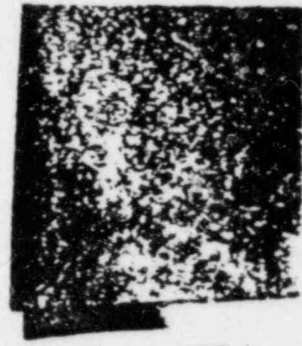
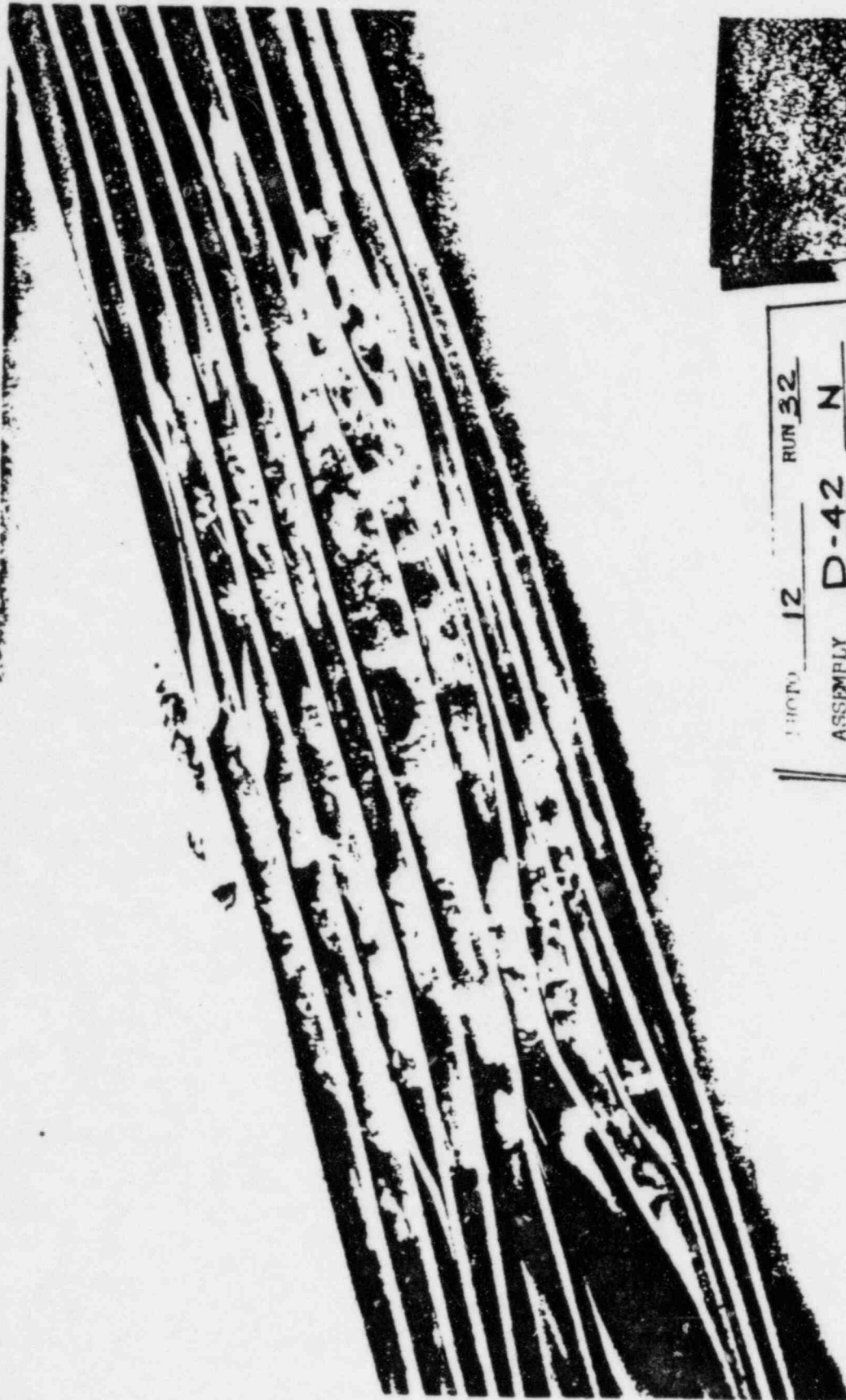


PHOTO	12	RUN	32
ASSEMBLY	D-42 N		
POSITION	F-5		
PLATE	1949		

Fig. 2- Edge view of fused plates, position F5 -- 4 6-msec test

IV. THE DESTRUCTIVE TEST

1. PREDICTABILITY OF TEST RESULTS

In accordance with the objectives of this program, power excursions were to be initiated with successively larger reactivities to obtain data on the nature and extent of damage encountered in the short period region and to probe for factors which might be responsible for the type of destructive pressure pulses which apparently occurred in the Borax test in 1954 [2] and more recently in the case of the SL-1 accident [11, 12].

The results of experiments leading up to the destructive test have been discussed in the preceding section but will be briefly reviewed with regard to extrapolability of the data to shorter periods. As discussed in the previous section, the measured power, energy, temperature, pressure, and the compensated reactivity had all shown regularity and predictability as the period was shortened. No evidence was observed in any of the data which would indicate the occurrence of unusual or unpredicted behavior in the period region just below 4.6 msec.

Although damage from thermal deformation had been produced in nearly 80 percent of the core and melting in about 3 percent, neither of these phenomena had produced a tendency toward the generation of large pressures despite the fact that fuel plate temperatures in many cases exceeded the critical temperature of water. In the 5.0-msec period test and the 4.6-msec period test, both melting and warping occurred, yet their occurrence was accompanied neither by the generation of significant pressures nor the displacement of materials.

2. TEST CONDITIONS

In the absence of any known threshold at periods proximal to 4.6 msec, the last test was approached with the specific objective of reducing the period by a substantial amount and establishing melting over a large fraction (about 40 percent) of the core. As with all preceding tests with periods below about 6.0 msec, the last test was conducted with the anticipation that an explosion such as occurred in the Borax-I test might occur although such could not be extrapolated or predicted. The period for the test was selected to be that which would produce fuel plate temperatures in the range 1000 - 1700°C. The 1000°C lower range limit was selected to ensure widespread core melting and the upper range limit of 1700°C was selected to avoid enhancement of the potential chemical reaction since studies at other laboratories [19] had indicated that near this temperature the chemical reaction between aluminum and water becomes more rapid.

A period of 3.3 msec was selected which required the insertion of about 3.5\$ excess reactivity. A peak power of 2.3 GW and a total nuclear energy of 33 MW-sec were predicted for this test.

In preparation for the test, a pneumatically operated transient rod ejection system was installed which was capable of ejecting the entire transient rod in about 85 msec.

The test was conducted under special procedures and with specified weather conditions. Safeguards which were adopted included evacuation from the area of all personnel not essential for the test and an alert status with various safety support services at the National Reactor Testing Station. Weather requirements for the test consisted of lapse conditions with no rainfall, wind from the southwest (190 to 250°) between 10 and 20 mph and a three hour predicted persistence of these conditions after the test. The wind direction was chosen to prevent a possible release of radioactive fission products from being airborne to other NRTS installations.

An extensive radiological effort (Appendix B and G) was planned, including ground-level dose measurements on a grid system extending downwind of the reactor building, and cloud tracking by airplane.

The area surrounding the reactor was inspected by airplane just prior to the test in order to assure that personnel were not inadvertently close to or downwind from the reactor.

Special instrumentation and reentry procedures were adopted to ensure the safety of personnel engaged in the reentry operation following the test since it could not be assured that normal control of the reactor would be possible nor that the usual operational information on the reactivity status of the reactor would be available.

Following completion of all pretest preparations, a period of about two weeks was spent in a state of readiness before meteorological conditions favorable for the test developed. The test, Run 54, was initiated at 12:25 p.m. on November 5, 1962.

3. TEST EVENTS

Immediately following ejection of the transient rod, a loud noise in the reactor area was heard over the intercom systems and a plume of water was observed to rise about 80 feet above floor level of the reactor building (Figure 29). Pictures on both television monitors in the control room were immediately lost apparently as a result of water hitting the cameras which were aimed directly at the core. It was found that the reactor control-rod-drive system could not be operated normally and that positive indication of the control rod positions could not be obtained. However, neutron levels (as indicated by neutron sensitive chambers) were declining normally.

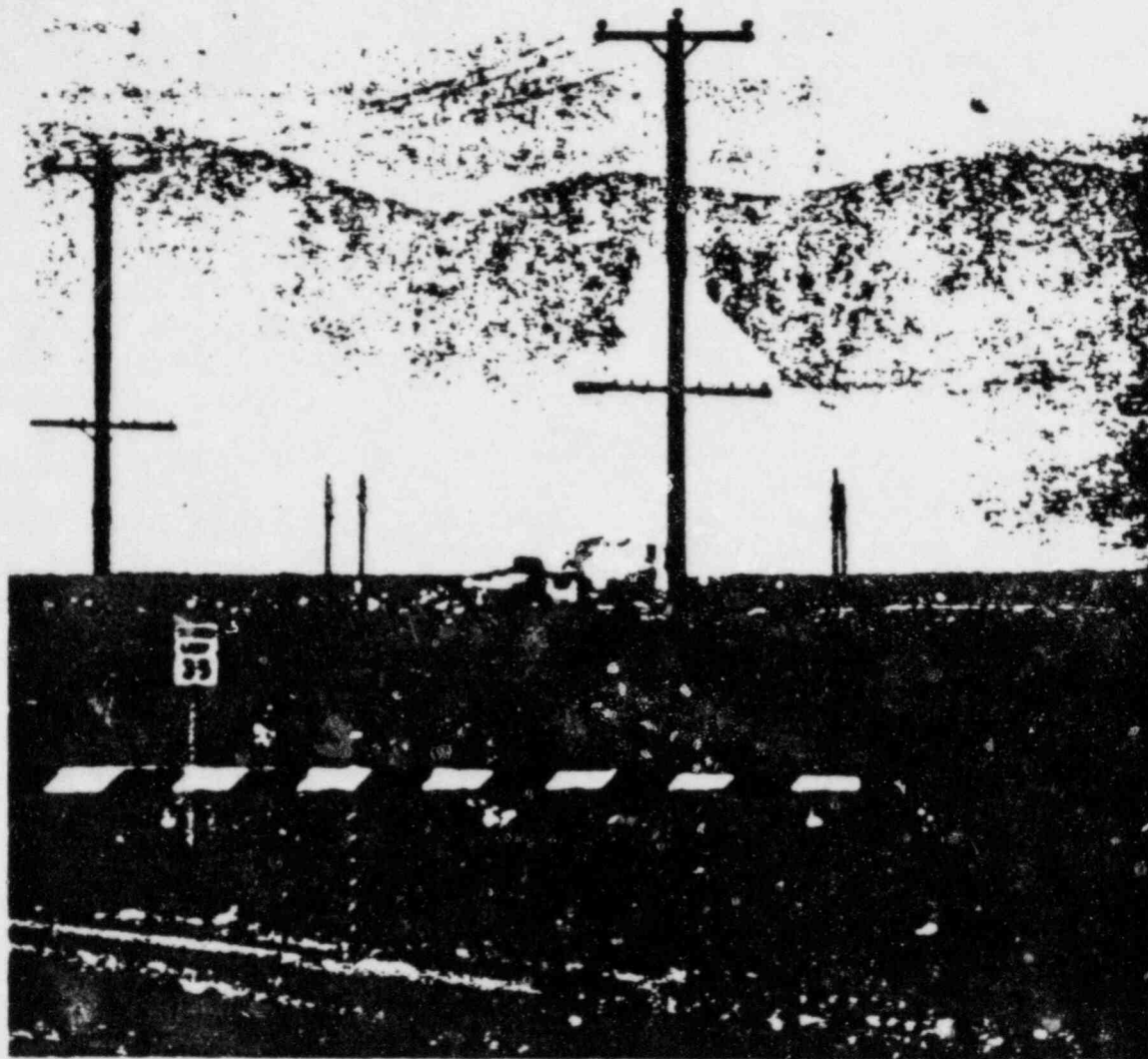


Fig. 29 Plume of water rising about Spert I during 3.2-msec test.

4. REENTRY

In accordance with procedures for reentry which had previously been established in the event that a positive indication of the shutdown condition of the reactor could not be determined (by means of the control system and the nuclear instrumentation), all water in the reactor vessel was drained by remote activation of a sump pump. As the water level reached 6-inch and 3-inch levels

above the vessel floor, a float-actuated, blast-protected, water level instrument [a] provided this information to the Control Center. Verification of the proper operation of this device was accomplished by partially refilling and redraining the vessel to test repeatability. Draining was completed and personnel reentry began about four hours after the test.

The first reentry team, equipped with several layers of protective clothing, self-contained breathing apparatus, and radiation monitoring equipment, approached the reactor while in radio contact with personnel in the Control Center and established that radiation levels in the reactor area were sufficiently low to permit recovery operations to begin around the reactor building. Short-time visual examination of the destroyed core in the vessel also was possible even though the normal shielding of water was absent. Although air activity in the reactor area was negligible following the test, all personnel in the first several reentry teams were required to use filter breathing apparatus for protection against contaminated particulate matter which might be airborne by the strong wind blowing at the time.

The radiation level at floor level over the open vessel (about 10 feet from the normal core center) was about 25 r/hr at the time of first reentry (3 hours and 55 minutes after the test). Other radiation measurements taken at this time indicated dose rate levels of 1.1 r/hr at roof level directly above the vessel (about 18 feet from the core), 85 mr/hr at "head" level about 5 feet from the edge of the vessel, and approximately 2 mr/hr at floor level about 50 feet in front of the reactor building.

After checking radiation levels, the reentry teams removed all motion picture cameras from the reactor area. The films were removed and processed immediately.

[a] See Appendix B for a description of this instrument

V. DESTRUCTIVE TEST RESULTS

1. DAMAGE TO THE CORE AND FACILITY

Immediately following the test it was possible to see that some of the control-rod-drive extensions were bent. Figure 30, a photograph showing a view of the front of the reactor building shortly after the test, shows the bent rod-drive extensions extending from the upper bridge (supporting the drive motors) to the magnet plates and dash-pots mounted on the lower bridge just below the lip of the tank. The lower bridge (visible at about floor level in Figure 30, and again in a rear view, Figure 31) had been raised and tilted. The lower bridge is normally about three feet below floor level and supported at each end by I-beams welded to metal plates in the concrete floor of the building. These end supports can be seen at each side of the reactor vessel. One end of the bridge had been thrust upward about three feet by the explosion and came to rest about two feet above normal level. Some debris and an overhead light from the reactor building can be seen on the floor in front of the vessel.

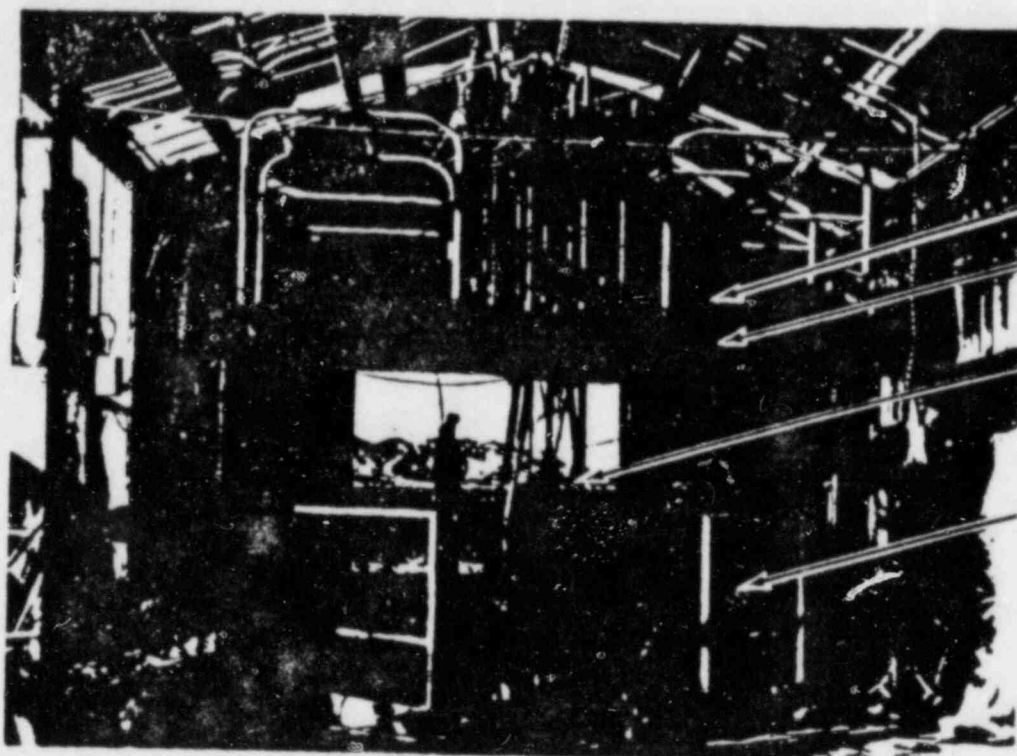
As shown in Figures 32 and 33, one of several roof support beams of the reactor building was bent upward, presumably by the water ejection.

Figure 34 shows the appearance of the reactor core prior to the test and Figure 35 is a similar view after the test showing the extent of destruction achieved by this test. The lower bridge, seen at the top of both figures, supports several items including instrument leads, control and transient-rod blades, and a periscope (the large black tube in the center of Figure 34). Figure 36 is a close-up view of the debris in the vessel. The periscope can still be seen at top, center. Immediately to the left of the periscope can be seen the transient rod extending down to the two aluminum blades, which have been spread into an inverted Y-shape. The transient rod blades are normally parallel and reside in a fuel assembly in the center of the reactor.

The condition of these blades suggests that a destructive pressure pulse probably originated between them in the central assembly of the core. Just to the front and to the right of the transient blades can be seen two of the four control-rods. The control rod blades, by contrast, are pressed together into a crescent shape.

On the right of the picture, Figure 36, the reactor vessel can be seen to be bulged outward between reinforcing rings which were attached to the exterior of the vessel. Since the vessel was back-filled, the bulging would have caused displacement and compaction of the surrounding earth. Other items identified in Figure 36 and in Figure 37 include ion chambers, core support structure, several damaged fuel assemblies, many fragments of fuel plates, underwater lamps, pressure transducers, etc.

Figures 38 and 39 show the general types of damage obtained in fuel assemblies and plates. In general, the central portions of fuel plates have been melted and subsequently disintegrated, leaving only the tops, bottoms, and the unfueled edge strips still intact. Further photographs of the test damage are presented in Appendix E.



CONTROL ROD
DRIVE MOTORS

UPPER
BRIDGE

CONTROL
ROD
EXTENSIONS

LOWER
BRIDGE
SUPPORT

Fig. 30 Front view of reactor building showing damage incurred to control rods.



PERISCOPE

LOWER
BRIDGE
SUPPORT

LOWER
BRIDGE

Fig. 31 Rear view of control rods and lower bridge.

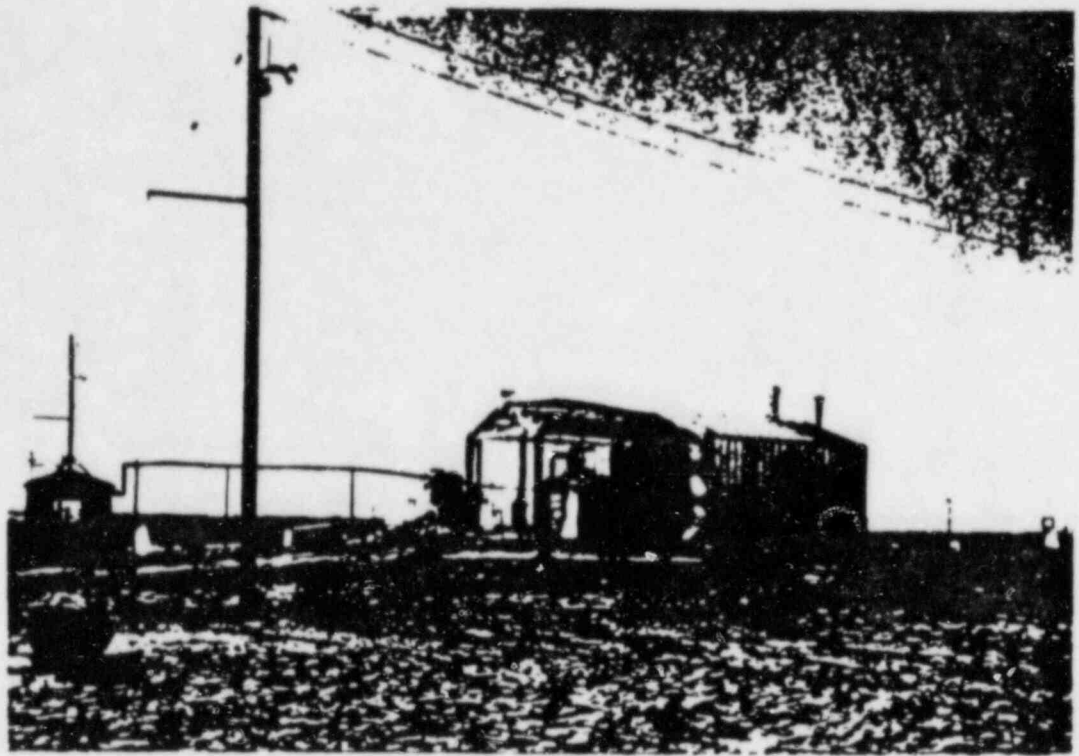


Fig. 32 Side view of reactor building showing bent roof purlin.

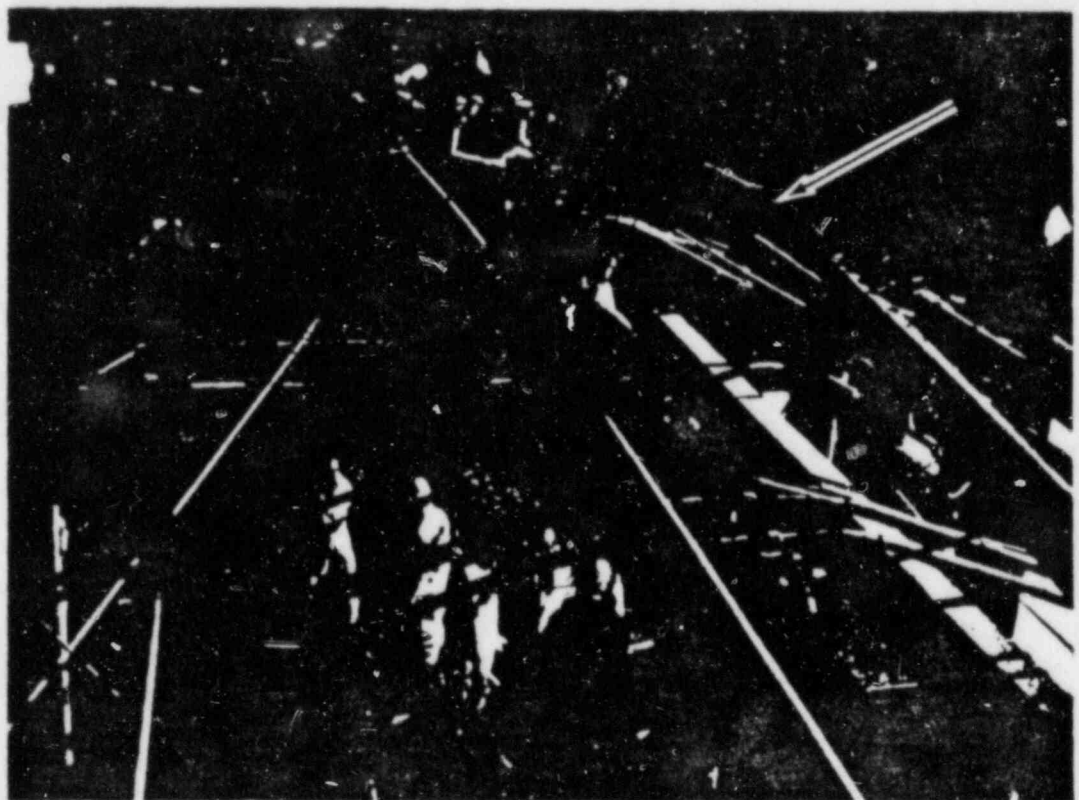


Fig. 33 Close view of bent roof purlin.

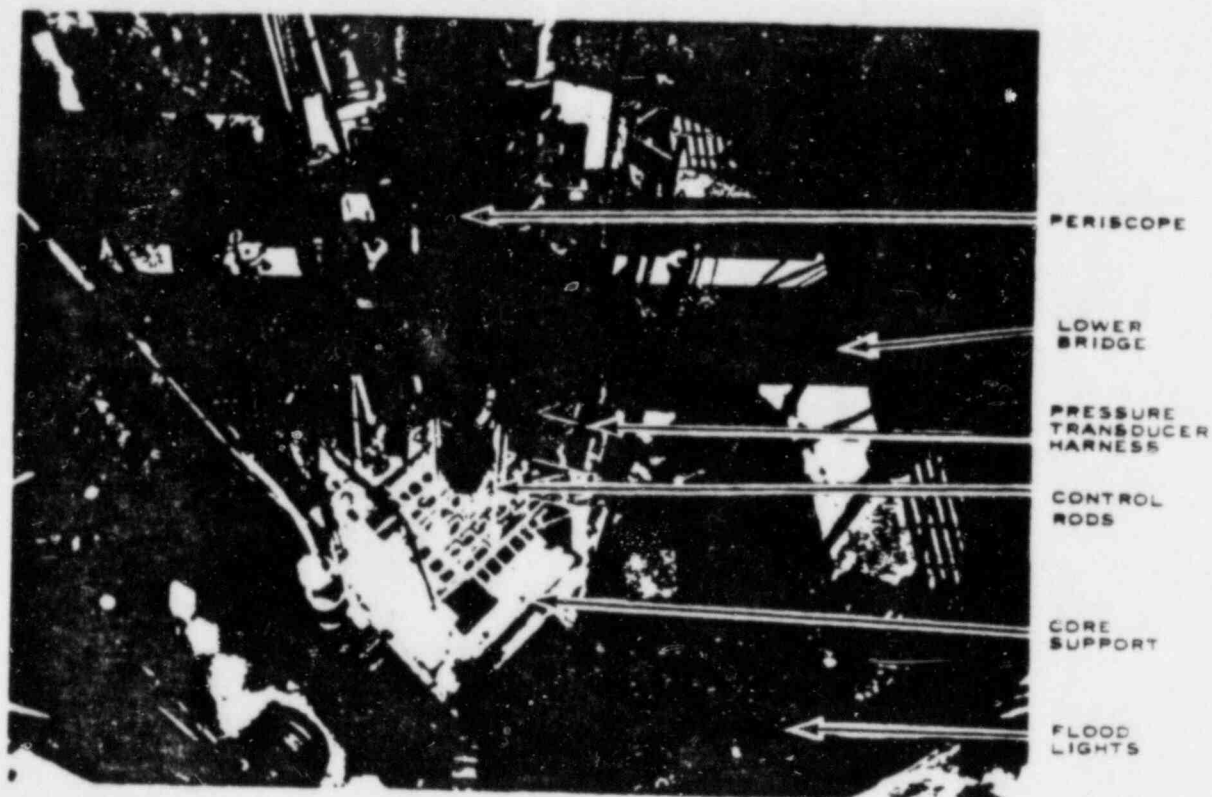


Fig. 34 View of reactor before destructive test.

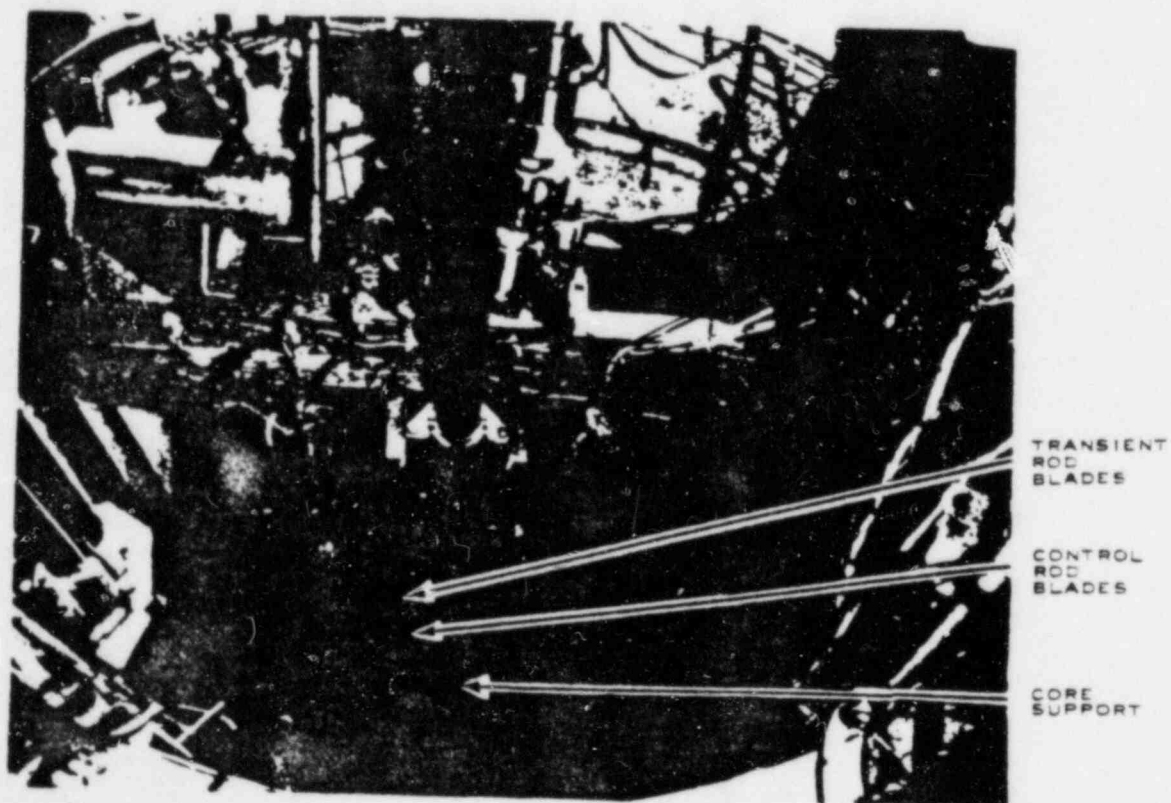


Fig. 35 View of reactor after destructive test.

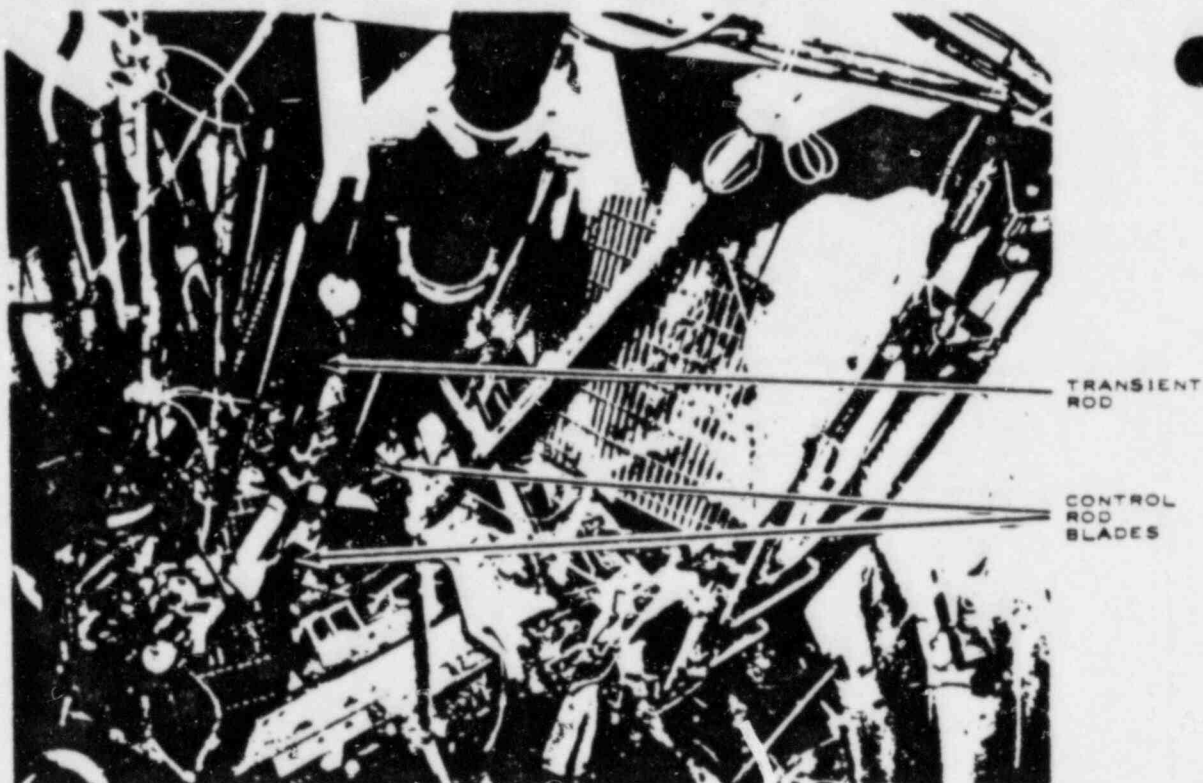


Fig. 36 Close view in vessel after destructive test.

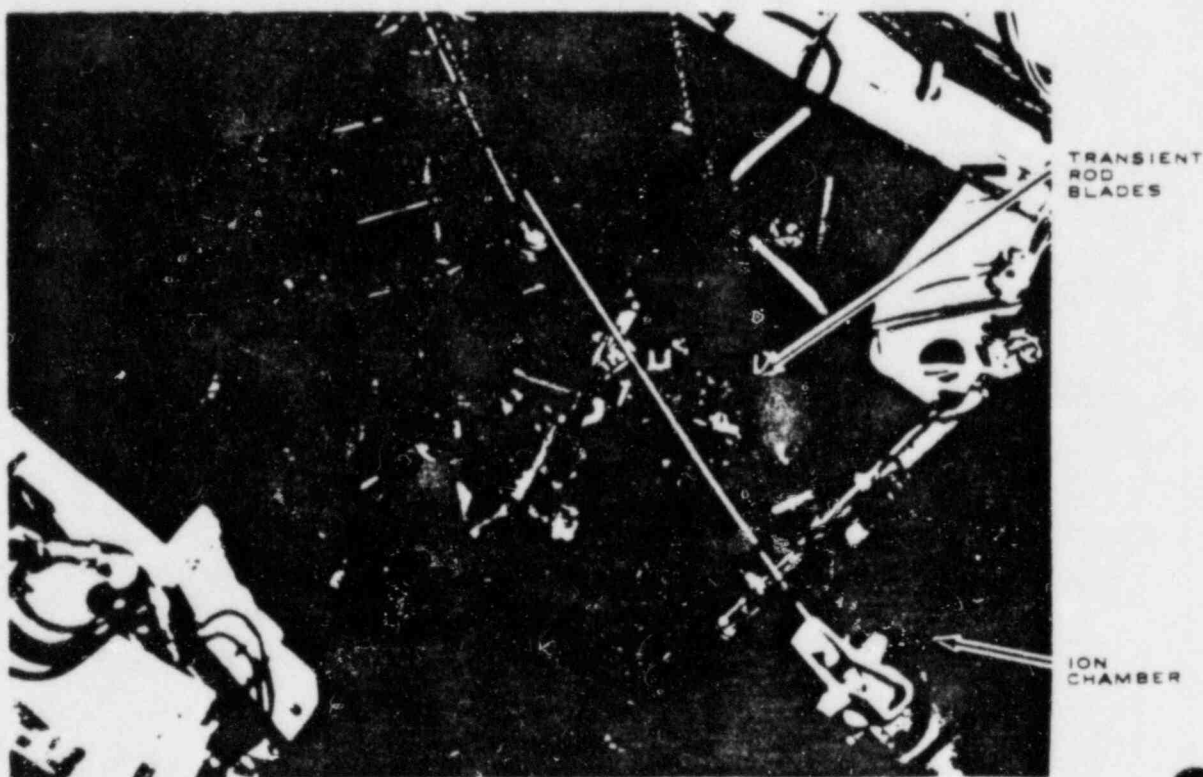


Fig. 37 Close view in vessel after destructive test.



Fig. 38 Typical plates from peripheral assembly-edge view, position G6.



Fig. 39 Fuel plate end fragments from assembly D5.

2. TEST DATA

2.1 General Behavior

Data from the destructive test indicate clearly that the power excursion was essentially complete and the reactor in a typical post-burst shutdown condition at the time the explosion began. The power, shown in Figure 40, had completed a normal excursion, with a period of 3.2 msec and a peak of 2.3 GW. The total nuclear energy release was 31 MW-sec. The reactivity compensation as inferred from the burst shape reached about 6.5\$ total compensation prior to the explosion. At the time of the first indication of the explosion, the power had declined to a level less than five percent of peak, and it is estimated that less than 0.6 MW-sec of nuclear energy was released in the remainder of this power excursion after the explosion began. In other words, the power excursion had released essentially all of the expected nuclear energy before the explosion.

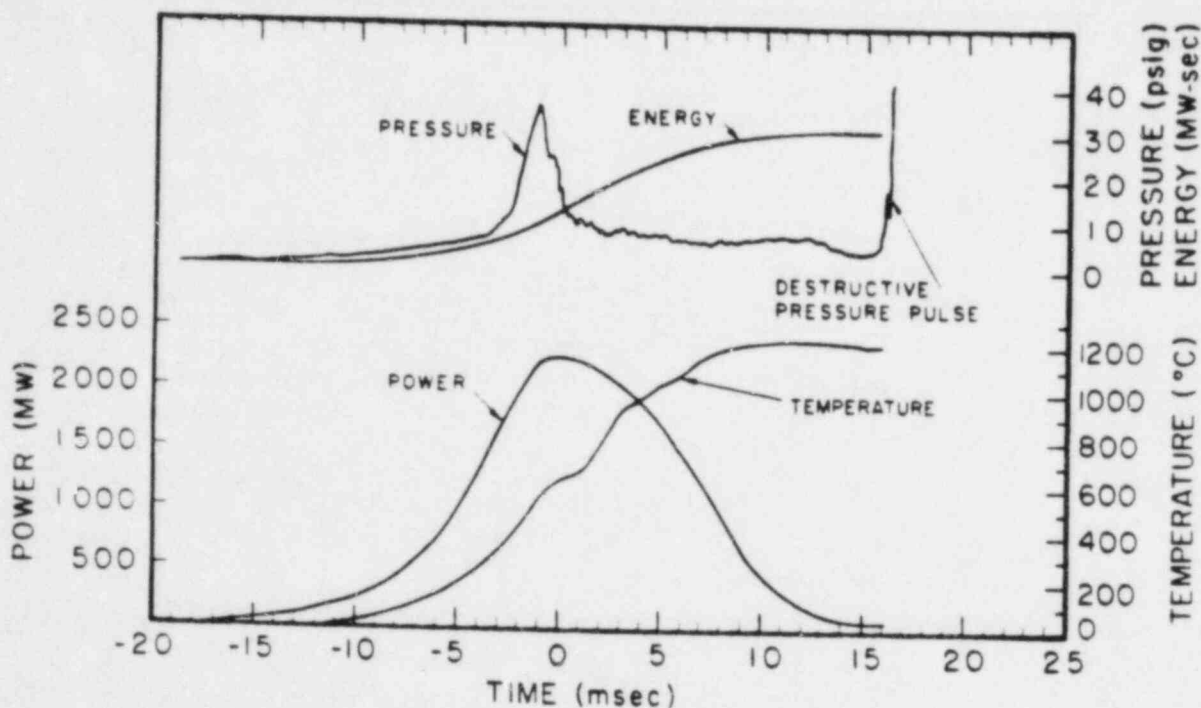


Fig. 40 Plot of data from Run 54, the destructive test.

This sequence of events, that is, a complete power excursion (including shutdown) taking place before the explosion, is in apparent contrast to the Borax-I destructive test. In the Borax test, the data do not permit a definite separation of the two events (in time) and seem to indicate the occurrence of some explosive effects even before peak power.

Since the nuclear energy release was nearly complete before the first indication of an explosion, the temperatures of the fuel plates very likely had reached their maxima and were beginning to decline. Measurements of fuel temperatures obtained from fuel capsules (Appendix B) which approximate actual fuel plate meat temperatures indicate that maximum temperatures were probably reached several milliseconds before the explosion (Figure 40). Con-

ventional thermocouples attached directly to the fuel plates near the core hot-spot, however, had either failed or were considered to be inaccurate at the above-melting temperatures attained.

Calculations of fuel plate temperature at the core hot-spot (see Reference 13 and Appendix F) indicate that maximum meat temperatures did not exceed 1400°C and that at the moment of the initial explosive pressure, fuel plate surface temperatures were probably near the melting point of aluminum (660°C).

The pressure trace shown in Figure 40 is typical of several traces obtained during the destructive test from low-range pressure transducers up to the time of the explosion. As with all previous pressure data, the pressure pulses appearing at about the time of peak power are associated with the onset of boiling in the core. Maximum shutdown (or boiling) pressure for this test (shown in Figure 11) was about 35 psig which constitutes a significant increase above the 9 psi pressure obtained from the 4.6-msec period test and which is slightly higher than predicted.

Additional plots of destructive test data are shown in Appendix C including temperature, pressure, strain, and power. Details of measurements of the total energy release, and maximum temperatures are given in Appendices B and F, respectively.

As a consequence of breakage and electrical shorting of many of the transducer cables during the explosion, the data recorded on oscillograph records (Figure 41) are extremely difficult to read. Most of the instrumentation which was located in and adjacent to the core was immediately destroyed by the explosion and produced erratic signals on the oscillograph record which tended to mask much of the remaining data.

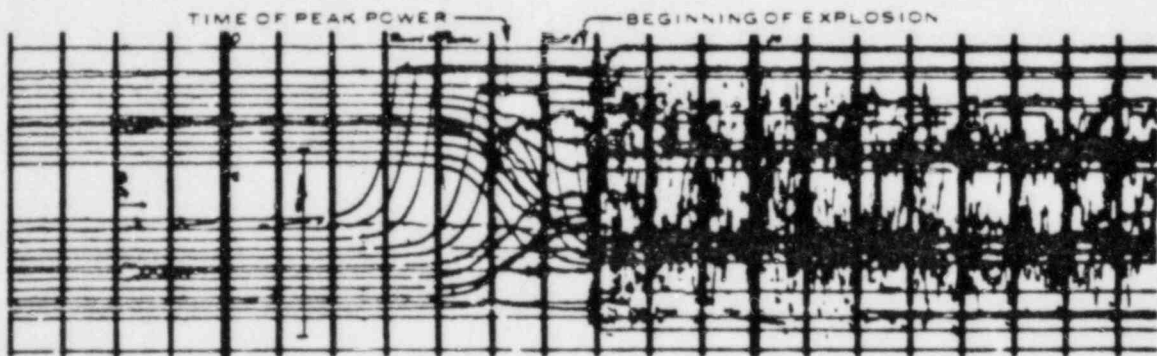


Fig. 41 One of four oscillograph records obtained during Run 54, the destructive test. The time elapse between vertical lines is 10 msec.

2.2 Discussion of the Destructive Pressure History

Detailed analysis of the oscillographic records has resulted in the conclusion that the initial rise of destructive pressure in the water near the core was extremely fast and probably was not recorded accurately due to the inadequate bandwidth of the recording galvanometers (nominally, 5 kc). The indicated rate of the pressure rise varies considerably from one transducer signal to another but the oscillograph trace which could be followed and measured with the greatest confidence (Figure 42) indicates that the pressure increased from zero to a first

peak of about 2800 psig in less than 300 μ sec, with a rise time (ie, 10 to 90 percent) of about 150 μ sec. Many other traces which could not be followed all the way to a first maximum also indicated rise times of 150 μ sec and less: One pressure signal recorded on magnetic tape was observed to rise from 0 to 30 psig in about 20 μ sec (close to the rise time limit of that system).

The 2800 psig maximum pressure recorded at the beginning of the explosion (Figure 42) is open to some question because of the difficulty in following the trace and because the pressure pulse itself apparently contained a broader frequency spectrum than the galvanometer was capable of recording. Data from several other transducers were not usable because of interference from other traces and also, more commonly, because of failure of the transducer. A single 100,000-psig range transducer, which did not fail, yielded a small amplitude signal which was difficult to measure accurately. Oscillations of this trace, both negative and positive, could be contained within an envelope of ± 3000 psig during the first two milliseconds of the pressure burst and within about ± 8000 psig for several more milliseconds before becoming quiescent.

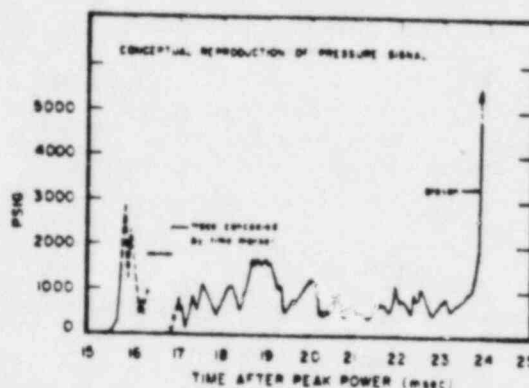


Fig. 42 Pressure recording obtained during Run 54, the destructive test. Dashed line indicates region in which original recording was too faint to follow with confidence.

At the onset of destructive pressures, nearly all of the low-range pressure transducers failed (as expected) usually within the first millisecond. The failure of some high-range transducers (ie, 0 to 10,000 psig), such as the one which provided the data shown in Figure 42, was unexpected since the pressures apparently did not exceed the rated range values of these transducers. Such failures, it has since been learned, are attributable to a characteristic of the strain-gauge type transducers which leads to fracture of the strain-gauge wires whenever the environmental pressure contains frequencies approaching (or above) the resonant frequency of the transducer, which in most cases was between 10 and 20 kc.

Although it was possible to establish that destructive pressures commenced to develop only after the nuclear excursion was essentially complete, ie, about 15 msec after peak power, it is not possible to deduce with certainty from any of the recorded data the exact nature of the pressure history after the pressure rise was initiated. For instance, there is no recorded evidence that the explosion consisted of just a single pressure pulse. In fact, preliminary studies based upon photographic measurements of the time and velocity of water ejected from the reactor vessel strongly suggest that a considerable fraction of the total pressure impulse occurred at a much later time, viz, more than 40 msec after peak power, such as might occur as a result of a series of pressure pulses covering a time span (from the first pulse to the last) of at least 25 msec or more.

It was possible to obtain additional data on the maximum pressure from an examination of damaged pressure transducers. Several of the pressure transducers used for the destructive test were of the diaphragm type rated for relatively low pressures (0 to 300 psig), and permanent deformation of the diaphragm occurred during the explosion. Laboratory studies of these transducers indicated

that such diaphragm deformations could be calibrated for both static and dynamic (or pulsed) pressure. Pulses with rise times as short as $100\text{ }\mu\text{sec}$ were generated to establish the calibrations, and in Figure 43 the results are shown for a typical transducer rated at 0 to 300 psig.

From the calibration of Figure 43, and the deformations observed on six different transducers used during the destructive test, peak pressures were established for several points external to the core. These pressures together with the single recorded pressure of Figure 42 (at position No. 12) are shown on a schematic of the core in Figure 44.

Pressures of about 4000 psig are indicated at symmetrical positions 8 and 13, each about 10 inches from the sides of the core. Positions 3 and 4, respectively, 11 inches and 8 inches from the top and bottom of the core (on the Z-axis) also show similar pressures around 2500 psig. A higher, and seem-

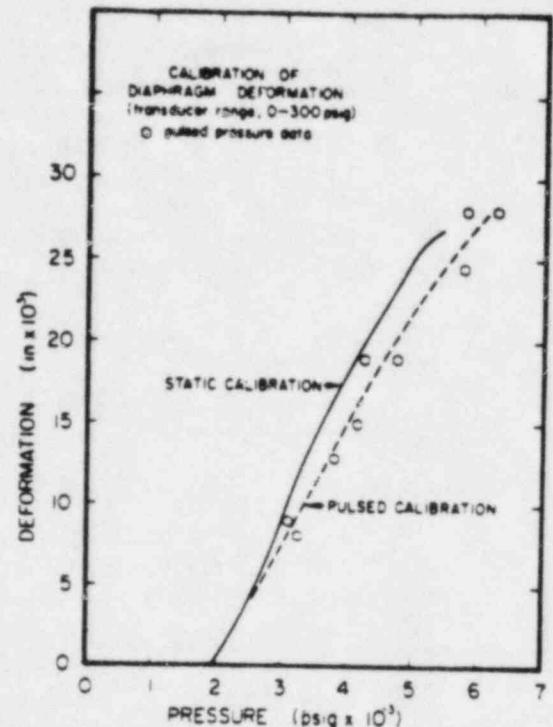


Fig. 43 Static and pulse calibration of permanent deformation of diaphragms of 0 - 300 psig range pressure transducers.

ingly anomalous, pressure at position 6 is attributed to reinforcement as a result of pressure reflection from the concrete floor of the vessel.

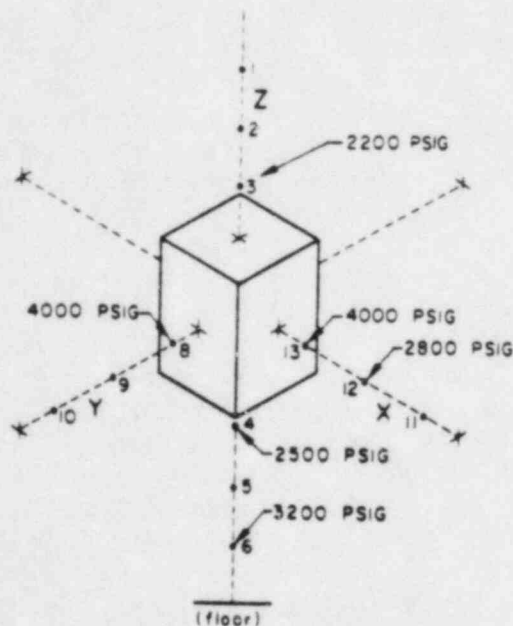


Fig. 44 Map of peak pressures around core during destructive test. All pressures were obtained from measurement of deformed diaphragms except at position 12 which was obtained by recording. See Table B-II for actual locations.

Studies of deformation also were made of the deformation of other selected items near the reactor, but these were generally inconclusive due to the complexities of geometry, materials, and pressure distribution. For the bulged vessel itself, yield pressure is about 140 psi but the actual pressure required to cause the vessel damage could not be computed due to the presence of the earth backing. Inside of the core, a crushed, air-filled tube indicates that pressures probably exceeded 3600 psig (Figure E-11).

2.3 Fisside Release

An array of air monitors had been placed on a grid system extending downwind of the reactor to measure the release of radioactive material from the reactor. Data obtained from these

samples are presented in Appendix G together with a description of the method used in computing the total release of fission products to the atmosphere. Based upon these calculations, (which use the $t^{-1.2}$ rule-of-thumb decay rate) it is estimated that about 2.4×10^5 curies were released to the atmosphere as a result of the destructive test. The fission product inventory of the core at the time of the release was almost totally due to the fissioning which took place during the power excursion with only a small contribution from the long-lived radioisotopes from previous tests. Using a value of the nuclear energy release of 31 MW-sec, it is estimated that the total fission product content of the core was 6×10^7 curies and that, therefore, this calculation indicates the fraction of this inventory which was released to the atmosphere to be of the order of 0.4 percent.

The fission product release calculation is severely limited in precision since only a few isotopes could be collected and corrected by decay back to the time of release. It appears that those isotopes which were collected were released as gases. No solid products were collected.

Improvements in the calculation of fission product release have been continued by the USAEC-ID Health and Safety Division. These calculations, which are still preliminary^[a], take into account the specific decay schemes of the collected isotopes, Sr^{91} , S^{92} , and Ba^{139} as well as an improved computer calculation of the noble gas inventory of the core at the time of the release. It has been calculated on this basis that about 7 percent of the noble gases were released to the atmosphere. Since neither solid products nor radioiodines were found, it is, therefore, estimated that the fission product release consisted mainly of the noble gases and amounted to about 0.7 percent of the total fission product inventory.

Although radioiodines were not detected following the destructive test, it has been possible to calculate the maximum release of radioiodines which could have taken place undetected. By this approach, it has been established that less than 0.01 percent of the radioiodines were released to the atmosphere^[a].

Most of the fission product release was swept out of the reactor building by the strong winds (≈ 20 mph) which were blowing at the time so that contamination both in the building and on the ground downwind of the reactor was slight (ie, about 40/disintegrations/min/cm² on smears taken from the reactor floor about 20 hours after the test).

[a] These results were obtained by the USAEC-ID Health and Safety Division and communicated personally by W. P. Gammill of that Division. This information along with the data and calculations is expected to be published as an IDO report in the near future.

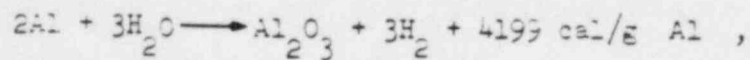
VI. ANALYSIS

1. METAL-WATER CHEMICAL REACTION

1.1 Chemical Analysis

Studies which have been carried out on the oxidation of molten aluminum in the presence of water indicate that this reaction can proceed at high rates with the release of a considerable amount of thermal energy. A review of some of these studies (References 14 through 21) was, therefore, made to help determine the feasibility of explaining the Spert I explosion on the basis of a rapidly reacting metal-water reaction.

For melted aluminum at about 660°C, this reaction takes the form:



where the product oxide is usually in the form, α - Al_2O_3 (alpha alumina). Other reactions are possible which lead to forms of alumina other than the α -phase and to various hydrates of alumina; but the above reaction appears to be the principal reaction at elevated temperatures such as were obtained during the destructive test [22].

Normally, in laboratory tests a quantitative measure of the extent of the oxidation reaction is obtained from the hydrogen reaction product which is collected. Since this was not possible during the Spert destructive test, a chemical analysis of the destructive test core debris was made. This method is based on the assumption that the α - Al_2O_3 product is quantitative, and that the accuracy of measuring the amount of this product in the radioactive debris recovered from the reactor vessel is adequate.

The debris collected from the reactor vessel originally contained all sorts of "foreign" material including nuts, bolts, paint, glass, sand, etc, in addition to fragments of fuel plates and selective removal of these items was necessary before the samples could be chemically analyzed. All foreign materials large enough to be conveniently seen and grasped with handling tools were removed from the debris as were all intact portions of the fuel plates (Figure 39) since unmelted aluminum would not have contributed significantly to the reaction.

A total of about 22 kg of debris was collected, and, of this, six samples totaling about 1420 grams were chemically analyzed at the Idaho Chemical Processing Plant. In order to remove as much metal from the samples as possible and to increase the relative concentration of α - Al_2O_3 , the samples were initially dissolved in HCL. Figure 45 outlines a complete typical analysis procedure. X-ray diffraction methods were used to detect and measure the alumina but, due to the presence of large quantities of ordinary sand in the x-ray samples, results were not precise.

Alpha-alumina was found separately in the form of small globules or spheres (the order of 0.004-inch diameter) and as incrustations upon aluminum metal

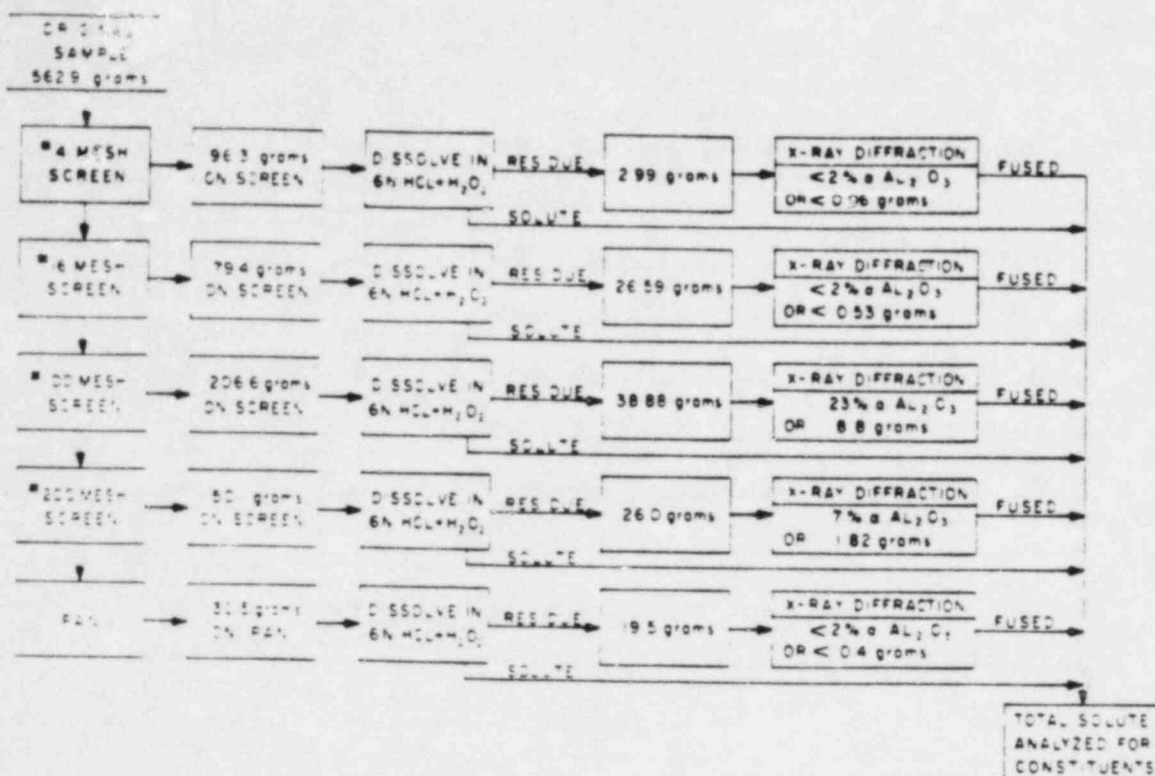


Fig. 45 Diagram of analysis and results of a typical sample of metallic debris collected from the Spert I vessel after Run 54.

fragments of all sizes. Many tiny globules and fragments were found in grab-samples of the debris. Analysis of individual globules in a Debye-Shirrer X-ray powder camera revealed that γ -alumina was a principal constituent along with several other undetermined crystal components.

Prior to chemical analysis two large samples of debris collected from the floor of the vessel were screened in order to obtain an approximate size distribution of the particles. The results of this size fractioning are plotted in Figure 46. Mean particle diameters appear to be in the range of 600 to 800 microns. It should be noted that the data in Figure 46 were taken directly from the screenings and no interpretation is made as to effective spherical size or as to the amount of exposed surface area.

From this analysis, it was determined that γ -alumina constituted between 1.6 and 2.0 percent by weight of the original cleaned samples of debris.

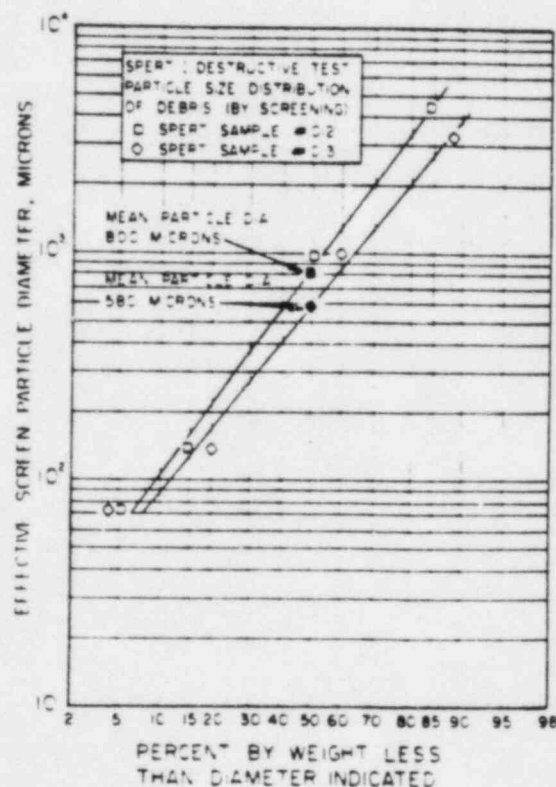


Fig. 46 Particle size distributions obtained from two samples of debris taken after the Spert Destructive Test.

Other constituents of the debris included aluminum 65 percent by weight, uranium 6.7 percent by weight, and the remainder consisting of sand, glass, etc.

Based upon an average content of 1.8 percent γ -alumina in a total of 22 kg of debris, it appears that about 200 grams of aluminum metal (or 0.4 percent of the aluminum in the core) was consumed in the reaction releasing, as a consequence, about 4 MW-sec of energy.

1.2 Interpretation

From a review of the results of several studies of the chemical reaction kinetics, it is concluded that the chemical reaction between aluminum and water would not be explosive under the conditions which were attained in the Spert I reactor before the explosion. After initiation of the explosion, it appears that dispersion of the molten fraction of the core could have produced conditions conducive to a rapid metal-water reaction, although, even under these conditions there is little experimental evidence to indicate explosive reactions.

Higgins and Schultz [17] report that the chemical "reactivity" of aluminum is nil at temperatures up to 1170°C, but that aluminum becomes more reactive at temperatures above 1170°C. The completion fraction depends importantly upon the particle size, becoming greater with small particles. It was found by Higgins and Schultz that as a result of dispersing molten metal into water to produce fine particles, pressure pulses were generated which were due primarily to the liberation of hot hydrogen gas, and that the rise time of the pressure pulses were sufficiently long that the metal-water reaction could be separated from the domain of "high order explosions". In two samples given [17] with metal temperatures of 1399 and 2021°C, the pressure pulses required 15 msec and 10 msec, respectively, to attain peak magnitude (73 psia and 191 psia, respectively). These results are in contrast with the Spert destructive test results which, although starting from a condition of somewhat intact, fuel plates apparently attained several thousand psig pressures in a fraction of a millisecond.

Extensive research done more recently both in-pile and out-of-pile at ANL also has failed to produce pressure pulses with the rise times required to explain the initiation of the Spert I explosion. Nor did an additional and specific test, in which sections of a Spert D-core fuel plate were subjected to ANL fast heating tests in the TREAT reactor, give any indication of an explosive reaction [15, 16].

The ANL tests have shown that aluminum reacts slowly up to temperatures around 1750°C and that above these temperatures the reaction rate increases but still is not "explosive". The reaction rate is apparently controlled by incrustations of oxide on the metal surfaces, and it appears that explosive rates of reaction are possible only if the metal is first finely divided.

It has been concluded, therefore, that the initial short rise-time pressure pulse of the Spert I explosion probably was not the result of a metal-water reaction. However, the chemical reaction very likely did proceed rapidly after initial deflagration of the core, and contribute energy to the explosion. For a metal-water chemical reaction to have initiated the Spert explosion would have apparently required first that the core be finely and violently fragmented, a condition which is tantamount to requiring another explosion of a different source to occur first.

2. CONDITION OF THE CORE AT THE TIME OF THE EXPLOSION

From the data of previous transient tests in which core damage was confined to thermal distortion and limited melting, it is possible to construct a model of the core conditions which probably existed to some degree in the few milliseconds just prior to the explosion. This is shown as the following sequence of events:

- (1) During the early part of the power excursion, fuel plate temperatures increased exponentially to the boiling point of water and above;
- (2) Nucleate boiling began and produced a pressure pulse which was measured outside of the core at about 35 psi;
- (3) Nucleate boiling next subsided to film boiling as fuel plate surface temperatures exceeded about 200°C;
- (4) After vapor blanketing was established, the fuel plate temperature increased rapidly but was probably arrested or even reversed occasionally by momentary collapse of the steam layer. Collapse of the void is postulated to be the result of a water hammer effect as water returned to the core after being accelerated out of the core by initial void growth;
- (5) While still below melting temperature, the fuel plates deformed into typical configurations (Figures 24 through 28) and met opposing fuel plates in the water channel. Such behavior is expected to create multiple channel blockages, entrapments of steam and water, and additional momentary collapse of voids;
- (6) Subsequent to thermal distortion, molten fuel escaped through cracks in the unmelted clad.

This sequence of events, although not directly observed during the destructive test, is consistent with many other observations of kinetic boiling behavior and fits the progressive nature of fuel plate damage observed in longer period tests. It also establishes the core in the condition which most probably existed at the time that the specific phenomena -- causative to the explosion began to occur.

The intimacy of melted and nearly melted aluminum with water trapped in warped water channels and with water which has effected void collapse appears to approximate conditions described by Long [23] which are conducive to "steam explosions". After producing and studying many steam explosions, Long states that "... violent explosions occur when a thin layer of water is trapped under a sudden rush of molten metal ...". In his study, designed to duplicate industrial metal spills, the "sudden rush" of metal is a description of the experimental method used.

As a consequence, then, of the rapidity of melting, warping, and void collapse in the destructive test and the resulting potential for generation of superheated water in contact with hot fuel, the "steam explosion" hypothesis is readily admissible as an explanation of the origin and perhaps also the development of the Spert I explosion.

VII. CONCLUSIONS

Having described in some detail the objectives, observations, and studies of this destructive testing program with a plate-type core, an attempt is made here to summarize the various results, conclusions, and implications. In general, many of the results have been essentially equated to types of damage observed and are presented here in order of increasing severity of the test from which they were derived.

In the period region around 10 msec and less, thermal distortion of fuel plates was the principal type of damage. This damage, arising from large thermal gradients generated within the fuel plates, was characterized by bowing, rippling, and clad failure and eventually led to channel blockage when adjacent plates touched and fused together in the water channels. Such distortions are concluded to be the result of an expanding meat section of the fuel plates which is constrained by the colder cladding, by the unfueled edge strips which remain relatively cold, and by binding of the fuel plate edges in the assembly side plates. In conventional assembly construction this situation is further aggravated since the fuel plates are welded in place, to a nonfuel bearing assembly side plate.

The occurrence of melting in the D-core was first seen as a result of a 5.0-msec period test, in which melting affected about 160 inch² of the fuel plate surfaces. For the 4.6-msec period test, melting affected over 500 inch² of fuel plate surface. The nature of the melting in both tests indicates that the flow of molten fuel does not occur very rapidly; ie, there is no evidence that the fuel is expelled from the plate under any pressure, such as might be anticipated to arise from high internal stresses. Melted portions of the fuel remained with the plates themselves. There were no fragments of fuel found separated from fuel plates. The transient pressures measured during these tests give no indication of any increase with the occurrence of melting and thus substantiate the conclusion that the simple fact of fuel plate melting does not of itself constitute a sufficient condition for the generation of destructive pressures.

Both of the aforementioned damage responses, ie, thermal distortion and melting, were superimposed for periods of 5 msec and less and led to the touching and fusing-together of adjacent plates. The mechanism whereby fuel plates fuse together appears to be one in which warping first causes the fuel plate to rapidly extend far out into a water channel where it touches another plate. Melting, which occurs subsequent to the warping, then fuses the plates together. Since warping is expected to take place only during the short interval of time in which the temperature is increasing above about 100°C but still below the melting point at 640°C, it is reasonable to expect that the warping process was very rapid during the 3.2-msec period test, and that the entrapment of water and steam between plates is a likely consequence of this process.

During the 3.2-msec period test, a violent explosion occurred immediately after the power excursion. In this test complete fuel plate melting is estimated to have occurred in approximately 8 percent of the core and partial (ie, internal fuel) melting in about 35 percent of the core (ie, approximately 12×10^3 inch² of fuel plate area). Little recorded information is available about the nature of the explosion which destroyed the core after this melting; however, a number of postulates have been advanced and there is a significant amount of indirect

2. CONDITION OF THE CORE AT THE TIME OF THE EXPLOSION

From the data of previous transient tests in which core damage was confined to thermal distortion and limited melting, it is possible to construct a model of the core conditions which probably existed to some degree in the few milliseconds just prior to the explosion. This is shown as the following sequence of events:

- (1) During the early part of the power excursion, fuel plate temperatures increased exponentially to the boiling point of water and above;
- (2) Nucleate boiling began and produced a pressure pulse which was measured outside of the core at about 35 psi;
- (3) Nucleate boiling next subsided to film boiling as fuel plate surface temperatures exceeded about 200°C;
- (4) After vapor blanketing was established, the fuel plate temperature increased rapidly but was probably arrested or even reversed occasionally by momentary collapse of the steam layer. Collapse of the void is postulated to be the result of a water hammer effect as water returned to the core after being accelerated out of the core by initial void growth;
- (5) While still below melting temperature, the fuel plates deformed into typical configurations (Figures 24 through 28) and met opposing fuel plates in the water channel. Such behavior is expected to create multiple channel blockages, entrapments of steam and water, and additional momentary collapse of voids;
- (6) Subsequent to thermal distortion, molten fuel escaped through cracks in the unmelted clad.

This sequence of events, although not directly observed during the destructive test, is consistent with many other observations of kinetic boiling behavior and fits the progressive nature of fuel plate damage observed in longer period tests. It also establishes the core in the condition which most probably existed at the time that the specific phenomena -- causative to the explosion began to occur.

The intimacy of melted and nearly melted aluminum with water trapped in warped water channels and with water which has effected void collapse appears to approximate conditions described by Long [23] which are conducive to "steam explosions". After producing and studying many steam explosions, Long states that "... violent explosions occur when a thin layer of water is trapped under a sudden rush of molten metal ...". In his study, designed to duplicate industrial metal spills, the "sudden rush" of metal is a description of the experimental method used.

As a consequence, then, of the rapidity of melting, warping, and void collapse in the destructive test and the resulting potential for generation of superheated water in contact with hot fuel, the "steam explosion" hypothesis is readily admissible as an explanation of the origin and perhaps also the development of the Spert I explosion.

VII. CONCLUSIONS

Having described in some detail the objectives, observations, and studies of this destructive testing program with a plate-type core, an attempt is made here to summarize the various results, conclusions, and implications. In general, many of the results have been essentially equated to types of damage observed and are presented here in order of increasing severity of the test from which they were derived.

In the period region around 10 msec and less, thermal distortion of fuel plates was the principal type of damage. This damage, arising from large thermal gradients generated within the fuel plates, was characterized by bowing, rippling, and clad failure and eventually led to channel blockage when adjacent plates touched and fused together in the water channels. Such distortions are concluded to be the result of an expanding meat section of the fuel plates which is constrained by the colder cladding, by the unfueled edge strips which remain relatively cold, and by binding of the fuel plate edges in the assembly side plates. In conventional assembly construction this situation is further aggravated since the fuel plates are welded in place, to a nonfuel bearing assembly side plate.

The occurrence of melting in the D-core was first seen as a result of a 5.0-msec period test, in which melting affected about 160 inch² of the fuel plate surfaces. For the 4.6-msec period test, melting affected over 600 inch² of fuel plate surface. The nature of the melting in both tests indicates that the flow of molten fuel does not occur very rapidly; ie, there is no evidence that the fuel is expelled from the plate under any pressure, such as might be anticipated to arise from high internal stresses. Melted portions of the fuel remained with the plates themselves. There were no fragments of fuel found separated from fuel plates. The transient pressures measured during these tests give no indication of any increase with the occurrence of melting and thus substantiate the conclusion that the simple fact of fuel plate melting does not of itself constitute a sufficient condition for the generation of destructive pressures.

Both of the aforementioned damage responses, ie, thermal distortion and melting, were superimposed for periods of 5 msec and less and led to the touching and fusing-together of adjacent plates. The mechanism whereby fuel plates fuse together appears to be one in which warping first causes the fuel plate to rapidly extend far out into a water channel where it touches another plate. Melting, which occurs subsequent to the warping, then fuses the plates together. Since warping is expected to take place only during the short interval of time in which the temperature is increasing above about 100°C but still below the melting point at 640°C, it is reasonable to expect that the warping process was very rapid during the 3.2-msec period test, and that the entrapment of water and steam between plates is a likely consequence of this process.

During the 3.2-msec period test, a violent explosion occurred immediately after the power excursion. In this test complete fuel plate melting is estimated to have occurred in approximately 8 percent of the core and partial (ie, internal fuel) melting in about 35 percent of the core (ie, approximately 12×10^3 inch² of fuel plate area). Little recorded information is available about the nature of the explosion which destroyed the core after this melting; however, a number of postulates have been advanced and there is a significant amount of indirect

information to support the hypothesis of a steam explosion resulting from a momentary superheating of water.

Of major significance from this 3.2 msec test is the observation that, prior to the initiation of the destructive pressure burst, which occurred 15 msec after the power-peak, the reactor underwent a complete self-limiting power excursion with burst parameters systematically predictable from longer period tests. It should be further noted that the reactor evidenced no difficulty in effecting self-shutdown for such short periods (reactivity insertions as large as 3.5\$).

The maximum reactivity compensation data obtained during several of the shortest period excursions indicate that, for this core, rapid compensations in excess of 6\$ are possible from thermal and boiling shutdown mechanisms. However, a tendency toward the production of high superheats and consequent pressures at the onset of boiling during such excursions and an apparent depression of the void growth rate during the initial steam formation may lead to an unpredictable increase in energy release and to core damage at periods shorter than those tested, ie, periods less than 3.2 msec.

It should be further noted that since the explosion occurred at a time after nuclear shutdown was complete and when the power, the reactivity, and fuel plate temperatures were all decreasing, conditions leading to the explosion do not appear to be directly a consequence of the excess reactivity, the period, or the shutdown process, except insofar as these factors determine the energy release. In other words, the major differences of initial core conditions between the 3.2-msec period destructive test and, say, the 4.6-msec period test lie in the domain of energy release effects such as maximum temperature and degree of melting.

The time at which the Spert I explosion took place (about 15 msec after peak power) may be a consequence both of the internal fuel plate temperatures and the rate of heat transfer from the meat to fuel plate surfaces. Calculations of fuel plate temperature distributions [13] indicate that fuel plate surfaces at the core hot spot may have been passing through the melting temperature at the time of the explosion. Centerline meat temperatures at the core hot spot possibly reached 1400°C maxima but are calculated to have decreased to about 1000°C at the time of the explosion. Thus, it is expected that during a shorter period power excursion with a consequent increase in the amount of energy released, complete fuel plate melting would occur earlier, and possibly, even before nuclear shutdown was complete.

An analysis was conducted to determine the extent of a possible metal-water chemical reaction, and it was determined that approximately 4 MW-sec of energy may have been released in this process. However an evaluation of the results, in the light of the pressure and temperature conditions obtained in the reactor during the 3.2-msec period test and those used in out-of-pile studies of this chemical reaction, indicates that the chemical reaction was not responsible for initiating the observed explosion. The reaction rates required to support such a postulate and the temperatures obtained in the test are not consistent with current experimental information on the kinetics of the chemical reaction. In fact, it is necessary to postulate a separate explosion or trigger mechanism to even establish the necessary condition for the high rates of the metal-water reaction itself. It is, therefore, concluded that the observed metal-water reaction (amounting to the consumption of roughly 200 grams of

aluminum) was a "side reaction" which proceeded as a consequence of the explosion, and added energy to it.

Another significant result of the destructive test concerns the release of fission products to the atmosphere resulting from melting and violent dispersal of the core. It has been calculated that about 0.7 percent of the total core inventory was released to the atmosphere in the form of noble gases. Solids were not detected in the atmosphere. Radioiodines also were not detected and, as a consequence, less than 0.01 percent of the iodines are calculated to have been released.

The conclusions which have been drawn here regarding the explosion in the Spert I reactor and regarding the conditions which existed in the core prior to the explosion may bear significance in the analysis of the two other cases of reactor explosions, the Borax test explosion in 1954, and the accidental SL-1 explosion in 1961. In all three reactors, the materials and geometries of the cores were similar (ie, low-melting point (aluminum) metal in plate-type water moderated systems), and the energy release in each case was sufficient to induce melting, and, a priori, severe warping of the plates.

Thermal warpage in both Borax and SL-1 cores probably was sufficient to cause adjacent fuel plates to touch each other. In the Spert core, ripple amplitudes greater than 0.22 inch have been observed (following a nonexplosive, 4.6-msec period test) whereas the water channel thickness was only 0.18 inch. There is a distinct possibility then that warping in the Borax core could have been sufficient to span the 0.117-inch plate spacing and cause adjacent fuel plates to touch, even though a stiffener plate was used in that core which reduced the effective fuel plate width to about half of the nominal 2.8-inch-wide plate in Spert I.

Plate and channel dimensions in the SL-1 core were considerably different from either Spert I and Borax but, there again, it seems that touching of plates is highly probable in any excursion attaining temperatures at or near melting. SL-1 plates had a free width of 3.5 inches, and the coolant channel thickness was 0.310 inch. If the Spert I ripple amplitude mentioned above is scaled-up by the ratio of plate widths, then amplitudes of deformation in SL-1 of about 0.275 inch can be expected which are considerably in excess of the half-channel thickness.

As was noted above, the increased energy expected at shorter reactor periods would be expected to result in melting of fuel earlier in the excursion possibly before nuclear shutdown was complete or even during the power rise, a situation which may have been evidenced in the Borax test.

Also with regard to the Borax test, it should be noted that the pressures derived from the momentary superheating of water prior to the onset of boiling may have played an important role in initiating that explosion. If the Borax explosion occurred around the time of peak power, then shutdown pressures associated with initial boiling of the moderator in colder fractions of the core could still have been occurring at the beginning of the explosion. Thus, the need for a separate triggering mechanism is not nearly as evident in the Borax test as it appears to be in the Spert I test. Shutdown pressures in a 2.6-msec period power excursion may be sufficient to initiate dispersion of melted fuel plates.

One implication of the Spert I test results arises from the fact that in the Spert I core, as with Borax and SL-1, each assembly (consisting of 12 fuel plates) was separated from adjacent assemblies by the unheated assembly walls which remain cold and, therefore, strong and rigid during each test. Thus, it is reasonable that only one assembly need be considered in formulating a model for a triggering mechanism (recognizing that pressure disturbances may "couple" more than one assembly). Also it was noted that the center assembly which had the highest fuel plate temperatures also produced the highest pressures, and also may have been the source of the initiation of the explosion. Because of the placement of the transient rod blades, the largest group of fuel plates in this assembly is four plates. Thus, the very distinct possibility of being able to conduct meaningful investigations of the nature of the initiation of the explosion in small scale mechanism experiments is evident.

The possibility that only a small number of fuel plates may have been responsible for initiating the Spert I explosion combined with the fact that the explosion does not appear to be involved in any aspect of integral core kinetics (ie, shutdown behavior, etc) points out the possibility of performing other tests in small sub-assemblies, possibly even with nonnuclear heat.

Another conclusion resulting from the Spert I destructive test is again based upon the yet unproved assumption that melted fuel plates are essential to produce the explosion. That is, it appears that the use of higher melting point metals for fuel plate cladding (ie, zirconium- stainless-steel, etc) would be effective in reducing the probability of either a steam explosion or a metal-water chemical reaction simply because of the higher melting temperatures (provided of course, that other effects of these materials such as lower heat conductivity and thinner cladding thicknesses do not abrogate the advantage of a higher melting point).

Some advantage also may be obtained with aluminum by using an alloy which is less susceptible to hot-short cracking than is the 6061 alloy used here. In most of the very short period tests, clad cracking was extensive and contributed to the early release of molten fuel even though the clad surface was not itself melted.

With regard to creating conditions within the core which deter or prevent an explosion, the relative merits of fuel plates which are constructed either "thick" or "thin", or with either thick cladding or thin cladding are not certain. A core consisting of plates with thick cladding, for instance, will have a higher heat capacity and will be able to sustain excursions with greater energy release; however, it appears that the thicker clad also may delay the onset of boiling and the completion of nuclear shutdown with the result that a higher energy release necessarily takes place. It also is possible that the reduced flexibility of thick plates would lead to cracking and rupture earlier in a transient than their thin counterparts.

Finally, it is felt that a significant volume of information has been added to the study of plate core reactor kinetics as a result of this program and that the justification of pursuing the investigation of the many facets of the destructive test in subassembly test programs has been more firmly established.

VIII. REFERENCES

1. T. F. Wilmott et al, Time Behavior of Godiva Through Prompt Critical, LA-2029 (April 1956).
2. J. R. Dietrich, Experimental Investigation of the Self-Limitation of Power During Reactivity Transients in a Subcooled, Water-Moderated Reactor. Borax-I Experiments, ANL-5323 (March 1957).
3. A. H. Spano and R. W. Miller, Spert I Destructive Test Program Safety Analysis Report, IDO-16790 (June 1962).
4. R. W. Garner, An Analysis of Nonboiling Reactivity Feedback Mechanisms in Pressurized Power Excursions in the Spert III Reactor, IDO-16819 (January 1963).
5. G. O. Bright (ed.), Quarterly Progress Report - October, November, December, 1957, IDO-16437 (March 1958) p 58.
6. R. W. Miller, "An Experimental Study of Transient Boiling During Spert I Power Excursions", Trans. Am. Nucl. Soc., 4, 69-70, June 1960.
7. R. W. Miller, Calculations of Reactivity Behavior During Spert I Transients, IDO-16317 (June 1957).
8. F. L. Bentzen (ed.), Quarterly Progress Report - October, November, December, 1959, Reactor Projects Branch, IDO-16537 (September 1958) pp 52-61.
9. G. F. Brockett and E. Feinauer, Summary Data Report for Spert Transient Pressure Measurements in the Interval 1955-1961, IDO-16930 (April 1964).
10. J. Dugone and L. L. Wieland, Fuel Plate Experience During Spert I Destructive Test Series with an Aluminum-Clad Plate-Type Core, IDO-16885 (July 1963).
11. Final Report of SL-1 Recovery Operation, May 1961 through July 1962, IDO-19311 (July 1962).
12. J. F. Kunz (ed.), Additional Analysis of the SL-1 Excursion, IDO-19313 (November 1962).
13. J. E. Houghtaling, Alain Sola, and A. H. Spano, Transient Temperature Distributions in the Spert I D-12/25 Fuel Plates During Short-Period Power Excursions, IDO-16884 (June 1964).
14. R. C. Liimatainen et al, Studies of Metal-Water Reactions at High Temperatures II. Treat Experiments: Status Report on Results with Aluminum, Stainless Steel-304, Uranium, and Zircaloy-2, ANL-6250 (January 1962).
15. Reactor Development Program Progress Report, ANL-6658 (November 1962) p 68.

16. R. O. Ivins, "A Study of the Reaction of Aluminum/Uranium Alloy Fuel Plates with Water Initiated by a Destructive Reactor Transient", Trans. Am. Nucl. Soc., 6, 101-102, June 1963.
17. H. M. Higgins and R. D. Schultz, The Reaction of Metals with Water and Oxidizing Gases at High Temperatures, IDO-28000 (April 1957).
18. W. F. Zelezny, Metal-Water Reactions: Rates of Reaction of Aluminum and Aluminum-Uranium Alloys with Water Vapor at Elevated Temperatures, IDO-16629 (November 1960).
19. L. F. Epstein, "Correlation and Prediction of Explosive Metal-Water Reaction Temperatures", Nucl. Sci. Eng., 10, 247-253, July 1961.
20. H. M. Saltsburg, Metal-Water Reactions, KAPL-1495, April 1956.
21. S. C. Furman, Metal-Water Reactions: V. The Kinetics of Metal-Water Reactions-Low Pressure Studies, GEAP-3208, July 1959.
22. R. O. Ivins and L. Baker, Argonne National Laboratory, Personal Communications.
23. G. Long, "Explosions of Molten-Aluminum in Water -- Cause and Prevention", Metal Progress, 71, 107-112, May 1957.
24. F. de Hoffman, Intensity Fluctuations of a Neutron Chain Reactor, MDDC-382, October 1946.
25. F. Schroeder (ed.), Quarterly Technical Report, Spert Project, January - March, 1962, IDO-16788 (August 1962) pp 5-9.
26. R. L. Johnson, A Statistical Determination of the Reduced Prompt Neutron Generation Time, Λ/β , in the Spert IV Reactor, IDO-16903 (July 1963).
27. M. R. Zeissler, Non-Destructive and Destructive Transient Tests of the Spert I D, Fully Enriched, Aluminum-Plate-Type Core: Data Summary Report, IDO-16886 (November 1963).
28. U. S. Weather Bureau, Meteorology and Atomic Energy, AECU-3066, July 1955.
29. C. A. Hawley, Jr., et al, "Radiological Data from the Destructive Test", Trans. Am. Nucl. Soc., 6, 139-140, June 1963.

APPENDIX A

START-UP AND STATIC EXPERIMENTS

APPENDIX A

START-UP AND STATIC EXPERIMENTS

1. INITIAL CORE LOADING

Initial loading of the D core began on March 3, 1962, and an initial critical loading was achieved with 20 fuel assemblies and the control rods withdrawn 17.95 inches on March 5, 1962. The associated critical mass was approximately 2.8 kg of U-235. Loading then proceeded until an operational core consisting of 25 assemblies containing 3.8 kg of U-235 was achieved on March 6, 1962. The reactor was critical at ambient temperature with the control rods withdrawn 9.20 inches. The available excess reactivity of the core was determined to be $\approx 8.2\%$ and the shutdown reactivity margin to be $\approx 4.4\%$; these were considered adequate for the proposed test program.

2. ROD CALIBRATIONS

2.1 Control Rod

The differential reactivity worth of the control rods over the range of rod travel from the critical position to the fully-withdrawn position was measured by the reactor period method. Both boric acid solution and transient rod poison insertion were used as reactivity shims to permit measurements of reactor period over the range of control rod travel.

Differential and integral reactivity worths of the control rods are shown in Figure A-1. Scatter in the differential reactivity worth data is attributed to uncertainties of ± 0.02 inch in the rod position increment and to possible inhomogeneity in the concentration of the boric acid solution used to shim the reactivity. The integral curve indicates an available excess reactivity of 8.2% , which, if inserted as a step, would result in about a 1-msec period power excursion.

A shutdown reactivity of 4.4% was inferred from integration of a linear extrapolation of the differential rod worth curve from 9.20 inches to zero inches withdrawn.

2.2 Transient Rod

Reactivity worth of the transient rod was determined by intercalibration with the control rods, and the integral transient rod reactivity worth is shown in Figure A-2. The total worth of the transient rod was 7.1% , which indicated that the minimum period possible for test purposes was about 1.3 msec, based upon a measured reduced prompt neutron lifetime of 8.2 msec.

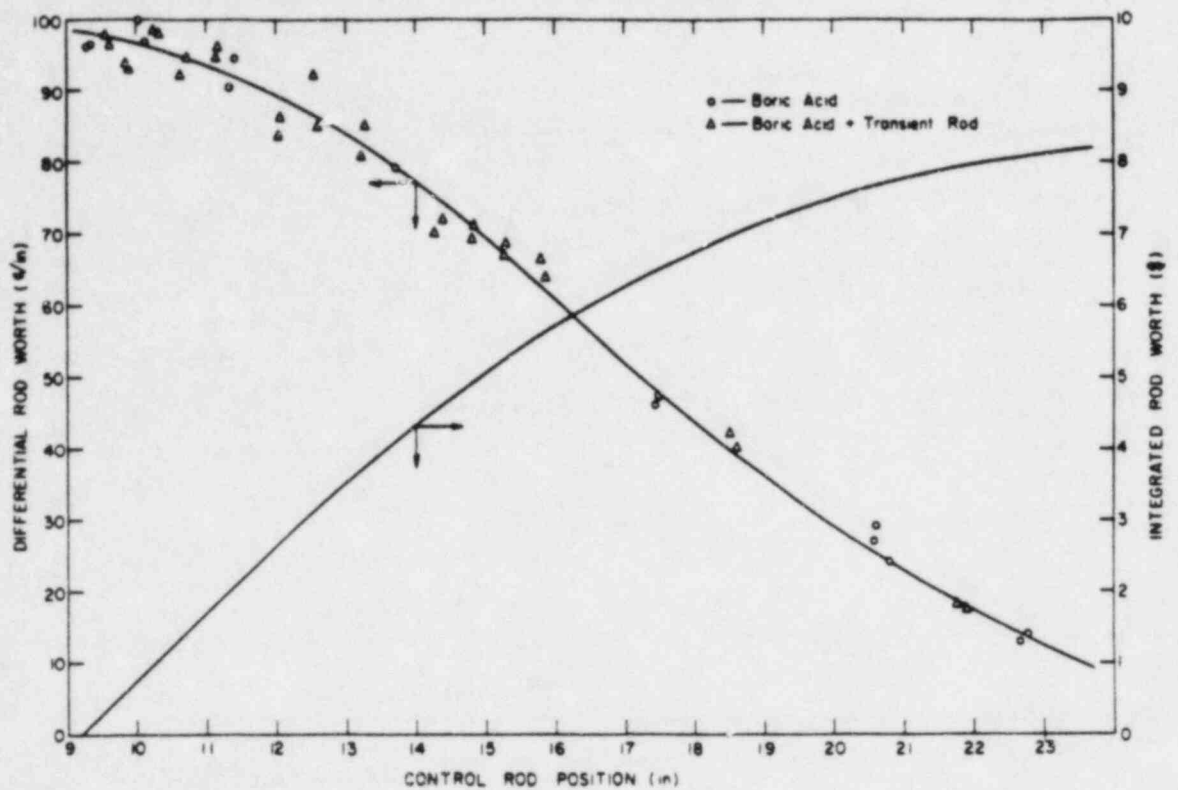


Fig. A-1 Differential and integral control rod calibration curves.

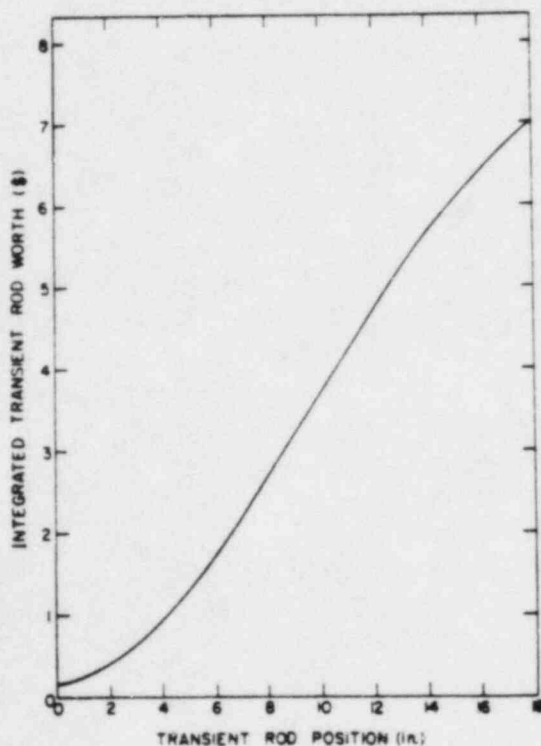


Fig. A-2 Integral transient rod calibration curve.

3. VOID COEFFICIENT

Void coefficient measurements were made for uniformly distributed voids in the core and for voids distributed at various axial positions in the central region of the core. The influence of a change in the volume of the void in the peripheral regions of the core on the value of the central void coefficient also was studied.

3.1 Uniform Void Coefficient

The measurement of the uniform void coefficient was performed by inserting 30-inch long by 0.610-inch wide by 0.159-inch thick magnesium strips in alternate channels of each non-rodded fuel assembly to simulate a uniform distribution of voids throughout the core. The lateral positions of the magnesium strips in the channels were staggered to reduce interaction. Following the determination of the critical position of the control rods with all the strips in place,

selected strips were removed, a new critical position established, etc, until all the strips were removed from the core. Reactivity loss for each set of strips removed was obtained from the change in the calibrated control rod positions. The void coefficient was calculated by correcting the reactivity effect for neutron absorption by the magnesium and by considering only the magnesium within the active length of the fuel assemblies as a void. No correction was made for neutron scattering. Results of these measurements, shown in Figure A-3, indicate a value for the coefficient of $36\phi/\%$ decrease in moderator density (or $-0.067\phi/\text{cm}^3$ of water removed).

3.2 Central Void Coefficient

Central void coefficient measurements were performed by use of 4-inch long by 0.610-inch wide by 0.157-inch thick magnesium strips located in the central region of the core. Each strip was attached to the transient rod drive mechanism to enable remote vertical positioning of the voids. The vertical profile of the void coefficient was obtained from the control rod worth by determining the critical rod position as a function of void position. The results of this measurement are shown in Figure A-4. The peak of the local void worth curve occurs at a void position of about 8.5 inches above the bottom of the fuel. The maximum central void coefficient was about $-84\phi/\%$ decrease in moderator density (or $-0.16\phi/\text{cm}^3$ of water removed). This coefficient was determined to be independent of void volume for void volumes as large as 370 cm^3 .

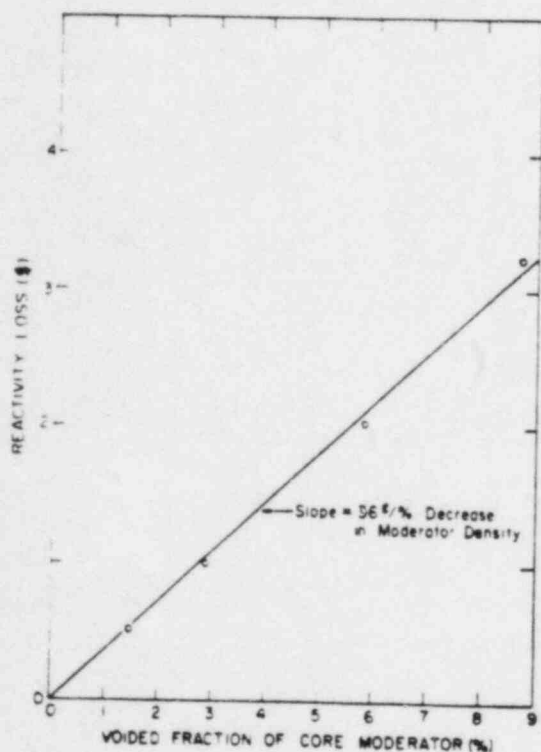


Fig. A-3 Reactivity loss as a function of void fraction for a uniform distribution of voids.

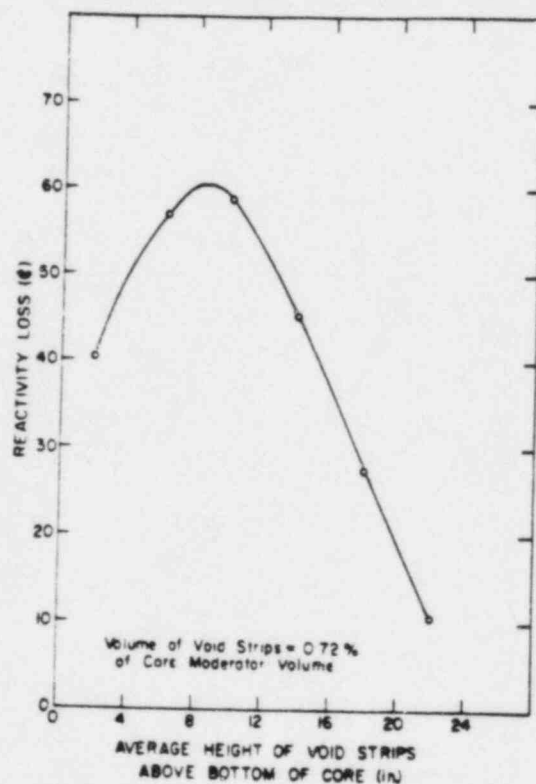


Fig. A-4 Reactivity worth of centrally-located, 4-inch long void strips as a function of height above the bottom of the core.

3.3 Void Interaction of Central and Peripheral Regions

The void distribution during a transient probably does not correspond to a uniform void only, or to a central void only, but is rather some more complicated distribution which changes rapidly with time as the boiling point is exceeded. For example, it is likely that during a short-period self-limiting excursion, water channels in the centermost regions of the core are almost completely voided while water channels in the peripheral region of the core, which receive less heating, are only slightly voided. A strongly voided core, by virtue of the consequent redistribution of neutron flux, might be expected to have a markedly different void importance distribution from that obtained in the previous measurements. Additional void worth measurements were, therefore, conducted to determine if the central void coefficient was significantly affected by the presence of voids in peripheral regions of the core.

Four experiments were performed using aluminum strips (26 inches long x 3/4 inch wide x 1/8 inch thick) to simulate voids. For these experiments a 6- x 6-inch region centered about the transient rod was defined to be the "central region", with the remainder of the core defined as the "peripheral region". The four experiments included one in which the central and peripheral regions were voided uniformly, and three experiments in which the central region was more heavily voided than the peripheral region. The reactivity effect due to each of the various void distributions was measured from the change in the critical position of the calibrated control rods. Specific values for the four void configurations along with the results of the experiments are listed in Table A-1.

TABLE A-1
VALUES FOR THE FOUR VOID CONFIGURATIONS AND EXPERIMENT RESULTS

Experiment No.	Region	Number of Strips in Region	Void Volume (cm ³)	Region Voided (%)	Reactivity Change From Unvoided Critical Core (¢)	Central Region Void Coefficient ^[a] (¢/cm ³)
1	Central and Peripheral	95	3503	6.68	-315	---
2	Central Peripheral	40 80	1475 2950	17.81 6.68	-455	-0.096
3	Central Peripheral	40 44	1475 1622	17.81 3.67	-345	-0.090
4	Central Peripheral	40 0	1475 0	17.81 0	-214	-0.090

[a] Void coefficients are corrected for absorption cross section of aluminum only.

The results show that the central void coefficient as measured with voids only in the central region is not significantly affected by void fractions as large as seven percent in the peripheral regions. Higher void fractions in both regions would probably have accentuated any interaction between voids. However, the experiments described here were sufficient for present purposes since they produced reactivity decrements in excess of the reactivity compensations necessary for the destructive test program.

An additional result of these experiments has been a comparison of the relative void coefficients obtained by using two different materials, magnesium and aluminum, to simulate voids. The independent calculations of these two determinations yield -0.067% /cm³ for magnesium and 0.063% /cm³ for aluminum which agree within 10 percent when both values are corrected for the absorption cross sections of magnesium and aluminum, respectively.

4. NEUTRON FLUX DISTRIBUTION

The steady-state neutron flux distribution was determined from activation of 29 cobalt wires located in the core as shown in Figure A-5. The wires extended the full length of the fuel plates and were irradiated for 135 minutes at power level of about 90 kW.

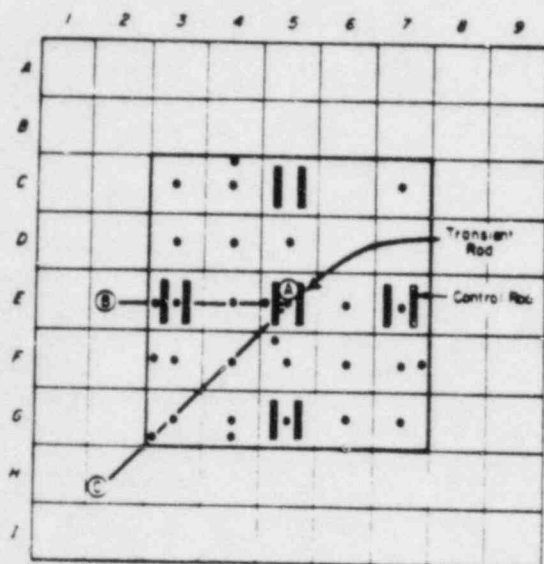


Fig. A-5 Flux wire activation positions.

Figures A-6 through A-10 illustrate representative vertical and horizontal flux profiles at selected core positions. The normalized flux distributions are plotted as functions of height above the bottom of the core or distance from the core centerline. The maximum flux was determined to be in position E5-5 at about 8 inches from the bottom of the core (E5-5 means the 5th water channel numbered from the west or left side of the fuel assembly in the E5 grid position). The peak-to-average flux ratio was determined to be 2.4. Individual values of the flux are estimated to be accurate within 20 percent: 15 percent due to uncertainty in the exact location of the wire detector and 6 percent due to the counting error.

5. POWER DISTRIBUTION IN A VOIDED CORE

The flux distributions discussed previously were obtained during an experiment in which the power level of the reactor was kept at low values insufficient to raise the temperature of the core above the boiling point of water. By contrast, however, many of the transients anticipated during the destructive test program would cause boiling to occur over large fractions of the core; and, the following experiment was designed to determine to what extent the power distribution in the core would be affected by the presence of a nonuniform void distribution such as might be produced during one of these tests.

The experiment consisted of measuring the power distribution both with and without simulated voids in the core. Thin foils of a 93 percent enriched uranium-aluminum alloy (5/32 inch diameter by 0.006 inch thick) were used to monitor

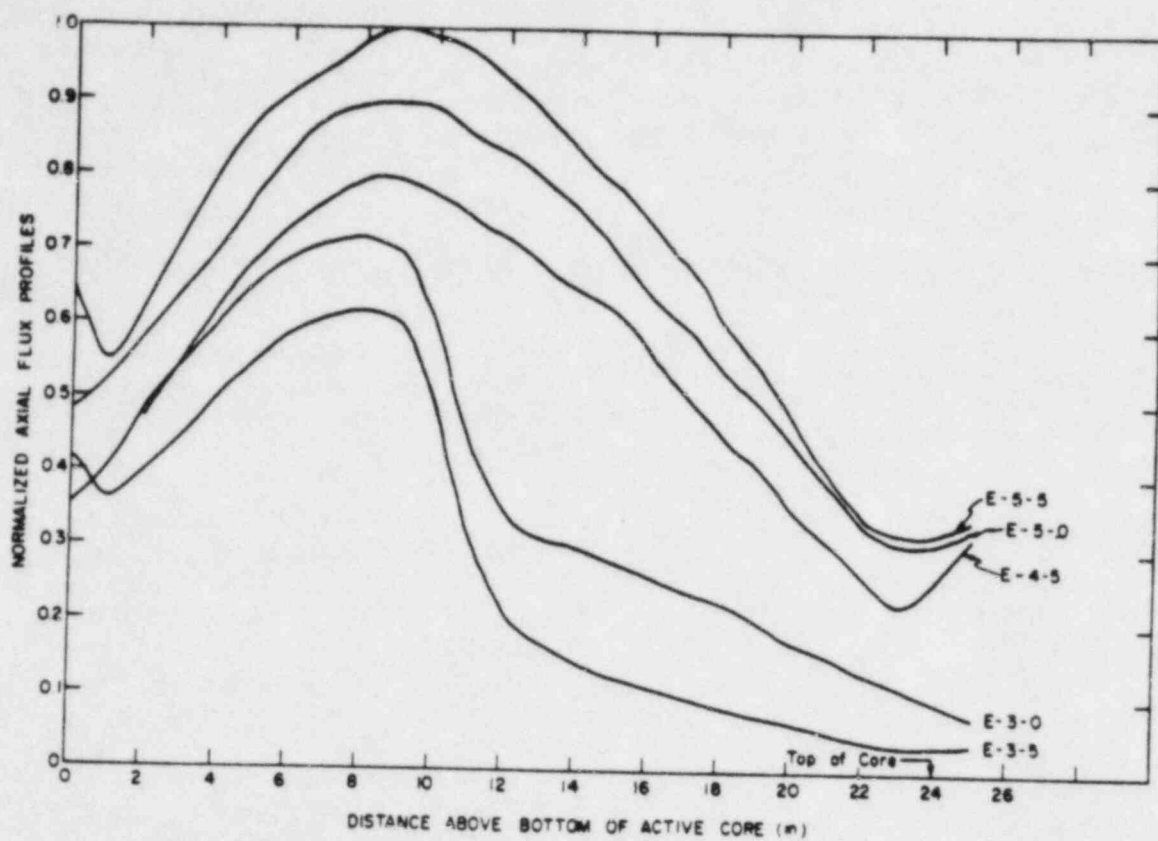


Fig. A-6 Vertical flux profiles in fuel assemblies E-3, E-4, and E-5.

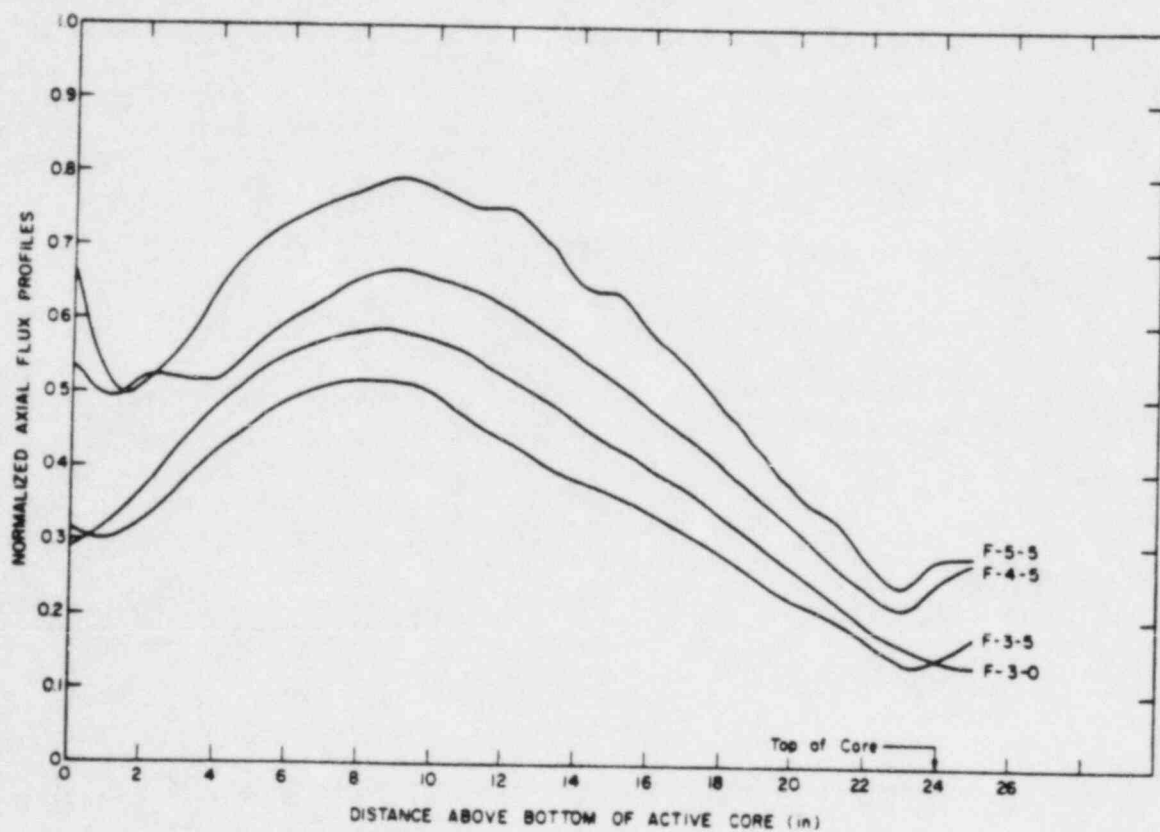


Fig. A-7 Vertical flux profiles in fuel assemblies F-3, F-4, and F-5.

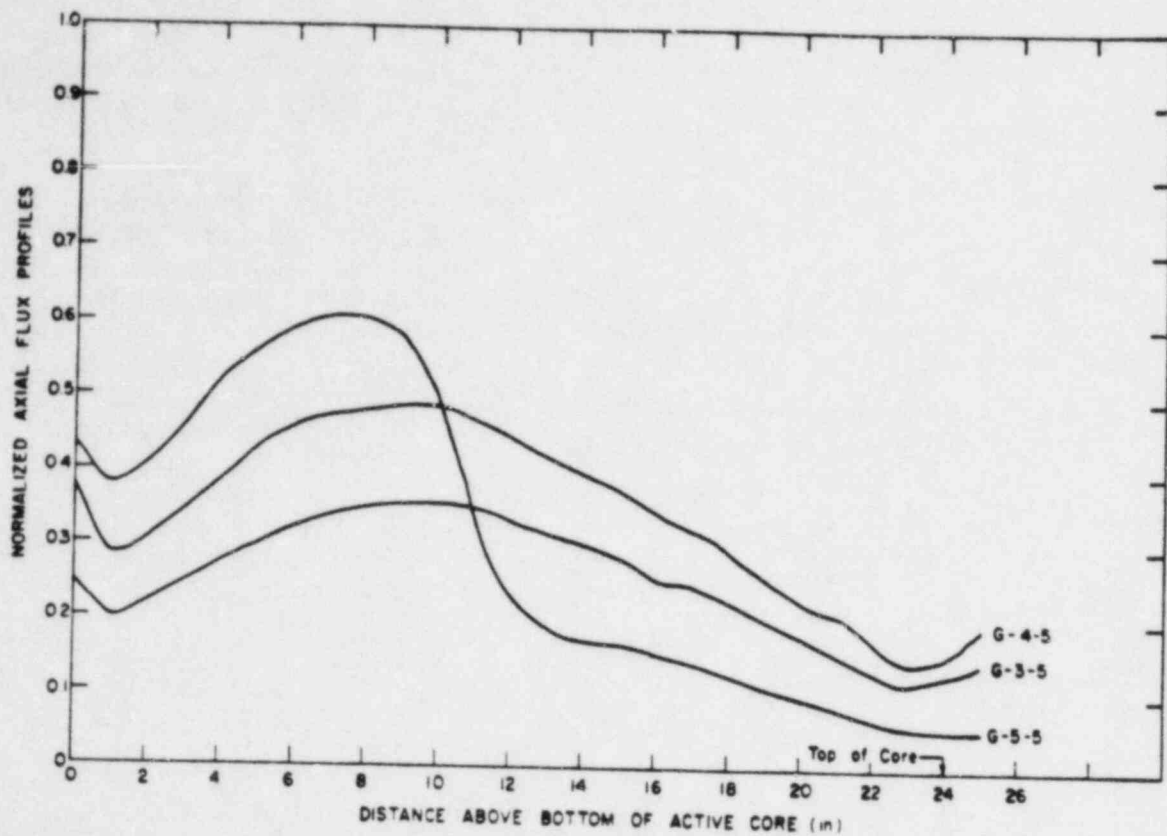


Fig. A-8 Vertical flux profiles in fuel assemblies G-3, G-4, and G-5.

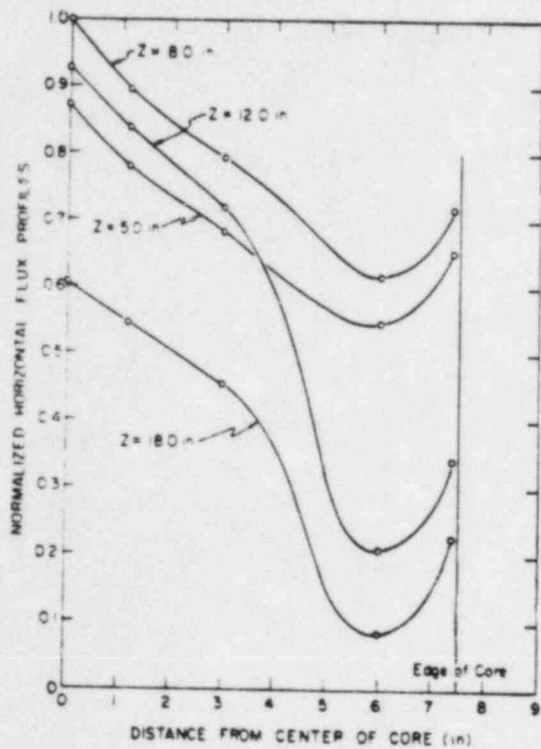


Fig. A-9 Horizontal flux profiles along direction A-B (Fig. A-5). Lines drawn in to connect data points.

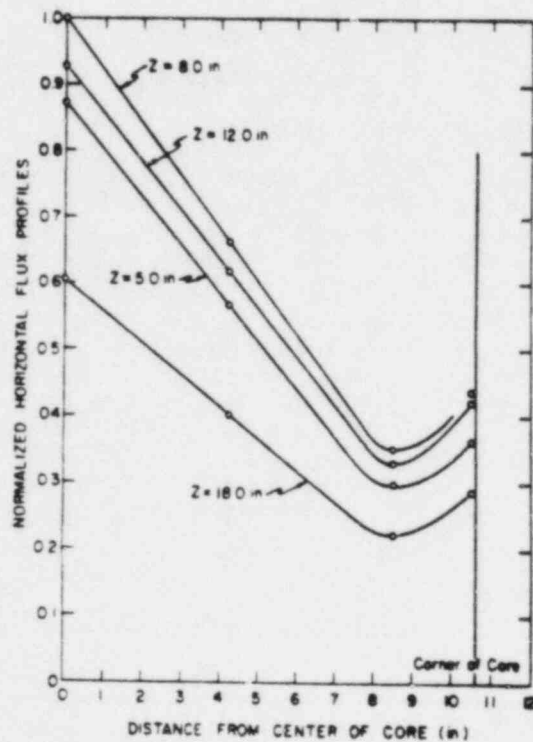


Fig. A-10 Horizontal flux profiles along direction A-C (Fig. A-5). Lines drawn in to connect data points.

the flux, and aluminum strips were used to simulate the voids. Only a central region (shown in Figure A-11) was voided to simulate the void distribution which might occur during the early part of an excursion. This region was voided to about 18 percent.

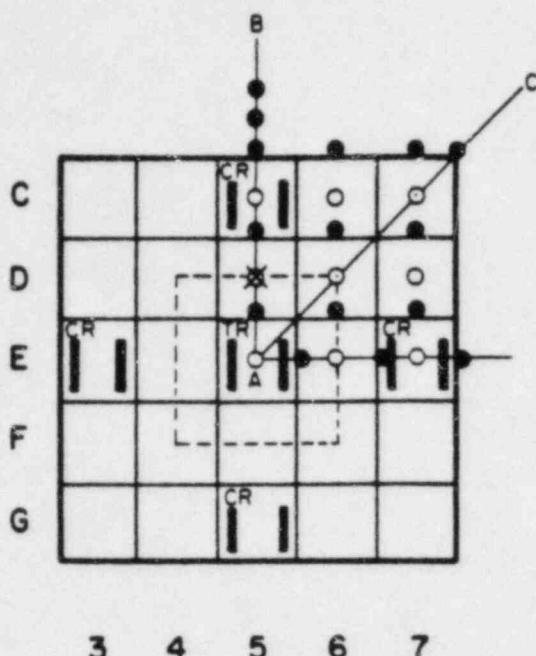


Fig. A-11 Location of uranium-aluminum alloy foils for comparison of the flux invoided and unvoided core.

○= Foils located at +3, 0, -4, -7, -10, -13, -16, -19, -22, -25, and -28 inches.

○= Same as 0 with addition of cadmium covered foils at $-1\frac{1}{2}$, $-1\frac{1}{2}$, $-8\frac{1}{2}$, $-14\frac{1}{2}$, $-17\frac{1}{2}$, $-20\frac{1}{2}$, and $-26\frac{1}{2}$ inches [a].

●= Foils located at 0, -7, -13, -16, -19, and -25 inches [a].

✕= Same as 0 with an additional foil at $-17\frac{1}{2}$ inches; this was the master foil used in the counting analysis [a].

[a] All dimensions are from the top of the core; ie, +3 indicates a position three inches above the top of the core.

8.3 ± 0.4 msec as compared to a value of 8.16 ± 0.04 msec obtained from step-transient tests. The quoted uncertainty in the second value is the standard deviation based on the deviation of the data points from a least squares fit and is probably an underestimate.

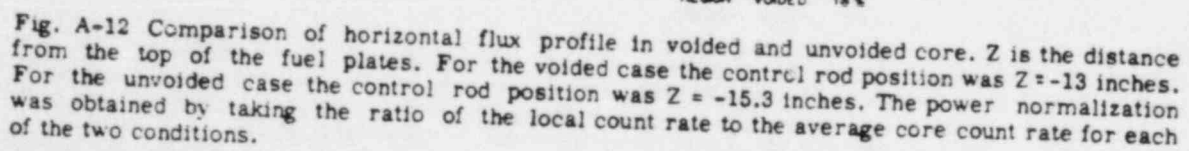
The foil locations used for both the voided and unvoided activations are shown in Figure A-11. The foils were mounted on plexiglass strips with mylar tape, and the strips were positioned in one quadrant of the core; since analysis of the cobalt wire activations obtained during the power calibration indicated quadrant symmetry, only one quadrant was investigated. The total weight of U-235 in all foils was only 1.5 g in each experiment. Figure A-12 shows the results of these flux measurements.

6. ISOTHERMAL TEMPERATURE COEFFICIENT

An isothermal temperature coefficient of approximately $-2.1\%/^{\circ}\text{C}$ was determined from the change in control rod critical position during a 9.6°C temperature rise obtained during the flux distribution measurement.

7. REDUCED PROMPT NEUTRON LIFETIME

A value of the reduced prompt lifetime, $\lambda/\bar{\epsilon}$, for the D-12/25 core was determined from an analysis of subcritical statistical behavior of the neutron population [24, 25, 26]. The value of the reduced prompt neutron lifetime obtained in this experiment was $\lambda/\bar{\epsilon} =$



APPENDIX B

DETAILS OF TRANSIENT INSTRUMENTATION FOR RUN 54

APPENDIX B

DETAILS OF TRANSIENT INSTRUMENTATION FOR RUN 54

1. POWER

Measurement of the reactor power level during the excursion was accomplished by seven neutron-sensitive ionization chambers variously located in the reactor core, in the reflector water, and in underground tubes immediately adjacent to the reactor vessel. Those chambers located in the reflector water and subject to damage from large pressure excursions were contained within heavy-walled watertight canisters for protection. Three of the chambers were of miniature size (about 1/8 inch diameter x 1 inch long). The relatively insensitive miniature chambers were placed in and adjacent to the core. The location of these miniature chambers is indicated in Table B-I.

TABLE B-I

MINICHAMBER LOCATIONS [a]

<u>Chamber</u>	<u>X (in.)</u>	<u>Y (in.)</u>	<u>Z (in.)</u>
GE-176	- 9.7	9.62	9.5
GE-679	- 3.0	8.5	- 6.0
GE-686	- 1.3	- 1.6	- 3.0

[a] Dimensions are in inches from the geometric center of the core. The X, Y, and Z coordinates form a left-handed system with the Z dimension pointing vertically up from the core. The core itself is approximately 15 inches square x 24 inches high.

With provision for duplication and multiple-ranging of some of the power instruments in order to provide power coverage from a few watts to about 200 GW, a total of 28 power signals was recorded by optical recording galvanometers. Six of these power traces also were recorded on magnetic tape to provide better frequency response, and easier reduction and preparation of data for analysis.

2. ENERGY RELEASE

The energy release from the excursion was obtained by integration of the power data recorded as described above. During the destructive test, six cobalt wires also were placed in the core in order to provide additional information on the nuclear energy release by activation measurements.

3. TEMPERATURE

Fuel plate temperatures in the core were measured by 34 thermocouples installed on 16 different fuel plates. Of these, 12 were surface-type and 22 were buried-type thermocouples. The surface-type thermocouples (Figures B-1 and B-2) consisted of 10-mil diameter chromel-alumel wires, flattened and trimmed

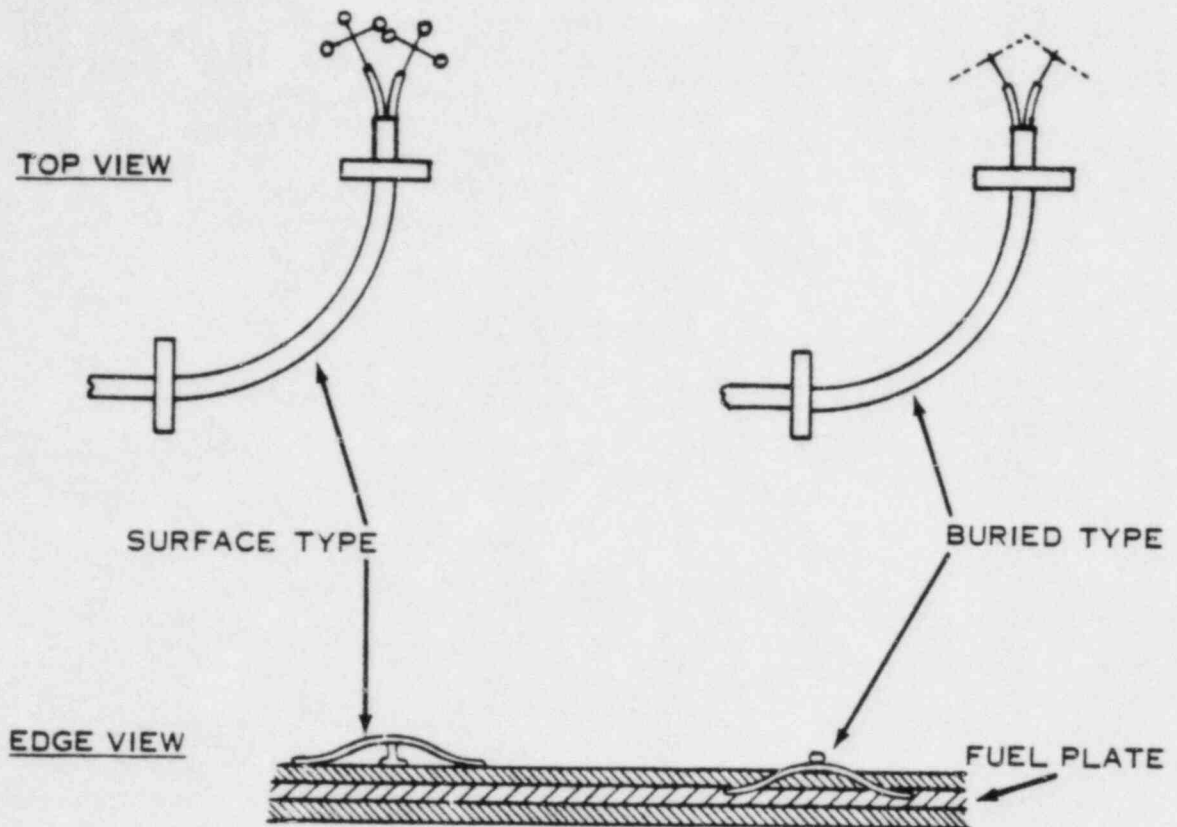


Fig. B-1 Mounting technique for thermocouples.

to tabs approximately 0.5 mil thick, which were resistance-welded to the surface of the fuel plates to establish a low-mass junction. The buried-type thermocouples consisted of two chromel-alumel wires imbedded into the meat of the fuel plate with the cladding peened over the top of the wires to hold them in place (Figure B-1). These buried thermocouples provided thermal and electrical contact with the plate for a longer time after plate melting than would have been the case for the wires attached to the surface and were, therefore, used in regions of the core that were expected to exceed the melting point of aluminum. In the attempt to obtain a measure of the actual fuel temperature in the core during the destructive test, two special capsules were constructed and installed in the core prior to the test. These capsules consisted of a small quantity of the fuel alloy (from a conventional plate) contained in a high-melting-point container along with high-melting point thermocouples. Upon melting, the meat alloy was constrained to remain in contact with the thermocouples. The capsule consisted of a type-304 stainless steel cylinder, 3/16 inch in diameter, 3/4 inch long, with 20-mil walls, crimped into an elliptically shaped container. One end of the container was welded closed

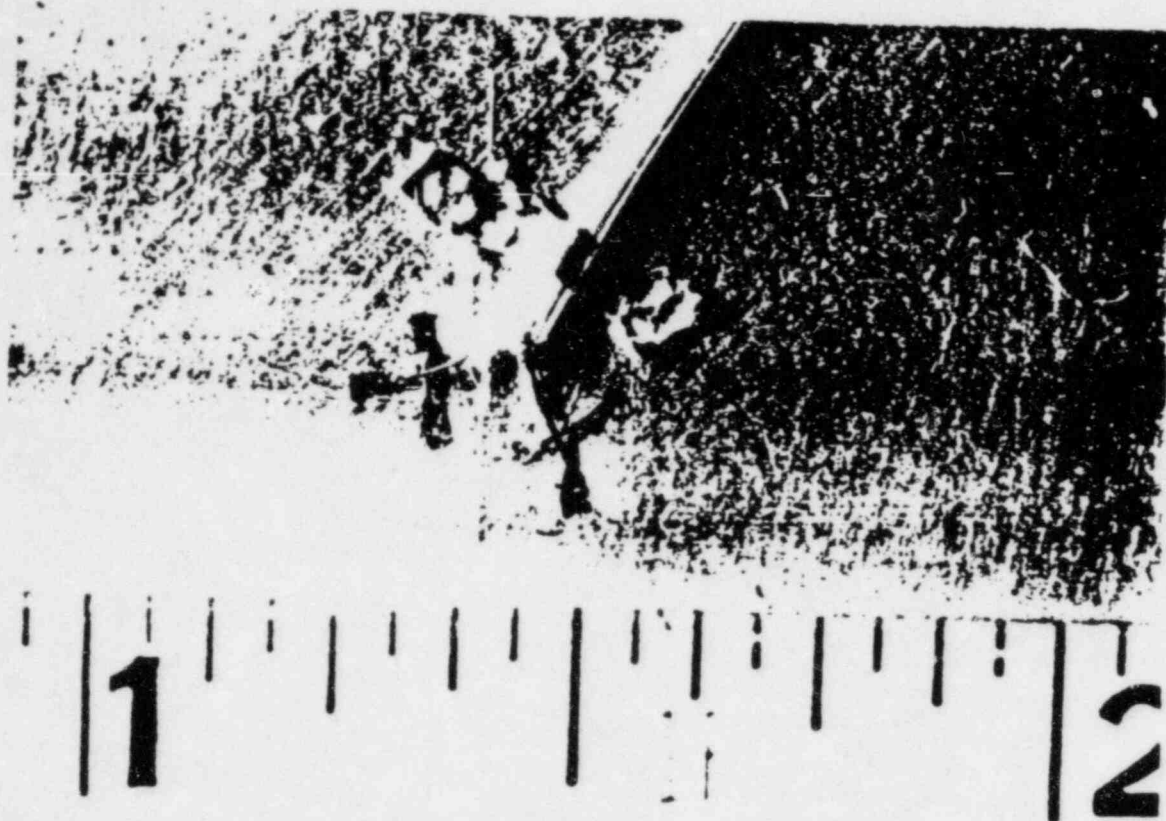


Fig. B-2 Photograph of typical surface-type thermocouple. (Welded tabs are ≈ 0.5 mil thick.)

with 0.125 inch of stainless steel. Two slabs of U-Al alloy from a regular fuel plate were placed in the container, forming a fuel slab about 0.04 inch thick. A tungsten, tungsten-rhenium thermocouple pair, contained in a stainless steel sheath, was placed in the fuel. The stainless steel sheath extended into the cylinder but not into the fuel. The top of the container was then welded closed with stainless steel, adding 0.250 inch of stainless steel on the top side of the fuel capsule. The capsule was again crimped and heated past the melting point of the uranium-aluminum alloy to ensure good contact between the thermocouple wires and the fuel. Figure B-3 is a photograph of the fuel capsule.

One of the fuel capsules was placed near the central hot spot of the reactor core and the other at a point just outside the expected melting region of the core.

4. PRESSURE

A total of 19 pressure transducers at 15 different locations surrounding the reactor core was used during the destructive test. The location and ranges of these transducers are shown in Figure B-4 and in Table B-II. The location of pressure transducers used during all other tests also appears in Table B-II. This arrangement was selected to provide information on the time behavior of transient pressures as a function of position surrounding the core. More than one transducer was located in some of the positions in order to cover the range from the modest pressures extrapolated from previous data to the destructive pressure pulses anticipated for the series. No pressure measurements were made



Fig. B-3 Photograph of fuel-bearing capsule.

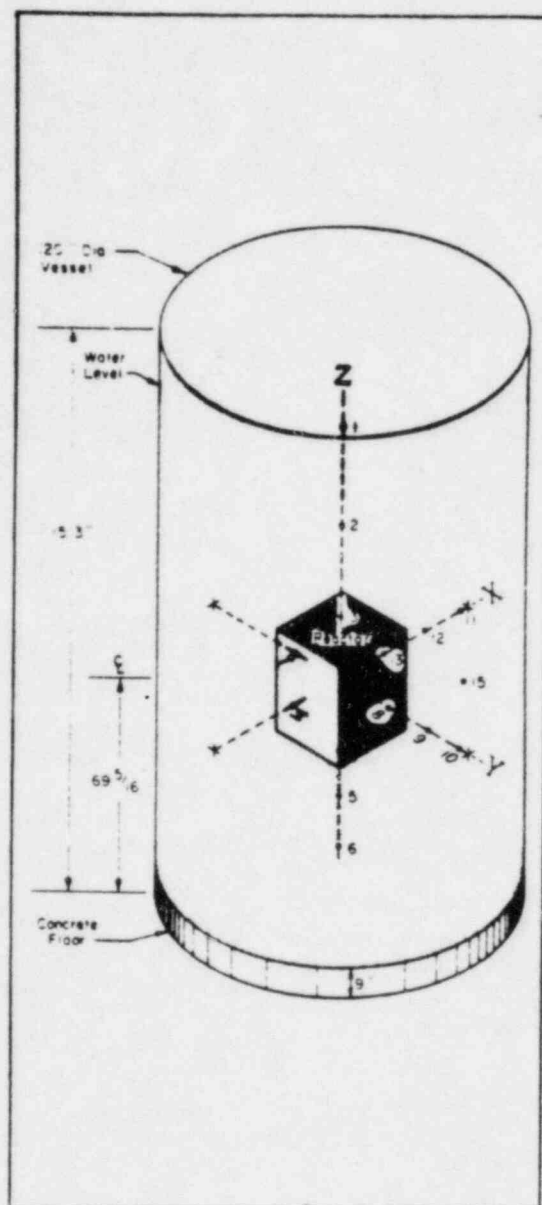


Fig. B-4 Location of pressure transducers for destructive test.

within the reactor core since no transducers were available which were sufficiently small to fit between the fuel plates and at the same time sufficiently insensitive to the radiation burst to permit useful measurements. The pressure transducers were carefully selected to minimize the radiation sensitivity of the transducer while at the same time preserving a maximum available frequency response. A total of 24 pressure signals was recorded by the optical recording galvanometers during the test.

5. STRAIN

Strain gauges were placed on several items in and around the reactor during the destructive test, utilizing strain measurement techniques which had been

TABLE B-II
PRESSURE TRANSDUCER INSTRUMENTATION

Transducer Serial No.	Location (See Fig. B-4)	Coordinates (in. From Core Center)			Pressure Range (psig)
		X	Y	Z	
1960	1	3	2	58.5	100
2444	1	6	3	58.5	1000
1976	1d	3	3	62	-15 to 35
2444	2d	3	3	39	-100 to 900
1975	3	3	3	19.5	100
2655	3d	5	5	23	-10 to 20 and -50 to 250
2060	3d	3	3	23	-100 to 700
16106	4	3	3	-27.5	100
2077	4d	3	-4.5	-20	-300 to 2700
2628	4d	3	-3.5	-20	-10 to 20 and -30 to 270
2074	5d	3	2	-36	-350 to 3150
16237	6	-4	-3	-51	100
2281	6	-2.5	3	-52	3000
2638	6d	3	2	-53.5	0 to 300
2208	7	0	-25	0	2500
2192	7d	3.5	-16.5	0	0 to 10,000
3949	8	0	10.5	0	150
2062	8d	1.5	16.5	0	0 to 3500
1977	8d	-1	17	0	-8 to 17 and -25 to 225
2639	9d	1	36.5	2.5	0 to 300
16275	10	-4.5	54	0	100
2232	10	5	53	0	1000
1990	10d	1	53.5	2	-7 to 58 and -200 to 450
1976	11	54	4	0	100
2192	11	54	-6	0	10,000
2196	11	55	8	0	8000
2475	11d	52.5	1	1.5	0 to 300
1977	12	25.5	0	0	250
2196	12d	35	0	2	-800 to 7200
3948	13	10.5	0	0	150
2281	13d	17	1	-1	0 to 3000
2646	13d	17	-2	2	-15 to 85 and -30 to 270
2553	14d	-17	1.5	0	0 to 1000
20123	15d	17.5	-22.5	-48.5	-10,000 to 90,000

Note: Locations of pressure transducers used during the 3.2-msec destructive test are designated by the letter "d". The pressure ranges indicated for the transducers used during other tests are maximum pressure ranges and were adjusted before each test by varying the gain of the connected amplifiers.

developed during the nondestructive portion of the testing program. The following specific items were instrumented with strain gauges during the test: the hold-down bars which provided vertical restraint on the fuel assemblies in the core -- longitudinal tension; the core clamps which provided lateral support to the core -- longitudinal compression; the core-support legs which support the core structure from the bottom of the reactor vessel -- longitudinal compression; a peripheral fuel assembly -- instrumented for strains in bowing and bulging of the assembly; and the reactor vessel -- hoop stress or bulging. A total of eight signal channels was recorded for the measurement of strain during the destructive test.

6. FLOW

The flow of moderator from the reactor core during short-period excursions is of interest because of its applicability to the study of the transient shutdown processes. Both the thermal expansion of the fuel plates and boiling of the moderator in the core lead to the expulsion of moderator from the core. Since these mechanisms apparently constitute the major shutdown processes occurring during short-period excursions, information as to the time and rate at which shutdown occurs can be obtained from the measurement of moderator flow from the top and bottom of the core.

Two different devices were utilized for the measurements of flow from fuel assemblies in the core. The first consisted of a small circular disc suspended on the end of a cantilevered beam over the center of the flow. The force on this drag disc was monitored by a strain gauge mounted on the beam and the force then related to the velocity of flow. While this device provided a sensitive indication of the initial flow motion of the moderator, the relationship between the force on the disc and water velocity was such as to make quantitative flow information difficult to obtain from the device. A more quantitative measurement of flow was obtained from a displacement transducer which utilized positive motion of a piston in a cylinder, with the velocity of the piston being measured by a moving-magnet technique. This flowmeter consisted of two separate piston-cylinder units mounted on each end of a fuel assembly (Figure B-5). Flow from the assembly was constrained to move into the cylinders and cause the pistons to move outward. Attached to each piston was a magnet moving through a coil to produce a signal proportional to the velocity of motion. For the destructive test, two drag-disc-type and two displacement-type flowmeters were in use, mounted on two fuel assemblies adjacent to the central assembly of the core.

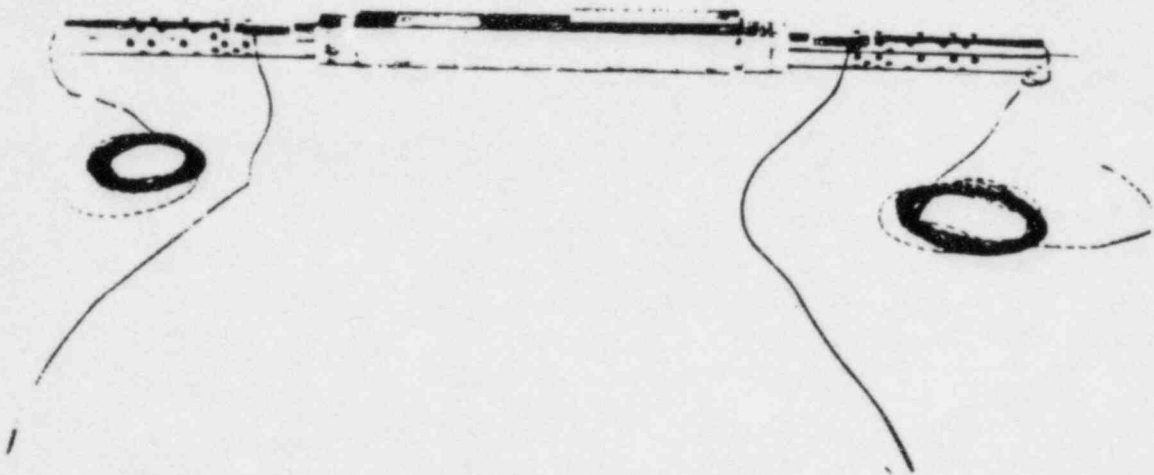


Fig. B-5 Photograph of displacement transducers mounted on fuel assembly.

7. PHOTOGRAPHY

For the destructive test, two high-speed (500 fps) cameras were used in conjunction with the periscopes to provide an underwater view of the reactor core.

A third, medium-speed (128 fps) camera viewed the core from above through a mirror. Six cameras ranging from high speed (600 fps) to conventional speed (24 fps) were variously positioned to record the expulsion of water from the vessel, disruption of the control structure, and ejection of missiles. Table B-III lists all the cameras which were used for the destructive test with their locations and speed.

TABLE B-III

LOCATION AND SPEED OF CAMERAS FOR DESTRUCTIVE TEST

Camera No.	Type	Speed (fps)	Location
1	Waddell	500	North edge of reactor tank using periscope to view across top of core
2	Waddell	500	North edge of reactor tank using periscope to view top of core
3	Waddell	600	Rear doorway of reactor building viewing directly over reactor vessel
4	Bell & Howell	128	Near reactor tank viewing top of core through mirror
5	Bell & Howell	64	Approximately 50 ft southeast of reactor viewing front of reactor building
6	Bell & Howell	24	Approximately 100 yd southeast of reactor viewing front of reactor building
7	Bell & Howell	128	Roof of Spert I terminal building viewing west side of reactor building
8	Arriflex	48	At the Control Center approximately 1/2 mi from the reactor
9	Bell & Howell	24	Approximately 125 ft west of Spert II reactor building, about 1/2 mi from the Spert I reactor

8. RADIOLOGICAL MEASUREMENTS

The radiological measurements obtained during the destructive test were conducted as a joint effort by personnel of Phillips Petroleum Co. and the Health and Safety Branch of AEC Idaho Operations Office. The measurements made included: (a) measurement of the integrated neutron and gamma dose as a function of position relative to the reactor vessel, including separate determination of the integrated dose during the power burst and the total integrated dose for about four hours after the test; (b) direct-radiation dose-rate measurements made with six remote-area monitors at several points for the purpose of estimating hazard to reentry personnel; (c) airborne radioactive contamination, using high-volume air samplers located in and around the reactor area; (d) the neutron spectra and the gamma-to-neutron ratios as a function of position relative to the

core, by use of nuclear accident dosimeters (NAD) suspended over the reactor; (e) the fission product inventory in the reactor water after the test, by water sampling; (f) air activity and fallout rate, at several grid positions downwind of the reactor; (g) the Na-24-induced activity in ordinary blood, as a function of proximity of the blood sample to the edge of the reactor vessel, in order to determine biological effects; (h) body absorption factors for a reactor excursion accident, by simultaneous exposure of film badges and bottles of tissue-equivalent solution; (i) comparison of several methods for accident analysis, by placement around the vessel of materials (small tools, various metals, etc) which might normally be found around a reactor which had undergone an accident; (j) determination of fallout by the use of grass plots, fallout plates, etc, positioned on the downwind grid; and (k) fisside cloud activity and progress by means of both airborne and surface mobile tracking equipment located downwind for a distance of 25 miles.

9. SPECIAL EQUIPMENT FOR DESTRUCTIVE TEST

In addition to the instrumentation described above and the normal control instrumentation for the reactor, a number of special items of equipment were provided specifically for the destructive test. Two television monitors were provided to view the reactor core and the top of the vessel. Monitors for these channels were placed in the reactor control room to provide information for post-test analysis of the condition of the core and facility prior to reentry.

In addition to the conventional water-level indicator for the reactor vessel, a separate, ruggedized, float-actuated device was mounted on the floor of the reactor vessel to provide indication when the water level reached six and three inches above the bottom of the reactor vessel. This was provided in anticipation that the normal full-range water-level indicator might be damaged by the violence of the test and to provide positive indication of successful draining of the vessel prior to personnel reentry of the area.

A remotely operated soluble-poison injection system also was provided to inject gadolinium nitrate solution into the reactor vessel in the event that, because of damage to components and hardware, it might not be possible to drain the water from the reactor vessel.

Figures B-6 through B-11 illustrate typical transient instrumentation for Run 54.



Fig. B-2 Miniature ionization chamber used for in-core power level monitoring.

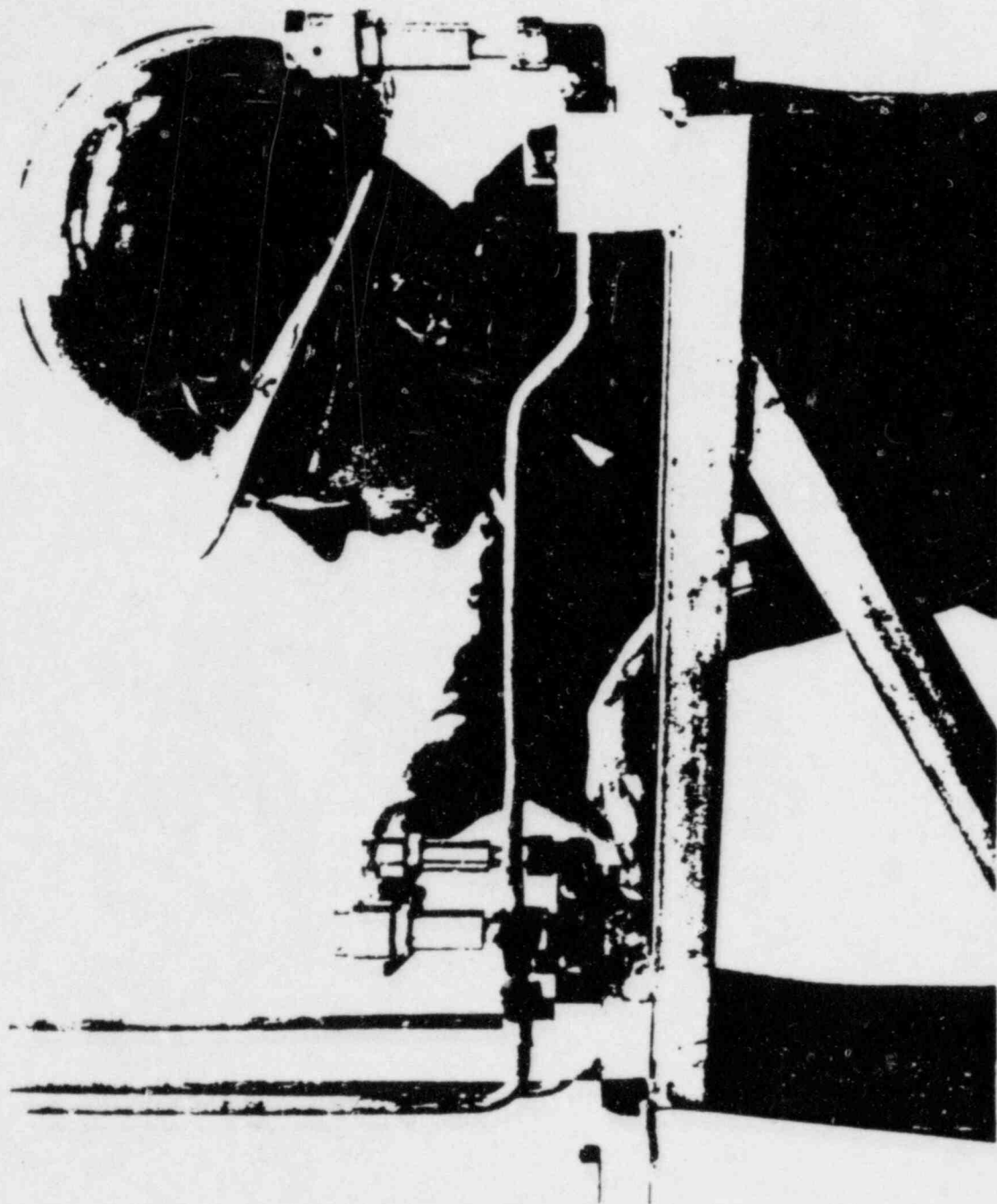


Fig. B-7 Typical installation of pressure transducers. Three transducers are shown attached to wall-mounted bracket. Lead wires exit through steel tubing.

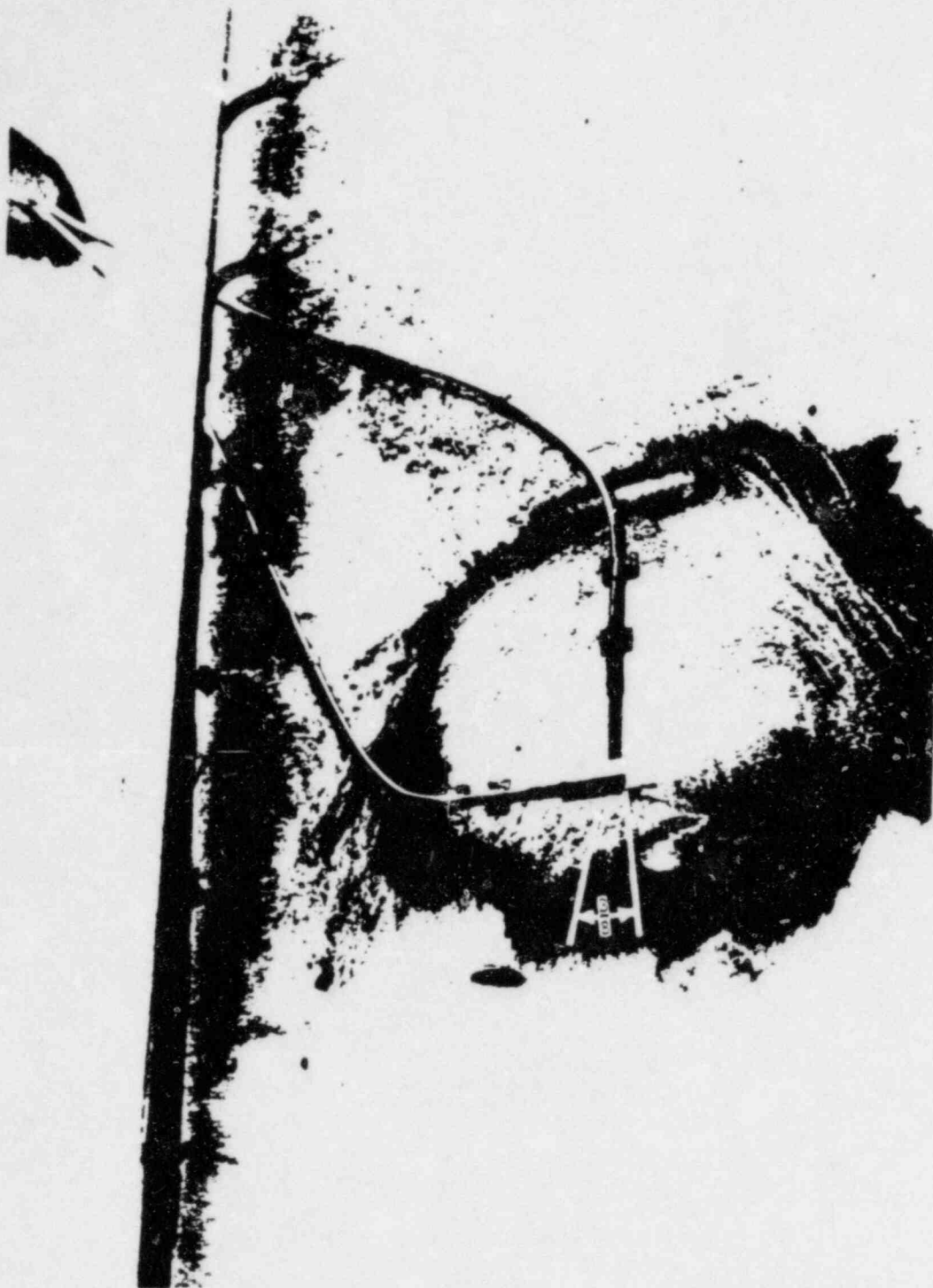


Fig. B-6 Typical installation of strain gauges. Two strain gauges are shown attached to the wall of the reactor vessel, one vertical and one horizontal.

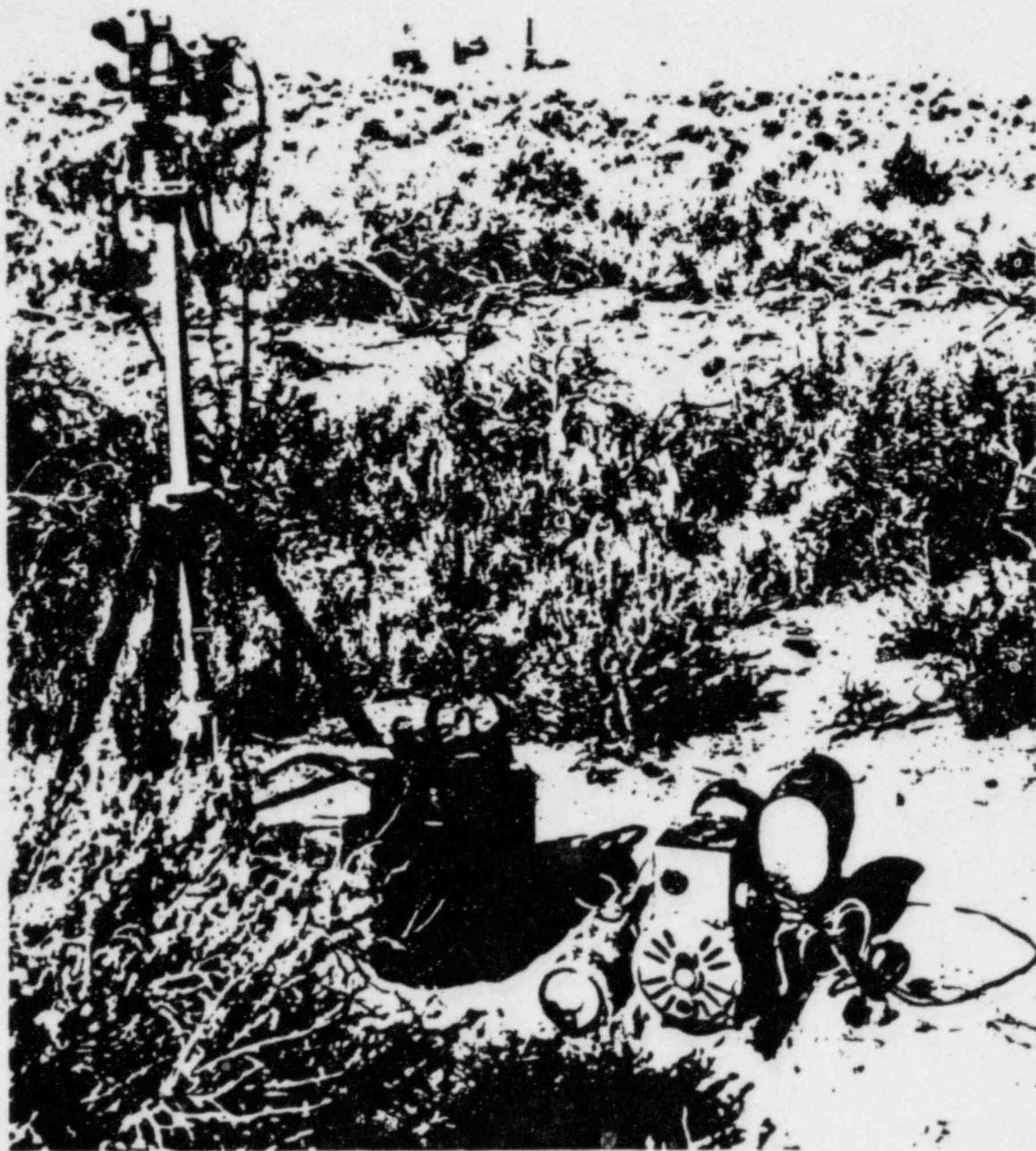


Fig. B-9 Installation of camera #6 for long distance photography. Camera has independent power supply and is started remotely by a sequence timer at the control center.

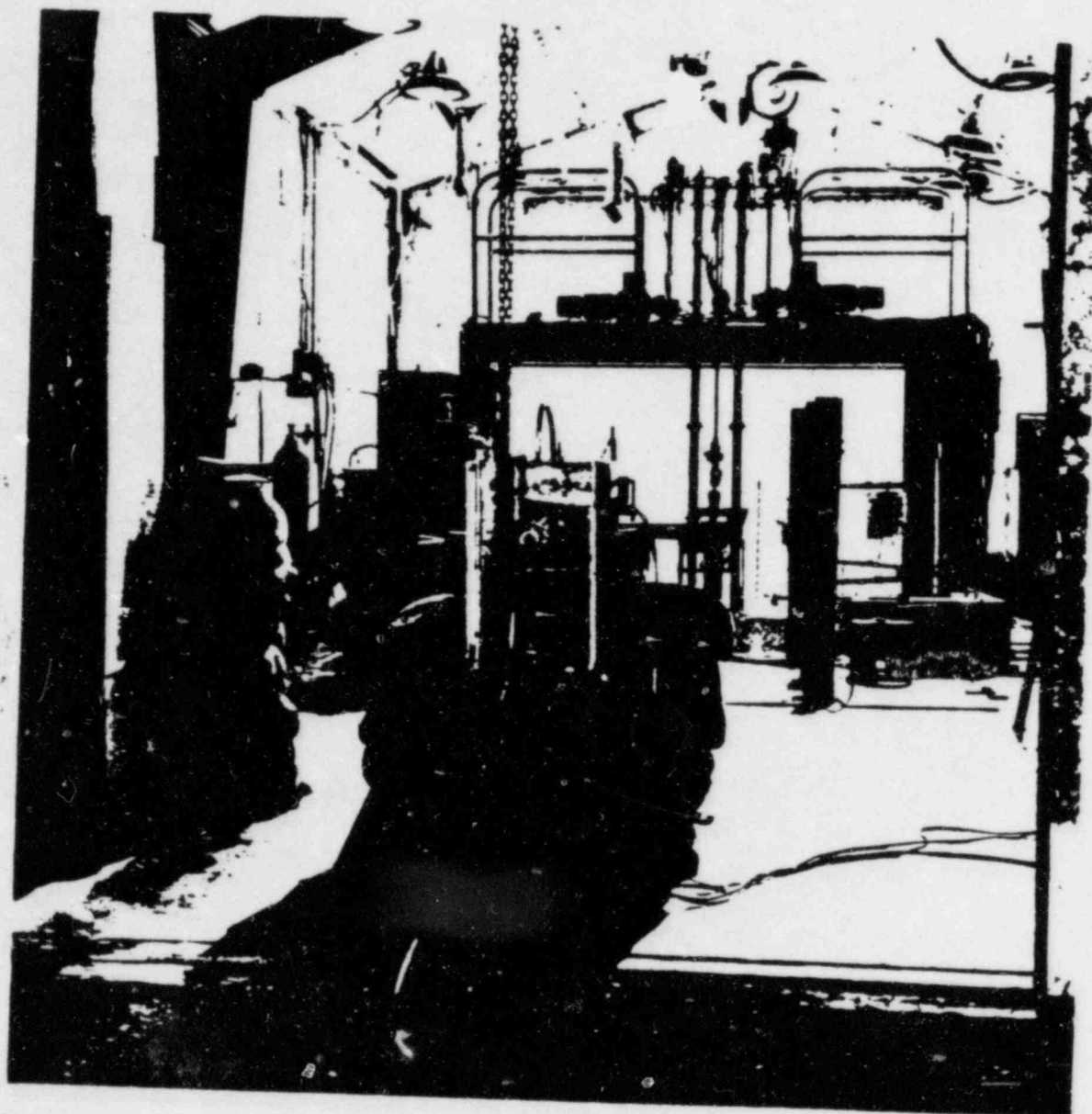


Fig. B-10 High speed (600 fps) camera #3 installation at the rear of the reactor building. Rope (attached at rear of housing) and inclined track are for remote removal of camera.

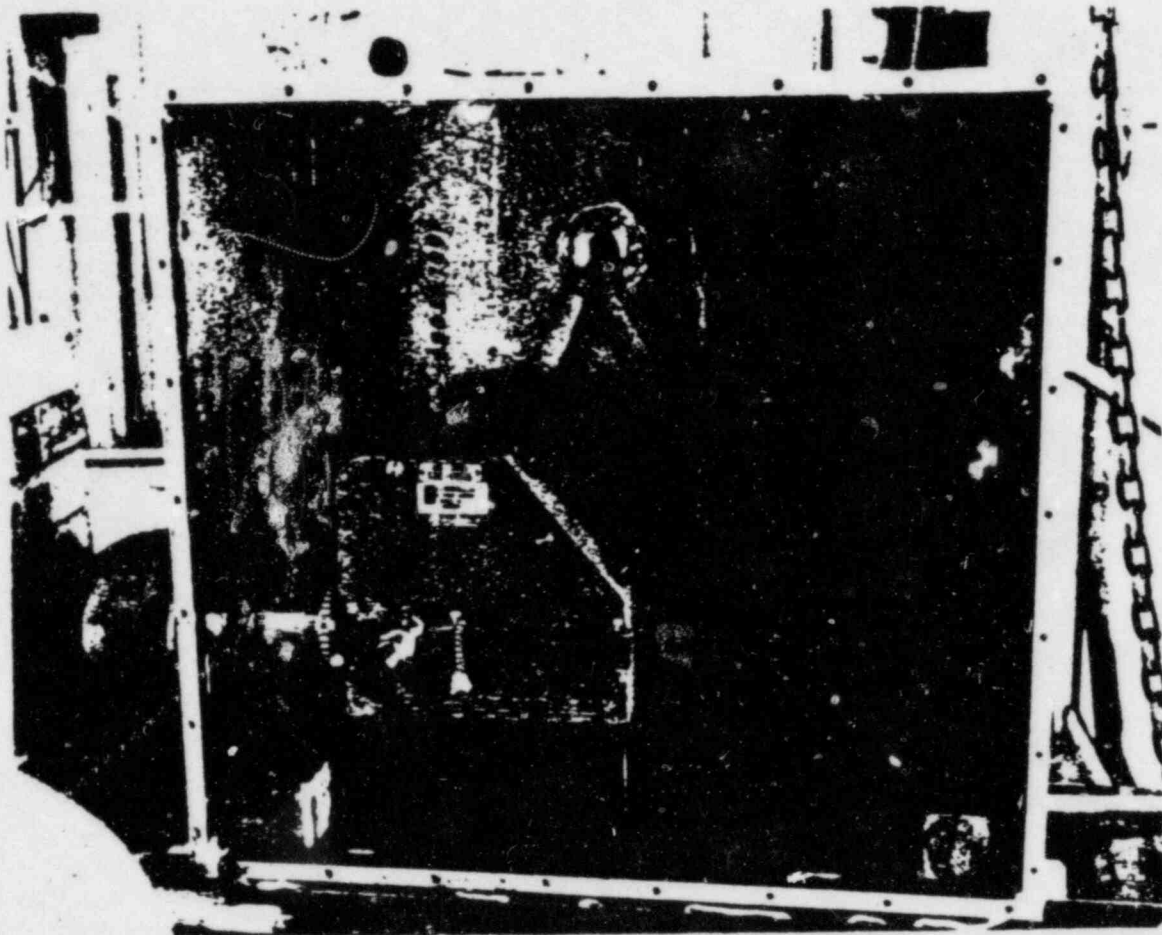


Fig. B-11 View of high speed camera inside of protective housing. Cables supply power for motors and light-timing device.

APPENDIX C

DATA SUMMARY

APPENDIX C

DATA SUMMARY

This appendix contains representative data taken from selected tests during the Destructive Test Series. For a more complete data summary see Reference 27. In the figures to follow, nomenclature designating the location of the measuring instrument is assigned to each temperature and pressure response curve. The location of pressure transducers is specified by a left-handed, Cartesian coordinate system having its origin at the center of the core (Figure B-4). A number which corresponds to specific coordinates (Table B-II) is assigned to each pressure transducer. The location of thermocouples is specified by a symbol having five characters: the first two specify the fuel assembly (Figure D-1); the third specifies the fuel plate (fuel plates are numbered 1 through 12, number 1 is the first fuel plate on the west side of the fuel assembly); the fourth specifies the side of the fuel plate to which the thermocouple is attached; and, the last is the z coordinate of the thermocouple location ($z = 0$ is at the vertical center of the core).

Figures C-1 through C-7 are general behavior plots of power, temperature, and pressure (pressure traces are shown only when a significant deflection was recorded) for the period region from 880 msec to 6 msec. Figures C-8 through C-10 are general behavior plots showing power, temperature, and pressure for a 5-msec period test. Figures C-11 through C-13 are general behavior plots of power, temperature, and pressure for a 4.6-msec period test. Figures C-14 through C-20 are behavior plots from the destructive test. Figure C-21 shows the maximum recorded temperatures for the Destructive Test Series.

Figure C-22 is a plot of burst parameter versus reciprocal period for all of the data recorded during the Destructive Test Series. The burst parameter is defined as $\beta(t_m)/E(t_m)\tau_0$. If the power increase to peak follows a pure exponential, then $\beta(t_m)/\tau_0$ is the energy release up to the time of peak power, $E(t_m)$. As τ_0 increases the power rise becomes sharper thus approaching a pure exponential and the burst parameter approaches unity. The change in slope and eventual decline of the burst parameter (shown in Figure C-22) for τ_0 greater than about 100 sec⁻¹ is due to burst broadening before peak power which is discussed in Section III-2.5.

Table C-1 contains a list of the initial step injection of reactivity, Δk_0 ; the period, τ_0 ; reciprocal of the period, τ_0^{-1} ; peak power, $\beta(t_m)$; energy release at the time of peak power, $E(t_m)$; total energy release, E_T ; maximum temperature at the time of peak power, $\theta(t_m)$; and maximum temperature, θ_{max} , for each of the 54 tests performed during the Destructive Test Series.

The best values of τ_0 , $\beta(t_m)$, and E_T for the destructive test are 3.21 ± 0.04 msec, 2260 ± 60 MW, and 30.7 ± 0.6 MW-sec, respectively. The quoted errors are the standard deviation of the experimental values. For $\beta(t_m)$ and $E(t_m)$ there also may be a possible 10 percent systematic error.

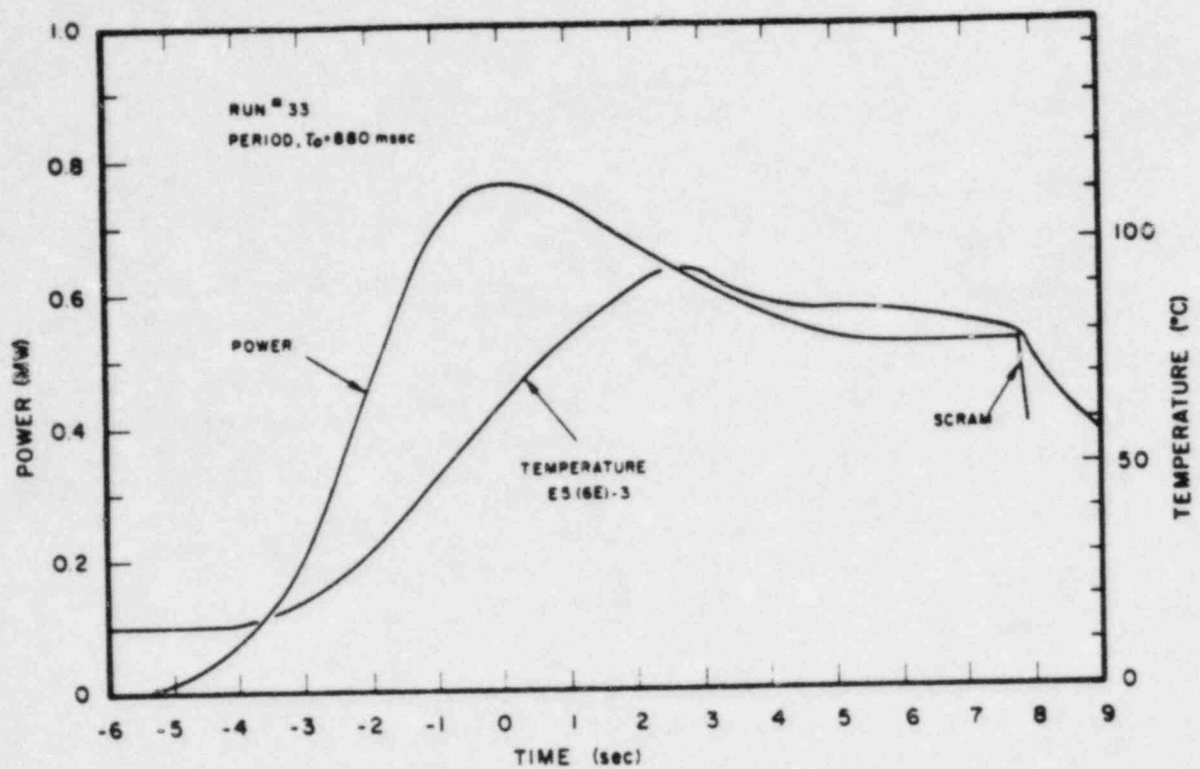


Fig. C-1 General behavior plot showing power and temperature for a 880-msec period transient test.

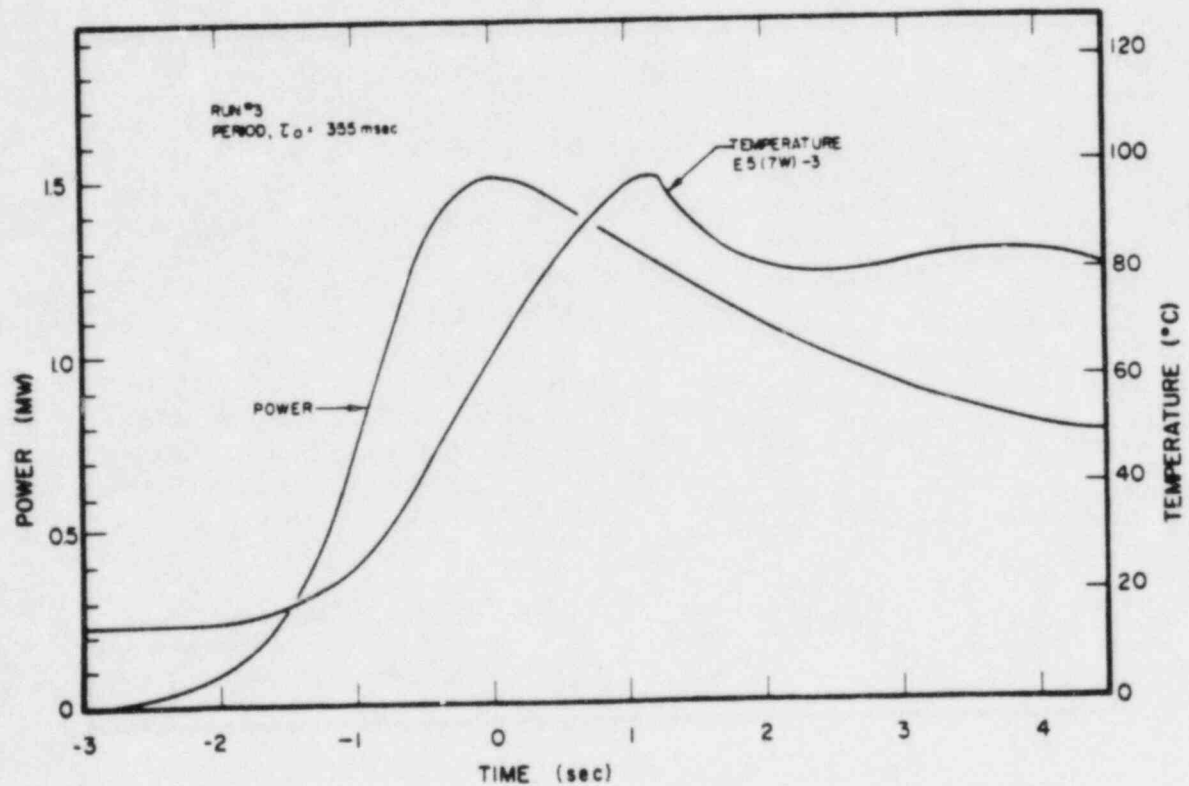


Fig. C-2 General behavior plot showing power and temperature for a 355-msec period transient test.

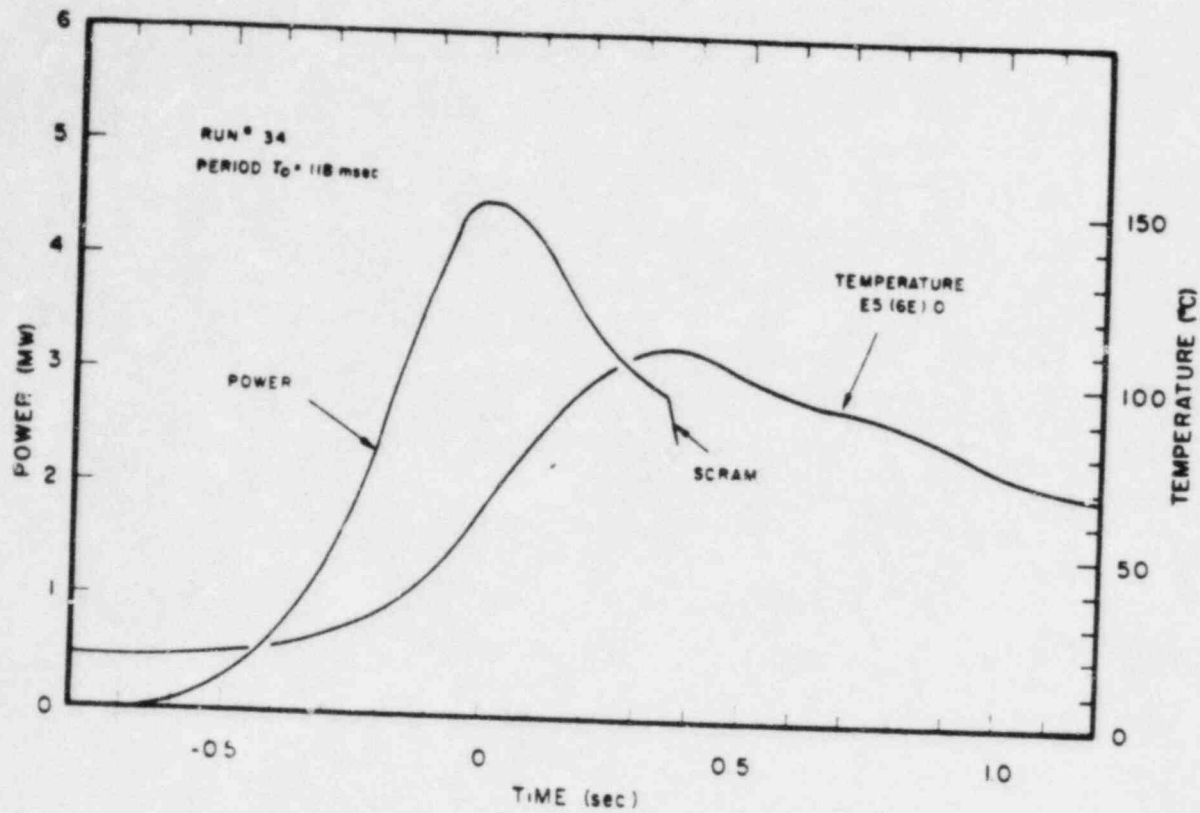


Fig. C-3. General behavior plot showing power and temperature for a 118-msec period transient test.

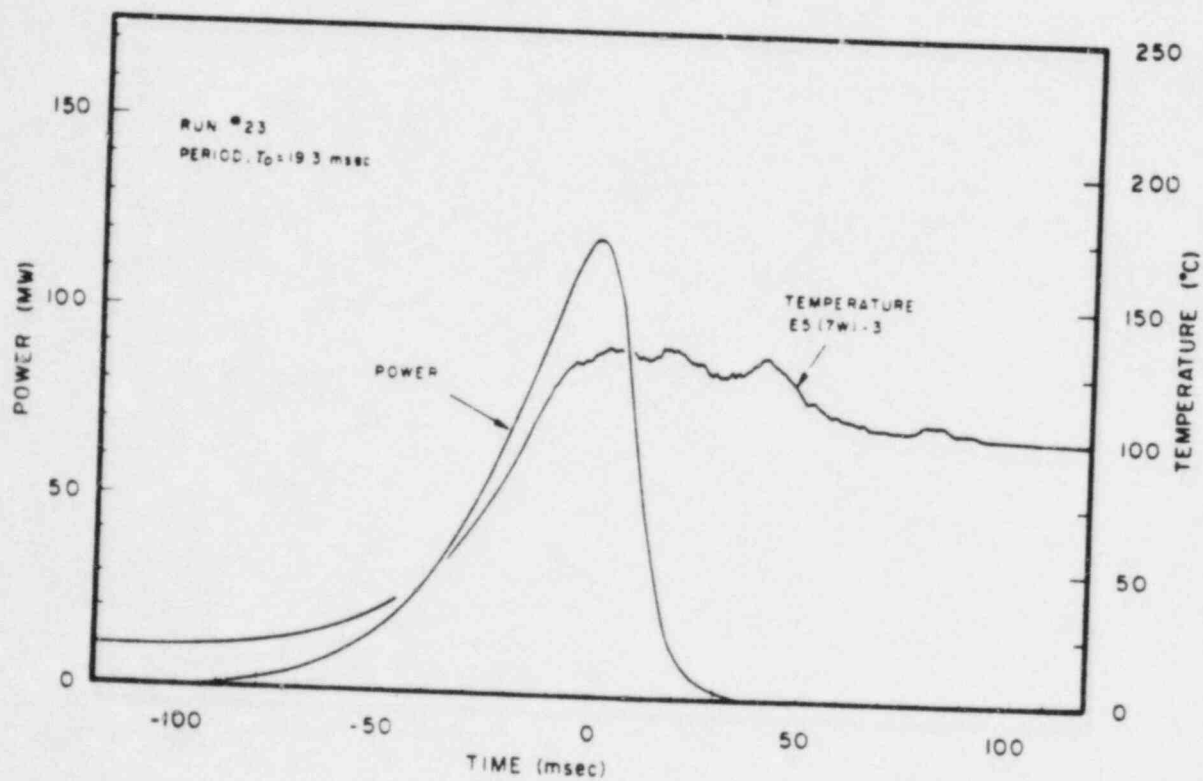


Fig. C-4. General behavior plot showing power and temperature for a 19.3-msec period transient test.

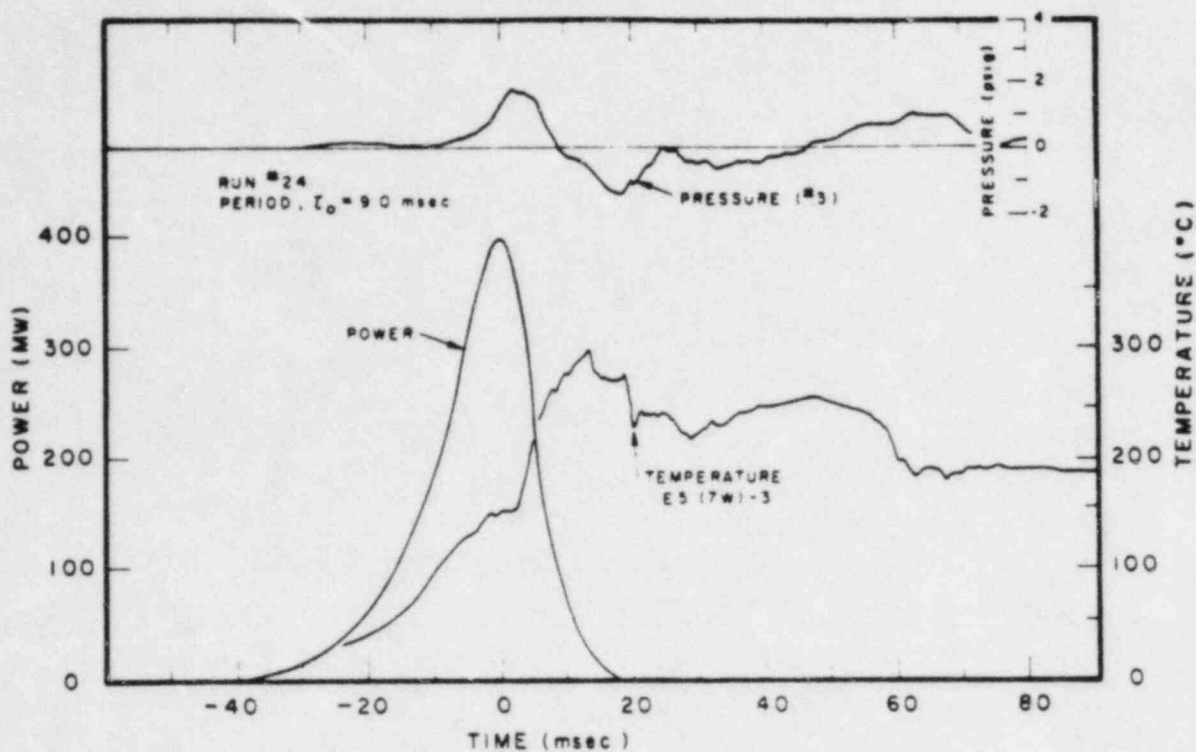


Fig. C-5 General behavior plot showing power, pressure, and temperature for a 9-msec period transient test.

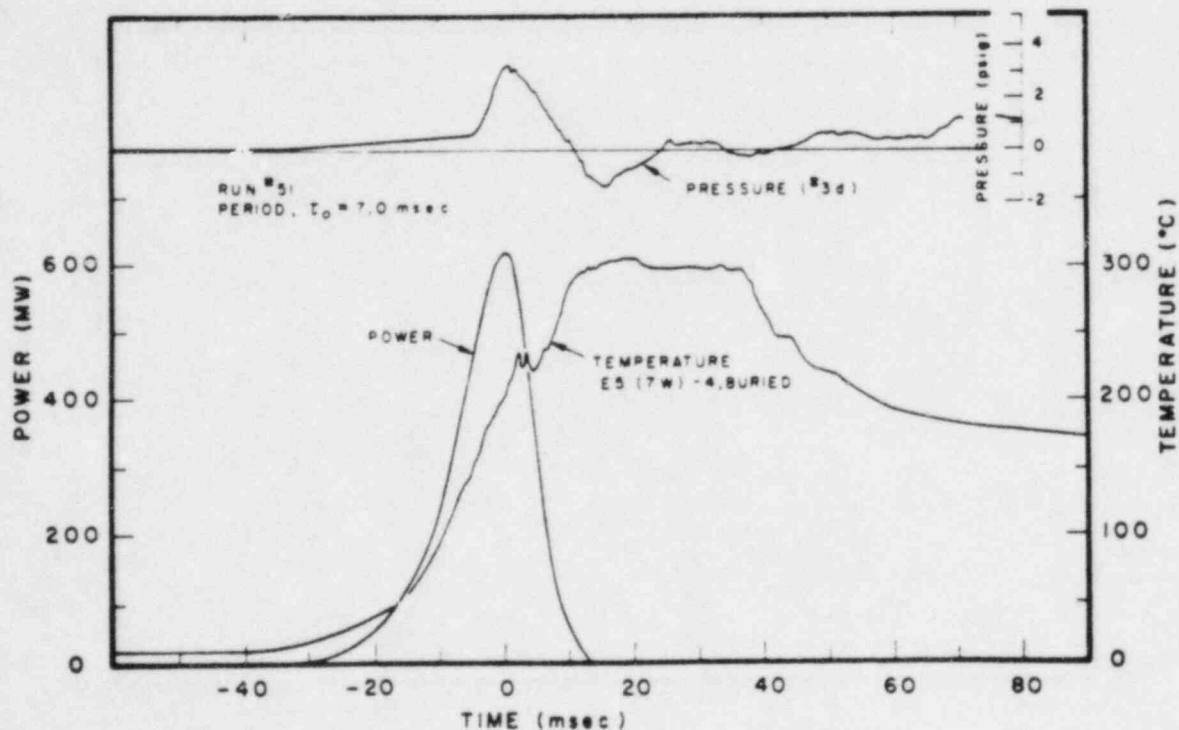


Fig. C-6 General behavior plot showing power, pressure, and temperature for a 7-msec period transient test.

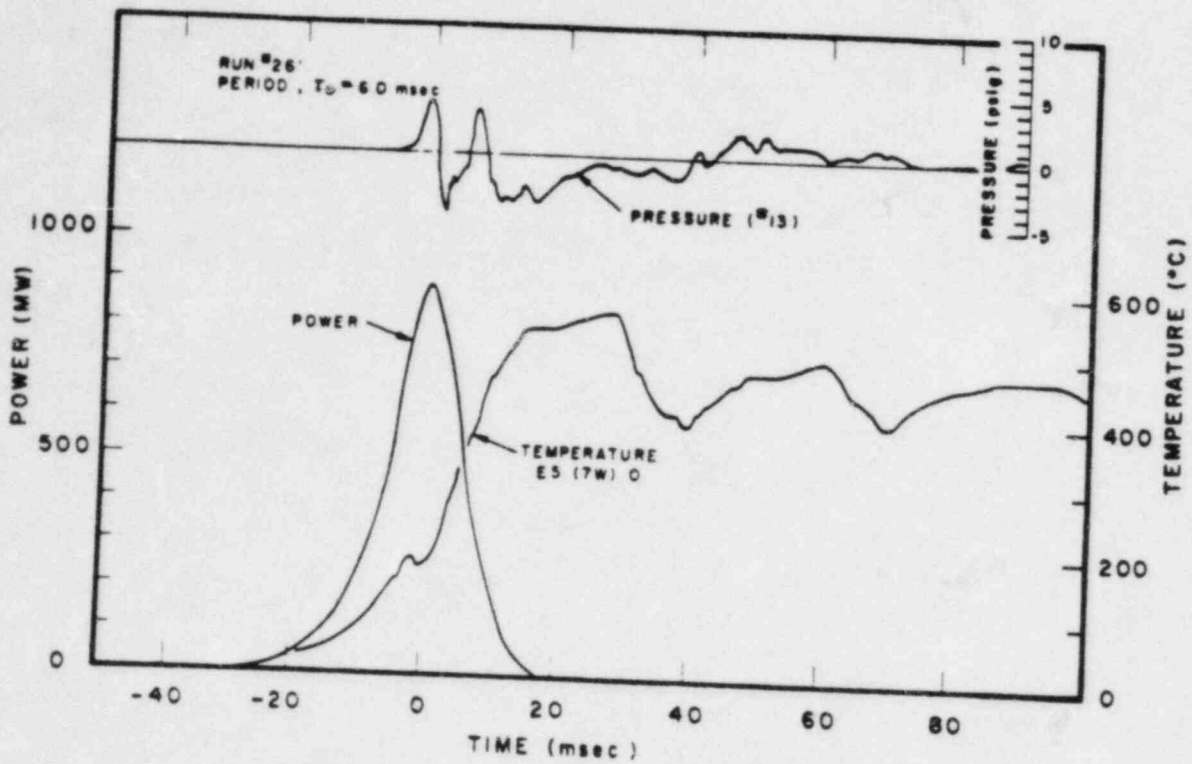


Fig. C-7 General behavior plot showing power, pressure, and temperature for a 6-msec period transient test.

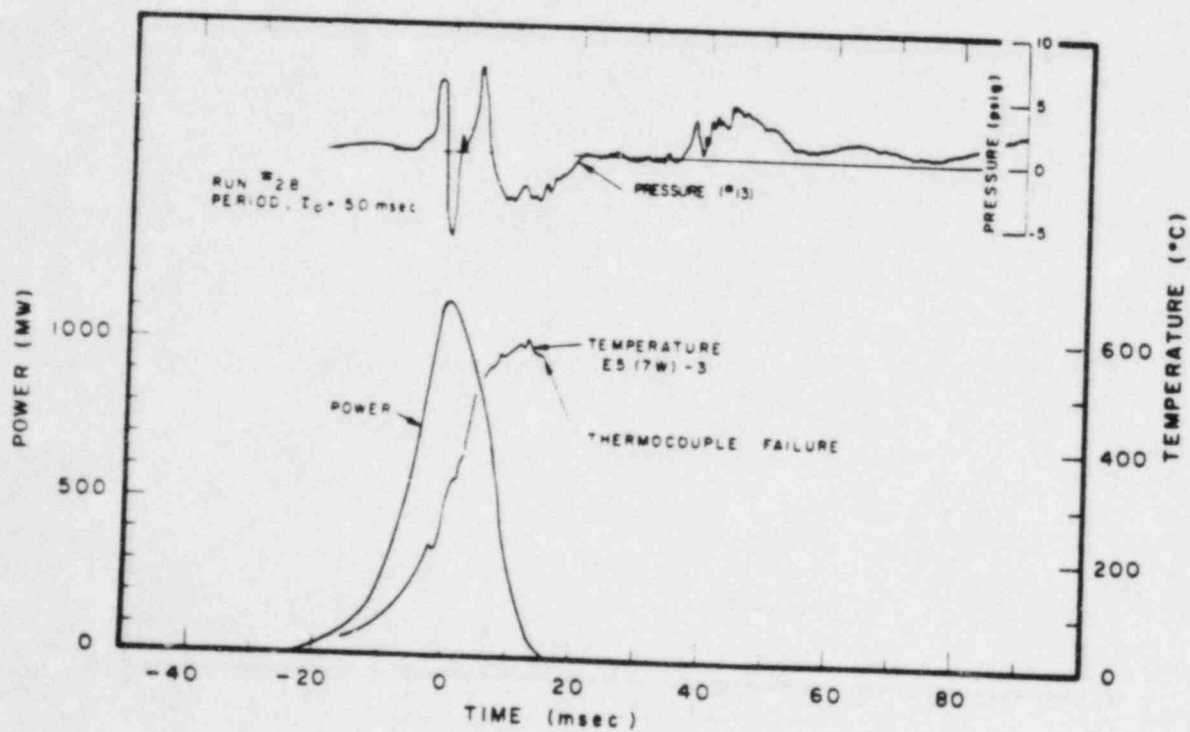


Fig. C-8 General behavior plot showing power, pressure, and temperature for a 5-msec period transient test.

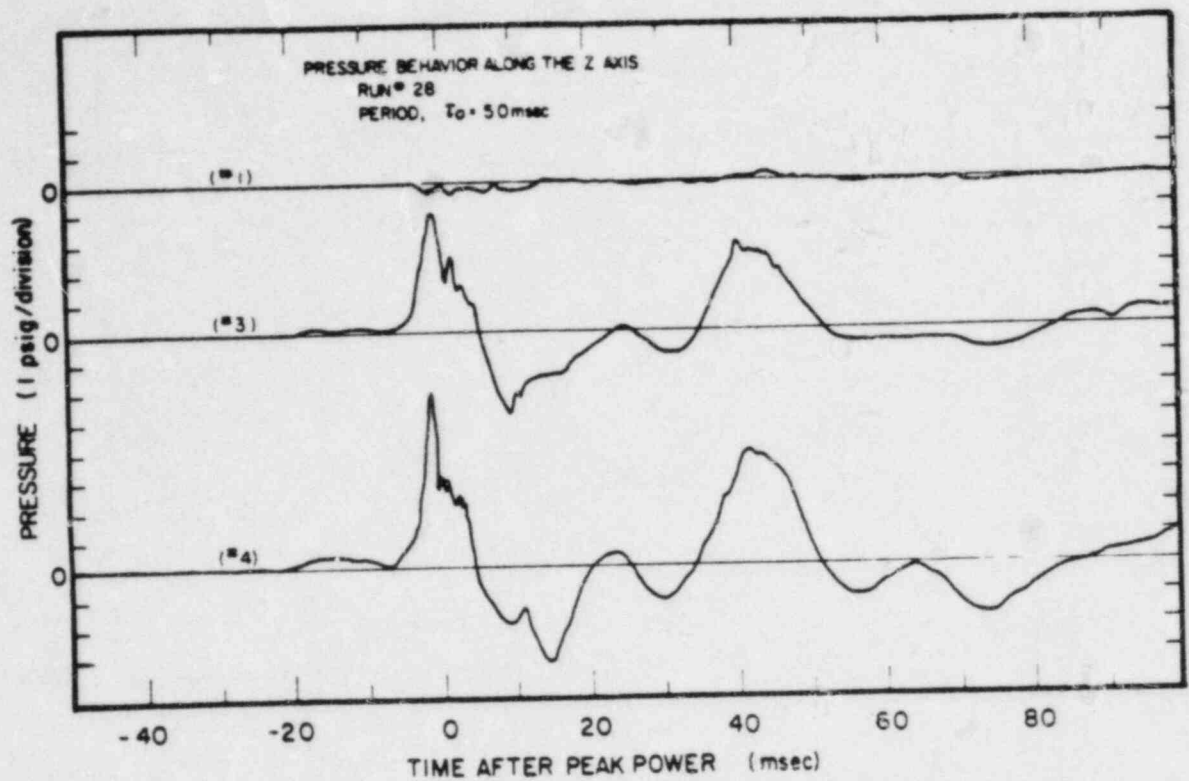


Fig. C-9 Vertical pressure profile showing pressure measured about five feet above the center of the core (#1), about two feet above the center of the core (#3), and 20 inches below the center of the core.

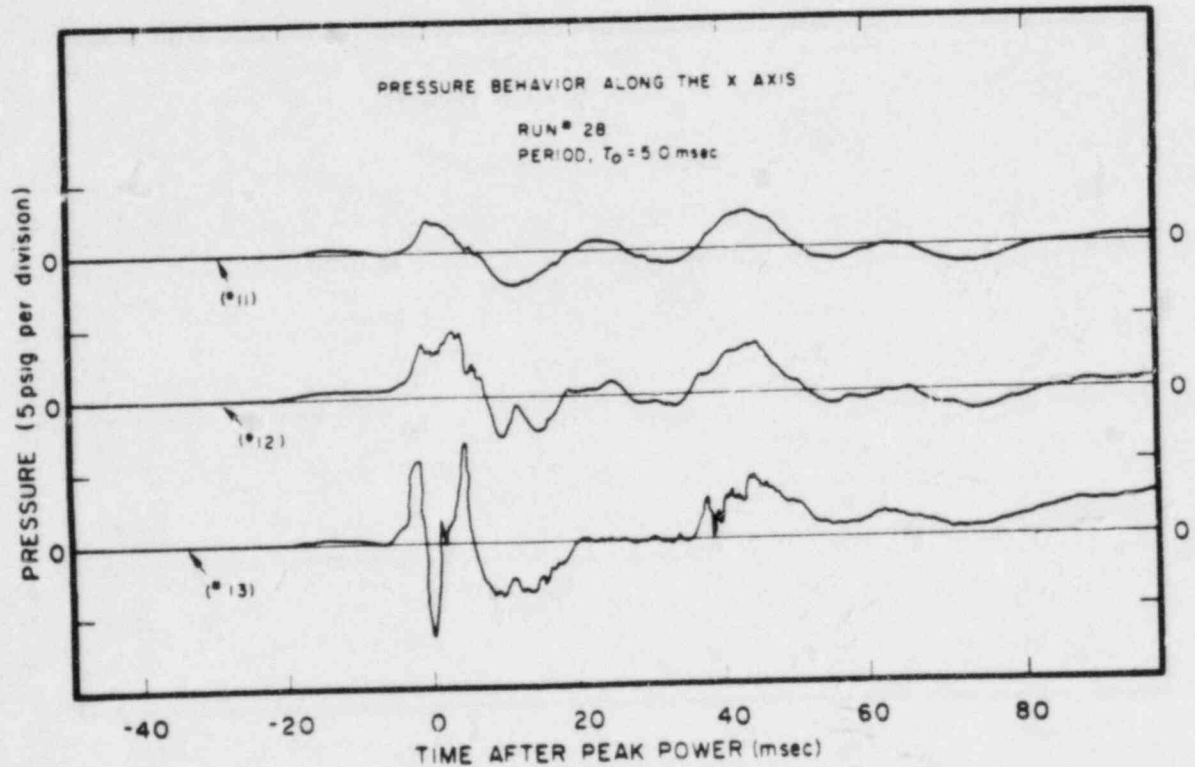


Fig. C-10 Horizontal pressure profile showing pressures measured respectively, 52 inches (#11), 35 inches (#12), and 17 inches (#13) horizontally from the core center.

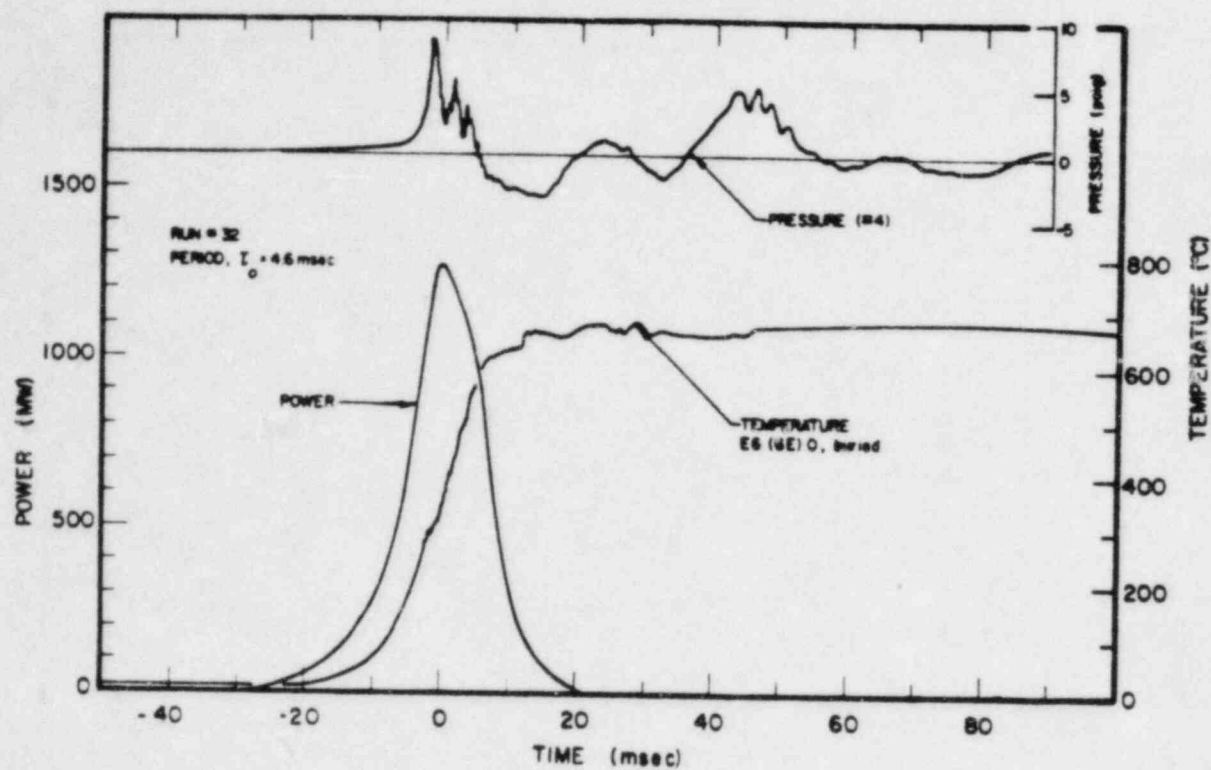


Fig. C-11 General behavior plot showing power, pressure, and temperature for a 4.6-msec period transient test.

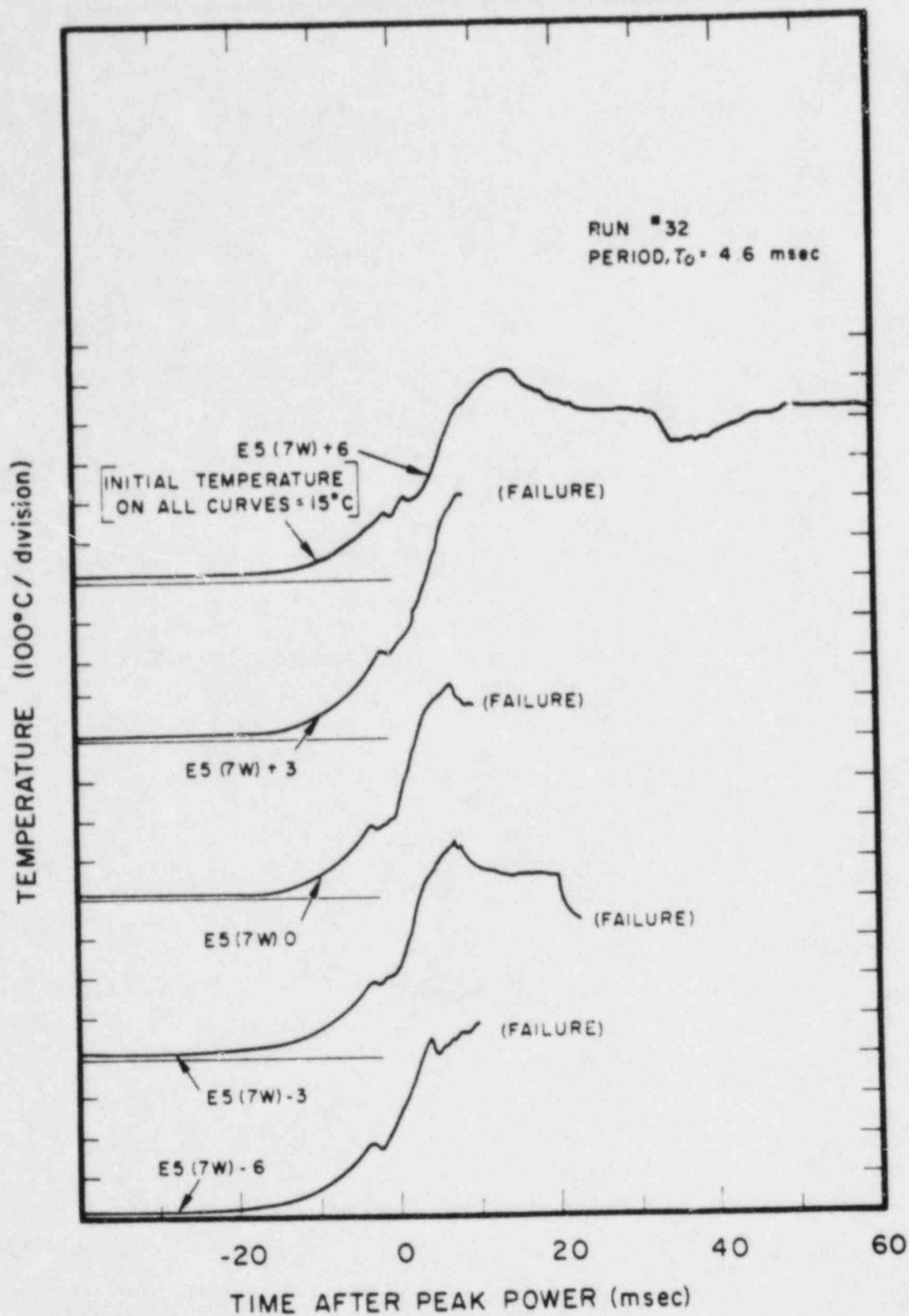


Fig. C-12 Vertical temperature profile measured on the west side of plate #7 in assembly E-5. The measurements were taken at the vertical center ($z = 0$) of the core and six inches and three inches above and below the vertical center by surface mounted thermocouples.

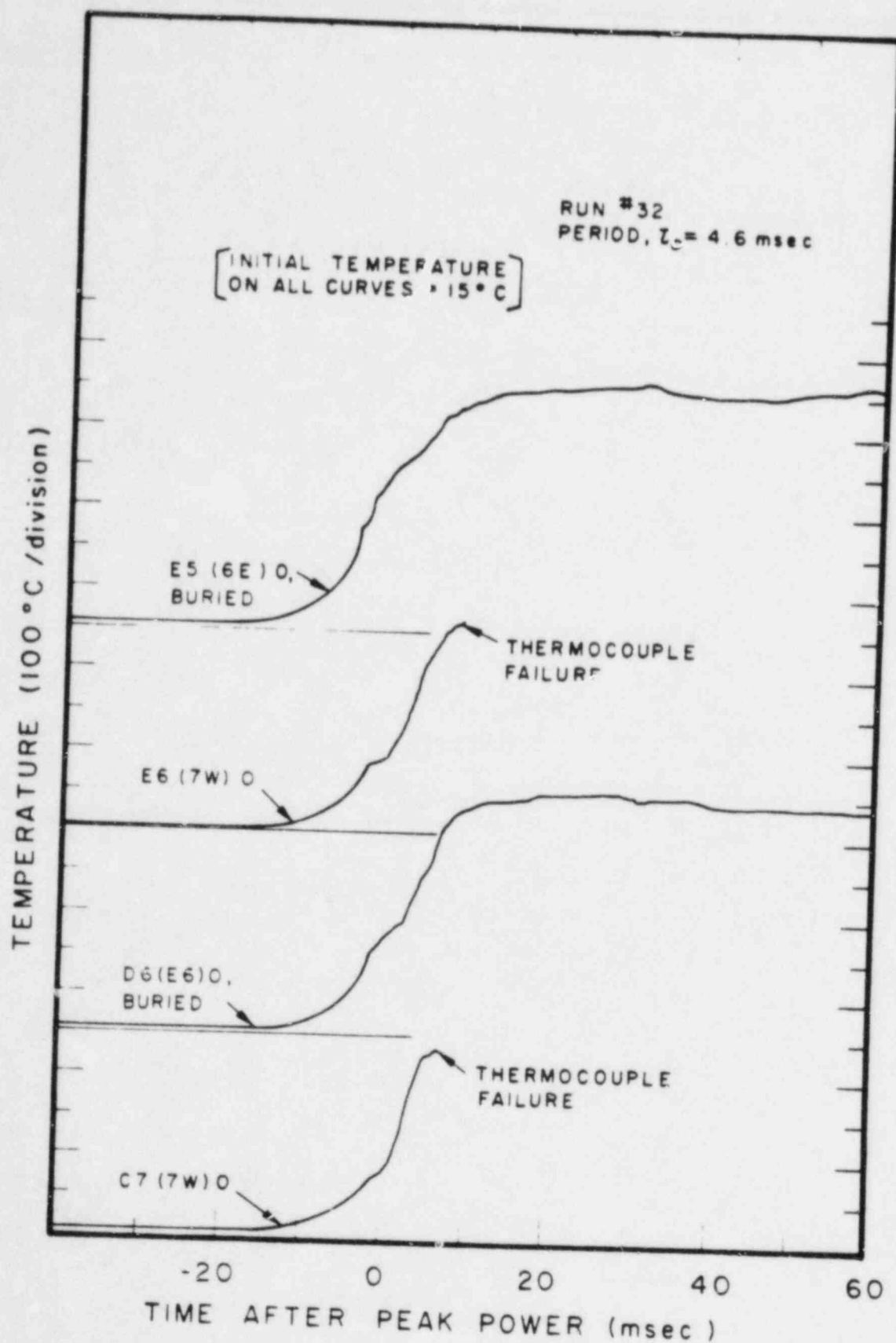


Fig. C-13 Horizontal temperature profile measured in the $z = 0$ plane.

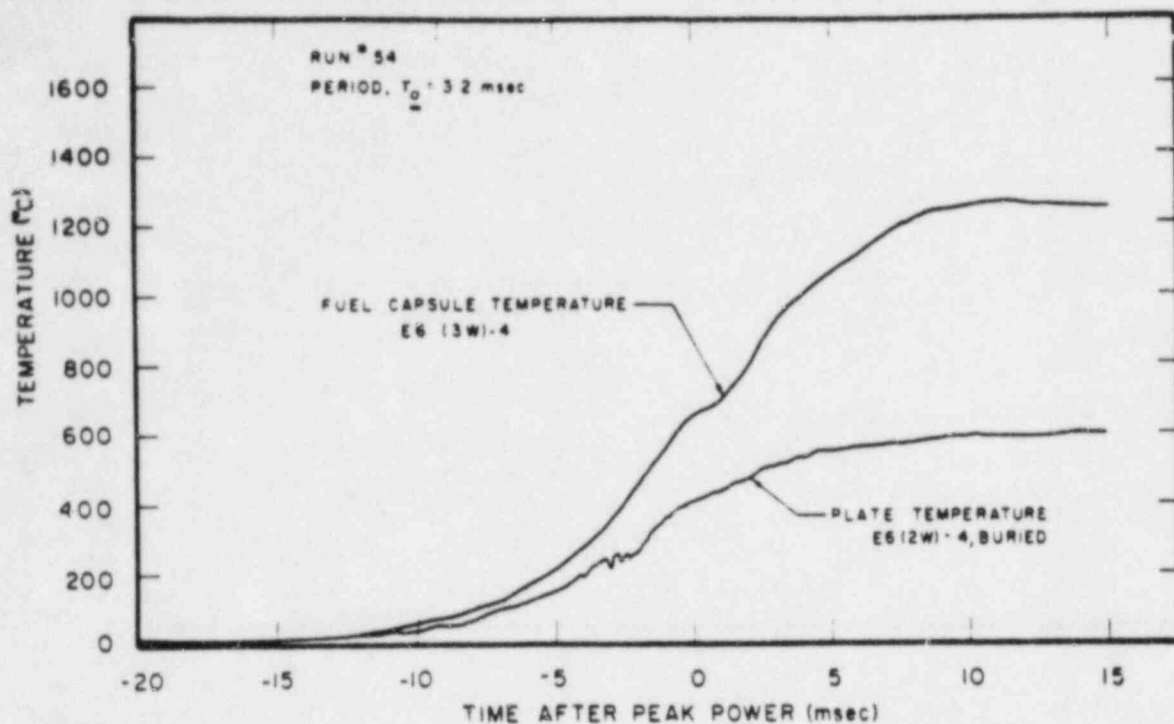


Fig. C-14 A comparison of fuel capsule and fuel plate temperatures during the destructive test.

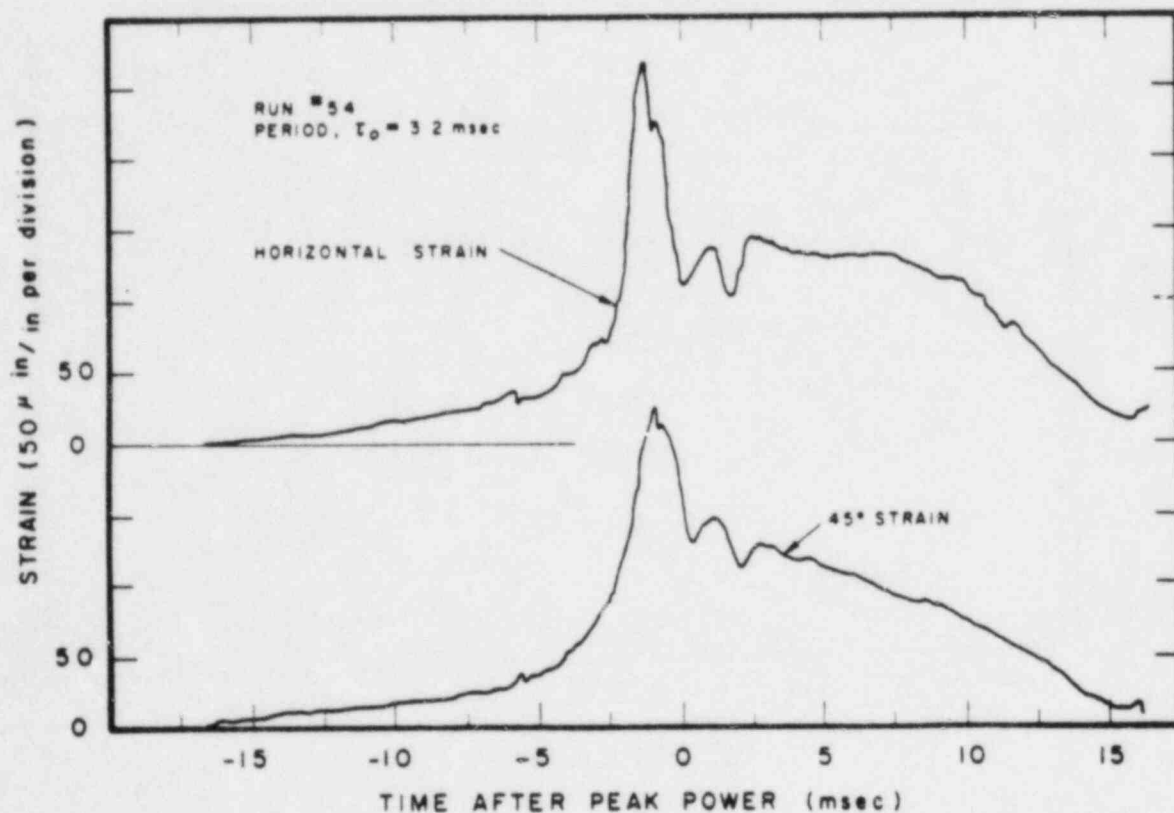


Fig. C-15 The strain response of the horizontal and 45° gauges of a rosette attached to the outside of a peripheral fuel assembly.

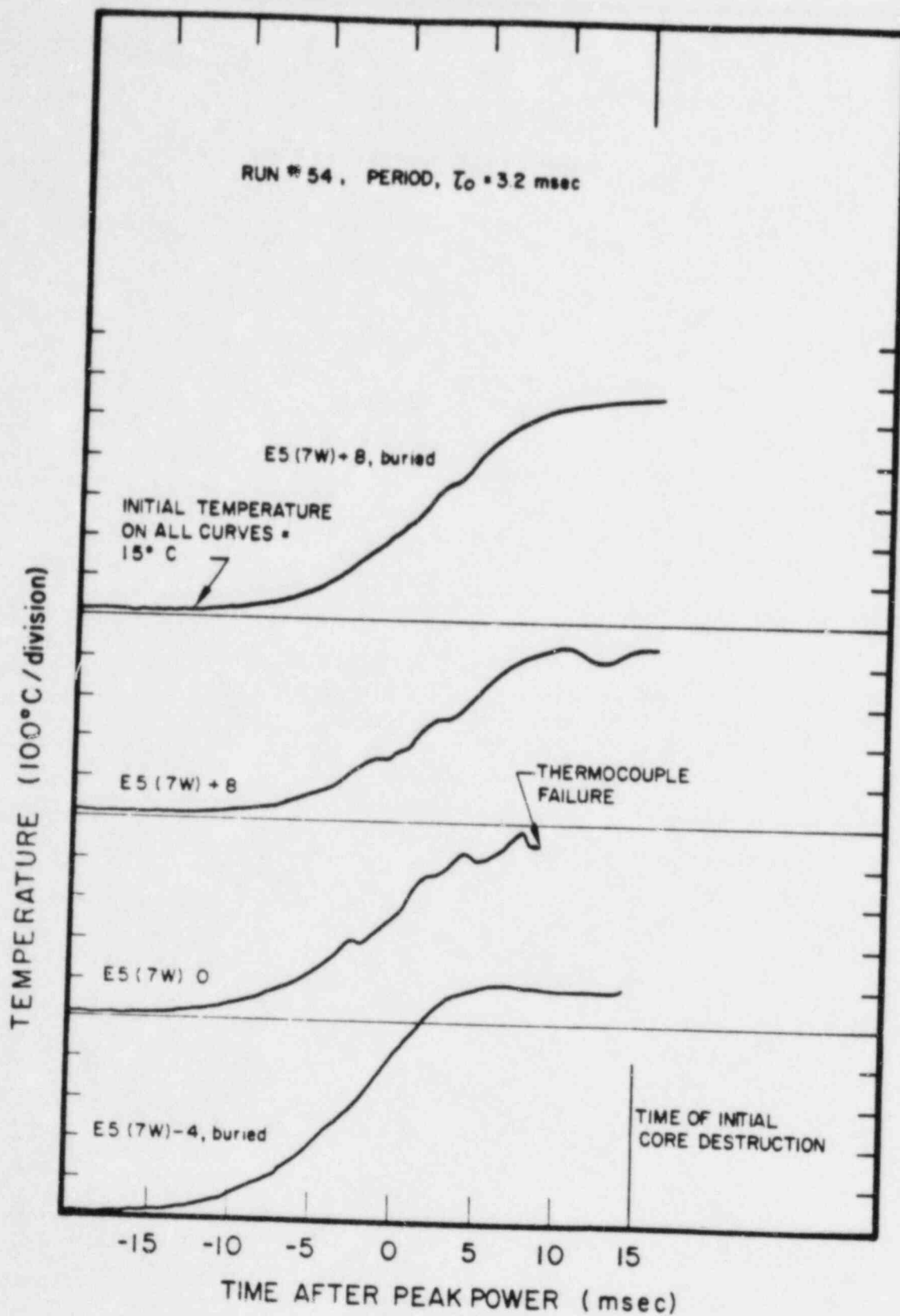


Fig. C-16 Temperatures measured on the west side of the plate #7, assembly E-5, during the destructive test.

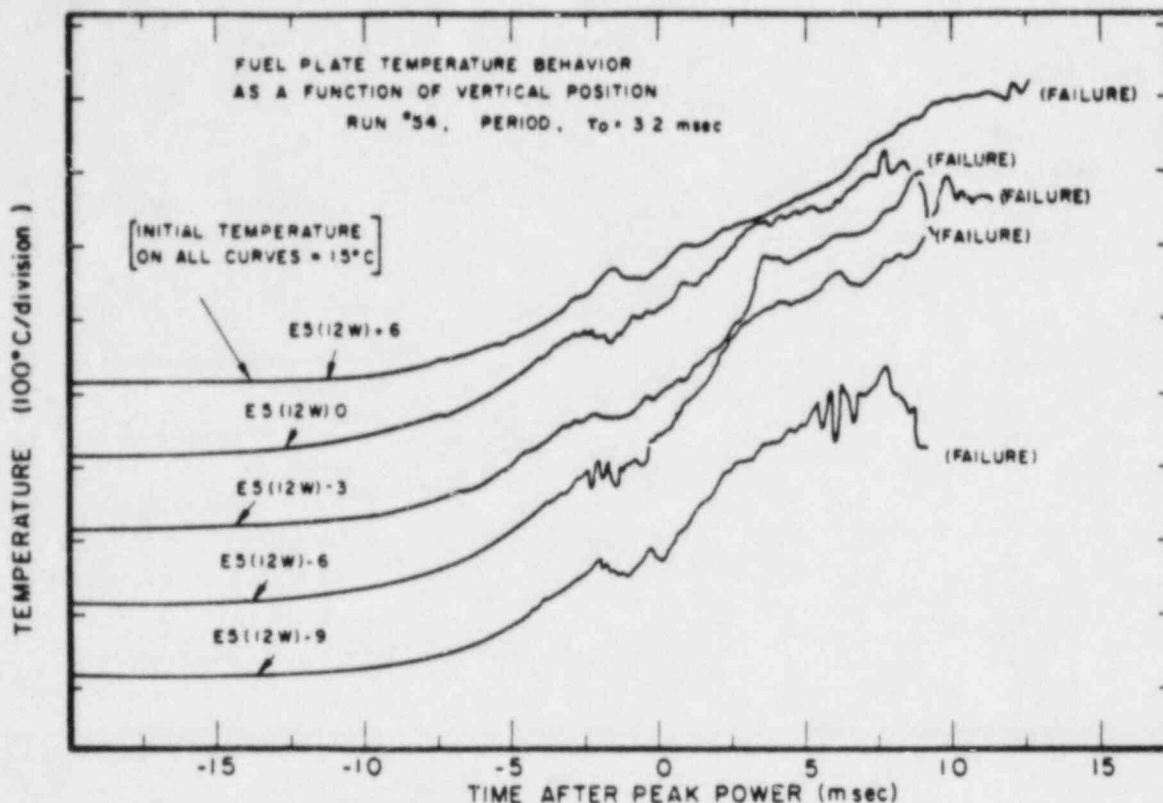


Fig. C-17 Vertical temperature profile as measured by surface-mounted thermocouples attached to the west side of plate #12, assembly E-5, during the destructive test.

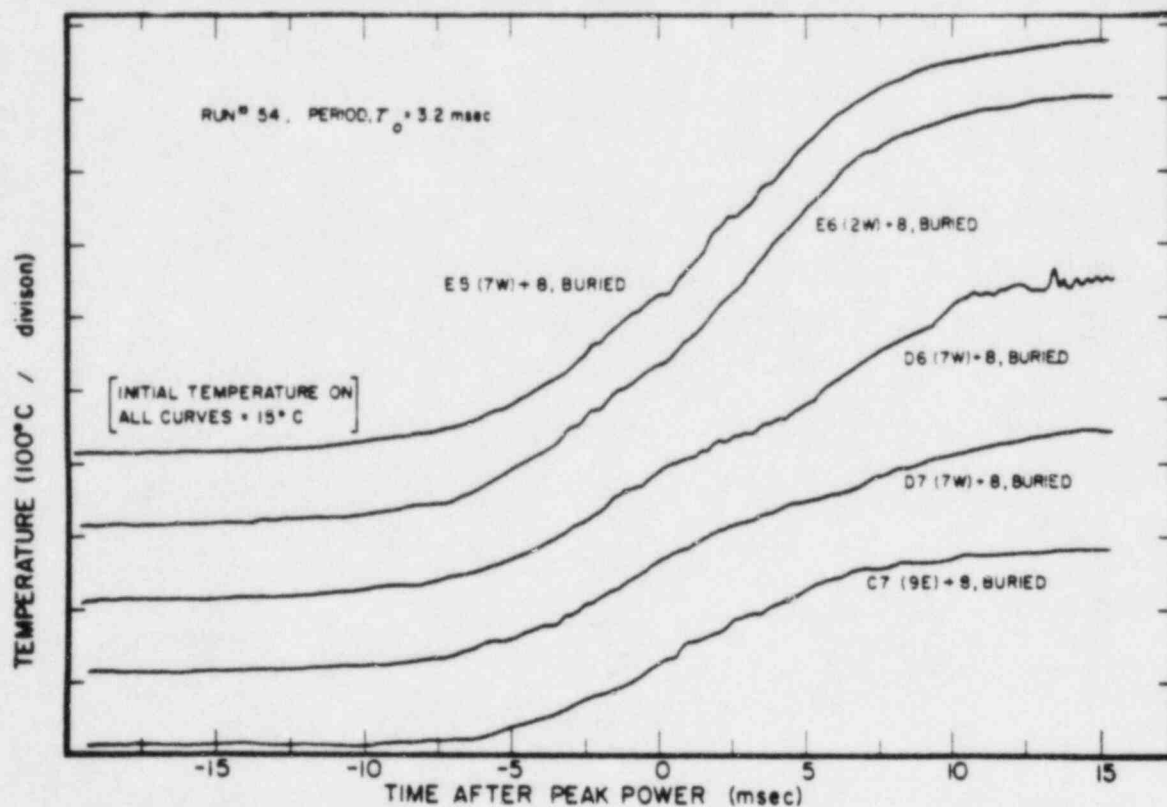


Fig. C-18 Horizontal temperature profile measured in the $z = -8$ plane by buried thermocouples during the destructive test.

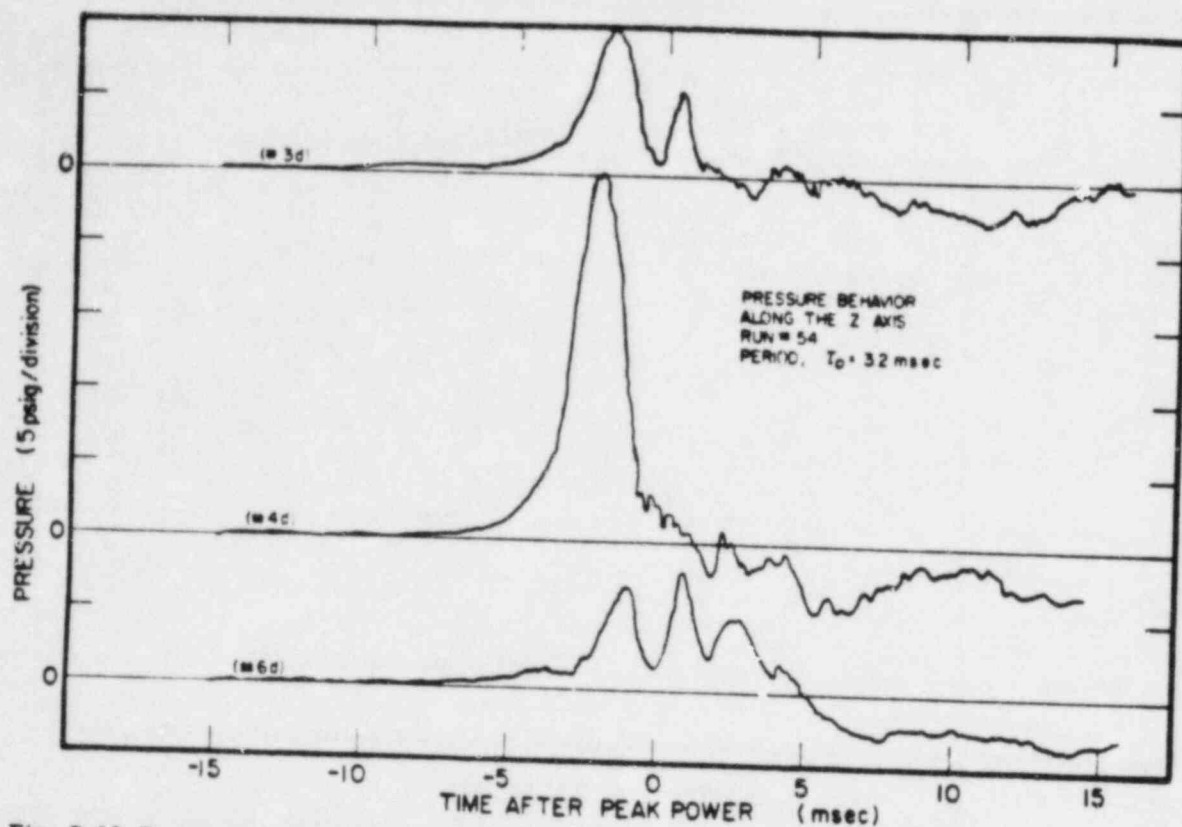


Fig. C-19 Pressure associated with moderator boiling as measured about 2 feet above the core center (#3 d), 20 inches below the core center (#4 d), and 53 inches below the core center (#6 d), during the destructive test.

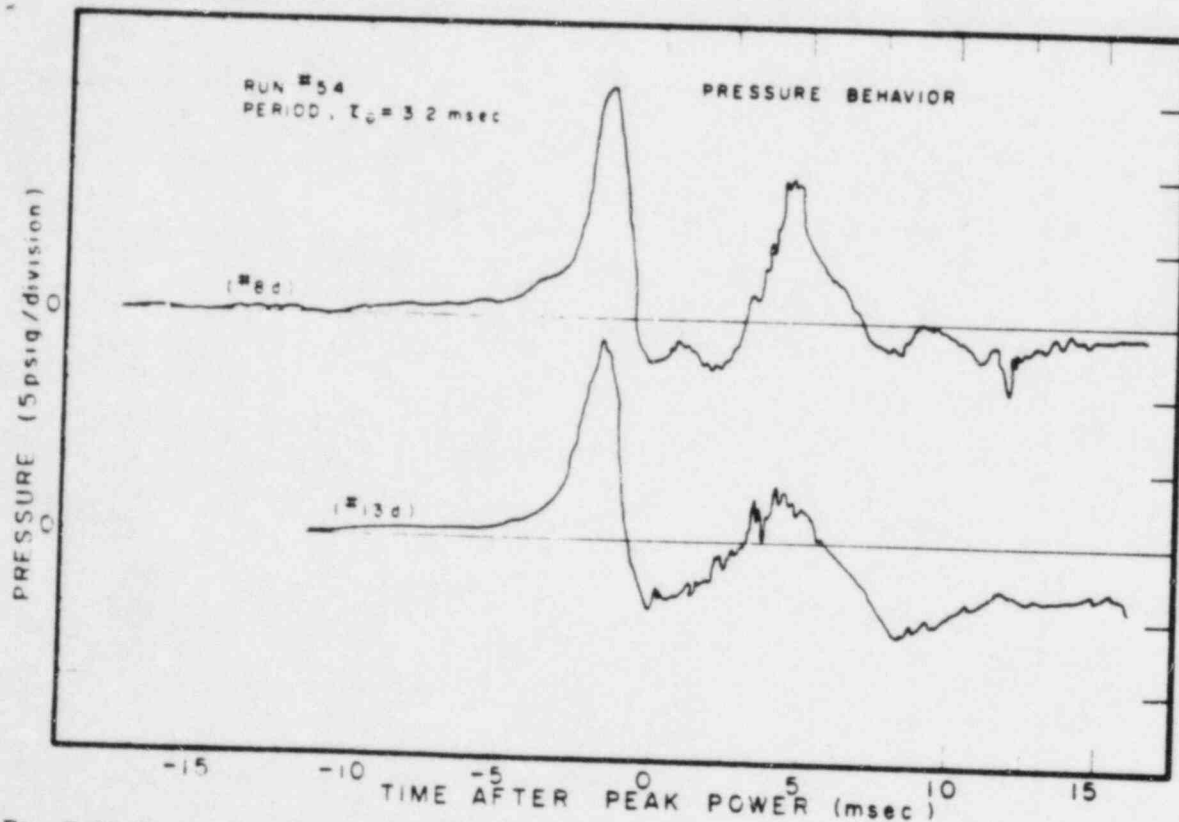


Fig. C-20 Pressure associated with moderator boiling as measured at the side of the core and 17 inches from the core center during the destructive test.

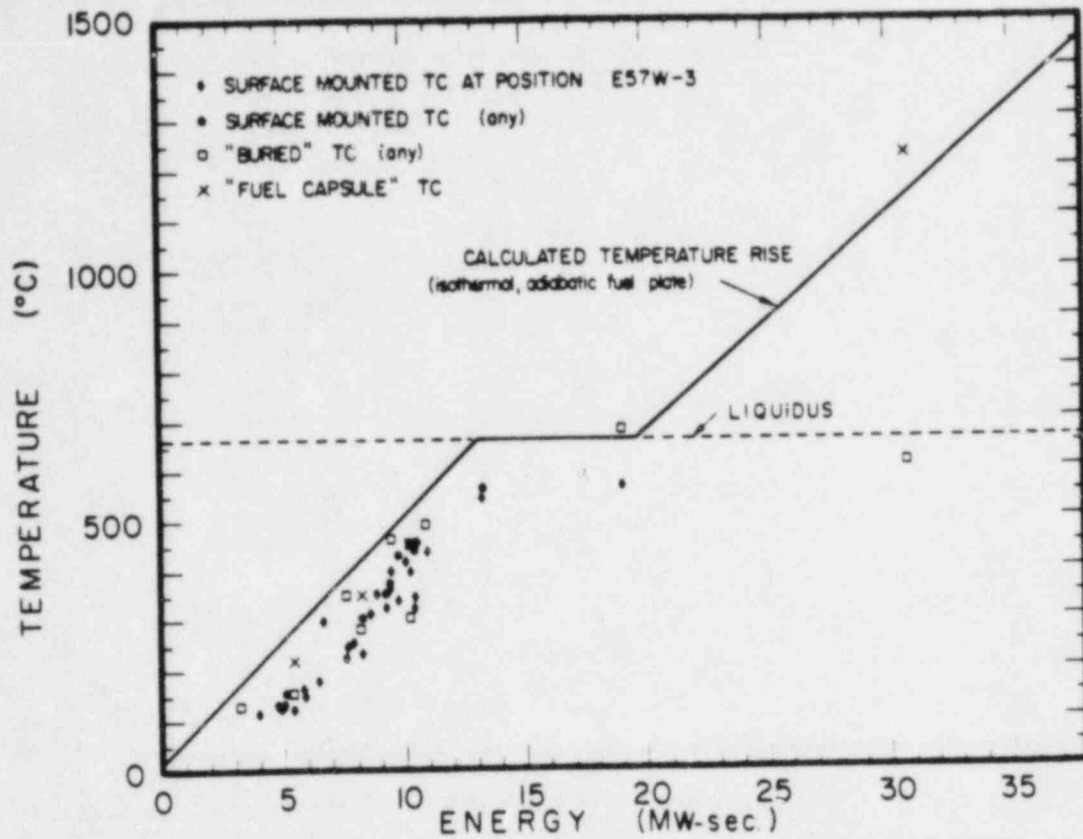


Fig. C-21 Maximum measured temperatures versus total energy release.

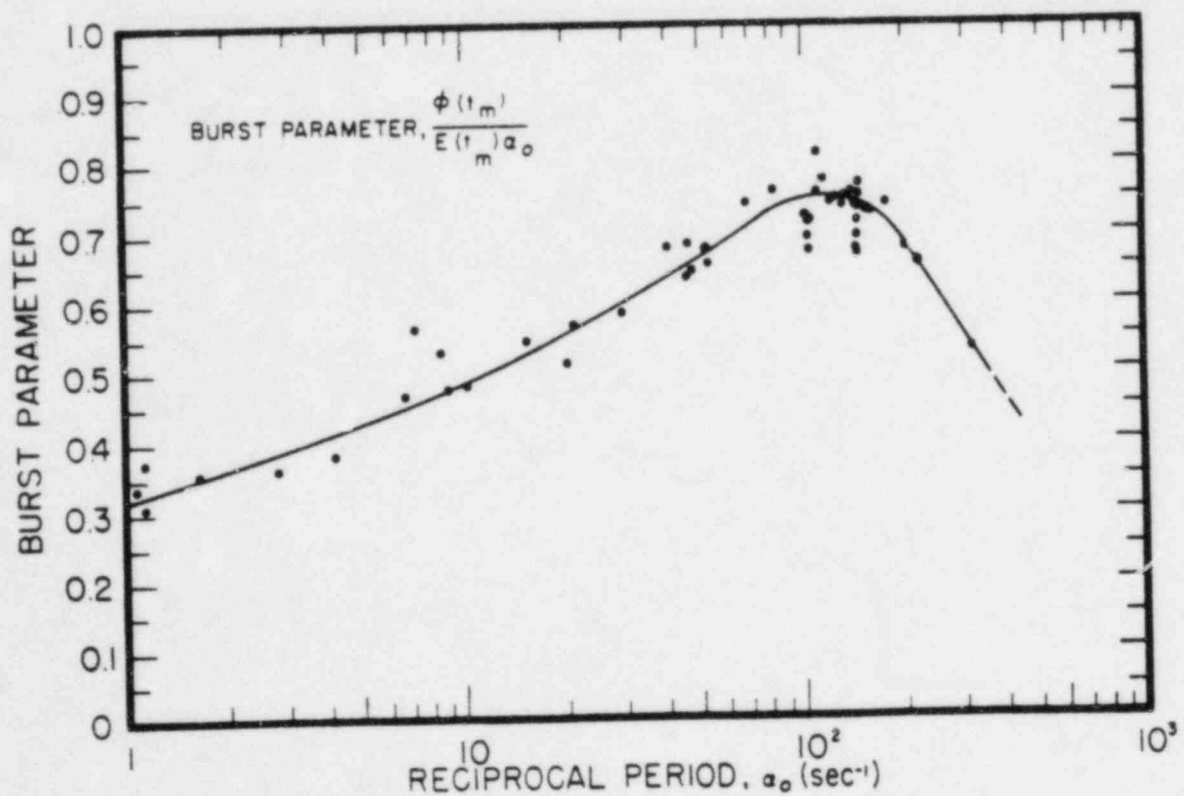


Fig. C-22 Burst parameter versus reciprocal period.

TABLE C-I

DATA SUMMARY - DESTRUCTIVE TEST SERIES

Run No.	T_0 (msec)	Q_0 (sec ⁻¹)	Q_0 (g)	$\theta(t_0)$ (m)	$E(t_0)$ (Mr-sec)	E_T (Mr-sec)	$\theta(t_m)^a$ (°C)	Q_{21}^b (°C)	Date (yycc)
1	930	1.00	0.80	0.67	1.84	(d)			
2	640	1.56	0.85	0.96	1.76	(d)	65(a)	89(a)	April 5
3	355	2.82	0.92	1.50	1.47	(d)	66	95	10
4	163	6.14	0.99	3.25	1.13	(d)	61	98	10
						(d)	60	104	10
5	98	10.2	1.05	6.50	1.34	(d)		105(a)	
6	65	15.4	1.10	14.2	1.66	(d)	73	110	11
						(d)	92	115	11
7	47	21.3	1.16	27.5	2.25		93(a)		
8	34	29.4	1.23	50.0	2.90	3.95	110	117	11
9	25	40.0	1.32	87.0	3.20	4.90	122	124	11
10	19	53	1.42	141	4.05	4.90	130	132	12
11	14.5	65	1.50	210	4.10	5.85	145	150	12
						5.80	156	165	12
12	12.1	83	1.67	290	4.60		164(a)		
13	9.5	108	1.80	380	5.15	6.45	166	180	12
14	9.5	108	1.85	430	5.70	7.55	180	227	12
15	6.8	128	1.99	530	5.85	7.85	186	255	13
16	7.8	139	2.13	630	6.00	8.55	181	315	13
						9.32	181	360	17
17	4.9	145	2.16	690	6.45			375(a)	
18	6.8	147	2.20	685	6.05	10.2	174	400	17
							203(a)		
19	6.4	156	2.27	745	6.60	10.00	186	420	19
							198(a)		
							176	455	19
							198(a)		
22	860	1.14	0.81	0.96	(d)	(d)			May
23	19.3	58	1.42	120	3.40		54(a)	94(a)	10
24	9.0	111	1.90	395	4.70	4.70	125	132	10
25	7.5	133	2.08	555	5.55	7.10	157	300	10
26	6.0	167	2.36	890	7.20	8.80	158	355	11
							185	545	11
27	8.1	124	2.00	505	5.45		210(a)	560(a)	
28	5.0	200	2.63	1130	8.35	9.20	177	325	16
						17.5	320	585	18
29	49.5	20.2	1.13	19.1	1.84				June
30	7.6	132	2.03	510	5.20	3.20	125(u)	129(b)	6
						9.40	172	400	6
31	6.9	145	2.14	620	6.40		250(u)	465(u)	
32	4.8	218	2.78	1270	8.90	10.9	190	440	8
							290(b)	490(u)	
						19.0	240	570	11
							420(u)	680(u)	
33	300	1.14	0.81	0.76	1.79	(d)			July
34	11.6	84.8	1.03	4.50	1.00	(d)	64(b)	94(b)	23
						(d)	59	102	24
35	21.7	46.1	1.37	107	3.40		67(b)	109(b)	
36	8.9	112	1.91	460	5.05	5.05	125	126	24
							149(b)	155(b)	
37	860	1.14	0.81	0.78	2.21	(d)	151	242	26
38	11.2	8.93	1.03	5.05	1.18	(d)	230(b)	350(b)	
						(d)	69(b)	87(b)	26
39	22.4	45.8	1.35	105	3.60		63	99	26
							68(b)	117(b)	
40	8.7	115	1.93	470	5.25	5.40	120	124	27
							146(b)	154(b)	
41	6.8	147	2.20	635	5.75	8.20	167	234	27
42	6.9	145	2.18	640	6.00	9.20	216(b)	305(b)	
						9.70	232(b)	355(b)	30
							156	340	31
							246(b)	430(b)	
43	6.9	145	2.18	660	6.35	10.4	160	340	August 1
44	6.9	145	2.18	665	6.60	10.4	243(b)	440(b)	
							161	325	2
							250(b)	440(b)	
45	13.0	0.76	0.75	0.39	1.49	(d)			October-
46	4.3	4.12	0.95	1.43	0.91	(d)	65(b)	80(b)	18
47	4.0	7.14	1.02	3.80	0.94	(d)	61(a)	93(a)	19
48	2.11	47.4	1.38	110	3.60	(d)	62(a)	112(a)	22
						5.40	148(b)	153(b)	22
50	9.6	104	1.85	350	5.00			220(c)	
51	7.0	143	2.16	620	6.45	7.15	195(b)	232(b)	24
								350(c)	
52	9.6	104	1.85	380	5.10	7.25	223(b)	305(b)	24
								455(c)	
53	9.7	103	1.84	360	5.05	7.45	208(b)	229(b)	24
								360(c)	
							204(b)	234(b)	24
								350(c)	
54	3.2	313	3.55	2250	13.8	30.7	430(b)	615(b)	November 5
								1230(c)	

* Surface temperature measured at E5 (TW)-3.

(a) Highest surface temperature measured at a position other than E5 (TW)-3.

(b) Temperature measured using "buried" thermocouple (see Appendix B).

(c) Maximum temperature measured using special "fuel cell" thermocouple.

(d) Total energy undefined due to absence at long periods of a distinct power cutoff.

APPENDIX D

MELTDOWN DATA

APPENDIX D

MELTDOWN DATA

Melting of fuel plates occurred for three of the power excursion tests conducted in the exploratory and destructive test series, with periods respectively of 5.0, 4.6, and 3.2 msec.

In the 5-msec period excursion test, melting occurred in seven fuel plates over a region about six inches high in the center of the core and involved about 0.5 percent of the total fuel plate area of the core. Photographs of several of the damaged fuel plates from this test have been shown previously in Figures 16 through 22. Figure D-1 is a cross section drawing of the Spert I core showing the radial distribution of the melted regions for this test. Figure D-2 shows the vertical distribution of the melted regions of the plates.

In the 4.6-msec period test, melting was obtained in 52 of the 270 fuel plates of the core, involving about two percent of the total fuel plate surface area of the core. Photographs of melted fuel plates from this test were shown previously in Figures 23 through 28. Figure D-3 is a cross section drawing of the Spert I core showing the radial distribution of the melted regions for this test. Figure D-4 shows the vertical melt pattern for each of the assemblies in which melting occurred.

In the 3.2-msec period destructive test, all of the 270 fuel plates in the core experienced melting to some degree. Figure 39 shows the top portions of typical fuel plates recovered from the reactor vessel. The unfueled edges of the plates can be seen still attached to the upper portions of the plates. The vertical pattern of fuel plate meltdown for the destructive test is shown in Figure D-5 for those recovered portions of the fuel plate which could be identified. The remaining pieces of fuel plates which were recovered, but which could not be identified as to position in the core, represent about 19 weight percent of the recovered plates. In Figure D-5 the vertical melt pattern is shown for each fuel plate of each assembly with the assemblies arranged in the appropriate positions of a horizontal cross section drawing of the core. The melt pattern was symmetrical about the central fuel assembly, which showed the largest amount of melting (approximately 78 weight percent). The damaged fuel assembly from core position G6 is shown in Figure 38. This assembly was recovered relatively intact and was cut open for disassembly before the photograph was taken. It can be seen that much of the melted region of the plates is missing but that most of the unmelted upper and lower ends of the plates are still connected by the unfueled edges.

The fuel plates of two of the corner assemblies (C3 and G7) remained in place even though the central portion of the plates was sometimes melted. The fuel plates from one of these two corner assemblies is shown in Figure E-1. The central portions of the plates were observed to crumble and flake easily.

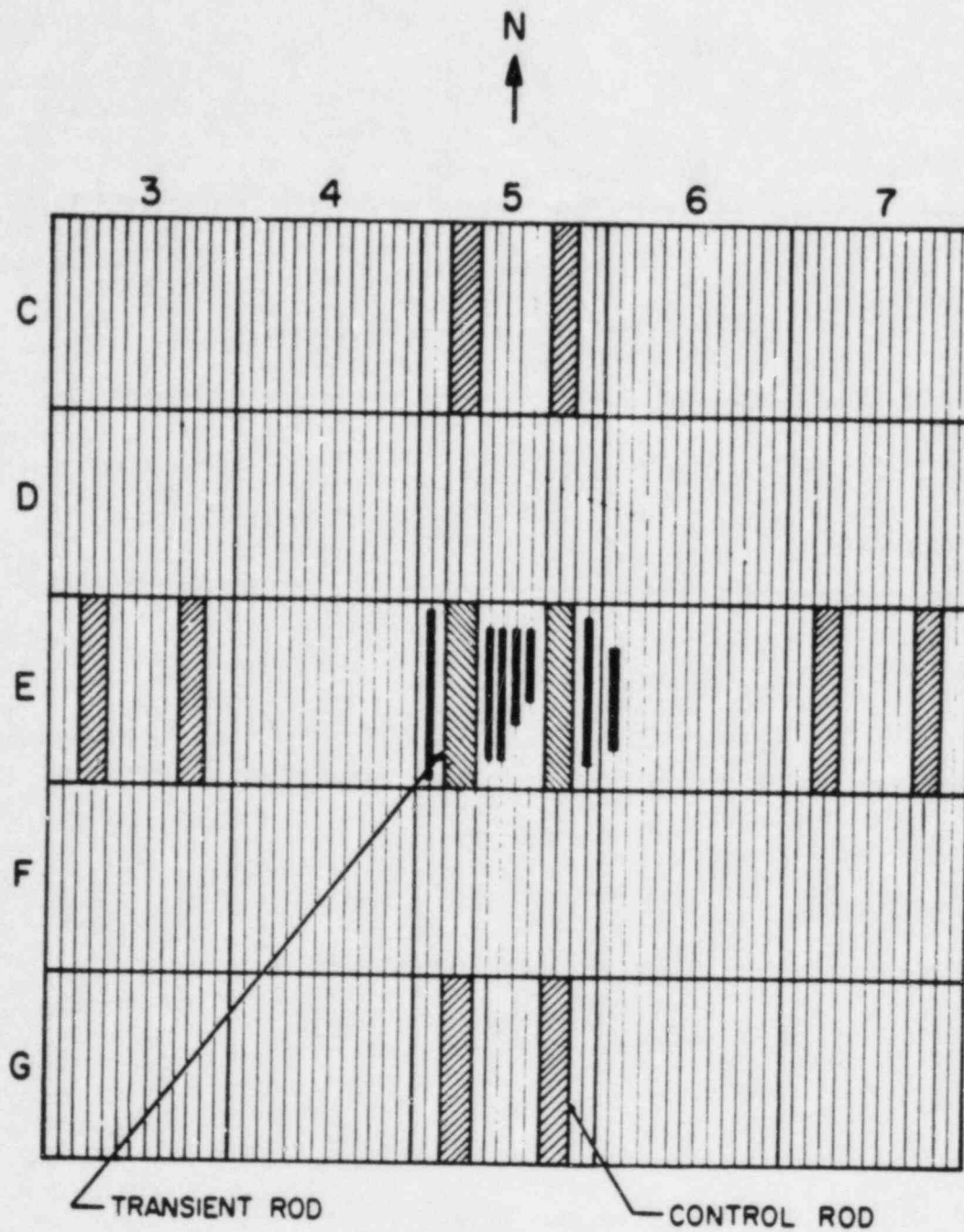


Fig. D-1 Cross section drawing of the core showing distribution of melted regions on fuel plates after 5.0-msec test.

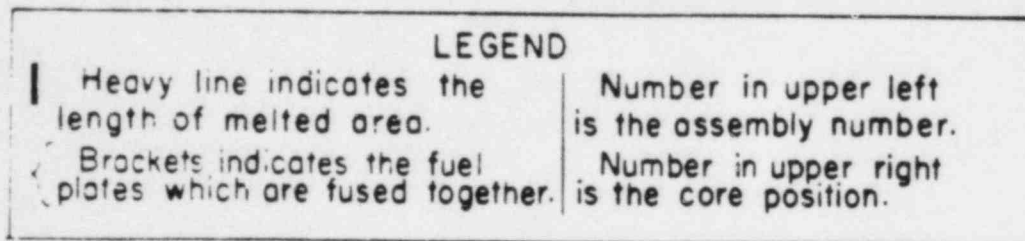
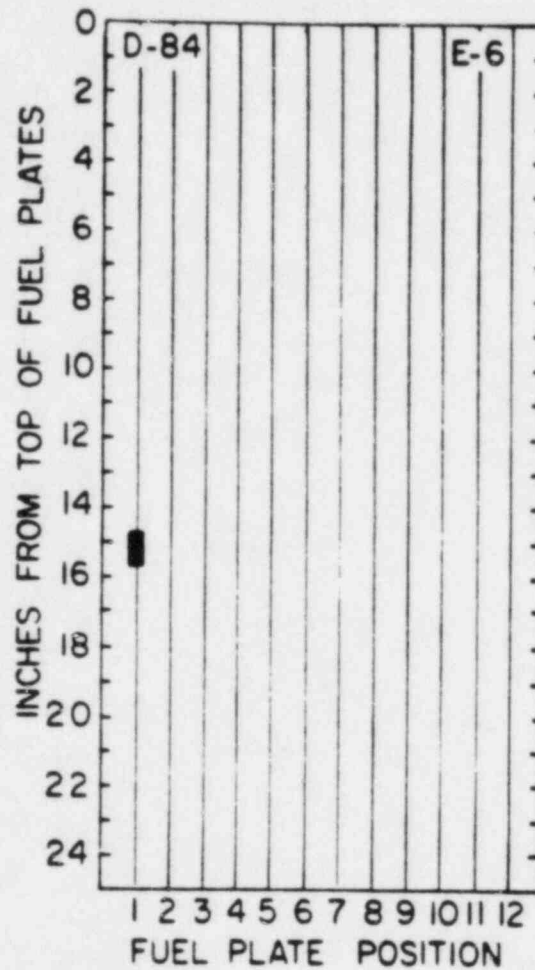
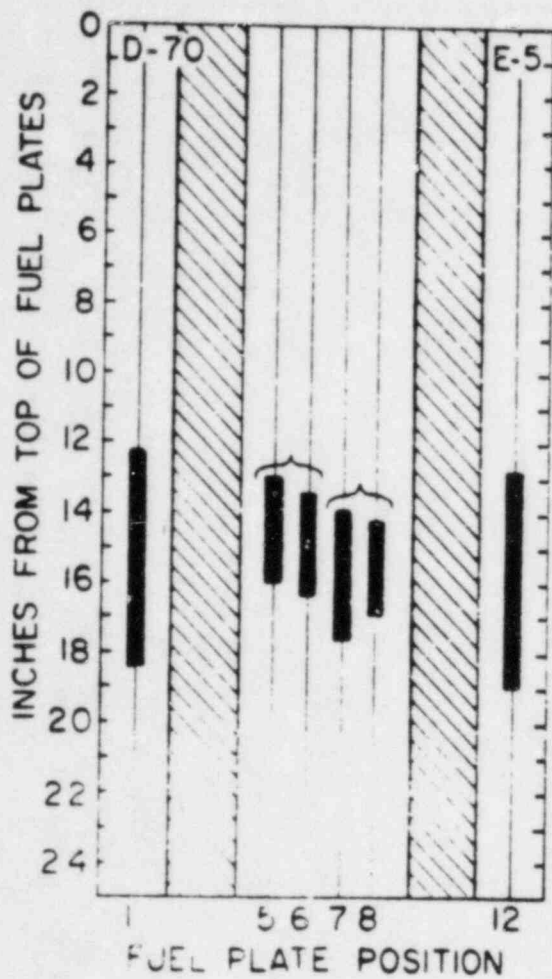


Fig. 1- Vertical drawing of assemblies showing melted regions on fuel plates after 5.0-msec test.

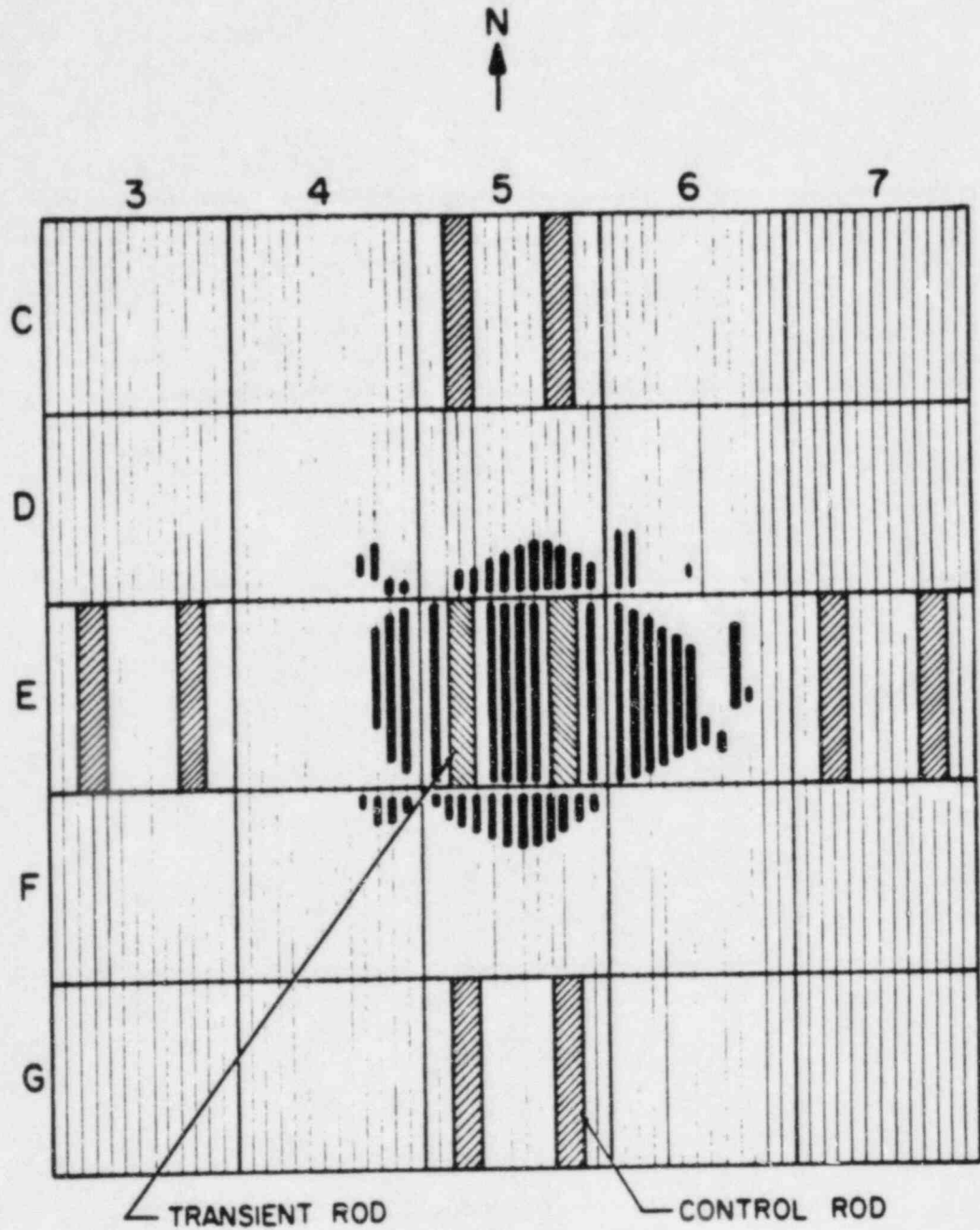


Fig. D-3 Cross section drawing of the core showing distribution of melted regions on fuel plates after 4.6-msec test.

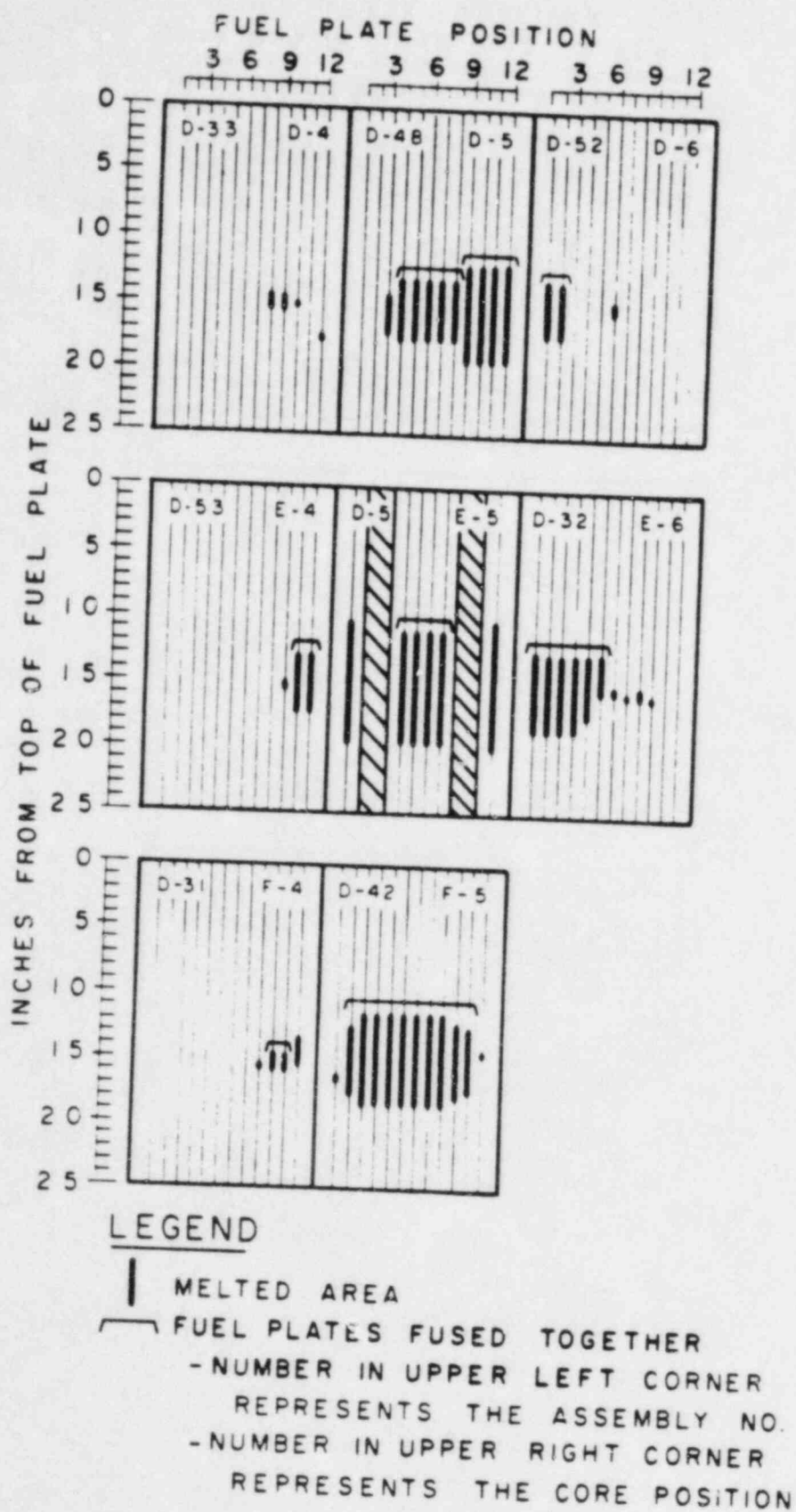


Fig. D-4 Vertical drawing of assemblies showing melted regions on fuel plates after 4.6-msec test.

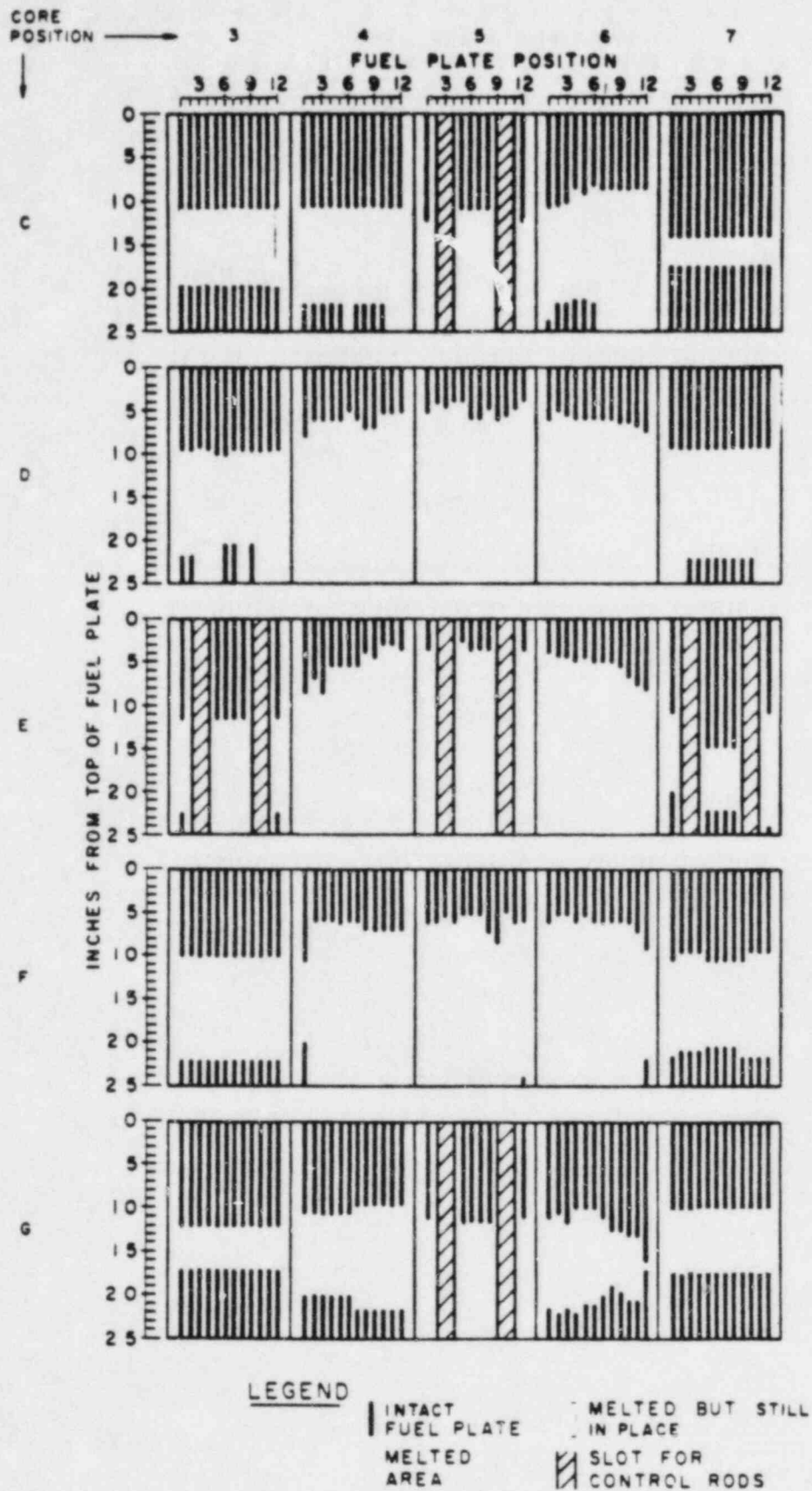


Fig. D-5 Vertical drawing of assemblies showing melted and disassembled regions of fuel plates after destructive test.

APPENDIX E

SUPPLEMENTARY PHOTOGRAPHS OF DESTRUCTIVE TEST RESULTS

APPENDIX E

SUPPLEMENTARY PHOTOGRAPHS OF DESTRUCTIVE TEST RESULTS

To further illustrate items which may be of interest, Figures E-1 through E-12 are included here as a supplement to Figures 30 through 44.

Figures E-13 through E-28 are selected frames from a motion picture taken of the destructive test by camera No. 6 (Table B-III). The camera was operating at about 24 frames per second and was located approximately 100 yards from the reactor building. The approximate time in milliseconds after peak power is indicated for each picture. The pictures shown are not necessarily successive frames.

Figures E-29 through E-44 are selected frames from a motion picture taken from the rear of the reactor building. The pictures shown are not necessarily successive frames. The camera was operating at approximately 600 frames per second, and the time after peak power is indicated for each picture.

The first motion observed in the motion picture is that of the floor as it is depressed around the lip of the vessel. (This motion is quite easily observed in motion projection but is difficult to see in individual pictures and, therefore, has not been included here.) Immediately following this, both periscopes (the large black tubes extending out of the vessel at the left and at the center) are observed to suddenly rise out of the vessel between $t = 57$ and $t = 70$ msec. Water finally emerges above floor level at about $t = 70$ msec.

Figures E-45 through E-60 are selected frames from a motion picture taken of the destructive test by camera No. 5 which was located approximately 50 feet southeast of the reactor building.



Fig. E-1 Fuel plates recovered from position C3 -- one of the two corners of the core in which the melted portions of the plates were relatively undisturbed. A cobalt wire used for integrated flux measurements is seen at the top.



Fig. E-2 Assembly from position C4.



Fig. E-3 Control rod bearing assembly from position E7. Upper part of control blades has been broken away. Lower blade extensions can be seen emerging from the bottom of the assembly.



Fig. E-4 Control rod bearing assemblies from core positions G5 (left) and E3 (right).



Fig. E-5 Control rod bearing assembly from position E7 after being opened for inspection. About half of the four fuel plates contained between the blades was melted and fragmented. The debris is typical of the material (in excess of 20 kilograms) collected.



Fig. E-6 Assembly from position G4 showing damage typical for internal assemblies.



Fig. E-7 Control rod bearing assembly from position C5.



Fig. E-8 Upper (nonpoison) section of transient rod blades as recovered from the reactor vessel. The fuel assembly bearing this rod (position E5) was completely torn apart. The bottom (poison) section of one blade was broken away. The condition of this rod indicates that large magnitude pressures were created within the four fuel plates which are normally located between the two blades.

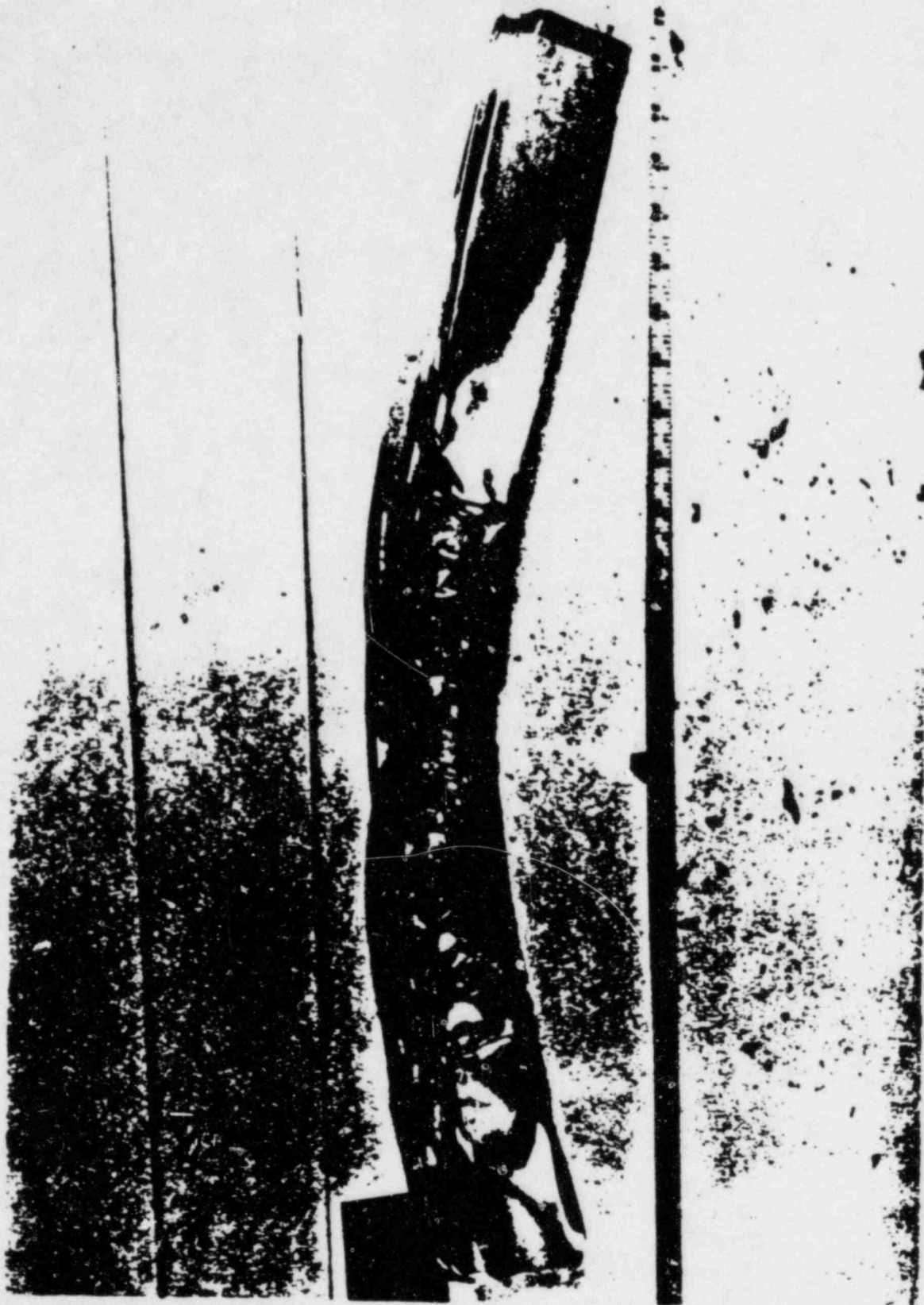


Fig. E-9 Several fuel plates from position G6 showing a stage in the progression from warping to melting and fusion of the plates. Wrinkles of soft but unmelted fuel plates at the extremities of the melted region probably blocked the channels and prevented pressure relief in the vertical direction of the core.

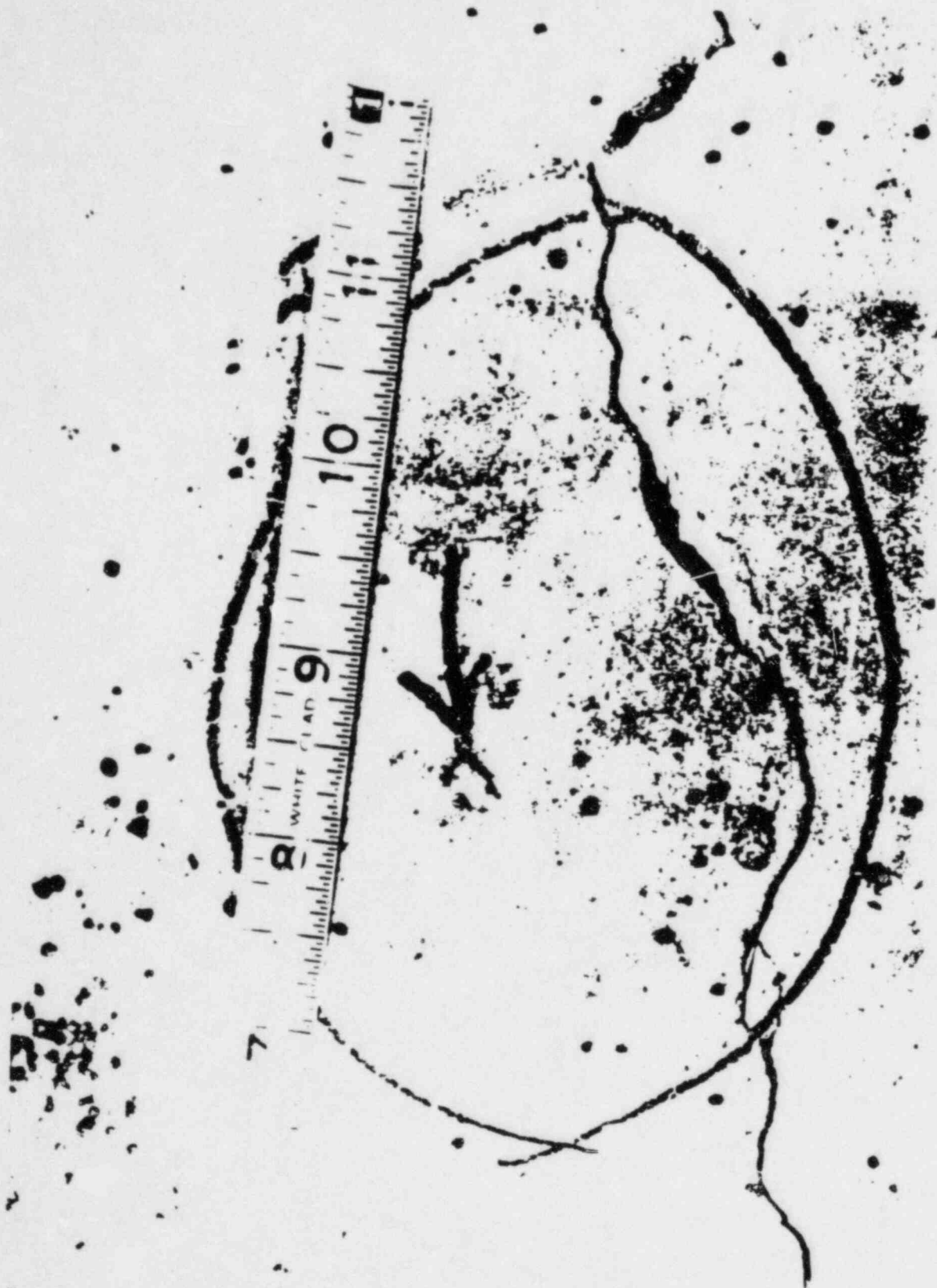


Fig. E-10 A fracture in the concrete floor which circumscribed the reactor vessel. In motion pictures, the lip of the vessel was observed to depress downward one or two inches and then to spring back up giving rise to this circumferential fracture. Arrow points to one of a few core fragments ejected from the vessel.



Fig. E-11 Section of an air filled tube located in the core during the destructive test. Pressure caused the tube to collapse as shown. It was estimated that over 3600 psi was required to cause this collapse.



Fig. E-12 Objective lens of periscope. This lens was located at the vessel wall directly opposite the core (about 3-1/2 feet horizontally from core). Motion pictures taken at about 600 fps through this periscope revealed no apparent motion of the core prior to lens failure.

FLASH
BULB

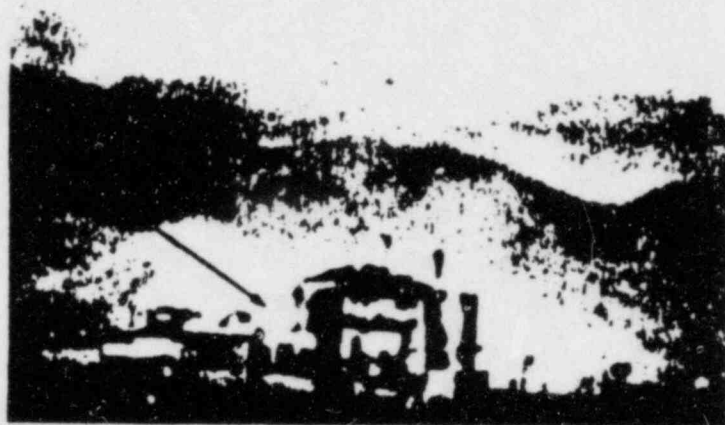


Fig. E-13 $t = -143$ msec. Flash bulb indicates transient rod release.

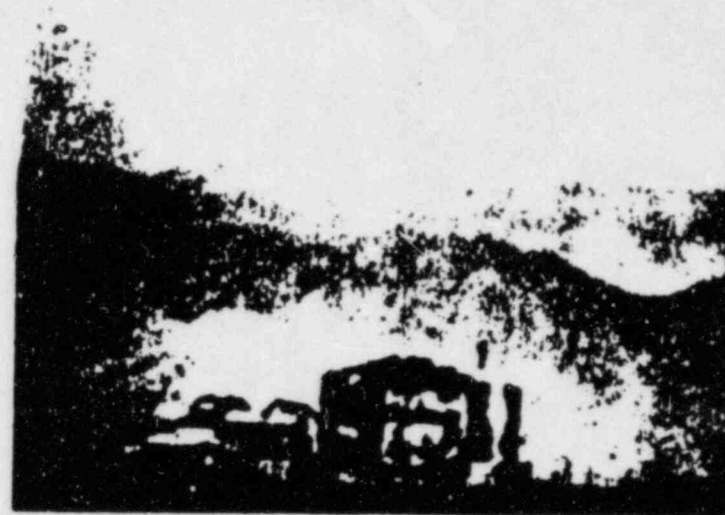


Fig. E-14 $t = 87$ msec.



Fig. E-15 $t = 130$ msec.

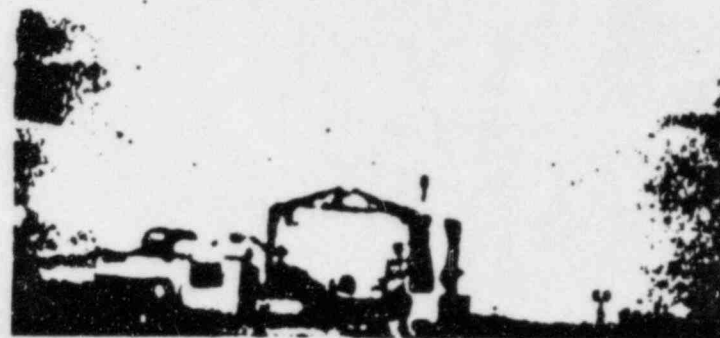


Fig. E-16 $t = 220$ msec.



Fig. E-17 $t = 360$ msec.



Fig. E-18 $t = 620$ msec.



Fig. E-19 $t = 900$ msec.



Fig. E-20 $t = 1030$ msec.



Fig. E-21 $t = 1300$ msec.



Fig. E-22 $t = 1620$ msec.



Fig. E-23 $t = 2160$ msec.



Fig. E-24 $t = 2630$ msec.

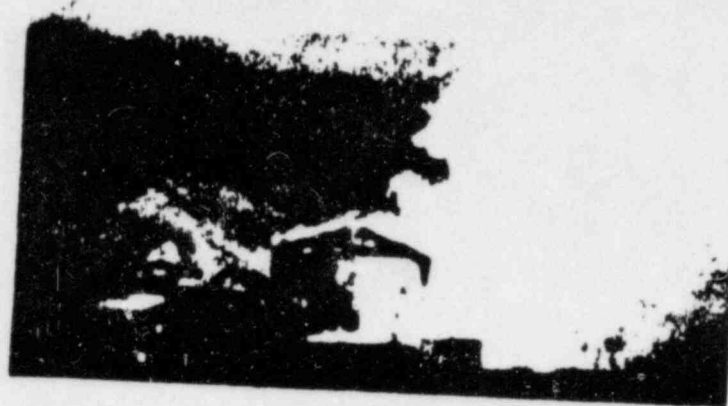


Fig. E-25 $t = 3280$ msec.

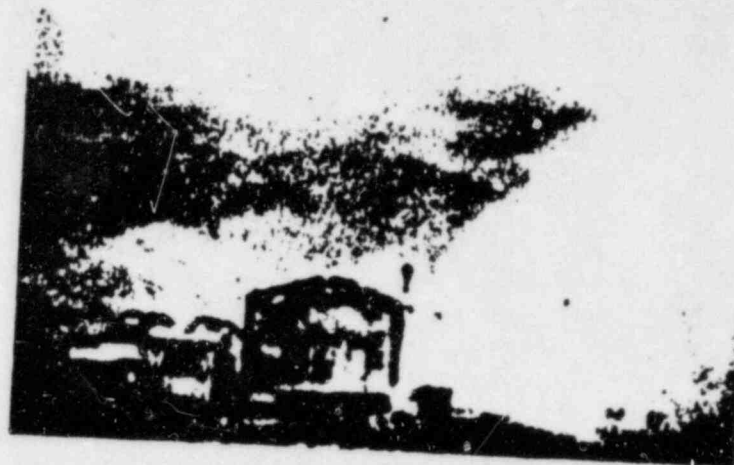


Fig. E-26 $t = 3820$ msec.

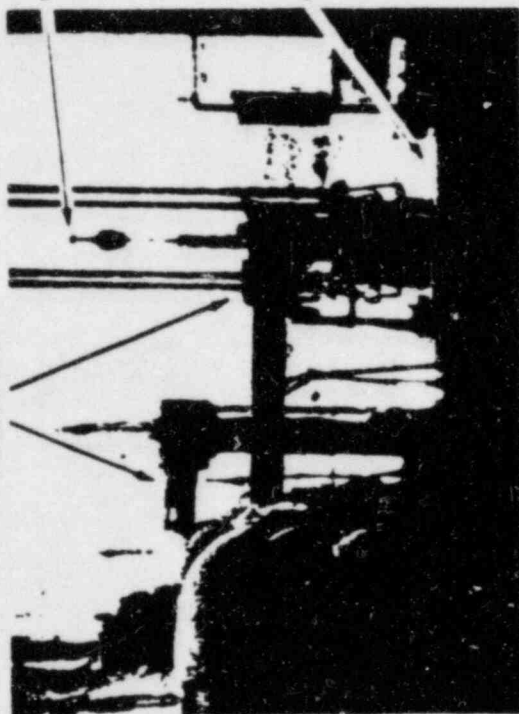


Fig. E-27 $t = 4400$ msec.



Fig. E-28 $t = 5300$ msec.

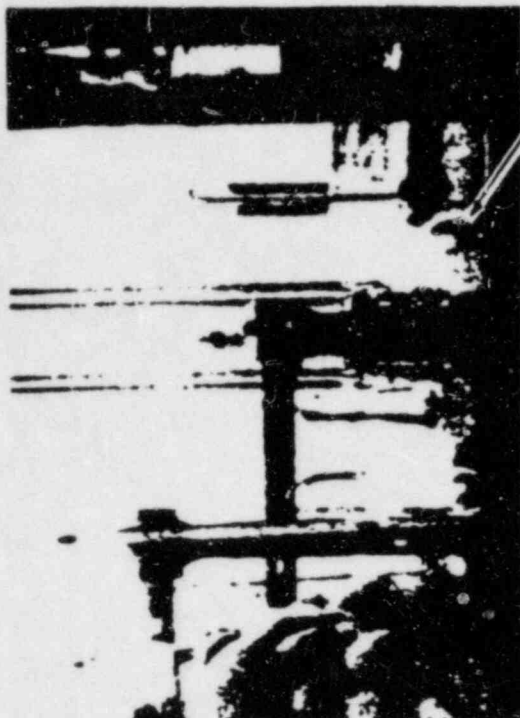
PERISCOPES



TRANSIENT
ROD

TIP OF
HEATING
ELEMENT

Fig. E-29 $t = -73$ msec.



THE SOUND TRANSDUCER
MOUNTING BRACKET

Fig. E-30 $t = 57$ msec.

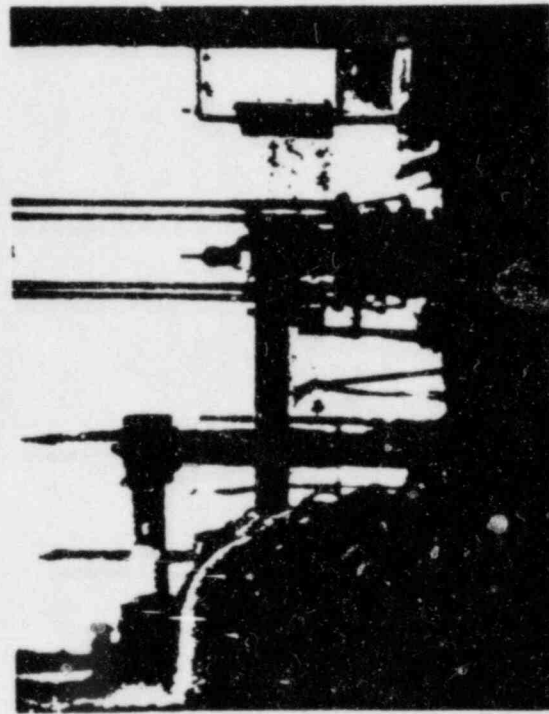


Fig. E-31 $t = 65$ msec.

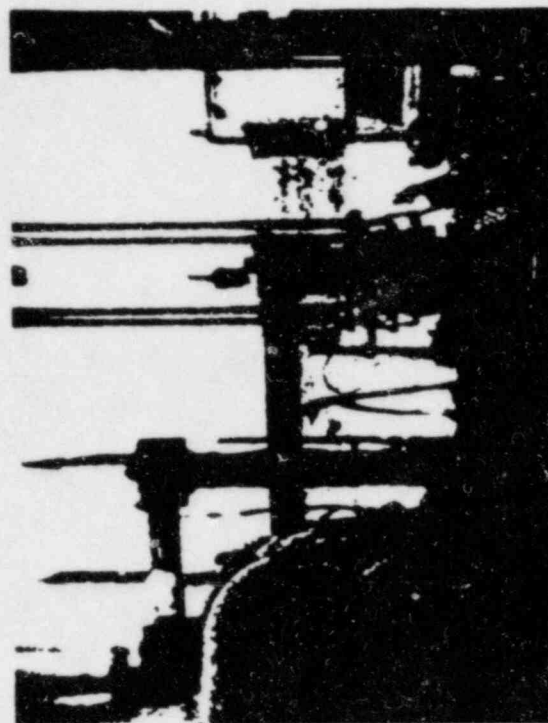


Fig. E-32 $t = 70$ msec.

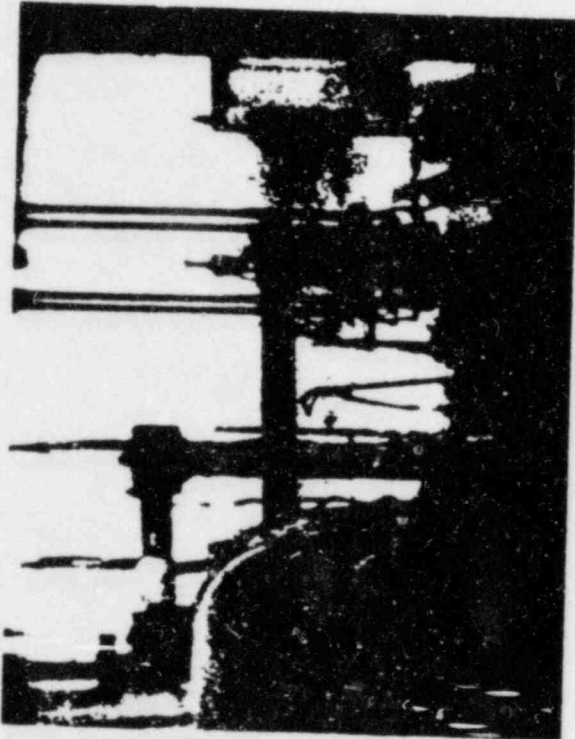


Fig. E-33 $t = 72$ msec.

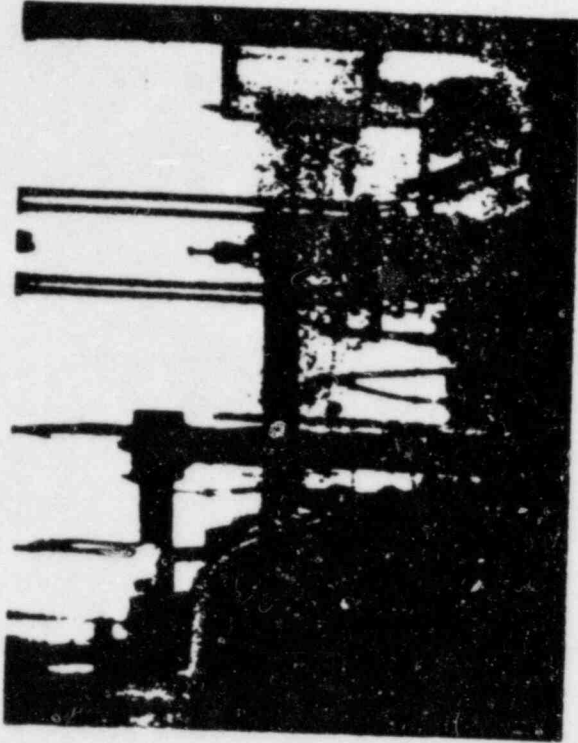


Fig. E-34 $t = 74$ msec.



Fig. E-35 $t = 79$ msec.

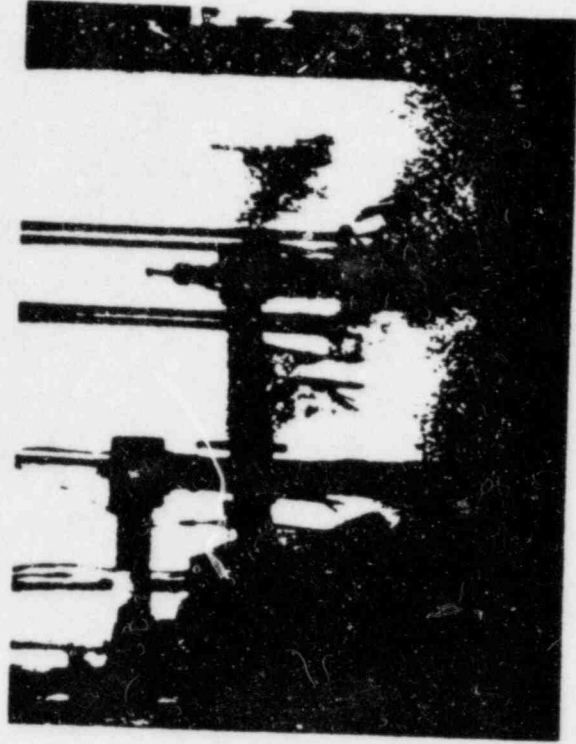


Fig. E-36 $t = 85$ msec.

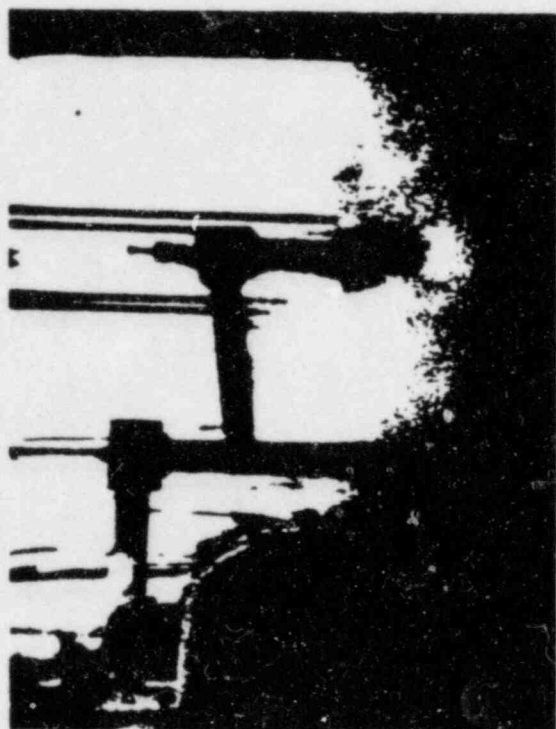


Fig. E-37 $t = 94$ msec.



Fig. E-38 $t = 97$ msec.



Fig. E-39 $t = 105$ msec.



Fig. E-40 $t = 114$ msec.



Fig. E-42 $t = 135 \text{ msec.}$

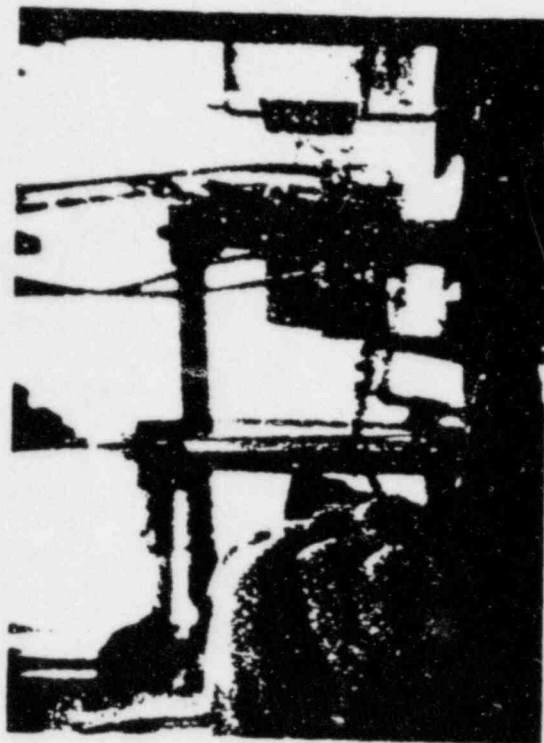


Fig. E-44 $t \approx 4 \text{ sec.}$



Fig. E-41 $t = 124 \text{ msec.}$



Fig. E-43 $t = 155 \text{ msec.}$

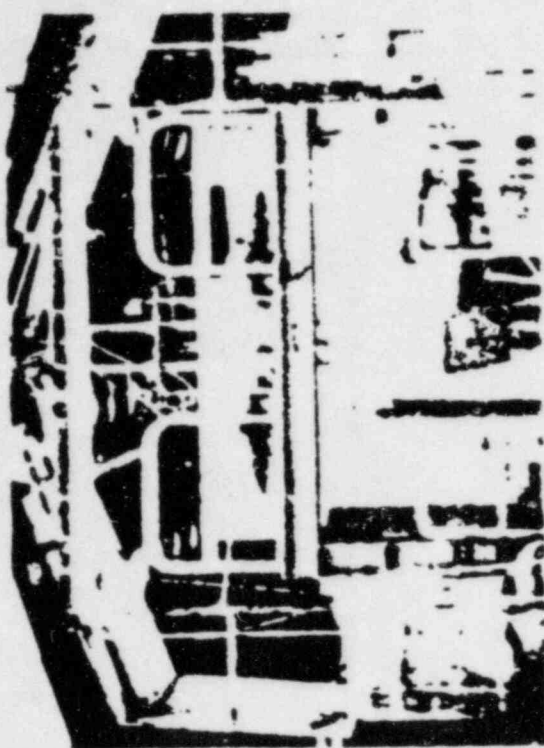


Fig. E-46 $t = 70$ msec.

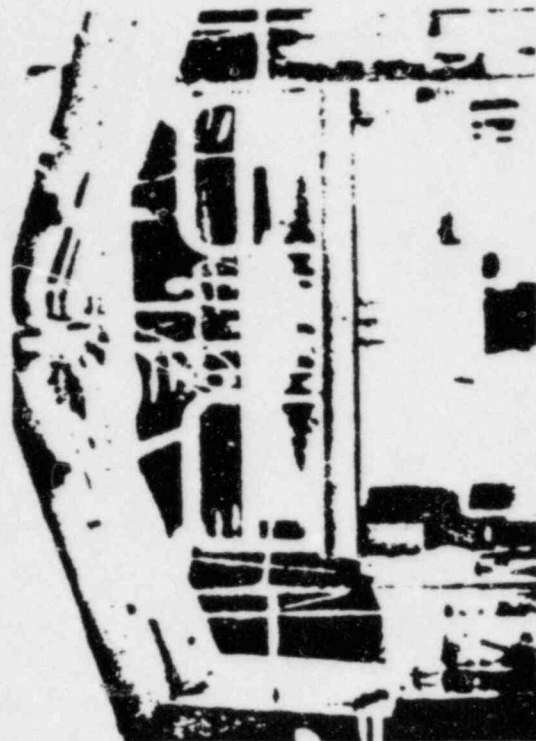


Fig. E-48 $t = 100$ msec.

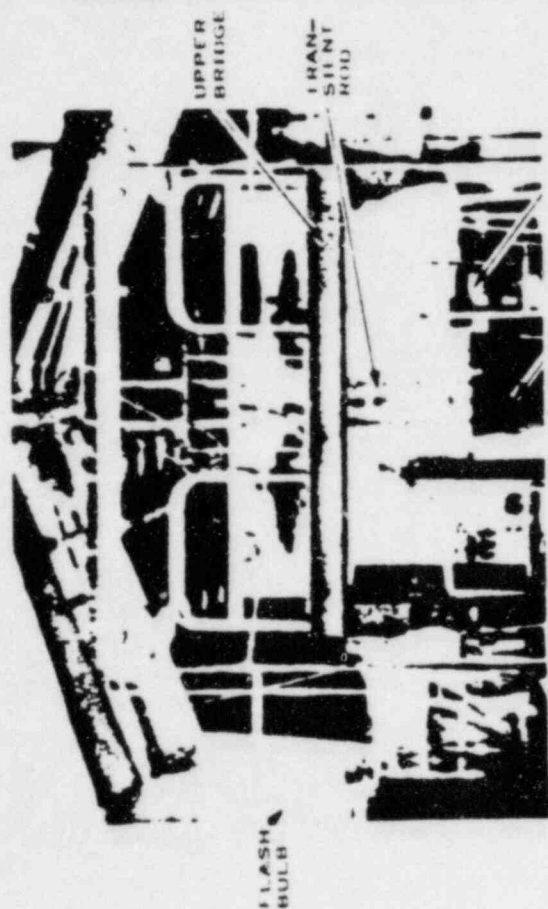


Fig. E-45 $t = -153$ msec.



Fig. E-47 $t = 86$ msec.

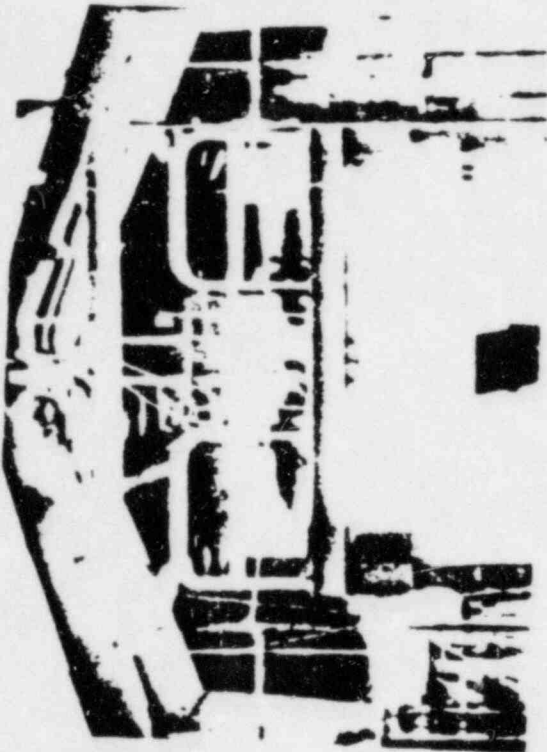


Fig. E-49 $t = 115$ msec.

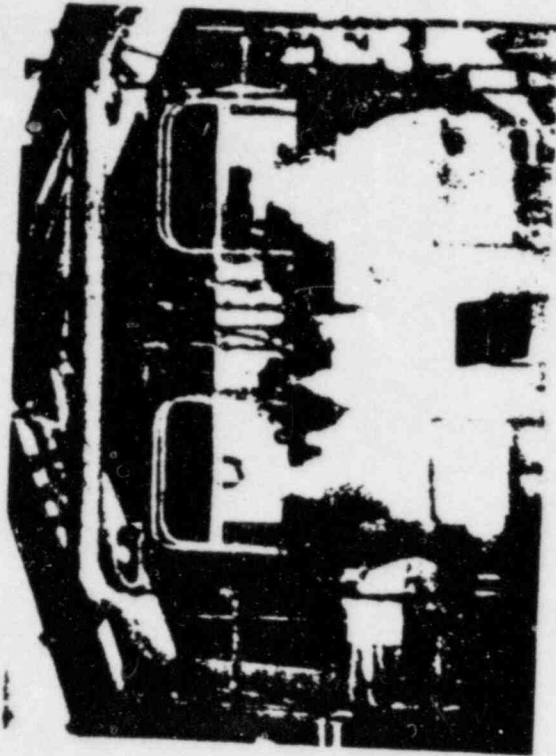


Fig. E-50 $t = 130$ msec.

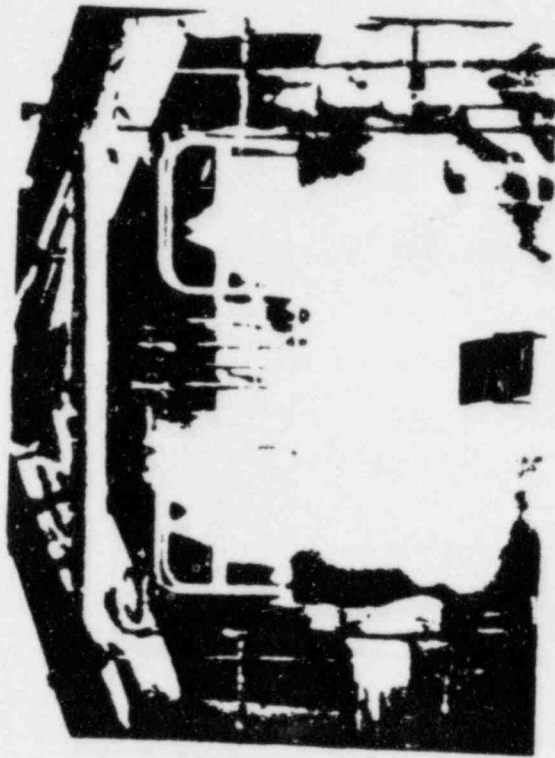


Fig. E-51 $t = 145$ msec.



Fig. E-52 $t = 160$ msec.

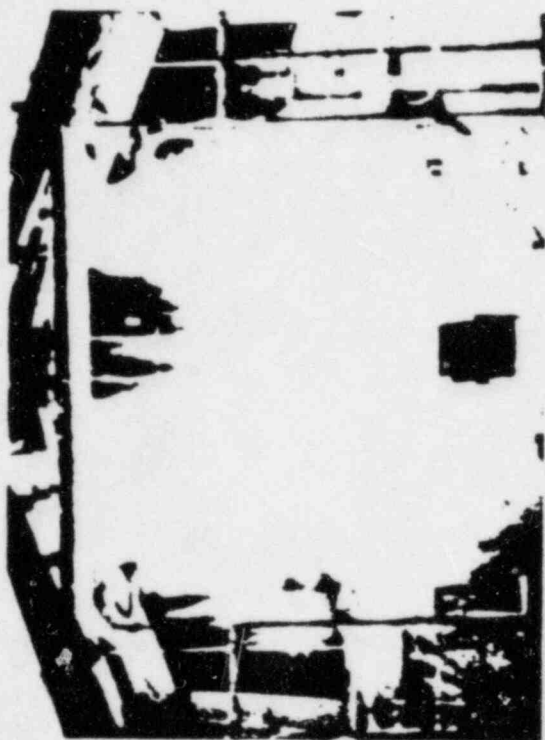


Fig. E-53 $t = 175$ msec.

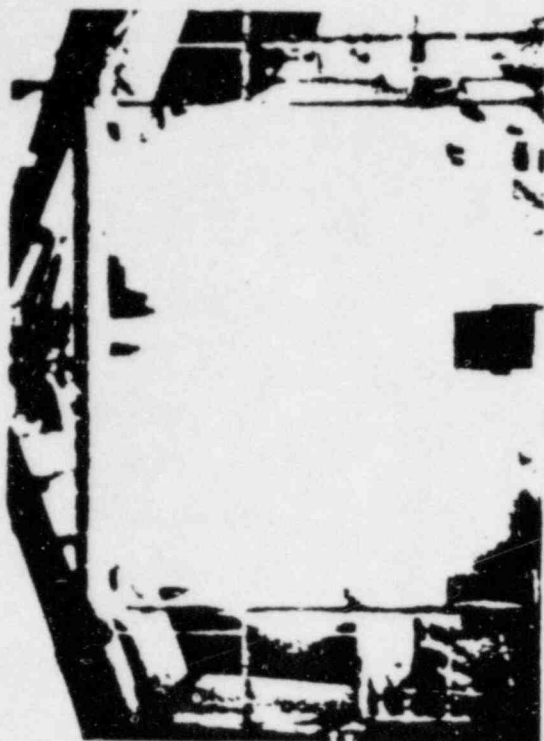


Fig. E-54 $t = 190$ msec.

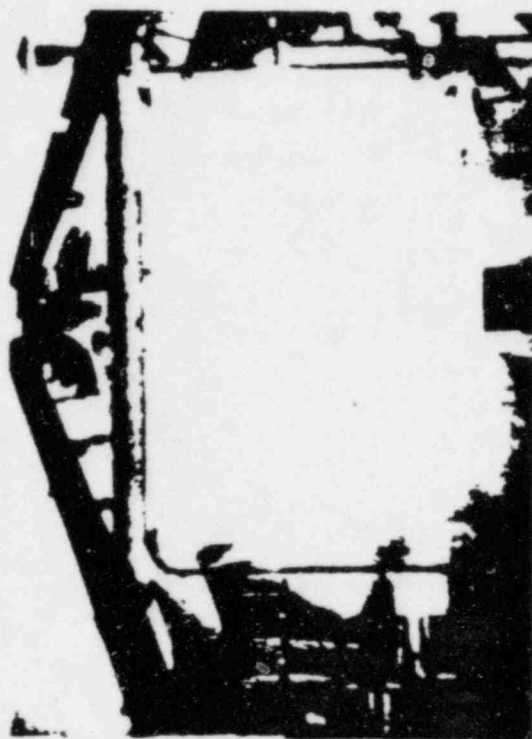


Fig. E-55 $t = 205$ msec.

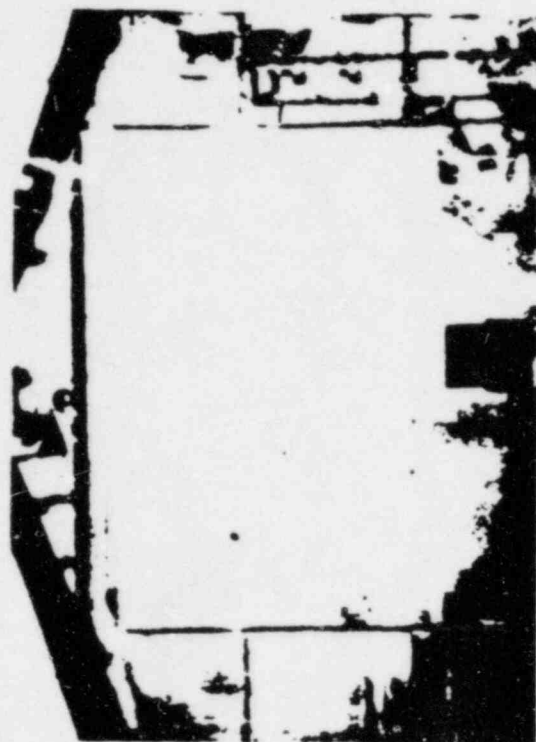


Fig. E-56 $t = 296$ msec.

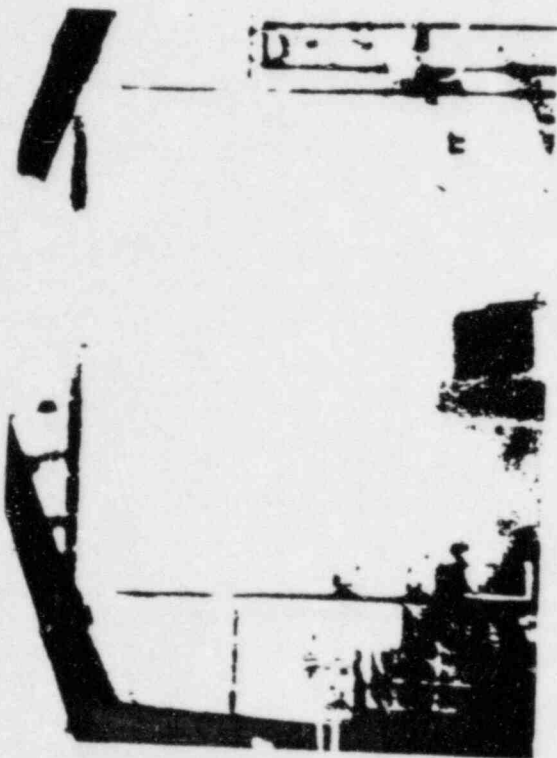


Fig. E-57 $t = 445$ msec.



Fig. E-58 $t = 1040$ msec.

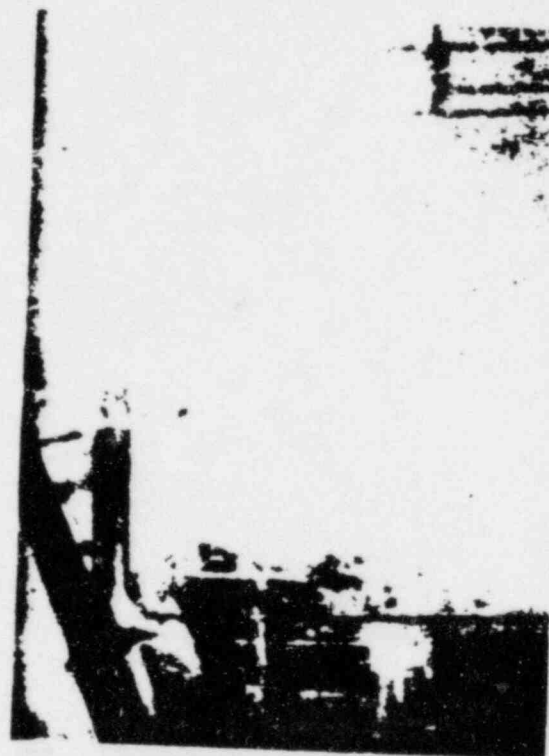


Fig. E-59 $t = 1940$ msec.

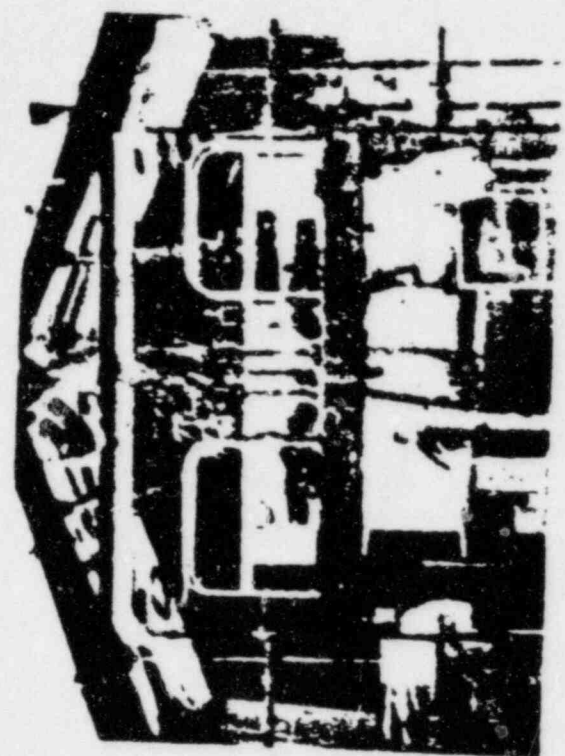


Fig. E-60 $t = 4340$ msec.

APPENDIX F

MEASUREMENT AND CALCULATION OF
MAXIMUM TEMPERATURE IN THE DESTRUCTIVE TEST

APPENDIX F

MEASUREMENT AND CALCULATION OF MAXIMUM TEMPERATURE IN THE DESTRUCTIVE TEST

1. EXPERIMENTAL RESULTS

1.1 Surface Thermocouple Temperature Measurements

Only four of twelve surface thermocouples remained intact during the power excursion up to the time of the destructive pressure pulse. Listed in Table F-1 are the location of the four surface thermocouples, the temperature indicated at the time of the explosion, the maximum temperature indicated by the thermocouples, and the time at which the temperature was recorded.

TABLE F-1

SURFACE THERMOCOUPLE INDICATIONS

Location	Temperature at $t = + 15$ msec [a] (°C)	Maximum Temperature (°C)	Time at Maximum Temperature [a] (msec)
E5 (7W) + 8	452	452	+ 10.5 and + 15
E6 (7W) + 8	443	470	+ 10
D6 (7W) + 8	359	359	+ 15
C7 (9E) 0	396	396	+ 15

[a] Time is taken to be zero at peak power.

The other surface thermocouples failed at various times between 4.5 and 11.5 msec after peak power. At the time of failure, surface thermocouples were indicating between 385 and 580°C. These temperatures are lower than the melting temperature of 649°C for 6061 alloy aluminum. Failure of the thermocouples is attributed both to the differential thermal expansion between the meat and the clad and to internal cracking in the plate.

1.2 Buried Thermocouple Temperature Measurements

All buried thermocouples were intact at the time of the explosion. Table F-II shows for each thermocouple the indicated temperature at the time of the explosion, and for the five cases where a higher temperature was recorded before the time of the explosion, the indicated maximum temperature and the time at which this temperature occurred. Figure F-1 shows the temperatures indicated by buried thermocouples which were located in a plane eight inches above the center of the core at the time of the destructive pressure pulse.

TABLE F-II
BURIED THERMOCOUPLE AND INDICATIONS

Location	Temperature at $t = + 15$ msec (°C)	Maximum [a] Temperature (°C)	Time at [a] Maximum Temperature (msec)
E5 (7W) - 4	620	---	---
D6 (7W) - 4	601	---	---
D5 (7W) - 4	578	---	---
E6 (2W) - 4	608	---	---
C7 (9E) - 4	597	---	---
E5 (7W) + 8	576	---	---
D6 (7W) + 8	454	---	---
D6 (3W) + 8 South	461	---	---
E5 (12W) + 8	586	---	---
D5 (7W) + 8 South	561	---	---
D5 (7W) + 8 North	403	---	---
E6 (2W) + 8	598	---	---
E6 (11E) + 8	354	---	---
D4 (6E) + 8	493	---	---
D7 (7W) + 8	344	---	---
C6 (7W) + 8	349	---	---
C7 (9E) + 8	285	---	---
F4 (6W) + 8	467	482	+ 11.5
E7 (7W) + 8	135	158	+ 9
E7 (12W) + 8	177	230	+ 9
C5 (8E) + 8	144	166	+ 8
C5 (12W) + 8	160	186	+ 8

[a] Except when indicated the maximum temperature is the temperature at $t = + 15$ msec.

The temperatures indicated by buried thermocouples were always 10 to 25 percent higher than temperatures at equivalent positions indicated by surface thermocouples. (Compare, for instance, the values for E5 (7W) + 8 and D6 (7W) + 8 in Tables F-I and F-II.) Since the thermocouple junctions of the buried type lie in temperature gradients extending from the center of a fuel plate to the surface, the measured temperatures are, at best, a lower limit of the temperature existing at the center of the meat.

The fact that no temperatures above the melting point of aluminum were measured at any position does not indicate that melting did not actually occur. As seen below, a large part of the core meat (U-235 alloy in the center of each plate) did actually melt as well as some cladding material before the time of the explosion. The low (below melting) temperatures recorded with the buried thermocouples possibly may be due to the hot-short cracking of 6061 alloy aluminum which caused scales of unheated aluminum to separate from the molten interior of the plate. (See microphotographs in Appendix H which illustrate the separation of cladding.) Hot-short cracking was prevalent in hotter parts of the core and probably was instrumental in reducing heat transfer from meat to clad.

1.3 Fuel Capsule Temperature Measurement

In Appendix B is found a description of another device, called a fuel capsule, which was designed to provide a continuous indication of meat temperatures even above the melting point of aluminum. A fuel capsule was located at position E6 (3W) - 4 which is estimated to have a flux level about 15 percent lower than the maximum flux in the core. (The value of 15 percent was determined from a static flux measurement and may, therefore, differ slightly from the actual value during the transient test.) The fuel capsule yielded a peak temperature of 1245°C about 11 msec after peak power and a temperature of 1225°C at the time of the explosion, 4 msec later (see Figure C-14). Upon disassembly of the capsule it was found that the fuel alloy had melted but that the stainless steel surrounding the capsule fuel had not melted indicating that the temperature of the stainless steel wall of the fuel capsule had not exceeded 1400°C.

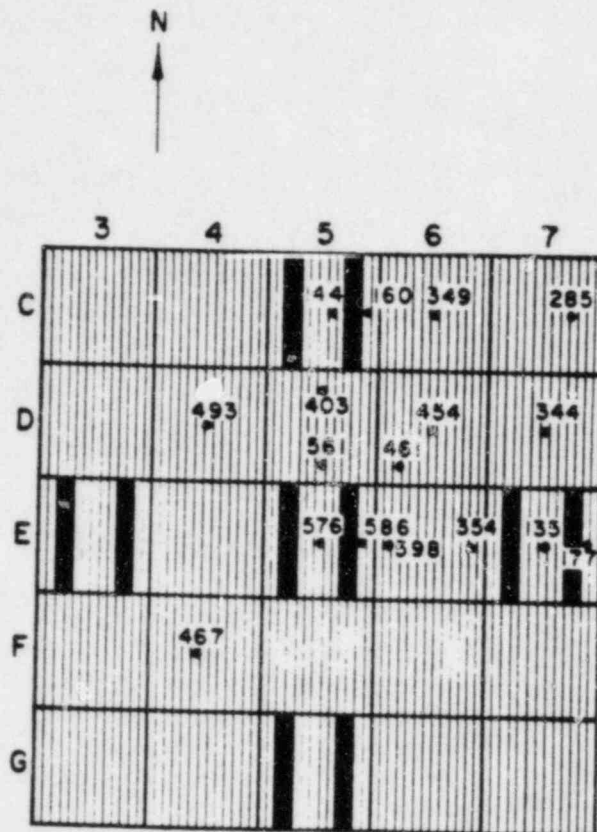


Fig. F-1 Temperatures at various points in the core in a horizontal plane eight inches above core center at about the time when destructive pressures arose ($t = +15$ msec).

2. CALCULATIONS OF MAXIMUM TEMPERATURE

2.1 Maximum Average Temperature of a Fuel Plate Near the Core Hot Spot; Location E5 (7W) - 3

Using the measured energy release for the excursion of 30.7 MW-sec and values of the temperature dependent heat capacity of the plate, a calculation based upon the assumption that the plate was thermally insulated (adiabatic) indicates that the maximum average temperature across the thickness of a plate placed at the hot spot of the core would have been 1275°C. Due to the adiabatic conditions, this represents an upper limit of the average temperature across a plate during the test.

2.2 Maximum Average Temperature in the Capsule

Using a computational method identical to the one above the maximum average temperature in the fuel capsule was computed to have been 1400°C. This value is in reasonably good agreement with the measured value of 1245°C.

If the energy density in the capsule is increased by 15 percent to take into account the fact that the flux at the capsule location may have been 15 percent lower than the maximum flux in the core, it is concluded that the maximum average temperature in the capsule would have indicated no more than 1630°C. Since conditions for heat transfer from the meat of fuel plates are more favorable than from the meat of the capsule, it is reasoned that 1630°C represents an absolute upper bound of the adiabatic plate meat temperatures.

Applying the same 15 percent correction to the 1245°C measured peak temperature in the capsule indicates that had the capsule been located at the core hot spot it would have yielded a measured value of the peak temperature of about 1500°C. From considerations of the temperature distribution in the capsule at the time of the explosion, 1500°C probably represents an upper limit of actual fuel temperature at the core hot spot. Therefore, peak fuel plate temperatures are expected to be lower than 1500°C.

2.3 Temperature Distribution in Fuel Plate at E5 (7W) 0

Detailed machine calculations also were made [10] of the transient temperature profile inside several fuel plates located at various positions in the core and near the hot spot, by solving the one dimensional, second order heat transfer equations for the meat and the clad. Solutions were obtained for a two region slab model using regional, temperature-dependent values of the thermal conductivity and volumetric heat capacity, and a time dependent prompt heat source derived from the experimental transient reactor power. The model consisted of a primary heat source region of U-Al alloy and a clad region of aluminum 6061. Exterior boundary conditions used were the Neumann condition (temperature gradient goes to zero at the boundary) applied at the center of the plate with the experimental plate surface temperature used for the outer boundary temperature of the fuel plate.

Figures F-2 through F-7 show the results of several of these calculations. A more complete discussion of the calculations can be found in Reference 10 which discusses the computational method, meaningfulness of the measured temperature and calculated results, as well as assumptions that were made.

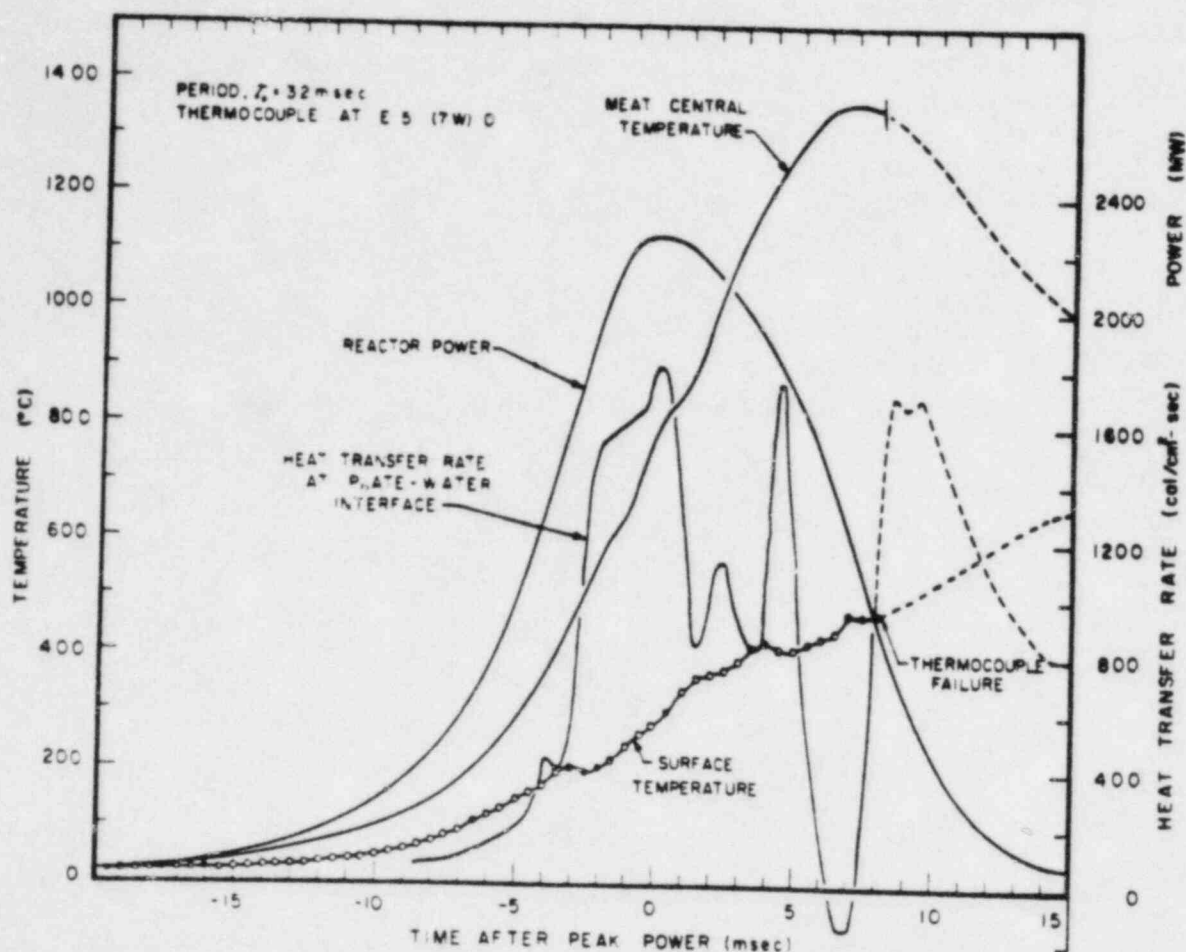


Fig. F-2 Calculated results of centerline meat temperature and of heat transfer rates from fuel plate surface to moderator. Experimental surface temperature (shown) was taken near core hot spot, E5 (7W) 0. Run 54.

Calculations of temperature distributions and heat transfer rates for a segment of fuel plate near the core hot spot, Figures F-2 and F-3, were complicated by failure of the thermocouple about 7 msec before the explosion. However, at this time the peak central temperature had apparently been reached and is calculated to be about 1360°C.

To continue the hot-spot calculation until the explosion, several "trial" or assumed surface temperatures were used, one of which is shown in Figure F-2 as the dashed portion of the surface temperature after thermocouple failure. Although a continuation of this surface temperature after thermocouple failure would reasonably go to lower temperatures (due to overall thermal relaxation and cooling of plate and rapidly decreasing power), the trial shown in Figure F-2 is based upon a nearly linear extrapolation of the temperature data and leads to a final surface temperature of about 650°C which is near the melting point of aluminum. Thus, this trial leads to a condition of incipient melting at the clad surface at the time of the explosion and a central temperature at this time of 1000°C (representing a 360°C drop from peak value).

This "trial" is considered to be reasonable with regard to peak surface temperature. Nevertheless, another trial was taken which assumed that adiabatic conditions existed after the thermocouple failure in order to compute the highest central and surface temperatures possible at the time of the explosion. From this limiting type of calculation, values of 960 and 1080°C are found, respectively, for the surface temperature and centerline temperature.

From these calculations (with their inherent calculational models and assumptions) the conclusion is formed that at the onset of the explosion, the peak (unexposed) meat temperature at the core hot spot was about 1000°C and probably not exceeding 1100°C. Fuel plate surface temperatures at the same time probably did not exceed the melting point. However, if one assumes that the fuel plate was completely insulated during the last 7 msec prior to the explosion, then temperatures may have exceeded the melting point by as much as 300°C.

At other positions in the core, of course, temperatures were lower.

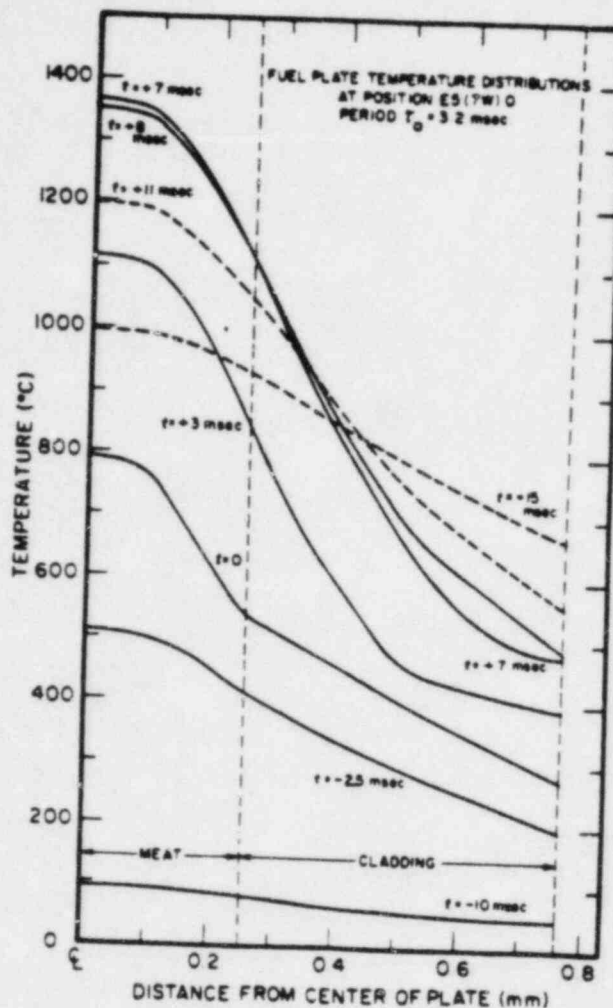


Fig. F-3 Calculated temperature distributions of a fuel plate section near the hot spot of the core. Times indicated are in milliseconds after peak power during the destructive test. Run 54.

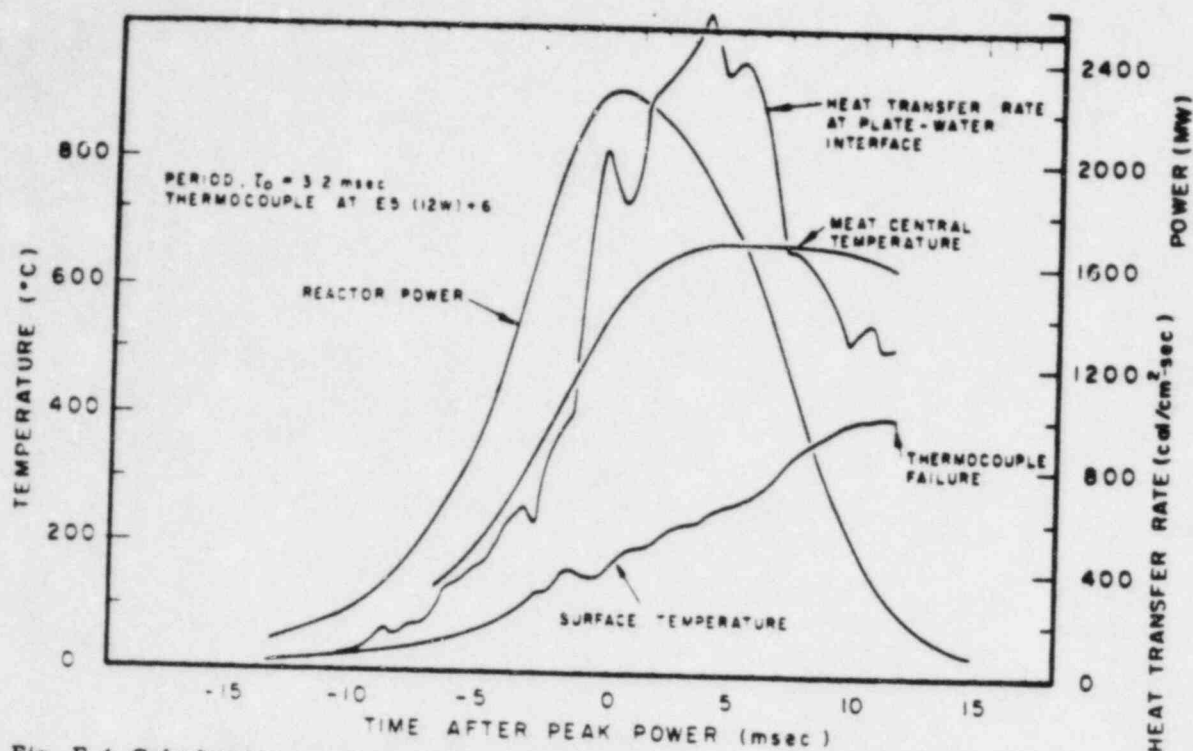


Fig. F-4 Calculated temperature and heat transfer rate shown with measured surface temperature at position E5 (12W) + 6. At this position, the thermal neutron flux was about 60% of the peak flux at the core hot spot. Run 54.

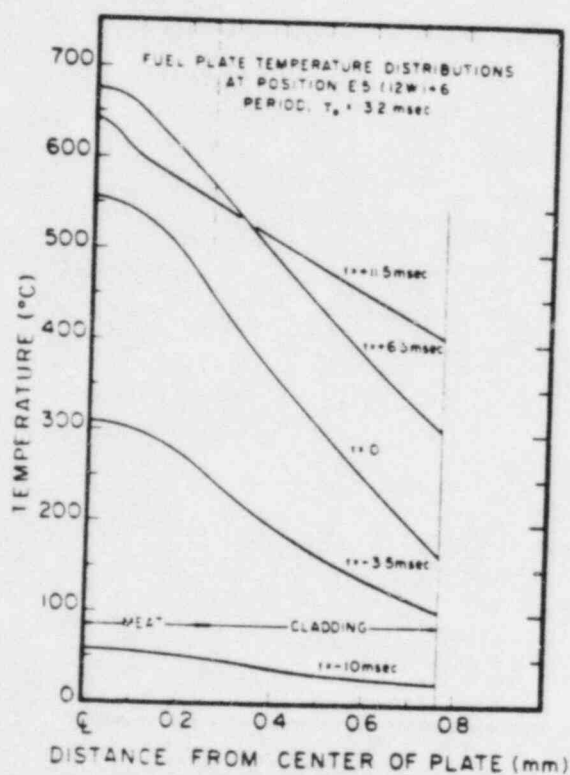


Fig. F-5 Calculated temperature distribution in a fuel plate segment at E5 (12W) + 6, (relative thermal neutron flux about 60% of peak at core hot spot). Times indicated are in milliseconds after peak power. Run 54.

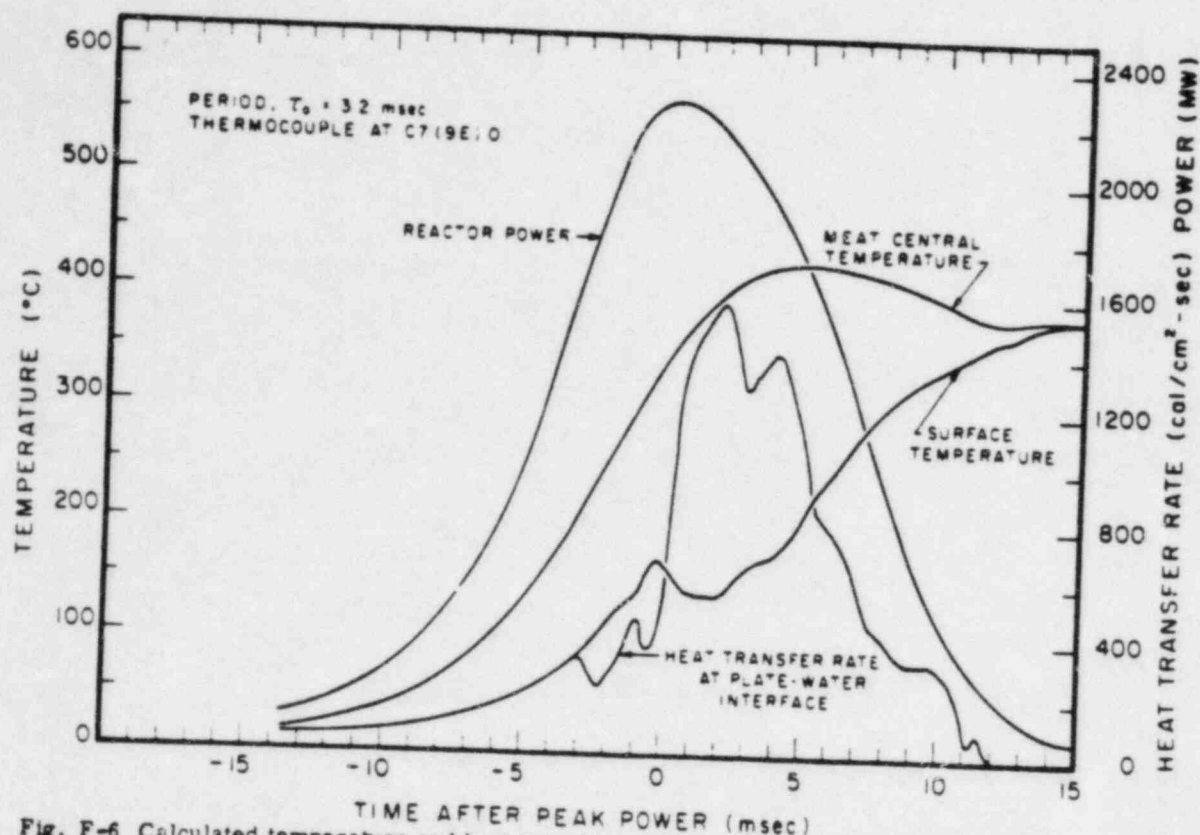


Fig. F-6 Calculated temperature and heat transfer rates shown with measured surface temperature at position C7 (9E) 0, during destructive test, Run 54. At this position the thermal neutron flux was about 45% of the peak at the core hot spot.

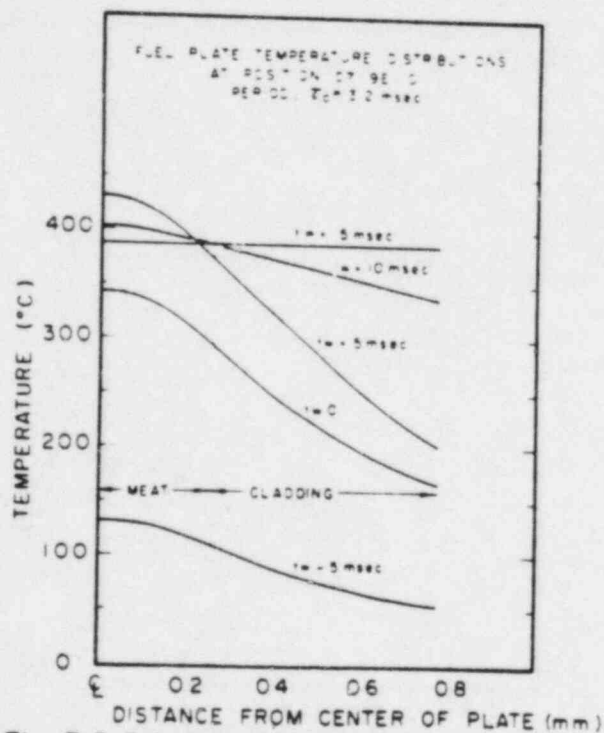


Fig. F-7 Calculated temperature distribution in a fuel plate segment at position C7 (9E) 0 (relative thermal neutron flux about 45% of peak at core hot spot). Times indicated are in milliseconds after peak power, Run 54.

APPENDIX G

CALCULATION OF FISSIDE RELEASE FROM THE DESTRUCTIVE TEST

APPENDIX G

CALCULATION OF FISSIDE RELEASE FROM THE DESTRUCTIVE TEST

The information presented in this section is based upon data provided by the USAEC-ID Health and Safety Division who cooperated with Phillips Petroleum Company in the performance of the destructive test and who had the responsibility for collection and analysis of fission product released data as well as coordination and collection of meteorological data for the destructive test. The data were taken from samples obtained with several prefilter, carbon trap, high volume air samplers placed on a grid system as indicated in Figure G-1.

The meteorological forecast conditions required for the destructive test were: wind direction $220^\circ \pm 20^\circ$, wind speed 10 to 20 mph, temperature lapse rate conditions and no precipitation for a three-hour period. Meteorological measurements recorded for the period between 1220 and 1420 Mountain Standard Time on November 5th are given in Table G-1. Values of the standard deviation of the wind direction variations are based upon instantaneous readings at one-minute intervals for the Spert I station and upon instantaneous readings at alternating two- and three-minute intervals for the three-mile arc station. The vertical temperature lapse rate was nearly neutral on the 250-foot meteorological tower at Central Facilities.

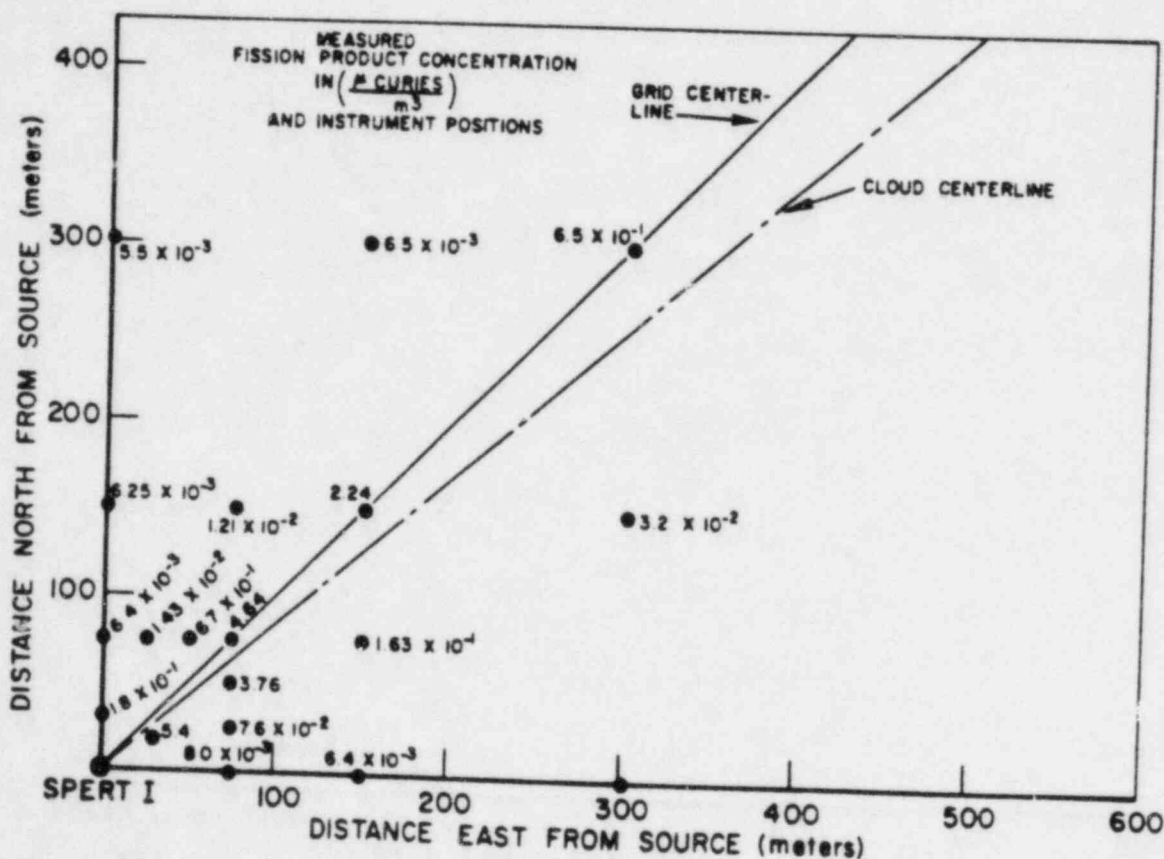


Fig. G-1 Air sampler locations and portion of the grid system showing values measured at each location (corrected to 1800 MST).

TABLE G-I

WIND MEASUREMENTS AFTER THE DESTRUCTIVE TEST

Station	Wind Speed \bar{u} (mph)	Mean Wind Direction	Standard Deviation
Spert I	23	226°	10.9°
Three-Mile Arc	29	238°	11.9°

The destructive test was initiated at 1225, but counting data from the air samples were not available until 1800 due primarily to the time required for reentry after the test. Air sampler data corrected for decay back to 1800, along with instrument positions relative to the Spert I reactor building, are shown in Figure G-1. The values given in Figure G-1 are the concentrations in μ curies/ m^3 rather than total integrated dose rates. Although cloud passage time was not actually measured, computed concentrations are based on the assumption that the cloud took two minutes to pass over the instruments. Concentrations in μ curies/ m^3 were first plotted versus their respective distances from the grid centerline [a] on semi-log paper. Gaussian curves were fitted to the data for approximate downwind distances of 100, 200, 430, and 736 m (not shown in Figure G-1) and the maximum value of each Gaussian curve was then the interpolated cloud centerline which, when multiplied by the assumed two minutes of cloud passage time yields the total integrated dosage, TID, at the cloud centerline.

If it is assumed that the Spert I destructive test fissile release falls into the category of an "Instantaneous point source at ground level" [28], then, Q , the total curie release to the atmosphere of the test may be computed from Equation (1).

$$TID = \frac{2Q}{\pi C^2 \bar{u} (\bar{u}t)^{2-n}} \frac{\text{curie-sec}}{m^3} \quad (1)$$

Sutton's parameters and other values used in this equation are:

\bar{u} = mean wind speed = 26 mph

n = stability parameter = 0.25 (neutral)

C_2 = diffusion coefficient = 0.0210

$(\bar{u}t)$ = downwind distance on cloud centerline from point source to measuring instrument - 100, 200, 430, and 736 m.

[a] Grid centerline shown in Figure G-1.

The diffusion parameters used are typical for the NRTS during meteorological conditions such as those which prevailed during the destructive test. Computed values of Q were averaged to obtain an estimate of 1.51 curies for the instantaneous point source strength. Correction for 5 hours 35 minutes was estimated for the Way-Wigner equation, $A(0) = A(t) t^{1.21}$, which yielded 2.44×10^5 curies. This release is to be compared with a total fission inventory in the core of about 5.7×10^7 curies immediately after the excursion (based upon 1.85×10^6 curies/MW-sec)[29] and amounts to about 0.4 percent. As noted earlier on page 47, however, recent calculations by the USAEC-ID Health and Safety Division (not published) indicate that the total release consisted only of about 7 percent of the noble gases or about 0.7 percent of the total fission inventory. No solid products were collected after this test, and, although radioiodines were undetected, less than 0.01 percent of the iodines are calculated to have been released to the atmosphere.

APPENDIX H

METALLOGRAPHIC EXAMINATION OF
DAMAGED FUEL PLATES FROM THE DESTRUCTIVE TEST

APPENDIX H

METALLOGRAPHIC EXAMINATION OF DAMAGED FUEL PLATES FROM THE DESTRUCTIVE TEST

A metallographic examination has been performed at the MTR hot cell on eight fuel plates which were melted as a result of the 3.2-msec period destructive test. The plates and their location in the core are shown in Table H-I.

TABLE H-I
METALLOGRAPHIC SAMPLE POSITIONS

<u>Plate No.</u>	<u>Core Position [a]</u>	<u>Plate Position [b]</u>	<u>Approximate Length of Recovered Plate (in.)</u>
D-2321	E-5	1	3-1/4
D-2433	E-5	12	3
D-1930	E-4	1	8-1/2
D-808	E-4	12	3-3/8
D-800	C-5	12	10-3/4 [c]
D-2392 [e]	C-3	4	25-1/8 [d]
D-1163	F-6	6	5
D-365	F-6	7	5

[a] See Figure D-5 for core position nomenclature.

[b] Plates are numbered from west to east within assemblies as positioned in the core.

[c] A bottom portion of the plate was attached to the top portion.

[d] Center of plate was melted.

[e] See Figure E-I

All samples were 3/4 inch in length and were examined in the unetched state using 50x magnification.

Examination of the composite photomicrograph (Figure H-1) for a sample taken at the ruptured edge of plate D-2321 reveals the melting of the meat and the cladding. The end is flared, indicating that it had been in a plastic state. Figure H-2, which is another photomicrograph of the same sample, but at a position further away from the ruptured edge, shows melting at the center and edge of the larger fuel particles, but no damage to the cladding. This sample is a longitudinal-type specimen, ie, the viewing surface is parallel to the long axis of the fuel plate. A transverse-type specimen (Figure H-3) from the rupture area shows some melting and change at the edges of the large fuel particles. This sample shows no indication of cladding damage.



Fig. H-1 Composite photo micrograph of ruptured end of fuel plate D-2321 (50x) (cross section).



Fig. H-2 Photomicrograph of plate D-2321 away from ruptured edge (50x) (cross section).



Fig. H-3 Photomicrograph of transverse-type specimen from the rupture area of plate D-2321 (50x).

The photomicrographs obtained of plate D-2433 are quite similar to those of plate D-2321.

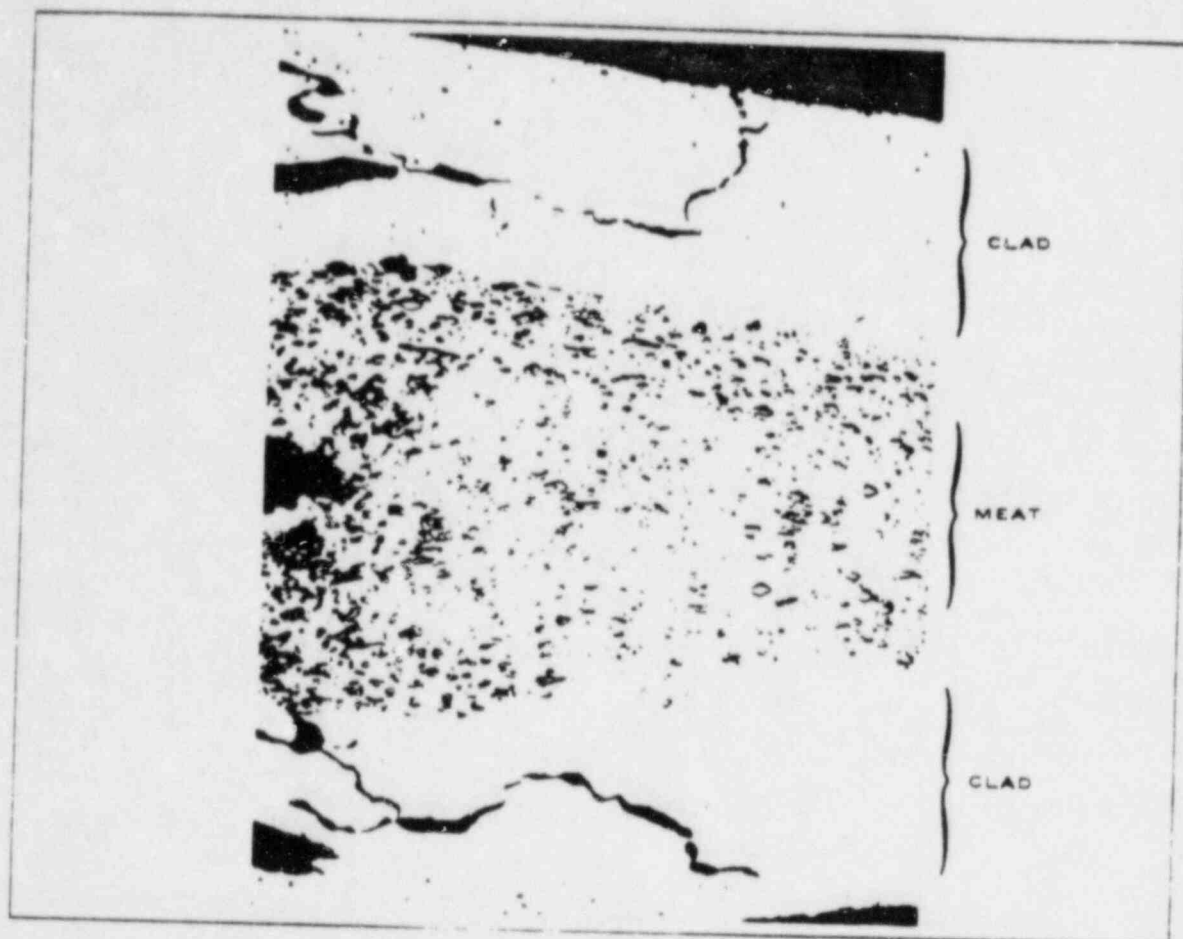


Fig. H-4 Photomicrograph of ruptured end of plate D-800 (50x) (cross section).

Photomicrographs of plate D-800 show the melting and mechanical damage of the fuel plate. Figure H-4 shows the ruptured edge of the fuel plate. The photomicrograph of Figure H-5 was taken immediately adjacent to that of Figure H-4 and shows the cladding damage. Figure H-5, which is an area about $\frac{3}{8}$ inch away from the area shown in Figure H-4, is typical of undamaged fuel samples. A sample from the bottom portion of the D-800 fuel plate is shown in Figure H-7. The sample exhibits a melted area at the fuel centerline and no cladding damage. The sample split through the fuel before mounting and only one-half of the sample is shown in the figure.

Figure H-8 shows a sample of plate D-808 near the ruptured edge. In this case the cladding is severely cracked, and the meat shows some centerline fuel outlining. A sample which was taken two inches from the ruptured end shows no apparent melting.

Samples from plate numbers D-1930, D-1163, and D-365 exhibited characteristics similar to the samples from plate D-808.

Samples taken at $5\frac{1}{2}$, 10, $13\frac{1}{8}$, and $16\frac{3}{8}$ inches from the top of fuel plate D-2392 were examined. The $5\frac{1}{2}$ - and 10-inch samples show typical areas with no melting. The $13\frac{1}{8}$ - and $16\frac{3}{8}$ -inch samples show no cladding damage and some outline melting of the larger fuel particles (Figure H-9).

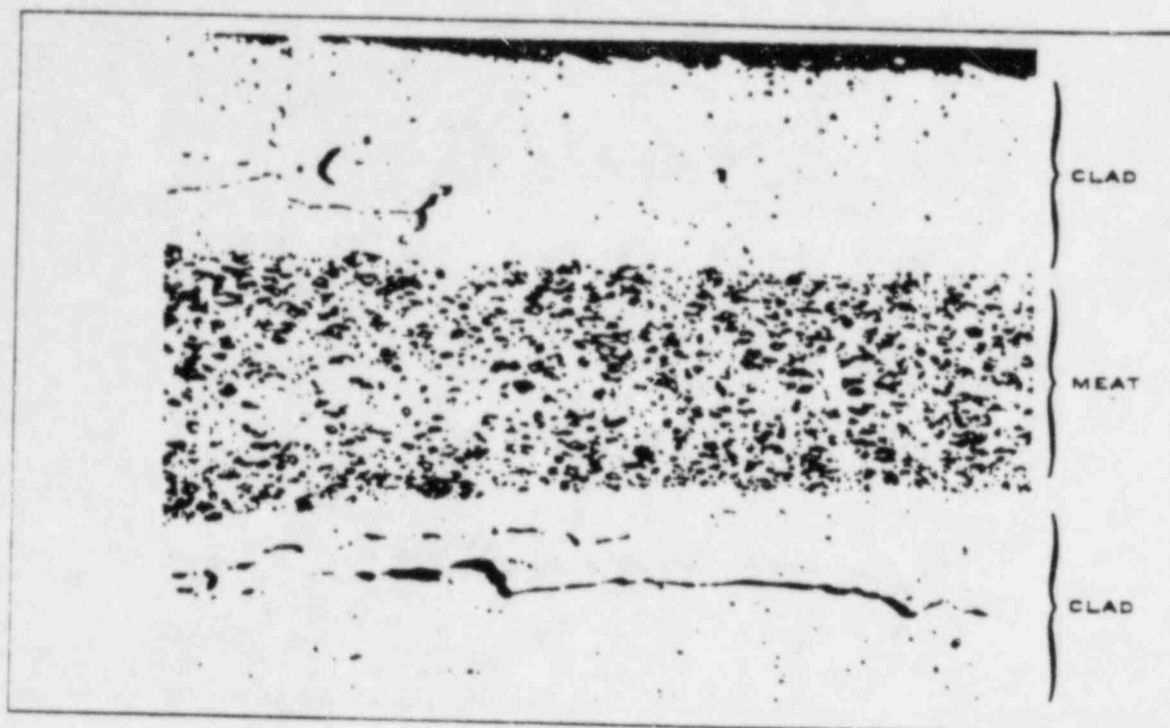


Fig. H-5 Photomicrograph of plate D-800. Sample taken immediately adjacent to that of Fig. 13 (50x) (cross section).

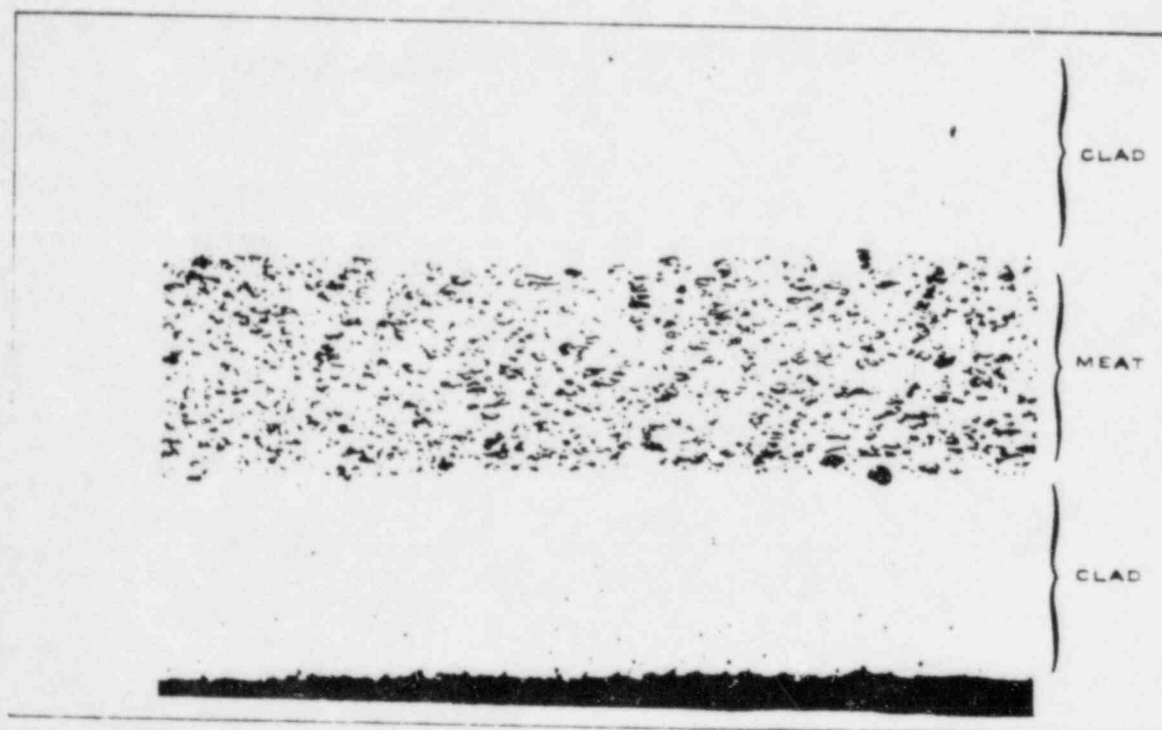


Fig. H-6 Photomicrograph of plate D-800. Sample taken about 3/8 inch from that of Fig. 14 (50x) (cross section).

Since the 13-1/8- and 13-3/8-inch samples were taken from the damaged area of the plate, it is somewhat surprising to see so little evidence of melting.



Fig. H-7 Photomicrograph of sample from bottom end of plate D-800. Only half of the sample is shown (50x) (cross section).

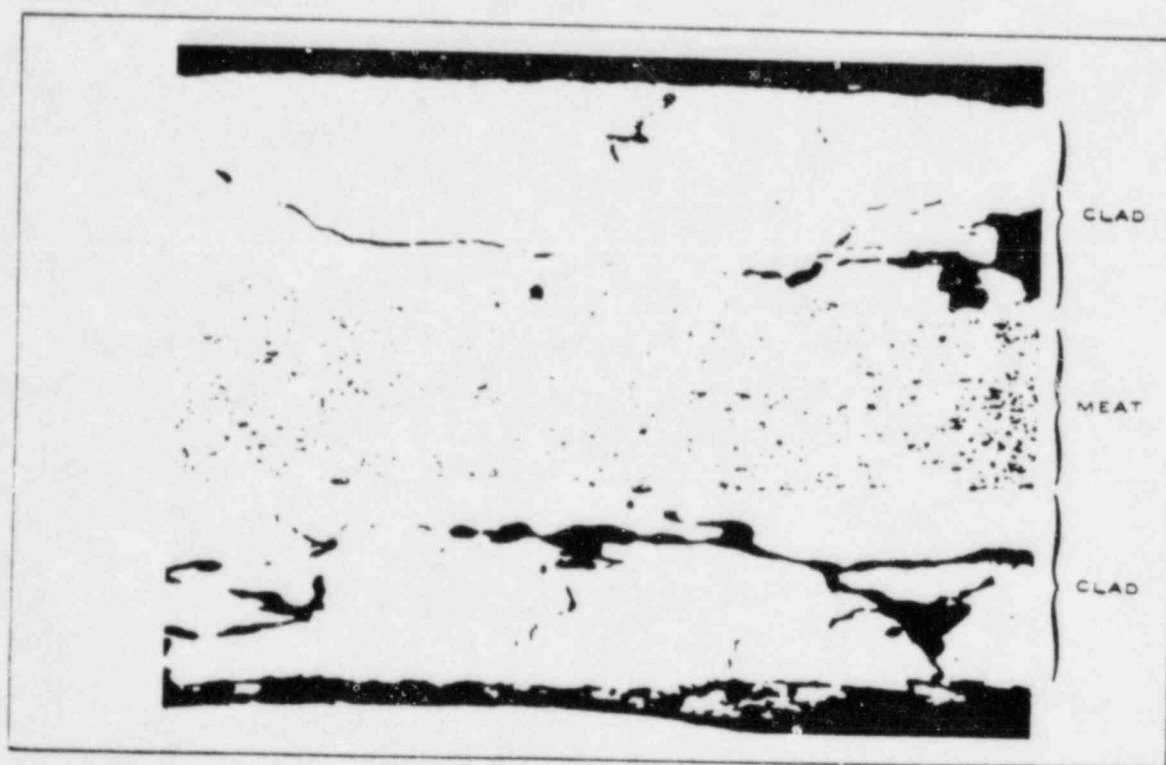


Fig. H-8 Photomicrograph of sample near the ruptured end of plate D-808 (50x).

In general, the melting of the fuel plates on the damaged ends extended into the plates about $1/8$ inch. At about $3/8$ inch from the ends, or in the middle of

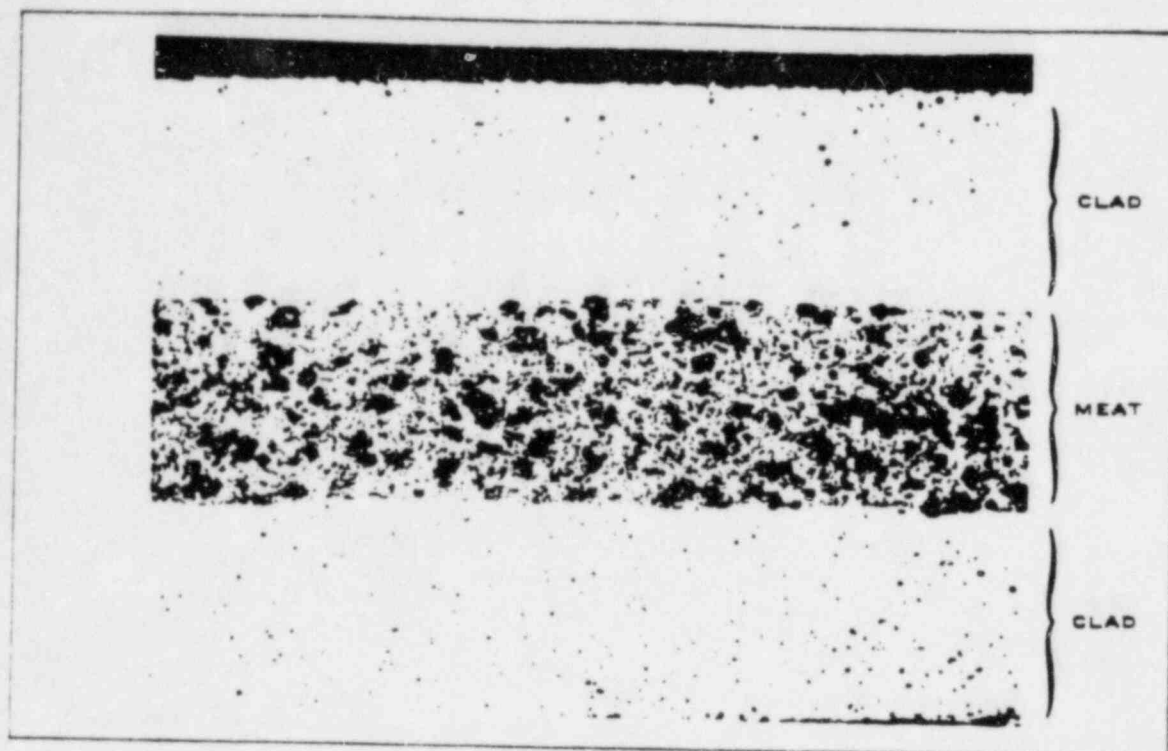


Fig. H-9 Photomicrograph of sample from plate D-2392 (50x) (cross section).

the specimens taken from the damaged ends, normal fuel plate structure was observed.

The failure of the fuel plates can be described as a combination of melting and mechanical damage. The observed intergranular cracking of the cladding and the melting of the meat near the ruptured ends shows that the plates must have reached a temperature of at least 640°C in this vicinity. Because of the absence of cladding and meat damage a short distance from the damaged end, it appears that the temperature gradient was large along the length of the plate. While this evidence, coupled with a temperature reading of 1230°C from the fuel-bearing capsule which was in the core, indicates that the temperature of the fuel plates was probably much higher than that recorded by surface thermocouples; there is no metallographic evidence that the maximum fuel temperatures approached the vaporization temperature of the alloy.

A more detailed presentation and discussion of metallographic data for the destructive test is contained in Reference 10.

APPENDIX I

RECOVERY AND CLEANUP OPERATIONS

APPENDIX I

RECOVERY AND CLEANUP OPERATIONS

Recovery and cleanup operations in the Spert I reactor vessel and surrounding area were initiated soon after the destructive test. For the first few days following the test, operations consisted primarily of the acquisition of information pertaining to the reactor condition and the recovery of radiation-sensitive items from the reactor area. These efforts included removal of motion picture cameras from their protective housing, removal of various activation samples, and a general documentation of the reactor condition by both motion pictures and still photography (see Figures 30-39). Upon the completion of these initial operations, it was necessary to recover those test components which had been ejected from the reactor tank and to make the necessary preparation for the more extensive core disassembly operations to follow. The items which had been expelled from the core, the majority of which were broken lights and light brackets, were noted as to location and identity, photographed, and removed to storage. After removal of certain items of equipment from the reactor building, such as the support stands for health physics experiments, the camera tables and tracks, some sand bags and blast shields for the cameras and electrical switch gear, several areas of the building were decontaminated to prevent the spread of the low-level contamination which was present; one of these areas was used as a clothing change area.

Systematic recovery of all items from the reactor vessel and the removal of the support bridges and the control rod drives was then initiated. The position and identity of each item was recorded and extensive written descriptions and photographic coverage was employed before it was removed to storage. All recovered fuel-bearing materials were weighed.

The majority of the recovery operations was accomplished with manually operated handling tools since most of the components were of small size. Large components were removed from the reactor tanks by using either long hook tools or ropes attached directly to the components. For the largest components, such as the lower support bridge, use was made of the building crane. During these operations the radiation level directly over the reactor tank was approximately 100 mr/hr. This relatively low direct radiation level and the low contamination levels present permitted the recovery operation to proceed rapidly with no unusual radiological problems.

Fifteen of the 25 fuel assembly cans in the core were found to be partially intact. Two of these assemblies were removed and transferred to a hot shop where they were cut open and photographed, using remote handling tools. The remaining 13 fuel assemblies were opened at the Spert I Terminal Building (Reference 1). The procedure used was to place a fuel assembly in a tank of water and to grind two of the edges from the fuel assembly permitting gradual opening. An electric motor was used to drive the grinding wheel through a flexible shaft. In this operation, the water served not only as a radiation shield but also to retain radioactive dust and chips resulting from the grinding operation. On completion of the grinding operation, the assembly was dried, using heat lamps, and then photographed. The fuel plates were then separated from the aluminum can and weighed, and the fuel and assembly parts removed to storage.

At frequent intervals during the recovery operation photographs were taken of the status of the reactor tank in order to document, in detail, the positions of various components. Samples of the metallic residue in the reactor vessel were taken periodically in order to obtain representative samples from all parts of the reactor vessel for subsequent analysis. Upon completion of the recovery operation, radiation levels in the reactor vessel were found to be near background and the facility was in such a condition as to allow restoration and repair to proceed for the next test program.

APR 1980

APR 30 1981

RECEIVED



Experimental Determinations of the Self-Regulation and Safety of Operating Water-Moderated Reactors

By J. R. Dietrich,* USA

INTRODUCTION

One of the important characteristics of a nuclear reactor is the degree of hazard which it creates in the surrounding area. If the usefulness of reactors, either for research or for power production, is to be exploited effectively, the hazard must be minimized, since isolation of the reactor compromises its utility and increases its cost. It is, therefore, important to find means for evaluating the hazards of specific reactors and methods of improving the safety of reactors in general.

The ultimate question in an evaluation of reactor safety is the question of what will happen if the reactor is inadvertently made supercritical and allowed to "run away" without any artificial limitation of its power. For, although safety devices which impose artificial limitations will certainly be provided for in the reactor design, the possibility of their failure as well as the consequences of their finite speed of operation must be recognized.

In general it can be said that the reactivity of a reactor will be related to its power level once the power has become sufficiently high to cause significant changes in the temperatures of the reactor parts. At moderate power levels this dependence can be such as to cause the reactivity either to decrease or to increase with power level, depending on the de-

sign of the specific reactor, but eventually at some power level any runaway reactor will become subcritical, through some degree of disassembly of itself if not by other means (Fig. 1). The safety question has to do with how violent the energy release becomes before the eventual shutdown is achieved.

The more important ways by which increasing power can cause a reactor to lose reactivity are by expansion of the fuel, by heating and expansion of the moderator, and, if strong resonance absorbers are present, by Doppler broadening of the resonances. In many cases the unknowns in the magnitudes of the applicable effects and in their speeds of operation make safety evaluations quite uncertain.

The most straightforward way of evaluating the unknown aspects of the reactor shutdown process is by observing experimental runaways of actual reactors. Some experiments of this kind on two reactor types which have particularly favorable power-limitation characteristics, the solid-fuel, water-moderated reactor and the water-moderated homogeneous reactor, are reported here. In addition to the instrumental measurements reported here, motion picture records, which add materially to the information on the safety characteristics of the reactors, are available.

Homogeneous reactors can, in general, be made to have negative temperature coefficients of reactivity. The negative coefficient results primarily from thermal expansion of the fuel solution, which decreases not only the density of the moderator, but that of the fuel as well. The coefficient is quite large for small reactors with high neutron leakage. Furthermore, since the heat of fission is liberated directly in the fuel solution, the action of the negative coefficient is very rapid, and insofar as such reactors can limit their power by temperature coefficient alone, they can be expected to be quite effectively protected against destructive runaways.

The solid-fuel water-moderated reactor may get a certain degree of power limitation from the Doppler coefficient if it contains a large fraction of U^{235} . Beyond this power limitation comes from the moderator temperature coefficient and expulsion of moderator from the reactor core by the formation of steam at the hot fuel element surfaces. The bulk temperature of the moderator does not change rapidly enough

* Argonne National Laboratory. Including work by C. C. Bigelow—Pratt and Whitney Aircraft Corp., R. A. Cameron—Argonne National Laboratory, B. C. Cerutti—Argonne National Laboratory, R. E. Coté—Pratt and Whitney Aircraft Corp., W. R. Davis—University of Washington, J. J. Dickson—Argonne National Laboratory, J. R. Dietrich—Argonne National Laboratory, J. M. Harrer—Argonne National Laboratory, R. O. Haroldsen—Argonne National Laboratory, P. R. Kasten—Oak Ridge National Laboratory, L. D. P. King—Los Alamos Scientific Laboratory, N. L. Krisberg—US Atomic Energy Commission, D. C. Layman—Argonne National Laboratory, H. V. Lichtenberger—Argonne National Laboratory, W. C. Lipinski—Argonne National Laboratory, R. N. Lyon—Oak Ridge National Laboratory, M. Novick—Argonne National Laboratory, V. K. Paré—Oak Ridge National Laboratory, R. L. Ramp—Argonne National Laboratory, W. M. Sandstrom—University of Washington, R. J. Schiltz—Argonne National Laboratory, O. A. Schulze—Argonne National Laboratory, A. R. Snider—California Research and Development Co., G. H. Stonehocker—Argonne National Laboratory, J. A. Thie—Argonne National Laboratory, A. J. Ulrich—Argonne National Laboratory, S. Untermyer—Argonne National Laboratory, S. Visner—Oak Ridge National Laboratory, G. K. Whitham—Argonne National Laboratory, C. Zabel—Los Alamos Scientific Laboratory, W. H. Zinn—Argonne National Laboratory, and C. B. Zitek—Commonwealth-Edison Company.

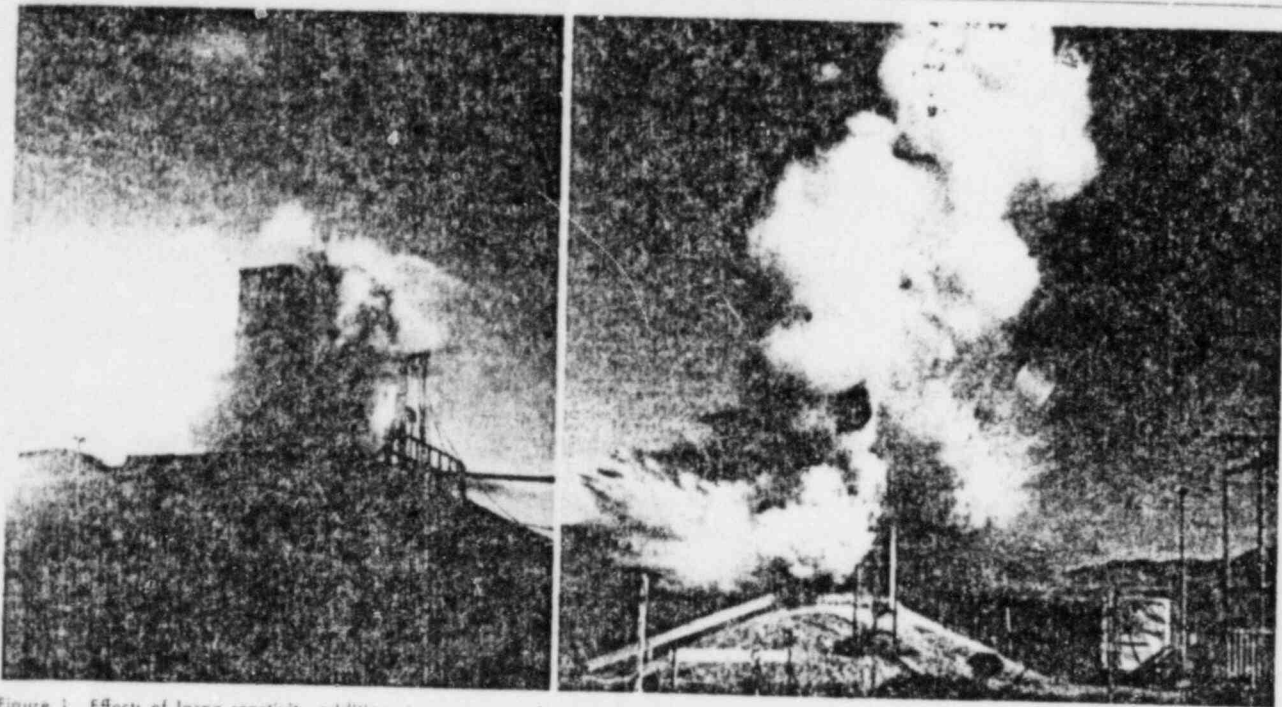


Figure 1. Effects of large reactivity additions to a water-moderated reactor; left, reactor shutting itself down safely by water expulsion after being made supercritical by 2.1% k_{eff} ; right, reactor destroyed by melting of fuel plates after being made supercritical by 3.3% k_{eff} .

to make the temperature coefficient effective against rapid power increases, but early laboratory experiments by Untermeyer and later ones by West, Weills, Hooker, and Schiltz showed that the expulsion of moderator by steam can be very rapid.^{1,2} The reactor experiments, initiated at the suggestion of Untermeyer, confirmed the effectiveness of the process. They were begun in the early summer of 1953 by Argonne National Laboratory as part of an experimental program on boiling water-moderated reactors. The effectiveness of boiling as a safety process was proved, and the following year the severity of the experiments was increased to the point of planned destruction of the reactor. A new reactor was built in 1954 with which similar experiments were made at elevated pressures.

In July and August of 1953 safety experiments were run on the Los Alamos "Supo" reactor by Lyon, Kasten, and others of Oak Ridge National Laboratory and King, Zabel, and others of Los Alamos Scientific Laboratory. Shortly thereafter a program of more drastic safety experiments was run on the Homogeneous Reactor Experiment at Oak Ridge National Laboratory by Paré, Visner and others. Although these experiments were not carried to conditions as severe as those used for the experiments on solid-fuel reactors, they demonstrated a high degree of inherent self-limitation of power in the homogeneous systems.

EXPERIMENTS WITH HOMOGENEOUS REACTORS

The runaway behavior of the non-boiling homogeneous reactor, whose power is limited by the temperature coefficient of reactivity, is the most straightforward of those investigated. Reactors of

this type may have very high negative temperature coefficients of reactivity which result primarily from the expansion of fuel solution out of the reactor proper as the temperature increases.

Figure 2 is a diagram of the Homogeneous Reactor Experiment, which was used for the tests described here. The core is normally full of the fuel solution of enriched uranium in water. If the solution heats and expands, the displaced fraction of the solution is accommodated by the pressurizer tank, where it contributes nothing to reactivity. The temperature coefficient of the reactor was about -0.1% k_{eff} per degree C. The volume of the core was 50 liters, and the effective prompt neutron lifetime was 7.5×10^{-5}

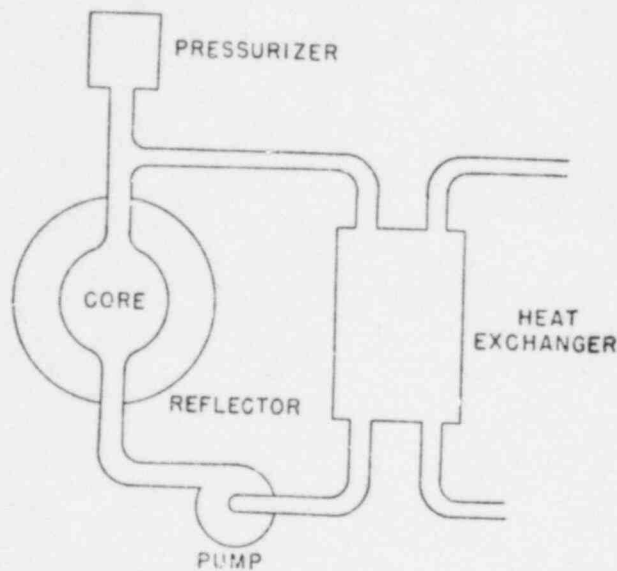


Figure 2. Diagram of homogeneous reactor system

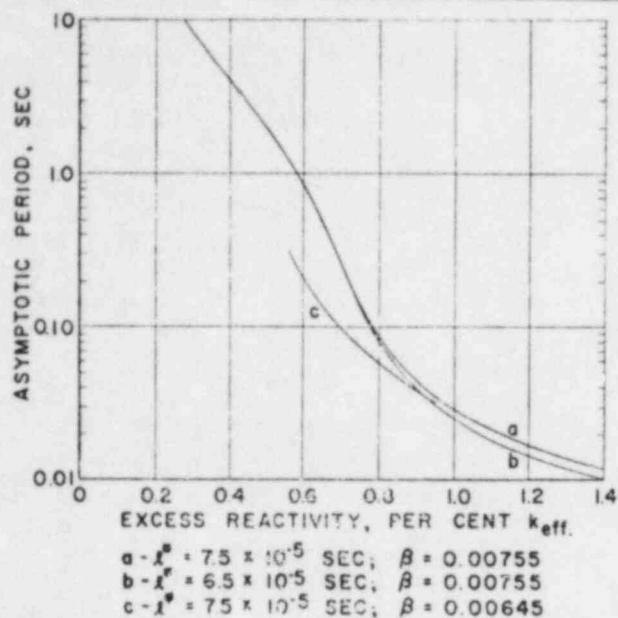


Figure 3. Relation between excess reactivity and reactor period

sec. The relation between excess reactivity and asymptotic reactor period is given by curve *c*, Fig. 3. The deficiency in delayed neutron fraction results from the circulation of the fuel solution. The reactor was pressurized to a pressure of 1000 psi.

If reactivity is added to such a reactor according to some law of time variation, $k_a(t)$, resulting in a period which is short compared to the residence time of the fuel solution in the reactor, then the law which expresses the variation of reactivity with time is simply

$$k(t) = k_0 + k_a(t) + C \int_0^t P(\tau) d\tau \quad (1)$$

where C is a characteristic constant of the reactor which includes the heat capacity and the (negative) temperature coefficient of reactivity, and $P(\tau)$ is the instantaneous reactor power. This equation must, of course, be coupled with the usual differential equations characteristic of the kinetics of the neutron chain reaction to specify the variation of reactor power with time. If the power increase is fast enough that the compressibility of the fuel solution is important, still further relations must be included to describe the dynamics of the system. Kasten has treated these considerations at some length.³ Regardless of the complications which may occur in specific reactors, the safety experiments which have been made indicate that the fundamental situation is reasonably well understood.

The reactor used for the experiments was not provided with special means for increasing reactivity rapidly, and hence the experimental situations were those relatively complex ones which would be characteristic of practical reactor accidents. Reactivity was increased experimentally by several methods: withdrawal of a weak control rod; increase of fuel concentration; raising of the reflector level;

rapid cooling of the circulating fuel; and pumping of precooled fuel solution into the reactor proper. The latter method gave the largest and fastest reactivity changes, and the results obtained by it are the ones reproduced here.

The experiments were made by stopping the circulating pump (Fig. 2), cooling the fuel solution in the heat exchanger to about 100°C, and then restarting the pump to inject the cooled solution rapidly into the reactor core, which had been maintained at a temperature of about 180°C. The severity of the experiment was adjusted by adjusting the initial power level of the reactor before the cold solution was injected. Figure 4 shows the measured power variations for two different initial power levels. Naturally, the lower initial level allows the greater increase in reactivity before the reactor begins to shut itself down and results in the higher maximum power. The temporary power decrease immediately after the pump starts is a result of the initial loss of delayed neutron emitters as the old fuel solution is displaced by the new.

This type of power transient can be characterized by specifying both the rate of addition of reactivity by the inflow of cold solution and the minimum reactor period reached during the transient. Figure 5 contains a set of theoretical curves giving the maximum power reached as a function of the minimum period reached during the transient, with rate of reactivity addition as the parameter. The experimental results are plotted in the same figure, with the rate of reactivity addition indicated by each. In view of the relatively complex experimental conditions, the agreement with theory is satisfactory.

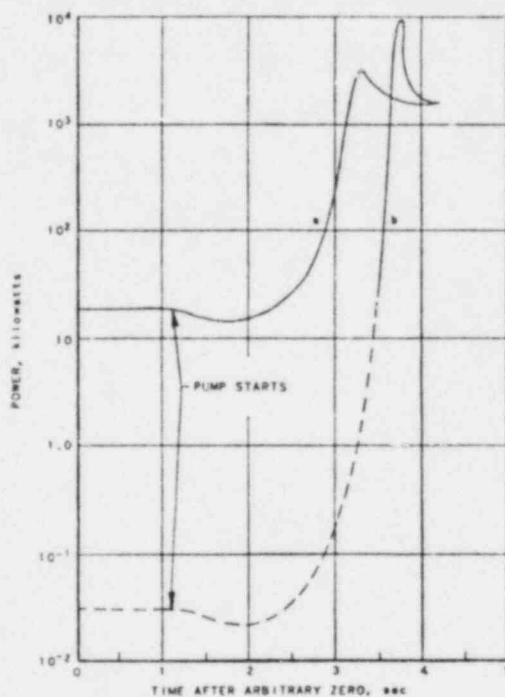
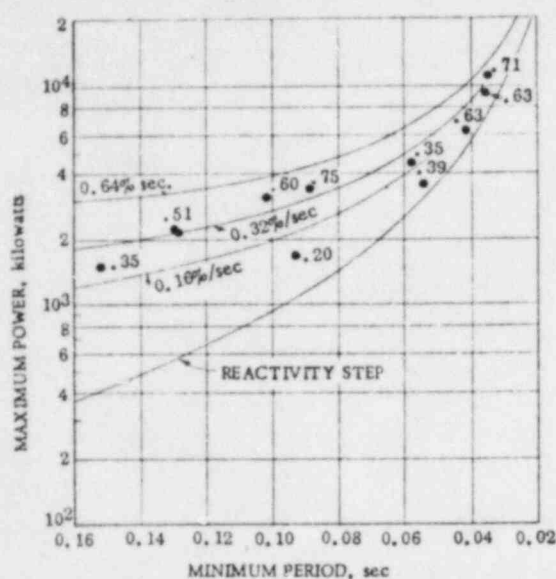


Figure 4. Power variations during injection of cold fuel solution in homogeneous reactor experiment



THE CURVES ARE COMPUTED FOR VARIOUS RATES OF REACTIVITY ADDITION. THE RATES OF ADDITION USED ARE MARKED BY THE EXPERIMENTAL POINTS.

Figure 5. Maximum power as a function of minimum period for homogeneous reactor power transients

The experiments indicated, further, that for the conditions tested the reactor would settle down to steady operation after the transient. The power level would then be determined simply by the rate of heat removal from the heat exchanger: the reactor power would be self-regulating via the temperature coefficient of reactivity.

The Supo reactor differs from the Homogeneous Reactor Experiment in that its fuel solution is not circulated; heat is removed by a cooling coil in the reactor vessel. Furthermore, the reactor vessel is not completely full of solution. The temperature coefficient is nevertheless strongly negative: about $-0.024\% k_{eff}$ per deg. The reactor has been described by King.⁴

The safety experiments were made in connection with an investigation of boiling operation of the reactor. The reactor was operated at powers of several kilowatts as a boiler, and the power under this condition fluctuated, but was self-regulating. Sudden reactivity additions up to about $0.4\% k_{eff}$ were made, under conditions of both boiling and non-boiling operation. In both cases the reactor power was self-limiting, but the excursion was terminated more rapidly under boiling conditions. The experiments indicated that there is no very long time delay in the formation of steam bubbles in a homogeneous reactor once the solution has reached saturation temperature. Once this is known, it is to be expected that steam would be by far the more effective shutdown agent for long-period power excursions at atmospheric pressure. For whereas about 5000 calories of heat are required to produce 1 cm^3 of effective void in liquid water by thermal expansion, only about 0.3 calorie is required to evaporate sufficient water to produce 1 cm^3 of steam at atmos-

pheric pressure. It is by no means evident, however, that the same situation would hold for very short period transients or at very high pressure.

EXPERIMENTS ON SOLID FUEL REACTORS

In the experiments made with solid-fuel, water-moderated reactors the expulsion of water by steam formation was the important process in transient limitation of the power. Since a quantitative theory of the process has not been developed, it is necessary to present the results and the experimental conditions in some detail.

The experiments were made in two different reactors which were also used for investigation of the steady-state characteristics of boiling reactors. The pertinent differences between the two reactors lay in their core characteristics. These differences will be described, but differences in the mechanical details of the two reactors will be ignored.

• Description of the Reactors

Figure 6 is a cutaway drawing of the first reactor, which was constructed outside and which was operated remotely from a control station half a mile away. The reactor tank was contained in a larger shield tank of ten-foot diameter which was sunk part-way into the ground and had earth piled around it for additional shielding. Adjacent to the shield tank was a pit with concrete walls in which was installed equipment for filling and emptying the reactor and shield tanks, and for preheating the water in the reactor tank. The reactor tank, four feet in diameter and about thirteen feet high, contained the reactor core, which consisted of an adjustable number of plate-type fuel elements held at the bottom by a supporting grid and at the top by a removable cover grid.

In operation the reactor tank was filled with water to a height of three to four and one-half feet above the top of the core; this water constituted the reflector, moderator, and coolant. The shield tank was filled with water only when the reactor was shut down.

The reactor contained five cadmium control rods which were operated by drive mechanisms located in the rectangular housing above the shield tank. The connection from the mechanism to the rods was through spring-loaded magnetic couplings. These couplings could be released in unison or individually, allowing the rods to drop freely downward under the acceleration of the springs plus gravity. When released, the center control rod dropped out of the reactor core to apply the excess reactivity used for the experiments. The other four rods when released dropped into the reactor core to terminate the experiments. Each rod traversed the length of the core in about 0.2 sec.

The fuel elements were made of aluminum-clad, aluminum-uranium alloy plates, of 60 mils total thickness, fastened into aluminum side plates to make boxes roughly 3 inches square. Figure 7 is a

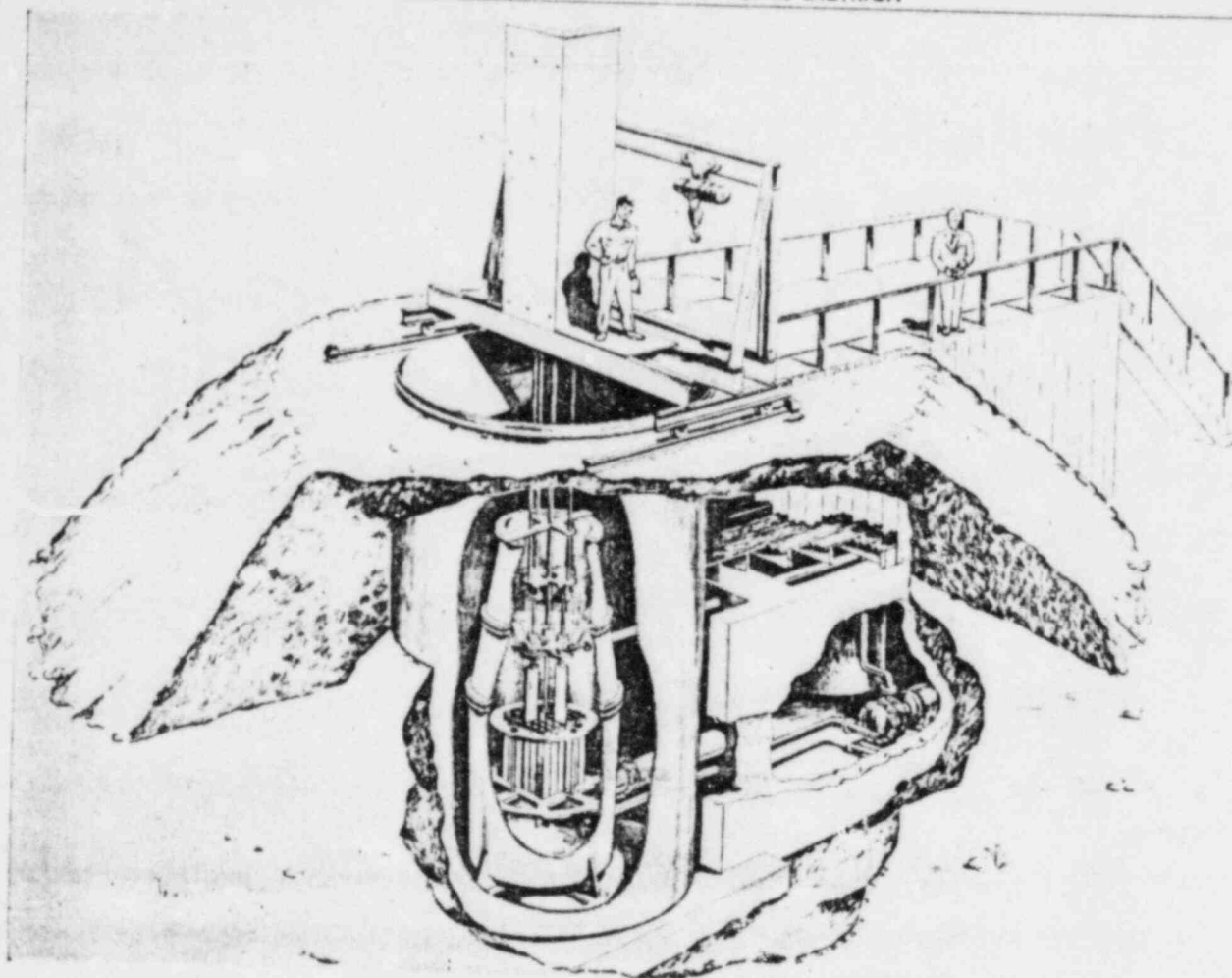


Figure 6. Cutaway drawing of reactor I

drawing of a fuel element for one of the reactors. The other reactor used elements of identical outside dimensions, but each element contained only ten of the fuel plates.

The two reactors will be designated I and II. Each reactor was loaded, for any given experiment, with the number of fuel elements which would give a convenient amount of reactivity. Typical loadings for the two reactors are diagrammed in Figure 8. Reactor II contained several elements of higher uranium content around its periphery to flatten the power distribution.

The relationship between asymptotic reactor period and excess reactivity for the reactors is given in Fig. 3 (curves *a* and *b*). For larger excess reactivities the period (τ) is given by

$$\tau = \frac{l^*}{k_{ex}(1 - \beta) - \beta} \quad (2)$$

where β is the total delayed neutron fraction and l^* the effective neutron lifetime. Other characteristics of the two reactors are summarized in Table I.

Typical Transient Behavior of the Reactors

The experiments were made by the following procedure. The reactor water temperature was adjusted

to the desired value, and the reactor was made critical at a low power (about 1 watt) by appropriate positioning of the control rods. The center control rod was then dropped out of the reactor core. The initial power was sufficiently low and the speed of rod ejection was sufficiently high so that in almost all cases the rod was completely out of the core and the reactor period reached its stable value before

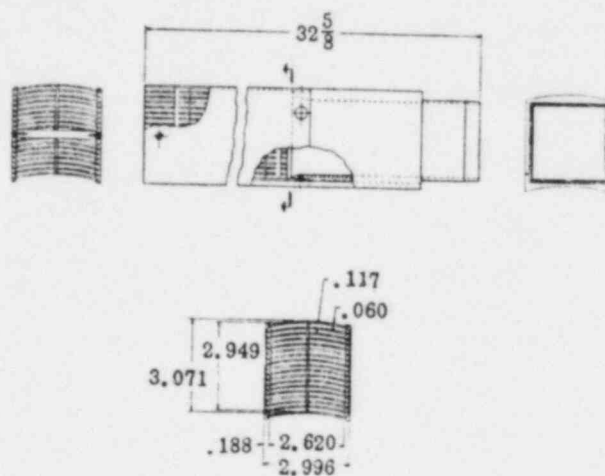


Figure 7. Standard fuel assembly

the reactor power had risen high enough to produce significant thermal effects. The power was allowed to continue to rise until the formation of steam in the reactor core reduced the reactivity below criticality and caused the power to fall to a low value. After it was evident that the power had been safely limited by the formation of steam, the remaining four control rods were dropped into the reactor to terminate the experiment, referred to as a power excursion. By proper adjustment of the number of fuel elements in the reactor core and of the positions of the four outer control rods, the reactor could be made critical with the center control rod inserted to any desired degree in the core. The magnitude of excess reactivity applied by ejection of the center rod could thus be adjusted at will.

Figure 9 is a reproduction of a typical chart from the multichannel magnetic oscillograph which recorded the data on the experiments. In this case the applied excess reactivity was $1.4\% k_{eff}$ and reactor I was used. The neutron flux (proportional to reactor power) was recorded over about three decades by three different neutron-sensitive ion chambers working through logarithmic amplifiers. The stable reactor period (τ) is indicated by the three ion chamber records as 0.0096, 0.0107, and 0.0109 second, respectively. The temperature of one of the fuel plates, which was situated at roughly the highest flux position in the core, is recorded by two fast-response thermocouples. Both of the couples were located near the position of maximum neutron flux; one was installed on the surface of the plate, the other at its central plane. There is little difference between the two temperatures, because of the high thermal conductivity of the thin plate.

The ion chambers, which were calibrated in terms of absolute power by thermal methods, indicate that the reactor power reached a maximum value of 220 megawatts before the formation of steam checked

Table I. Comparison of Reactors I and II

	Reactor I	Reactor II
Ratio, $\frac{\text{volume aluminum in core}}{\text{volume water in core}}$	0.626	0.422
U^{235} content per fuel element	138.6 gm	93.4 gm or 157.3 gm
Number of fuel plates per element	18	10
Plate spacing (between center lines)*	0.177 inch	0.324 inch
Measured reactivity loss with temperature increase:		
80°F to 200°F	0.82% k_{eff}	0.45% k_{eff} *
80°F to 280°F	1.93% k_{eff}	0.76% k_{eff} *
80°F to 420°F	--	1.57% k_{eff} *
Calculated loss of reactivity caused by replacement of 10% of core water by steam, at 200°F	2.4% k_{eff}	1.0% k_{eff} *
Effective neutron lifetime (l^*)	6.5×10^{-6} sec	7.5×10^{-6} sec*

* These values apply to the case in which the reactor is loaded only with fuel elements of low uranium content.

the rise. Further generation of steam reduced the reactivity below the critical value, and caused the power to decrease very rapidly to a value of about 0.2 megawatt.

Once the initial power excursion has been checked by boiling in the reactor the specific power variation depends both quantitatively and qualitatively upon the amount of excess reactivity to which the reactor was initially subjected, and upon the bulk temperature of the reactor water. Figure 10 contains tracings from excursion records for reactor I similar to those of Fig. 9, but of longer duration. They summarize the typical behavior of the reactor for various amounts of applied excess reactivity when the reactor water is initially at saturation temperature. When the excess reactivity applied is low, corresponding to a reactor period of about 0.03 sec or longer, the reactor power after the initial surge settles down to a relatively steady value in the neighborhood of half a megawatt (top curve, Fig. 10). For this type of excursion the self-regulating characteristic of the reactor operates rapidly enough to stabilize the power at a steady value characteristic of the amount of applied excess reactivity. After the power has reached this steady value, further reactivity could, of course, be applied, and the reactor would continue to operate stably in steady boiling at a higher power.

If the excess reactivity which is applied by ejection of the control rod exceeds that corresponding to a period of 0.02 or 0.03 sec, the initial power excursion is followed by a series of qualitatively similar excursions of smaller amplitude, which occur at intervals of about 1 sec (second curve, Fig. 10). The amplitudes of the successive excursions, although they vary in an irregular manner, have no sustained tendency to increase or decrease. This

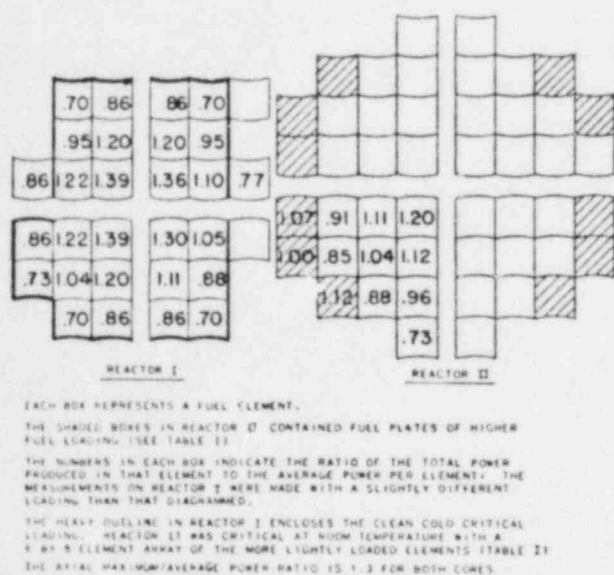


Figure 8. Core loading diagrams for reactors I and II

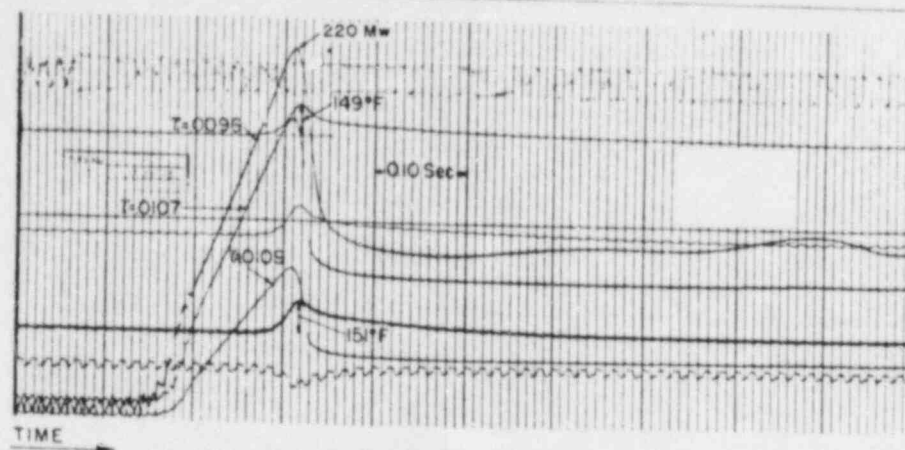


Figure 9. Typical record of power excursion

type of operation will hereafter be referred to as "chugging."

When the applied excess reactivity was greater than that corresponding to about a 0.01-sec period, the chugging was no longer observed, and the power after the first surge remained at a low value. This permanent shutdown was no doubt the result of expulsion of sufficient water from the reactor tank to partially uncover the reactor core. The occurrence of this behavior in other reactors would, of course, depend upon the specific design of the reactor in question.

When the applied excess reactivity was increased to about 2% k_{eff} to give periods in the 0.005-sec range, the qualitative behavior of the reactor power remained the same, but the fuel plate temperature did not drop immediately after the power surge (bottom curve, Fig. 10). The fuel plate temperature remained high for almost a second after the power surge and then decreased by small jumps, as though the plate had been blanketed by steam for some time after the power excursion.

Experiments of this type were not carried to periods shorter than about 0.013 sec when the reactor water was cooler than the saturation temperature. With this condition, which will hereafter be called the subcooled condition, chugging was never experienced. In all cases after the initial power excursion the reactor power stabilized at some more or less steady value. Figure 11 is a record of such an experiment on reactor I, in which the initial period was 0.014 sec. Although the reactor power oscillated after the excursion, the oscillation amplitude was very much less than that for typical chugging operation.

Some of the details of the nuclear and thermal behavior of the reactor during a power excursion are illustrated by Figs. 12a and 12b, which apply to the subcooled reactor I for excursions of two different periods. The curves show the time variation of reactor power, on a linear scale, and the fuel plate surface temperature. In these experiments the fuel plate, with thermocouple attached, was coated with a thermally insulating plastic over a section of

its length. The temperature of this section of the plate is also included in the figures. This temperature, except for the effect of a small heat loss through the thermal insulation, is proportional to the total nuclear energy liberated in the plate. The point at which there is a sharp deviation between the temperature of the bare section and that of the insulated section evidently marks the beginning of rapid steam formation at the bare plate surface. Up until this time the temperature of the bare plate, like that of the insulated plate, is roughly proportional to the time integral of the reactor power.

Since no single fuel plate can produce sufficient steam to shut the reactor down it is evident that the time relationship between peak reactor power and peak temperature of the bare fuel plate, as well as the ratio of maximum bare plate temperature to maximum insulated plate temperature, will depend upon the local value of power density at the plate location relative to the power density elsewhere in the reactor. The plate used for these measurements was located at or near the maximum power density, and the thermocouples were installed near the point of maximum power density in the plate. Nevertheless, Fig. 12a indicates that for long-period excursions

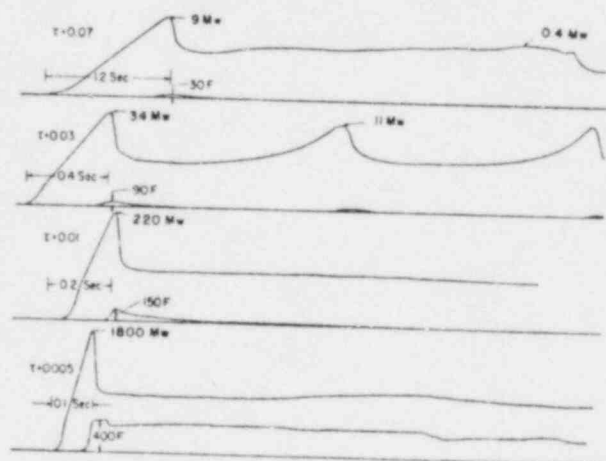


Figure 10. Representative records of excursions at saturation temperature with various excess reactivities

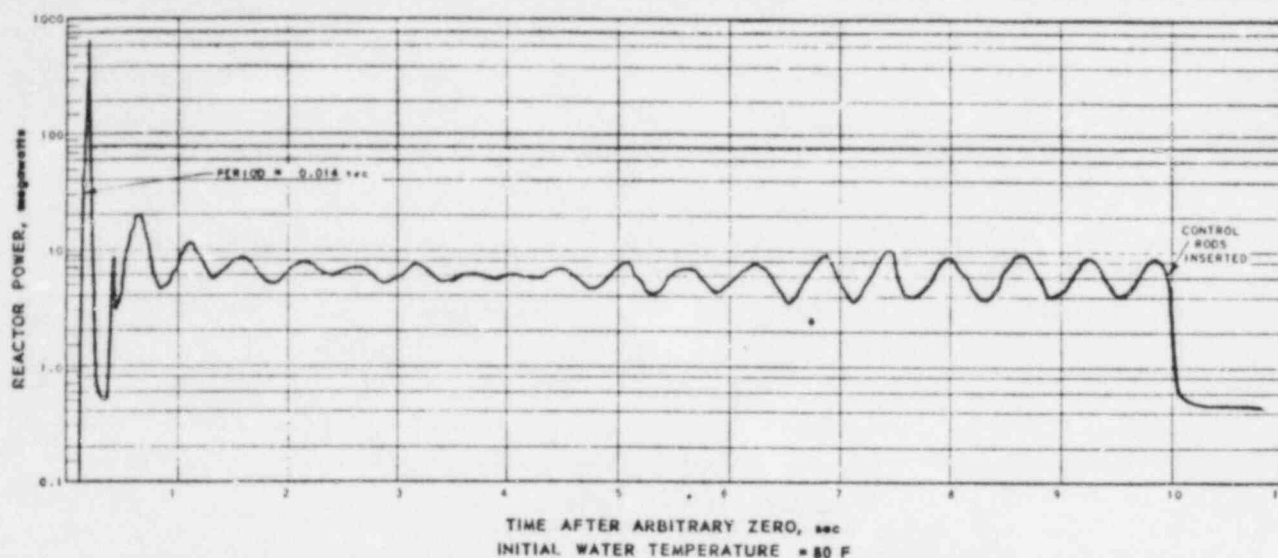


Figure 11. Reactor power variation during 10-second run following initial excursion of 14-millisecond period

sions other plates were responsible for the first formation of steam, since power began to decrease before plate temperature reached saturation.

Effects of Several Variables on Power, Energy and Fuel Plate Temperature

Both the total nuclear energy liberation and the maximum fuel plate temperature reached during a power excursion depend upon the amount of excess reactivity involved in the excursion. In the following presentation, the reciprocal of the stable reactor period is used to characterize the excess reactivity. The relation between the two is given in Fig. 3. In Fig. 13 the total energy† liberated by the power

† Throughout the section on solid fuel reactors the term energy will be used to refer to the prompt fission energy which is converted to heat in the fuel plates. The total energy release, including delayed emission and energy converted to heat directly in the reactor water, is about 15% higher. A consistent definition is used for reactor power. By the total energy of a power excursion is meant the energy liberation up to the time of the first minimum in reactor power.

excursion and the maximum fuel plate surface temperature are plotted as functions of the reciprocal period for the case in which the reactor water was at saturation temperature before the excursion began. The shapes of the two curves are quite similar; in fact, the maximum fuel plate temperature rise is roughly proportional to the energy of the excursion for all periods shorter than about 0.03 sec, and the peak temperature corresponds to the temporary storage in the fuel plate of 60 to 70 per cent of the total energy of the excursion.

The energy liberation and maximum fuel plate temperature for the condition in which the reactor was initially at room temperature are given, for reactor I, in Fig. 14. The plotted temperature is the maximum above saturation temperature at atmospheric pressure rather than the total temperature rise. The fuel plate temperature is somewhat higher (and the energy release is much higher) for a given reactor period than in the case of saturated reactor water.

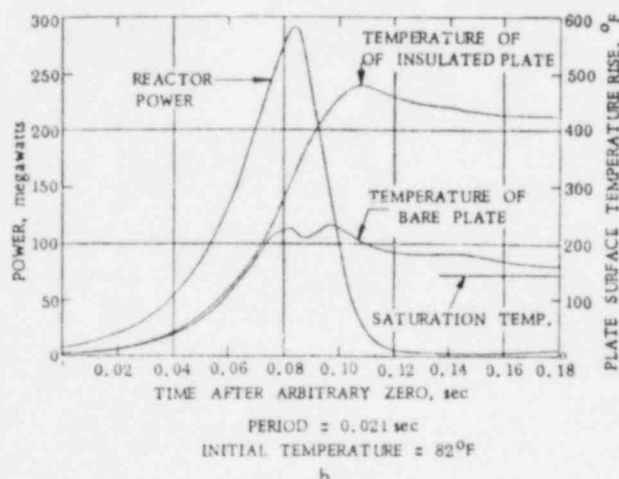
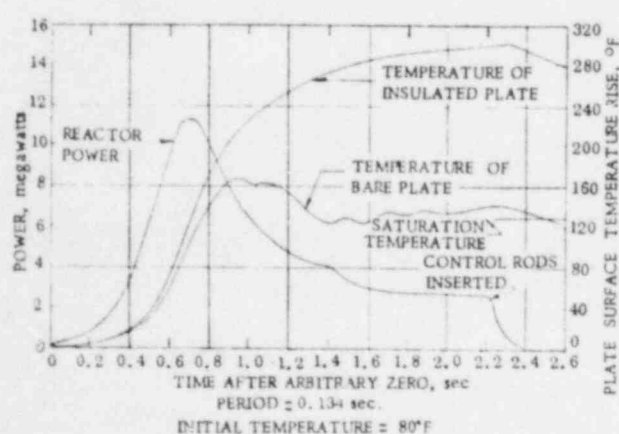


Figure 12. Power and fuel plate surface temperature rise during power excursions

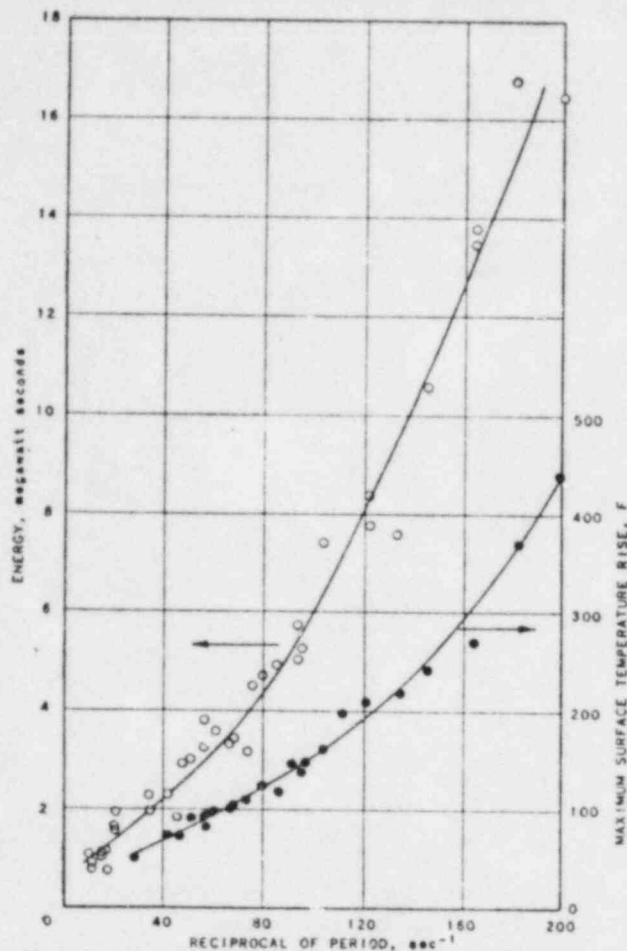


Figure 13. Maximum temperature rise at fuel plate surface and total energy release during power excursions of various exponential periods. Reactor I, at saturation temperature and atmospheric pressure

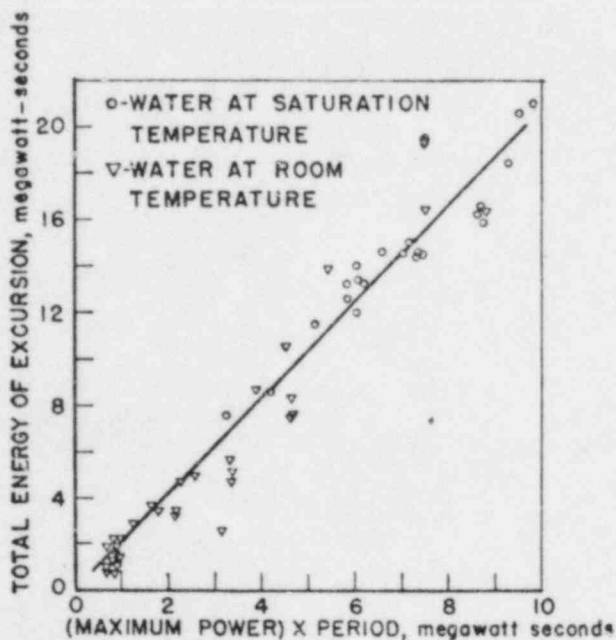


Figure 15. Relation of total energy, maximum power, and period. Reactor I

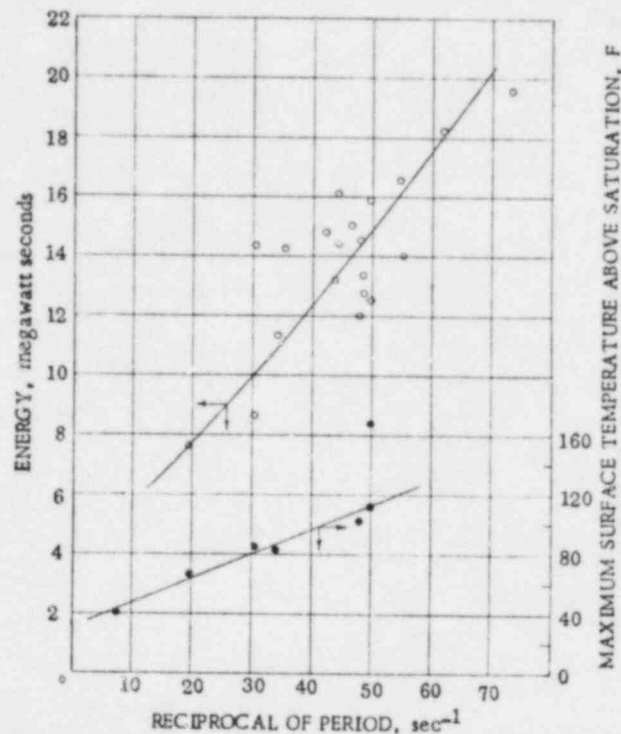
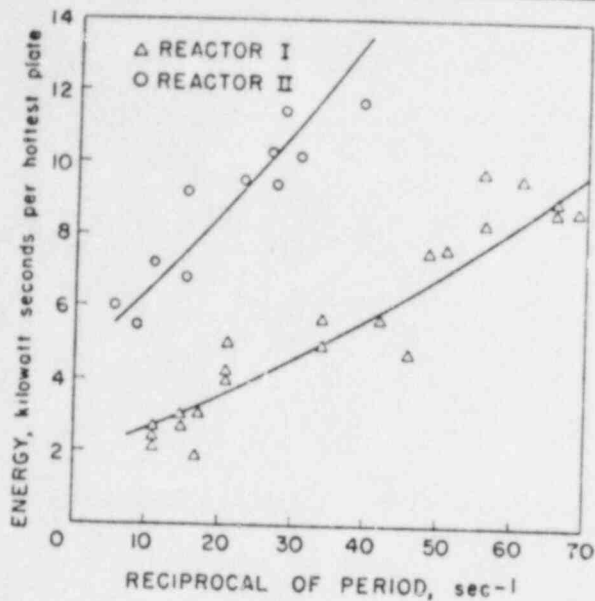


Figure 14. Maximum temperature of fuel plate surface and total energy release during power excursions of various exponential periods. Reactor I, at room temperature (approx. 80°F) and atmospheric pressure

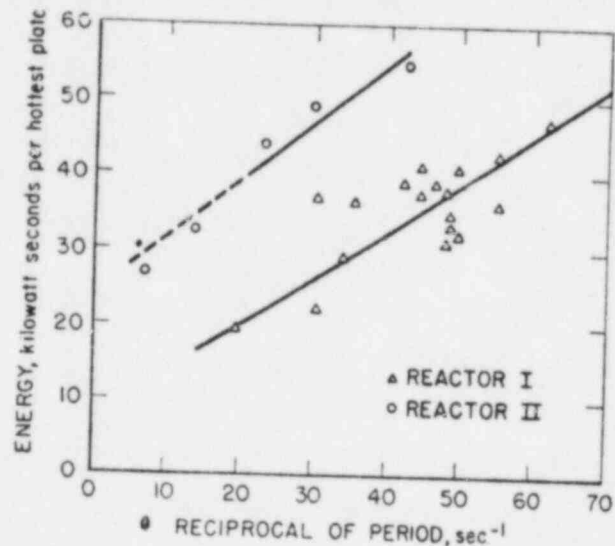
For the cases of both saturation temperature and room temperature water the total energy liberated during the power excursion was nearly proportional to the product of the maximum power and the period. These quantities are plotted in Fig. 15 for the experiments made with reactor I. The slope of the line is about two.

In comparing the behavior of the two reactors, I and II, which differed in core size, it is more informative to compare energy density or energy per fuel plate than to compare total energy. The latter comparison has been made. In Fig. 16 the energy release per fuel plate is compared, as a function of reciprocal period, for the two reactors: Fig. 16a is for the case of saturated reactor water, and Fig. 16b for the case of room temperature water. The dashed portion of Fig. 16b is an upper limit only. The plotted energy release is that of the fuel plate in the position of highest neutron flux. In comparing the behavior of the two reactors, reference should be made to Table I. Note that the volume of water associated with each fuel plate is about twice as great for reactor II as for reactor I. If the energy release per unit volume of water is compared, the values for reactor II are only slightly higher than those for reactor I, despite the fact that the steam coefficient of reactivity is more than twice as great for reactor I as for reactor II.

In reactor II the investigation of power transients was extended to reactor pressures as high as 300 psi. The pressurization of the reactor was by the vapor from the reactor water. Consequently, only the satu-



REACTOR WATER AT SATURATION TEMPERATURE
AND ATMOSPHERIC PRESSURE

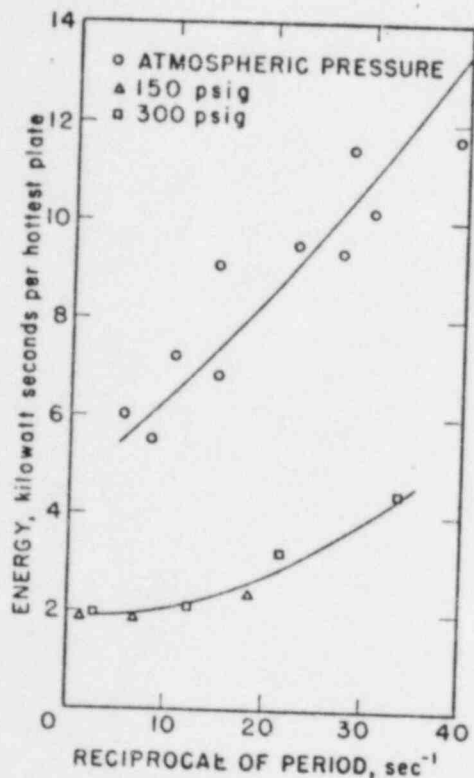


REACTOR WATER AT ROOM TEMPERATURE
AND ATMOSPHERIC PRESSURE

Figure 16. Energy release of hottest fuel plate during power excursions in reactors I and II; (a) left, reactor water at saturation temperature and atmospheric pressure; (b) right, reactor water at room temperature and atmospheric pressure

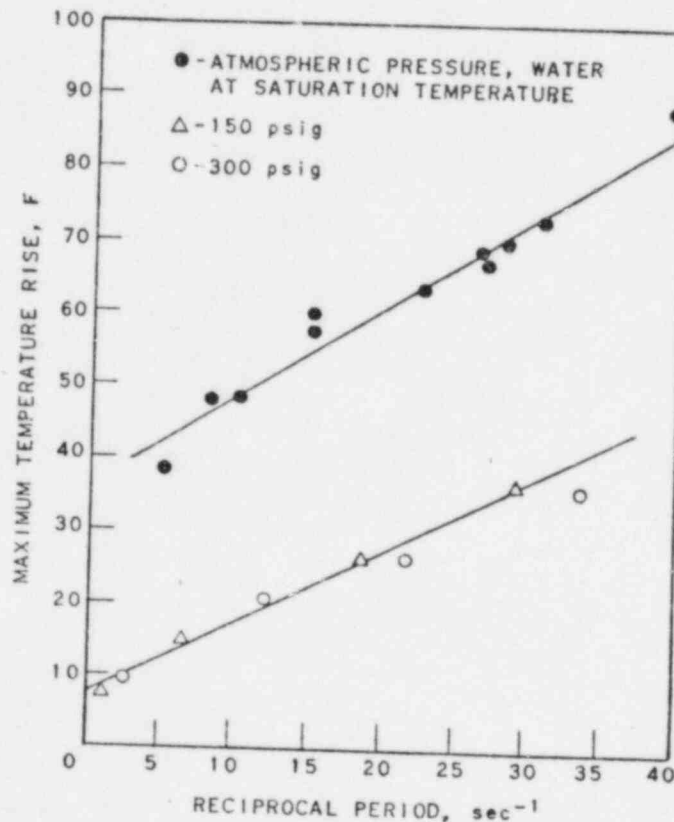
rated condition could be investigated. The power excursions were run with the reactor tank completely closed. In no case did the pressure in the steam space above the reactor water rise by more

than about 5 psi as a result of an excursion. The effect of pressurization is to decrease both the energy released in an excursion of given period and the maximum temperature rise of the fuel plates (Fig. 17).



WATER AT SATURATION TEMPERATURE

REACTOR II



REACTOR II

Figure 17. a, left, energy release of hottest fuel plate during power excursions at different pressures; b, right, maximum fuel plate temperature rise during power excursions: Comparison of unpressurized and pressurized cases

The Destructive Experiment

In the short period experiments with reactor I at atmospheric pressure, the steam pressure which built up in forcing the water rapidly from the reactor resulted in permanent deformation of the fuel plates. Because of this effect it was not possible to extend the experiments to periods shorter than about 0.005 sec without damaging the reactor to the point where it became unusable. Despite this mechanical damage the maximum temperatures reached by the fuel plates did not approach the melting temperature. It was decided that the reactor, which by this time had fulfilled its other purposes, should be sacrificed in an experiment which was violent enough to melt the fuel plates. For this purpose a control rod worth 4% k_{eff} was completely ejected from the reactor core. To increase the severity of the experiment it was run with the reactor water at room temperature. Although the ejection of the rod required only about 0.2 sec, the rod was only about 80 per cent out of the core when the reactor power reached its peak value. The minimum period resulting from the ejection was 0.0026 sec.

The power excursion melted most of the fuel plates. The pressure resulting from the molten metal in contact with the reactor water burst the reactor tank and ejected most of the contents of the shield tank into the air. The sound of the explosion at the control station, half a mile away, was comparable to that resulting from the explosion of 1 to 2 pounds of 40 per cent dynamite on the bare ground at the same distance. Figure 1b, taken from motion picture records of the experiment, shows one stage of the explosion, as compared to the nondestructive ejection of water from the reactor when the period of the excursion was 0.005 sec.

The total energy release during the excursion as determined by calibrated cobalt foils in the reactor core, was 135 megawatt seconds. Other data taken during the excursion are less reliable because of the violent mechanical effects of the explosion. Figure 18 is a reproduction of the transient record. The absolute values on the power curve (A) may be in error by 30 or 40 per cent, and the shape of the decreasing portion may not be correct. The fuel-plate thermocouple (curve B) failed long before peak power was reached. Curve C is a temperature record from an insulated fuel plate installed some distance outside the reactor core. It was used for an auxiliary determination of total energy and does not give good transient information, as it was connected to a relatively slow recorder. A pressure transducer, which was installed in the reactor tank adjacent to the reactor core, failed before it recorded a pressure of significant magnitude (curve D). Analysis of the mechanical damage of the transducer, however, indicated that the peak pressure was at least as high as 6000 psi, and was probably higher than 10,000 psi.

It was evident from examination of the reactor debris that many of the fuel plates had been prac-

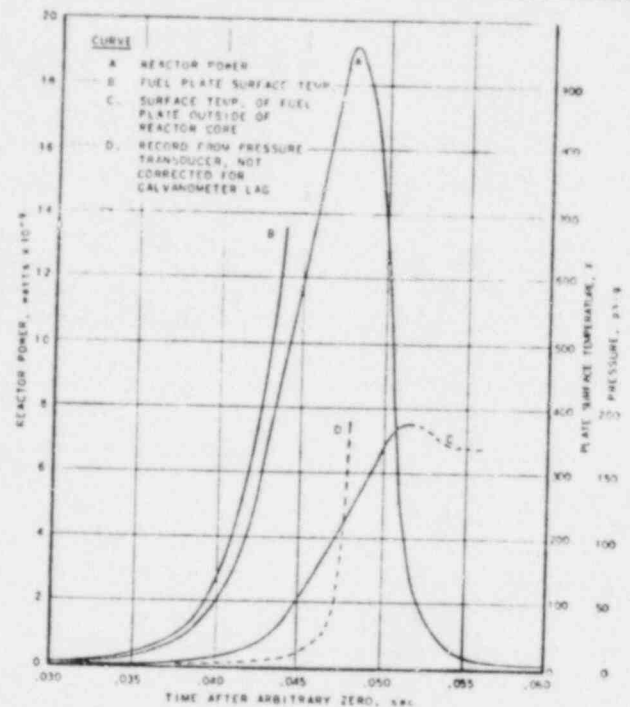


Figure 18. Replot of records from destructive experiment

tically completely melted. Others, evidently those at the edge of the core, had been only partly melted, and portions of them remained fastened to the side plates of the fuel elements (Fig. 19). Some of the fragments which had evidently been molten appeared as spongy metallic globules (Fig. 20). Other fragments appeared to have been molten inside, while the outside clad remained solid (Fig. 21).

Most of the heavy debris fell to the ground near the shield pit. The control rod drive mechanism, which weighed about a ton, fell on the side of the earth shield, after having been thrown about 30 feet into the air. Recognizable fuel plate fragments were thrown as far as 200 feet from the reactor site. Surveys of the total fission-product radioactivity of all the debris indicated that practically all of the fuel originally in the reactor could be accounted for within a radius of 350 feet around the original reactor location. Although these measurements necessarily lacked precision, they showed that no large fraction of the reactor core material left the site in the form of airborne material. At the time of the experiment, the wind velocity was 8 miles per hour at ground level, and 20 miles per hour at 250 feet above ground. Fifteen minutes after the experiment the total beta plus gamma activity level, 3 feet above ground, at a point 0.8 mile directly downwind of the reactor, was 5 mr/hr. At all points farther from the reactor the effects of fall-out were less than this value. Momentarily during the explosion, a gamma dose rate in excess of 400 mr/hr was indicated on a survey meter half a mile from the reactor. This indication decayed rapidly; the total dose received at the half-mile point (cross wind) was less than 10 mr.

Both the observed radiation intensities and the mechanical damage were roughly consistent with the measured nuclear energy release of 135 megawatt seconds. Although the explosion was spectacular, its effects were comparable to those which could be caused by a moderate amount of chemical explosive. The destruction of the reactor tank was not surprising, since it was constructed of relatively thin ($\frac{1}{2}$ -inch) steel. Most of the equipment outside the shield tank was either undamaged or repairable, and much of it, including the control rod drive mechanism, was decontaminated, reconditioned, and re-used on reactor II.

There was no evidence that the power-limitation process in the destructive experiment differed qual-



Figure 19. Fuel element side plate with attached cluster of fuel plate fragments



Figure 20. Pellet of spongy aluminum-uranium mixture



Figure 21. Fragments of fuel plates

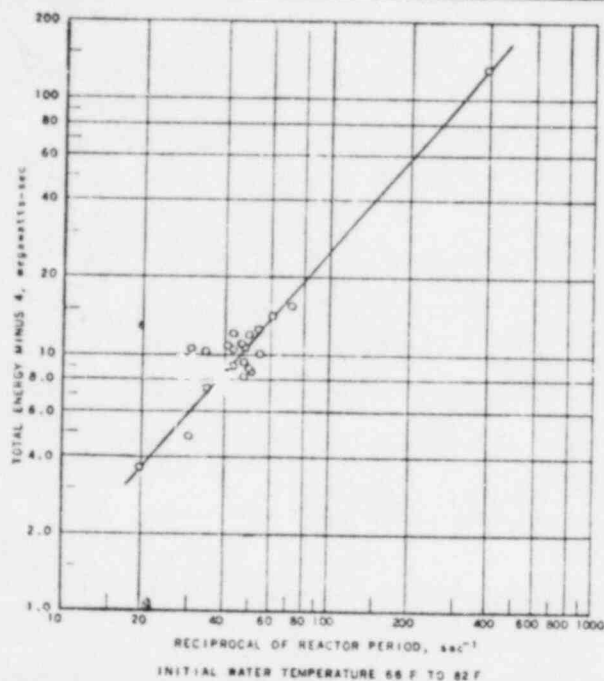


Figure 22. Total energy of excursion minus energy required (4 Mw-Sec) to raise temperature of center of average plate to the boiling point

itatively from that which was effective in the earlier, nondestructive experiments. It was quite evident that the nuclear power release was terminated at an early stage of the explosion; indeed, high-speed motion pictures recorded the light flash emitted by the reactor as it reached high power and showed that it was extinguished before any ejected material appeared above the top of the shield tank. The flash lasted about 0.003 second. The energy stored in the fuel plates as sensible heat and latent heat of fusion during the relatively short nuclear power burst was, of course, released during the much longer explosion process.

Figure 22 is a plot of energy released as a function of reciprocal period for all the power excursions made with cold water in reactor I. In plotting the curve, a constant energy of 4 megawatt-seconds has been subtracted from each value. This is the quantity of energy which has been released up to the time when the center temperature of the average fuel plate has reached the atmospheric boiling point of water. The highest point on the curve, which refers to the destructive experiment, does not appear inconsistent with the other values.

Discussion

The experiments that have been described prove that the reactors investigated possess a high degree of inherent safety, and indicate that it is possible to design practical reactors of these types which will be safe against any reactivity accident which can occur in practice. In this connection, the consistent and regular behavior of the reactors during the experiments is reassuring. Although such behavior would be expected in the case of the homogeneous

non-boiling reactor, anomalies would not have been surprising in the cases where shutdown depends on the rapid formation of steam. Actually, in the entire series of some two hundred experimental runaways, no inconsistencies of behavior were observed which could not be attributed to instrumental errors resulting from rather difficult experimental conditions.

A few general remarks may be made in connection with the application of the results to the estimation of the runaway behavior of other reactors. The behavior of the homogeneous, non-boiling reactor may be considered to be typical of the case in which the loss of reactivity is roughly proportional to the time integral of the transient reactor power. Thus the behavior of power as limited by a negative "prompt"† temperature coefficient in a solid-fuel reactor would be expected to be qualitatively quite similar. Quantitatively, of course, such "prompt" coefficients are generally small and their effectiveness is limited. In inferring the behavior of other steam-limited reactors from the results presented here, it should be remembered that the reactors used had fuel plates of such high thermal conductance that in all the non-destructive experiments the metal of the plate represented no important impedance to the transfer of heat to the water. Certainly the transient behavior will be strongly modified and the effectiveness of steam limitation of power will be decreased if a departure is made from this condition, as it may well be in certain power reactor designs. In such a case the difference between the behavior of the reactor with saturated water and with subcooled water may be a very important one, and reactors designed for operation as boiling reactors may have important safety advantages.

No complete theoretical treatment of the transient limitation of power by steam has yet been developed. Attention should be called to some of the general experimental results which will have important bearing on the formulation of such a theory. Perhaps the most obvious is that there is no apparent simple relation between the energy liberated during a transient and the energy content of a steam volume of the size necessary to remove the applied excess reactivity. For example, the heat of vaporization of sufficient steam to fill the entire core volume of reactor I at atmospheric pressure was only 0.087 megawatt-second, very much less than the energy generation in any of the experiments. Furthermore, in extending the experiments from reactor I to reactor II, the total energy release did not increase in proportion to the volume of steam required to produce a given decrease of reactivity. Finally, when the experiments were extended from atmospheric pressure to 300 psig (Fig. 17) the energy release for a transient of given period *decreased* by almost

a factor of 3, whereas the energy content of unit volume of steam *increased* by a factor of 16.

Certainly one of the important considerations is that although the energy required to vaporize a significant volume of steam is small, the temperature differences required to transfer this heat to the water in the short time available during the transient may be large. The heat capacity of all the fuel plates of reactor I was 0.05 megawatt-second per degree F, and the heat capacity of all the water in the core was 0.15 megawatt-second per degree F. Thus the establishment of steep temperature gradients required the expenditure of significant quantities of energy. A further consideration is that relatively high steam pressures must be built up to expel the water from the reactor core rapidly enough to terminate the short-period transients. A few pressure measurements were made in the reactor core which indicated that the peak transient pressure increase was about 15 psi during a transient of period 0.034 sec, and of the order 100 psi during the transient of period 0.005 sec. Consequently, even when transients are run with the reactor water at the ambient saturation temperature, the water is effectively in the subcooled state during the power excursion. Not only must the fuel plates be heated to temperatures corresponding to the transient saturation condition, but steam, once it forms at the hot fuel plate surface, may recondense in the cooler water.

Approximate theoretical treatments of the steam transient have been made by various workers to extend the results of the experiments to other reactor designs. Golian *et al.*§ have assumed that steam is formed in a laminar layer immediately adjacent to the fuel plate, and that the thickness of the layer grows by conductive transfer of energy across the layer to the water boundary. Edlund and Noderer¶ employ a model in which the transient pressure rise plays an important part. It is assumed that the heat transferred to the water is contained in a layer adjacent to the fuel plate, the average temperature of which equals the transient saturation temperature. The layer, which contains water and steam, grows in thickness as though by a thermal conductive process, but with a thermal diffusivity determined empirically from the experiments. Both approaches have shown reasonable agreement with the results of the experiments on reactor I.

The semi-empirical approach to extension of the experimental data is facilitated by the circumstance that all of the experimental power transients have quite similar shapes if time is measured in the non-dimensional unit of asymptotic reactor period. This characteristic is illustrated by Fig. 15. Despite this regularity, however, detailed examination of the power curves reveals significant differences in behavior as the conditions of the experiment are changed. In Fig. 23 the power curves for three

† The "prompt" coefficient is that component of the temperature coefficient of reactivity which depends on fuel-element temperature alone. It results from thermal expansion of the fuel element and Doppler broadening of resonances.

§ US Naval Research Laboratory.

¶ Oak Ridge National Laboratory.

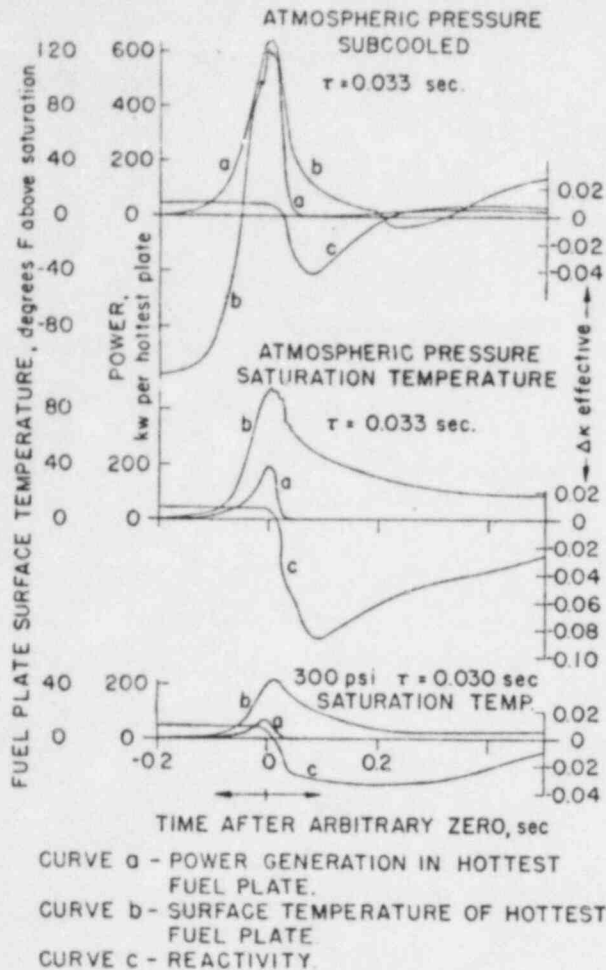


Figure 23. Time variation of power, fuel plate temperature, and reactivity during power excursions on reactor II

different reactor II transients of about the same period are reproduced along with the fuel-plate temperature records. The power curves have been analyzed to yield the variation of reactivity with time. The differences in magnitude of the power and temperature variations with subcooling and with pressure are striking, but it is interesting to note also the reactivity variations. At atmospheric pressure and saturation temperature the reactor shuts itself down by more than 8% k_{eff} . In the subcooled condition the degree of subcriticality achieved is considerably less, and the recovery to criticality is

rapid, no doubt because of condensation of the steam. At 300 psi the degree of shutdown is again small, evidently because of the relatively low heat storage in the fuel plates. The recovery to criticality is, however, quite slow. A striking characteristic in all cases is the small fraction of the total reactivity change which suffices to stop the initial power rise. As is to be expected theoretically, this is equal to the initial prompt excess reactivity.

The limitation of power in fast transients is one aspect of the self-regulating behavior of reactors with strong negative power coefficients of reactivity. Experience with the solid-fuel boiling reactors (e.g., Fig. 10) has shown that the self-regulation is normally stable but that a type of instability (chugging) can result if the reactor is subjected to sufficiently large reactivity variations. Fortunately, even under chugging conditions the power is limited and does not reach a dangerous level. It is no doubt true for all self-regulated reactors that for some amplitude of reactivity excitation the characteristic rates of change of power are too rapid for the self-regulating process to maintain control, and instability will result. In the boiling reactors it is believed that the rate of escape of steam from the core, rather than the rate of formation of steam, represents the limiting time constant in the regulating process. Consequently, in subcooled boiling operation, where steam can leave by condensation, the range of stability is increased (Fig. 11). In any case, however, the range of stable self-regulation of the reactors investigated is more than adequate for practical use and probably exceeds that which can be attained practically with artificial control systems.

REFERENCES

1. Untermeyer, Samuel, *Direct Steam Generation for Power*, Nucleonics, Vol. 12 No. 7, 43 (July, 1954).
2. Lottes, P. A., *Boiling Studies at Argonne Relative to Boiling Reactors*, Proceedings, 1955 Conference on Nuclear Engineering, University of California, Los Angeles; California Book Co., Ltd., Berkeley, California.
3. Kasten, Paul R., *Homogeneous Reactor Safety*, Proceedings, 1955 Conference on Nuclear Engineering, University of California, Los Angeles; California Book Co., Ltd., Berkeley, California.
4. King, L. D. P., *The Los Alamos Homogeneous Reactor, Supo Model*, LADC-1081 (Feb. 2, 1952).

Fundamental Aspects of Nuclear Reactor Fuel Elements

Donald R. Olander

*Department of Nuclear Engineering
University of California, Berkeley*

Prepared for the Division of Reactor Development and Demonstration
Energy Research and Development Administration

1976

Reprinted by the Technical Information Center
U. S. Department of Energy

Published by
Technical Information Center
Energy Research and Development Administration

Chapter 15

Fission-Gas Release

15.1 INTRODUCTION

Fission gases are considered to be released from the fuel when they reach any space that is connected to the free volume within the fuel pin. Gas collection zones include the fuel-cladding gap (if there is one), the central void, and porosity within the fuel which communicates directly with the fuel-pin gas space. Cracks or interlinked gas bubbles or pores are the most important type of open porosity. The following major differences exist between the gas in closed, gas-filled cavities in the fuel and that in the empty spaces:

1. Once the gas is released, the probability of its reentering the solid from the free volume is virtually nil.
2. The gas pressure in open porosity is equal to that in the free volume of the fuel pin. Because of the insolubility of xenon and krypton in solids, there is no direct influence of plenum fission-gas pressure on the rate of gas escape from the fuel.
3. While the fission gas contained by the fuel tends to cause swelling, fission gas that has been released promotes shrinkage by pressurizing the solid and thereby encouraging collapse of internal porosity and bubbles.

A summary of gas-release theories and the relationship of release and swelling was presented in Sec. 13.1. Regimes of gas release can be classified according to the extent to which they depend on fuel temperature and temperature gradient.

At low temperatures (less than about 1300°K), the mobility of fission-gas atoms is too low to permit appreciable gas-atom movement, either to release surfaces or even to sites where bubbles can form. The fission gases are frozen into the matrix of the solid, and only the gas formed very close to an external surface can escape. Release occurs both by direct flight from the fuel while the gas atom is still an energetic fission fragment (recoil) or by interaction of a fission fragment, a collision cascade, or a fission spike with a stationary gas atom near the surface (knockout). These release mechanisms are independent of both temperature and temperature gradient. Since they affect only the outer layer of the fuel (within $\sim 10\text{ }\mu\text{m}$ of the surface), the fraction of the total fission gas released by recoil or knockout is quite small.

At temperatures between 1300 and $\sim 1900^{\circ}\text{K}$ (in UO_2), atomic motion of the gas atoms in the solid becomes important, and release by diffusion to escape surfaces can

occur. Release by atom migration is described by the equivalent-sphere model or variants that include immobilization of gas atoms by natural or radiation-produced defects within the solid coupled with resolution of gas from the traps. In this temperature range bubbles can form, but they are not sufficiently mobile to migrate appreciable distances under the influence of the temperature gradient. Gas that collects at grain boundaries can be released if the intergranular bubble density is large enough to cause interlinkage that provides pathways to open porosity or to sufficiently weaken the grain boundaries so that stress in the fuel causes cracking.

At temperatures greater than 1900°K , gas bubbles and closed pores are sufficiently mobile to be driven by the thermal gradient over distances comparable to grain sizes in periods of days or months. Fission gas is released when either of these types of cavities reach a crack or other surface that communicates directly with the free volume in the fuel element.

15.2 EXPERIMENTAL TECHNIQUES

The quantities of xenon and krypton released from irradiated fuels are measured either by postirradiation annealing experiments or in-pile tests.

15.2.1 Postirradiation Annealing

In postirradiation annealing experiments, a sample is subjected to light irradiation at low temperature to provide an initial concentration of gas atoms in the solid and then is transferred to an apparatus where it can be held at high temperatures. The amount of gas released is monitored as a function of time. When fissile material such as UO_2 is studied, the initial irradiation is usually conducted in a nuclear reactor. The specimen may consist of a fuel pellet, powder, or small chips of fused material. The surface area for release is measured either by standard sieving techniques or by gas-adsorption methods. Evolution of one or more of the radioactive fission gases marked with an asterisk in Table 13.3 is followed in the anneal step.

Alternatively, radioactive gas may be injected into the solid by bombardment in the form of $\sim 10\text{ keV}$ ions produced by an accelerator. The solid to be studied need not contain a fissile species and is usually in the form of

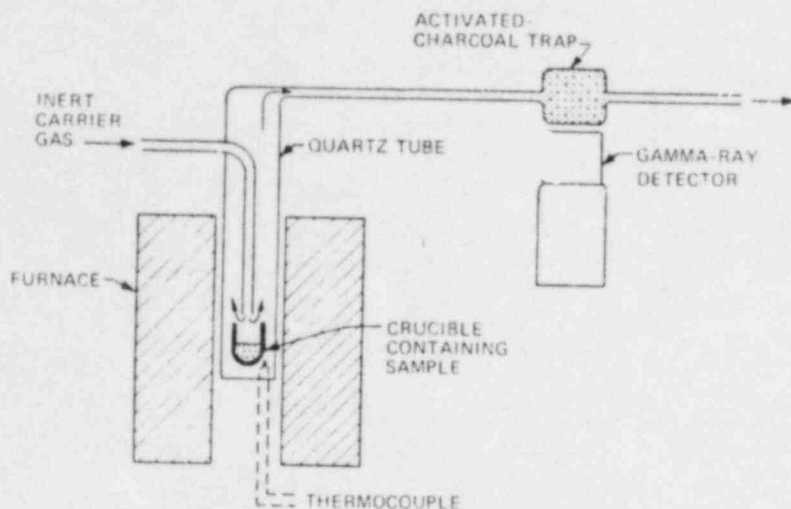


Fig. 15.1 Apparatus for measuring fission-gas release in postirradiation annealing experiments.

single-crystal disks. The disadvantage of this method is that the distribution of embedded gas is very nonuniform, being concentrated in a relatively thin layer near the surface. Reactor irradiation, on the other hand, produces a nearly uniform distribution of fission gas in the sample.*

Analysis of the radioactive gases emanating from the irradiated samples is the same for both methods of gas introduction. As shown in Fig. 15.1, the sample is placed in a furnace, and the released gases are transported to a gamma-ray detector by a stream of inert sweep gas. The detection system can be augmented by a charcoal trap to concentrate the radioactivity and thereby improve counting statistics. Alternatively, the activity remaining in the sample following each anneal can be measured. The total gas content of the sample is obtained by melting or dissolving the solid after the experiment has been concluded and adding the activity collected in this step to cumulative activity released during the anneals.

The postirradiation annealing technique using reactor-irradiated fuel samples, of which the work of Matzke and Springer¹ and Miekeley and Felix² are representative, is the most widely employed method of determining the fission-gas-release characteristics of fissile ceramics. It does not require complex equipment (except for the reactor) and can be applied to shapes and microstructure of actual fuel material. Ion bombardment experiments, which are directed more at probing the nature of the diffusional processes than at determining gas-release parameters, are typified by the work of Matzke and MacEwan,³ Jech and Kelly,⁴ and Ong and Ellman.⁵ In the last of these studies, radioactive gas is introduced into the specimen by fission recoil from a surrounding enriched-uranium metal foil.

15.2.2 In-Pile Release

Measurement of the rates of release of fission gases from fuels during irradiation provides a more realistic

*The surface layer of reactor-irradiated fissile specimens, however, is depleted of fission gas owing to recoil or knockout.

understanding of gas migration than can be obtained by the postirradiation annealing method. The main advantage of the in-pile studies is that production and release of the gases occur at the same temperature and in the same irradiation environment. In the postirradiation annealing studies, on the other hand, production occurs at ambient temperature in a low irradiation field, whereas release takes place at high temperature in the absence of a neutron flux. The main disadvantage of in-pile release experiments is their complexity and expense. A sample of fuel material is loaded into a test capsule for insertion into a reactor (Fig. 15.2). The specimen is heated by its own fission power, temperature control being achieved by varying the supply of cooling air flowing around the capsule. The fission gases are continually removed by a sweep gas passing over the sample and discharged into a gamma-ray detection system similar to that employed in postirradiation annealing studies (Fig. 15.1). A detailed view of a test capsule for in-pile investigation of gas release from single-crystal UO_2 specimens is shown in Fig. 15.3.

Less sophisticated measurements of fission-gas release can be obtained simply by puncturing an ordinary fuel element that has been in the reactor for a known length of time and by measuring the total pressure and composition of the gases inside the element. Information on the total release as a function of irradiation history is obtained often by using instrumented fuel elements equipped with a pressure sensor and thermocouples (Fig. 15.4). The disadvantage of measuring gas release from an entire fuel element is that the data represent averages over the axial temperature and fission-rate distributions in the fuel element.

The types of gas-release information provided by the post-irradiation anneal and in-pile methods are somewhat different. Postirradiation anneal experiments give the fractional release, which is the fraction of the initial quantity of gas in the specimen released during an anneal of time t . That is, the gas release is studied in an inherently transient manner. In-pile experiments using the apparatus shown in Fig. 15.2, on the other hand, generally analyze the activity of a short-lived fission product, such as ^{88}Kr . Because of

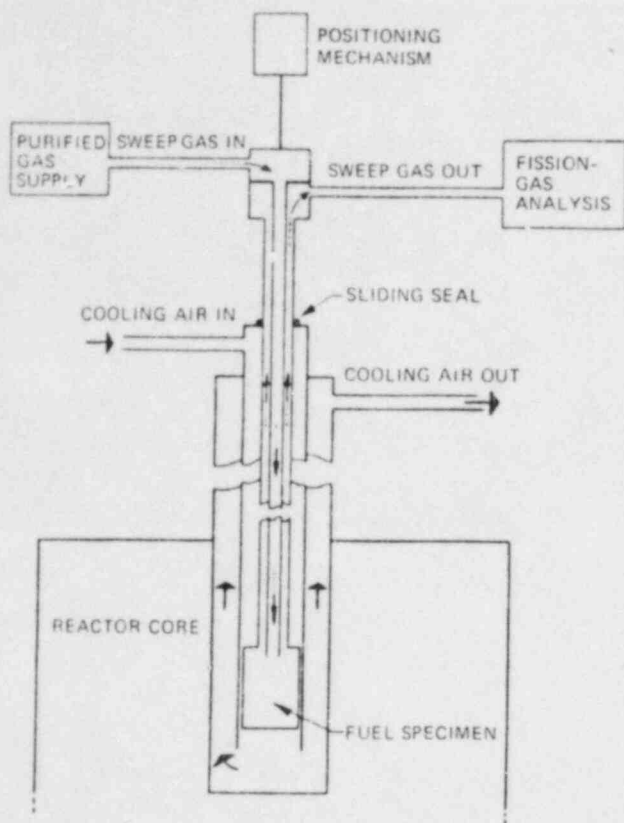


Fig. 15.2 Schematic flow diagram of an irradiation facility for continuous in-pile fission-gas release measurements. [After R. M. Carroll et al., *Nucl. Sci. Eng.*, 38: 143 (1969).]

the short half-life, these experiments attain a true steady state. The fractional release is defined for this experiment as the ratio of the rate of gas release to the rate of production from fission. This quantity is often called the release-to-birth rate ratio instead of the fractional release. Fuel-element puncture tests or continuous pressure measurements are usually reported as a fractional gas release, equal to the quantity of gas in the free volume within the fuel element divided by the total quantity of fission gases produced up to the time that the measurement was made.

15.3 RECOIL AND KNOCKOUT

Evidence for a temperature-independent mechanism of fission-gas release comes from data such as those shown on Fig. 15.5, in which the steady-state release rate of ^{88}Kr measured in the apparatus of Fig. 15.3 is plotted as a function of temperature. Below about 625°C (900°K) the emission rate is independent of temperature. Two distinct mechanisms are believed to be involved in the low-temperature portion of the release curve.

The first is direct recoil of fission fragments from within a layer equal to the range of the fission fragments in the fuel ($\sim 10\ \mu\text{m}$). To a good approximation, the fragments of a fission event travel through the solid in straight lines, losing energy en route primarily by interaction with the

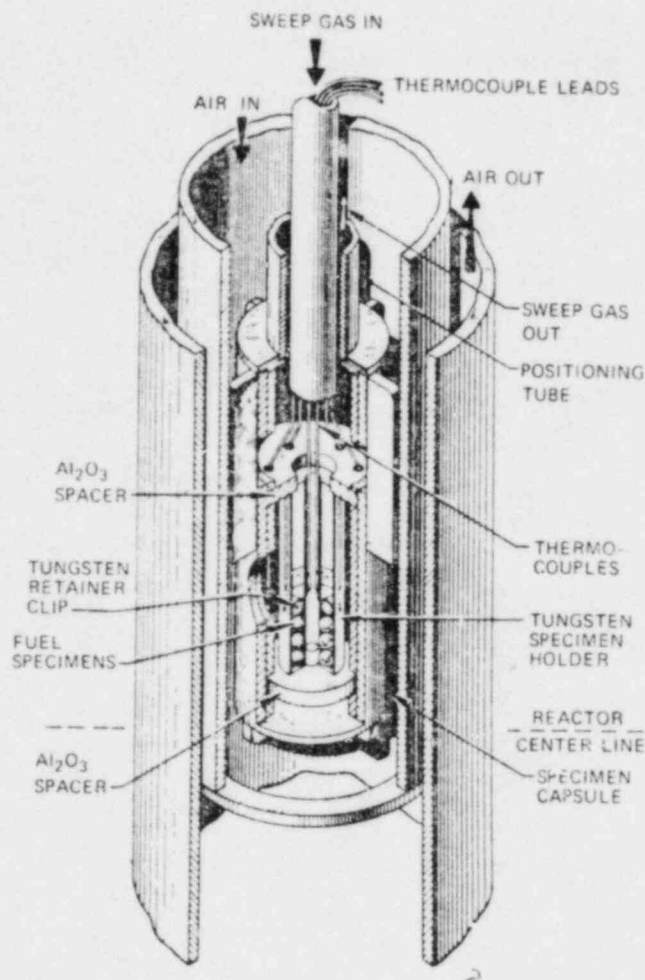


Fig. 15.3 Detail of capsule for in-pile fission-gas release investigation of fused crystal spheres of UO_2 . [From R. M. Carroll et al., *Nucl. Sci. Eng.*, 38: 143 (1969).]

electrons of the material. When the initial kinetic energy has been expended by the stopping power of the medium, the fragment comes to rest as a fission product.* However, if the fragment intersects a surface of the solid before its kinetic energy is depleted, it is released. Figure 15.6 shows fission-fragment tracks in a thin film of irradiated UO_2 which had been suitably etched to reveal the lattice distortion caused by the passage of the high-energy fragment. The track starting in the upper left corner of the electron micrograph and terminating in the lower right is $6.5\ \mu\text{m}$ in length and $\sim 150\ \text{\AA}$ in width.†

*Fission fragments are distinguished from fission products by their kinetic energy. Fission fragments possess all or part of the $\sim 80\ \text{MeV}$ received from the fission event, whereas fission products are stationary.

†Fission tracks are visible only in thin films of UO_2 , which have grain sizes less than $\sim 100\ \text{\AA}$. These fine grains trap the heat liberated by slowing down of the fragment. As a result of the very high local temperature, considerable disruption (essentially vaporization) of the lattice occurs. In large-grain material, on the other hand, the thermal spike is rapidly quenched and tracks are not visible.⁶

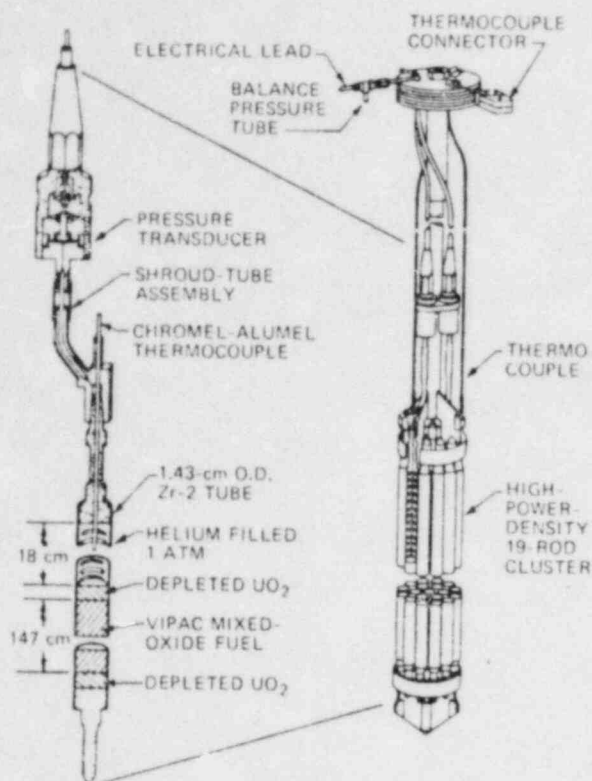


Fig. 15.4 Instrumented fuel element for measuring pressure buildup during irradiation. [After T. B. Burley and M. D. Freshley, *Nucl. Appl. Tech.*, 9: 233 (1970).]

The second mechanism of fission-gas ejection is called the knockout process. In passing through the solid, fission fragments occasionally make elastic collisions with the nuclei of atoms of the lattice, which become energetic particles in their own right. The fission track in Fig. 15.6 shows a slight change in direction near the middle of its path, which is probably due to such a collision. The atom struck by the fission fragment, which is called a primary knock-on, acquires energy of the order⁷ of ~ 100 keV. It too travels through the solid in a nearly straight line for a distance of ~ 200 Å before coming to rest. If the primary

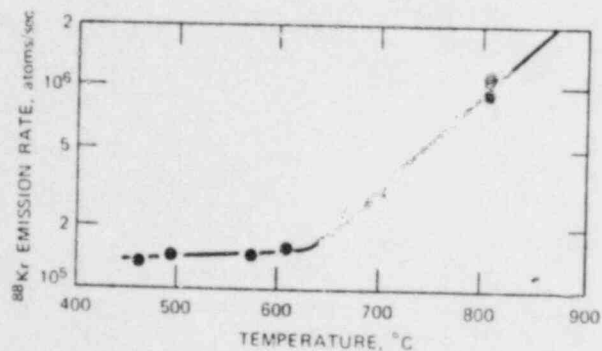


Fig. 15.5 Steady-state release rate of ^{88}Kr from single-crystal UO_2 for $\dot{F} \approx 2 \times 10^{12}$ fissions $\text{cm}^{-3} \text{sec}^{-1}$. [After R. M. Carroll and O. Sisman, *Nucl. Sci. Eng.*, 21: 147 (1965).]

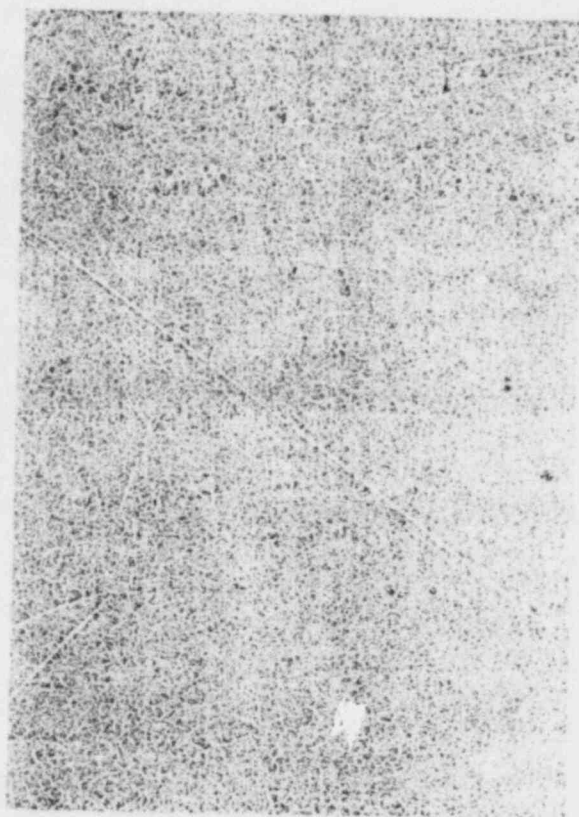


Fig. 15.6 Fission-fragment tracks in a 150-Å-thick film of vacuum-deposited UO_2 . [From M. D. Rogers, *J. Nucl. Mater.*, 16: 298 (1965).]

knock-on is created within this distance of the surface, it may be ejected. The primary knock-on is most likely to be a uranium or oxygen atom of the fuel, but occasionally a fission-gas atom lodged in the lattice may be struck by a passing fission fragment (of any kind) and become a primary knock-on that may have sufficient energy to escape from the surface before coming to rest.

Even if the primary knock-on does not emerge from the solid via a nearby surface, it can transfer its energy to other atoms in the solid by elastic collisions. The atoms struck by the primary knock-on are called secondary knock-ons. These in turn can strike other atoms to create a collision cascade whose members are generally referred to as higher order knock-ons. The mean energy and range of the higher order knock-ons are much less than those of the primary knock-on, but there are many more of the former than of the latter. The primary or higher order knock-on atoms that escape from the surface are said to be knocked out. To escape, the knock-ons must be produced no farther from the surface than their mean range.

The direct recoil and knockout mechanisms of release are illustrated in Fig. 15.7. The knockout process can remove any type of atom from the solid, either as a primary or a higher order knock-on. The energy for creating the collision cascade arises from a fission fragment, which need not escape from the fuel nor be one of the noble-gas fission products. Of course, only fission fragments can be released from the fuel by the direct recoil mechanism since the

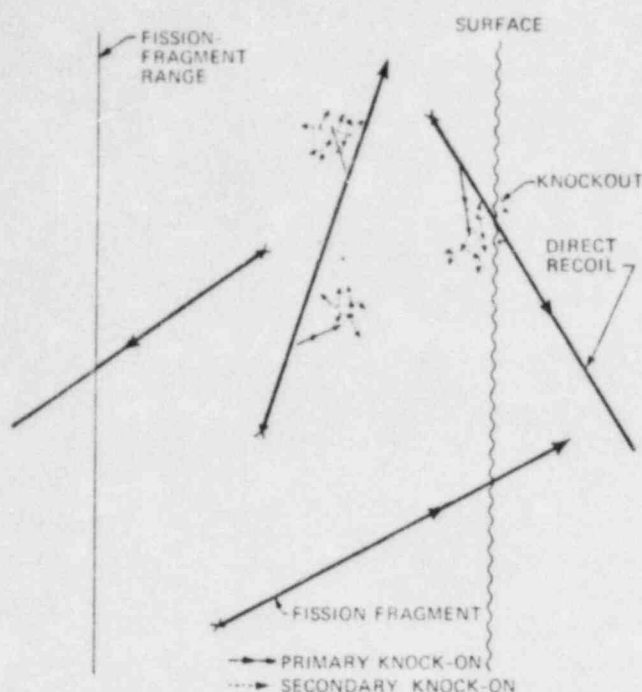


Fig. 15.7 Fission-gas release by direct recoil and knockout.

atoms of the fuel matrix do not directly receive any of the energy of fission. Table 15.1 summarizes the numbers, mean energies, and ranges of the energetic particles of importance in the direct recoil and knockout release mechanisms. The calculated parameters of the knock-ons refer to the uranium atoms of the UO_2 lattice. Analogous numbers can be obtained for the oxygen knock-ons.

In both the direct recoil and knockout mechanisms of fission-gas release, we must analyze a direct-flight particle transport problem near a free surface. Two quantities are of interest: the concentration profile of a particular fission-product species near the surface and the rate at which this species recoils out of the surface. To calculate the concentration distribution, we can balance the production and removal of fission products (not fission fragments) in a unit volume of solid. The method is similar to that applied to thermal neutrons in a reactor, in which fast neutrons are excluded from the thermal neutron balance and contribute to the latter as a slowing down source. In analogous fashion

Table 15.1 Characteristics of Fission Fragments and Knock-ons in UO_2 *

Particle	Number created per fission fragment	Mean energy, keV	Range, Å
Fission fragment	1	80,000	100,000
Primary uranium knock-ons	28	100	220
Higher order uranium knock-ons	21,000	0.2	44

*Based on Ref. 7.

we calculate the rate at which energetic particles of a certain type slow down and stop in a volume element of the solid. This process provides a source of particles to the balance. Similarly, particles struck by other high-energy species are lost from the stationary class.

Because the ranges of the energetic particles are small compared to the dimensions of the solid, all concentrations and generation rates can be considered as functions of the distance x from the solid surface. The rate of production of recoils of species i is defined by

$$P_i(x) = \text{rate of generation of recoils of species } i \text{ per unit volume at a distance } x \text{ from the surface}$$

The term "recoil" is used to denote fission fragments or knock-ons of any species in the solid.

We first compute the source term in the balance equation on a stationary species due to stopping of recoils in the solid. This quantity is defined by

$$q_i(x) = \text{rate at which particles of species } i \text{ are stopped in a unit volume of solid at a distance } x \text{ from the surface}$$

where q_i is analogous to the slowing-down density of neutrons at thermal energies treated in reactor physics calculations.

To determine q_i , consider a spherical volume element of radius ρ at a distance x from the surface, as shown in Fig. 15.8. The particles that come to rest in this volume element originated in a spherical shell a distance equal to the recoil range μ from the small sphere. The chord length through the small sphere intersected by a parallel line ranges from 2ρ if the particle passes through the center of the sphere to zero if the particle just grazes the sphere. The mean chord length can be obtained from elementary

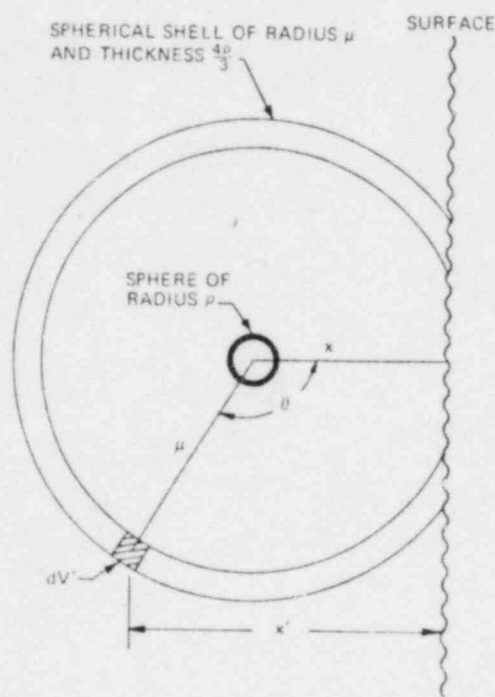


Fig. 15.8 Diagram for determining the rate at which recoils stop in a unit volume of solid.